REPORT DOCUMENTATION PAGE

Public reporting burden for this collection of information is estimated to average 1 hour per response, including the time for reviewing instructions, searching existing data sources, gathering and maintaining the data needed, and completing and reviewing the collection of information. Send comments regarding this burden estimate or any other aspect of this collection of information, including suggestions for reducing this burden, to Washington Headquarters Services, Directorate for Information Operations and Reports, 1215 Jefferson Davis Highway, Suite 1204, Arlington, VA 22202-4302, and to the Office of Management and Budget, Paperwork Reduction Project (0704-0188), Washington, DC 20503.

1. AGENCY USE ONLY (Leave blank)	2. REPORT DATE 29 June 92	3. REPORT TYPE AND DATES COVERED Annual Technical, 1 June 91- 31 May 92

4. TITLE AND SUBTITLE
Characterization of heterogeneities controlling transport and fate of pollutants in unconsolidated sand and gravel aquifers: First year report (Revised Aug. 1992)

5. FUNDING NUMBERS
G

AFOSR-91-0298

6. AUTHOR(S)
C. D. McElwee and J. J. Butler, Jr.

7. PERFORMING ORGANIZATION NAME(S) AND ADDRESS(ES)
Kansas Geological Survey
The University of Kansas
1930 Constant Avenue
Lawrence, KS

8. PERFORMING ORGANIZATION REPORT NUMBER
KGS
OFR 92-20

9. SPONSORING/MONITORING AGENCY NAME(S) AND ADDRESS(ES)
AFOSR/NL
Building 410
Bolling AFB DC 20332-6448

10. SPONSORING/MONITORING AGENCY REPORT NUMBER

11. SUPPLEMENTARY NOTES
This report revision supersedes all earlier versions.

12a. DISTRIBUTION/AVAILABILITY STATEMENT
Available from Publication Office of Kansas Geological Survey

12b. DISTRIBUTION CODE
OFR 92-20

13. ABSTRACT (Maximum 200 words)
The purpose of this project is to evaluate promising methodologies for characterization of heterogeneities in hydraulic conductivity. A major thrust of the first year of this project was an assessment of slug tests in heterogeneous formations. The theoretical components of this effort included the development of a time-continuous numerical model, a study of slug tests in layered aquifers, an examination of effective properties obtained from slug tests in the presence of well skins, and an examination of slug tests with observation wells. The field component emphasized multilevel slug tests. A prototype multilevel slug-test system was tested. Test results indicated that the tests are being affected by mechanisms not accounted for in the conventional theory. A series of experiments was carried out in order to clarify the mechanisms producing the observed behavior. These experiments served as the basis for the development of a new nonlinear model for the analysis of slug-test data. Additional field work included further hydraulic testing; a detailed aqueous geochemistry study; drilling and sampling activities; modification of the bladder sampler; laboratory analyses of cores; and a detailed seismic survey.

14. SUBJECT TERMS
Heterogeneities, alluvial aquifers, slug tests, site characterization, pollutant transport, pulse testing

15. NUMBER OF PAGES
209

16. PRICE CODE

17. SECURITY CLASSIFICATION OF REPORT	18. SECURITY CLASSIFICATION OF THIS PAGE	19. SECURITY CLASSIFICATION OF ABSTRACT	20. LIMITATION OF ABSTRACT

CHARACTERIZATION OF HETEROGENEITIES CONTROLLING TRANSPORT AND FATE OF POLLUTANTS IN UNCONSOLIDATED SAND AND GRAVEL AQUIFERS: FIRST YEAR REPORT

Carl D. McElwee and James J. Butler, Jr.
Kansas Geological Survey
The University of Kansas

with

Gwendolyn L. Macpherson
Department of Geology
The University of Kansas

Geoffrey C. Bohling, Richard D. Miller, Wenzhi Liu,
Christine M. Mennicke, and Zafar Hyder
Kansas Geological Survey
The University of Kansas

June, 1992

ABSTRACT

A considerable body of research has shown that large-scale spatial variations (heterogeneities) in hydraulic conductivity play an important role in controlling the movement of a contaminant plume in the subsurface. Quantifying these heterogeneities, however, can be a very difficult task. If we are to improve our predictive capabilities of the fate and transport of pollutants in the subsurface, it is critical to develop methodology that enables a more accurate characterization of hydraulic conductivity variations at a site to be obtained. The purpose of the research of this project is to evaluate, through both theoretical and field experiments, promising methodologies for the characterization of heterogeneities in hydraulic conductivity.

A major thrust of the first year of this project was an assessment of the type of information that can be obtained from slug tests in heterogeneous formations. This effort had both theoretical and field components. The theoretical components included the development of a time-continuous numerical model that can be used for the analysis of slug-test data from wells in heterogeneous formations, a detailed study of the viability of slug tests (and specifically multilevel slug tests) in layered aquifers, an examination of the effective properties obtained from slug tests performed in wells surrounded by a finite-radius zone of low permeability, and an examination of slug tests with observation wells.

The field component of this study of slug tests in heterogeneous formations mainly concentrated on an assessment of multilevel slug tests in highly permeable alluvium. A prototype multilevel slug-test system was tested at the Geohydrologic Experimental and Monitoring Site (GEMS), the field site for all of the work of this research. The results of the multilevel tests indicated that slug tests in the sand and gravel section at GEMS are being affected by mechanisms not accounted for in the conventional theory on which the standard methods for slug-test data analysis are based. The existence of these mechanisms were reflected by a concave downward curvature on log head versus arithmetic time plots, a dependence of slug-test responses on the magnitude of the induced slug (H_0), and systematic deviations between plots of the test data and the best-fit conventional models. A series of experiments was carried out at GEMS in order to clarify the mechanisms producing the observed behavior. Although these experiments have not yet been completed, they have served as the basis for the development of a new nonlinear model for the analysis of slug-test data. The initial form of this model appears to be superior to the conventional approaches for the analysis of slug-test data from the sand and gravel section at GEMS.

In addition to the research on slug tests in heterogeneous formations, a significant amount of the work in the first year of this project was directed at increasing our knowledge of the subsurface at GEMS. This work included hydraulic testing of wells in the aquifer and underlying bedrock at GEMS; a detailed study of the aqueous geochemistry of the upper clay and silt layer, the sand and gravel section, and the underlying bedrock; continued drilling and sampling activities; further modifications of the bladder sampler developed at the Kansas Geological Survey (KGS); continued laboratory analyses of the cores obtained with the bladder sampler; and a detailed seismic survey. These characterization efforts are directed towards the development of a detailed picture of the subsurface at GEMS, so that we can better assess the results of the hydraulic and tracer tests that are being performed as part of this research.

A considerable amount of construction and assembly of equipment took place during the first year of this project. This equipment included an additional bladder sampler, a laboratory calibration system for pressure transducers, a portable field trailer, a tripod and winch system for moving equipment in a well, and interfaces for data acquisition equipment.

The research team for this project is composed of professional staff from the KGS and the Department of Geology of the University of Kansas. Three graduate students (two directly funded by this project and one funded by the KGS) are using aspects of the work of this research as subjects for their doctoral dissertations. Additional graduate students are benefitting from this project as a result of the establishment of a computer lab for graduate students in hydrogeology and the incorporation of material from this work into courses at the University of Kansas taught by members of the research team.

TABLE OF CONTENTS*

IX. APPENDICES

* - Note that pages are numbered according to section and subsection.

L INTRODUCTION

A. RESEARCH OBJECTIVES

The accurate prediction of pollutant transport and fate in aquifers is one of the most difficult and pressing problems in hydrogeology today. Physical, chemical, and microbial processes all play major roles in controlling pollutant transport. Before we can begin to understand the influence of the chemical and biological side of this problem, however, we must fully understand the role of physical processes and, specifically, the influence of the physical hydrogeological properties. Many researchers now recognize (e.g., Molz et al., 1989) that if we are to improve our predictive capabilities for subsurface transport, we must first improve our capabilities for measuring and describing conditions in the subsurface. That is the focus of the research described in this report. The specific objective of this research is to assess the potential of advanced well-testing technology for providing more accurate estimates of spatial variations in the physical properties that control contaminant plume movement in saturated porous media. Although effective porosity is clearly an important consideration, the major emphasis of this work is on characterizing spatial variations (heterogeneities) in hydraulic conductivity.

Ideally, heterogeneities in hydraulic conductivity must be studied and characterized at several different scales in order to understand their influence on the movement of a contaminant plume. Although theoretical modeling work is an important element of any study of the influence of spatial variations in hydraulic conductivity, a rigorous study of this subject must have a major field component. A field site, at which researchers at the University of Kansas can pursue work on assessing heterogeneities in aquifer properties, has been set up as part of this research. The specific site of the field effort is the Geohydrologic Experimental and Monitoring Site (GEMS), which is located just north of Lawrence, Kansas on land owned by the University of Kansas Endowment Association. Figure 1 is a map showing the location of GEMS and some of the major features at the site. GEMS overlies approximately 70 feet (21.3 m) of Kansas River valley alluvium. These recent unconsolidated sediments overlie and are adjacent to materials of Pleistocene and Pennsylvanian age. A cross-sectional view of the subsurface at one of the well nests at GEMS is shown in Figure 2. The alluvial facies assemblage at this site consists of approximately 35 feet (10.7 m) of clay and silt overlying 35 feet (10.7 m) of sand and gravel. The stratigraphy is a complex system of stream-channel sand and overbank deposits. Thus, a considerable degree of lateral and vertical heterogeneity in hydraulic conductivity is expected at GEMS.

In the first year of this research, the focus of the work was on the use of slug tests to describe spatial variations in hydraulic conductivity. A theoretical and field examination of the potential of multilevel slug tests for providing detailed information about conductivity variations in the vertical comprises the majority of the work in this period. However, a considerable amount of additional work was directed at increasing our knowledge of the subsurface at GEMS. This effort involved additional slug and pumping tests, analyses of the aqueous geochemistry, continued drilling and sampling of the alluvium, laboratory analyses of sampled cores, and a detailed seismic survey. These characterization efforts are directed at providing the detailed information that will allow us to better assess the quality of the information provided by the various well-testing approaches evaluated in this work. In addition, this information will help us design the tracer tests to be performed in the third year of the project. The ultimate goal of these characterization efforts is to describe the site in so much detail that it effectively becomes an underground laboratory at which new technology can be evaluated.

B. BRIEF OUTLINE OF REPORT

The remainder of this report is divided into six major sections, each of which is essentially a self-contained unit. Pages, figures, and equations are labelled by section and, when warranted, subsection.

The first section describes theoretical work directed at developing a better understanding of the information that can be obtained from slug tests in heterogeneous aquifers. A continuous-in-time numerical model, which has proven very useful for the analysis of well-test data, is introduced. This model is then used in a detailed study of slug tests in layered aquifers. Some improvements that were made to SUPRPUMP, a well-test analysis package developed at the KGS, are described and an overview of the sensitivity analysis approach on which SUPRPUMP is based is given. SUPRPUMP is then used to carry out a study of effective properties obtained from slug tests in the presence of a well skin and an analysis of slug tests using observation wells.

The second section primarily describes field investigations of multilevel slug tests. A prototype multilevel slug test system, which has been developed at the KGS, is described and its use at GEMS is detailed. An extensive series of field experiments that were undertaken in order to understand the causes of anomalous behavior observed in slug-test data from wells in the sand and gravel section at GEMS are then described. The section concludes with the derivation of a new model, which accounts for some of the mechanisms affecting the GEMS slug-test data, and a discussion of the applicability of this model to the GEMS data.

The third section primarily describes activities directed at increasing our knowledge of the subsurface at GEMS. A program of slug tests carried out in the wells screened in the sand and gravel section is described. A preliminary analysis of a pumping test performed in a well in the bedrock underlying the alluvial section at GEMS is then reported. A detailed study of the aqueous geochemistry at GEMS is then given. After a description of the drilling and sampling activities that occurred over the last year at GEMS, work in the KGS core measurement laboratory is discussed. The section concludes with a brief report on the status of wireline logging activities and a detailed description of the shallow seismic survey that was undertaken during the past year at GEMS.

The fourth section describes new equipment that was built or purchased during the first year of this project.

The fifth section describes the personnel of the research team that has been organized to pursue this work, and lists relevant publications of the team over the last year. The section concludes with a discussion of the interactions with other research groups that have occurred over the last year.

The sixth section summarizes the report and briefly outlines the work planned for the second year of this project.
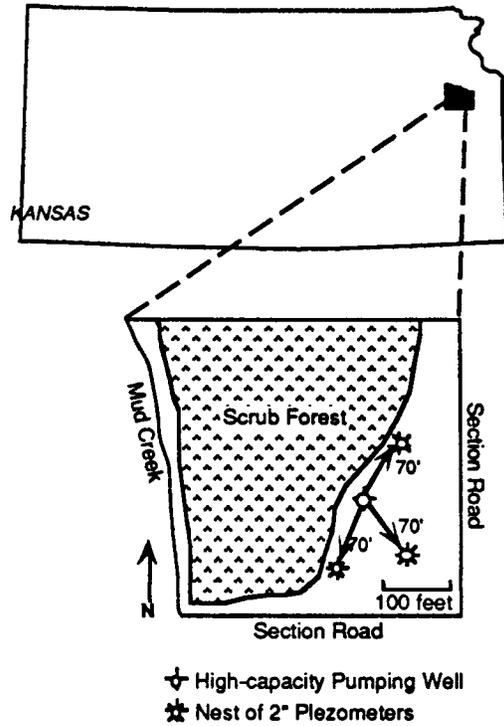
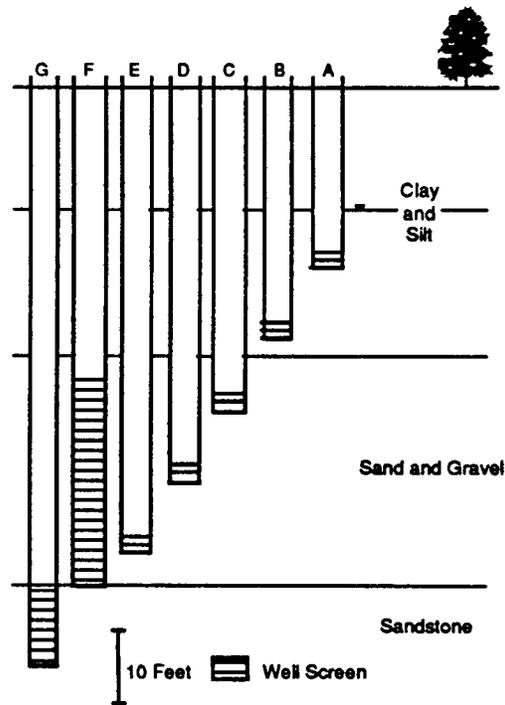Figure 1 - Location map for the Geohydrologic Experimental and Monitoring Site (GEMS).

Figure 2. A typical well nest cross-section

I.4

II. THEORETICAL INVESTIGATIONS OF SLUG TESTS IN HETEROGENEOUS MEDIA

A. A CONTINUOUS-IN-TIME NUMERICAL MODEL FOR THE ANALYSIS OF WELL TESTS IN THREE-DIMENSIONAL NONUNIFORN AQUIFERS

Introduction

Analytical solutions for drawdown in response to a pressure disturbance induced at a central well are the basis of conventional well-test analysis methodology. For the most part, these solutions consider hydraulic behavior in an idealized aquifer in which flow properties are invariant in space. Aquifers in nature, however, are characterized by a considerable degree of spatial variations (heterogeneities) in flow properties. Not surprisingly, analyses based on solutions to flow in idealized uniform systems may be of limited use in assessing heterogeneities in the vicinity of the stressed well. A better understanding of these near-well heterogeneities, however, is critical if we are to improve our ability to predict the fate and transport of pollutants in the subsurface. A component of the research in the first year of this project was therefore directed at further exploration of a numerical modeling approach that would allow the actual complexity of the geological system to be incorporated into the analysis of well-test data. This approach could then serve as a tool for both the development of insight into the role of heterogeneity in controlling well-test responses and the analysis of well tests and tracer tests in succeeding years of this project.

A general model for well-test analysis must allow the actual complexity of the geologic formation to be represented in the full three dimensions. Analytical solutions for well tests in simplified three-dimensional settings have been developed by a number of authors using traditional integral transform techniques (e.g., Russell and Prats, 1962; Papadopulos, 1966; Prijambodo et al., 1985; Hayashi et al., 1987; Raghavan, 1989; McElwee et al., 1990). Because of the complexities introduced by the vertical component of flow at the stressed well and within the aquifer itself, however, an exact analytical solution has yet to be derived for the general case of well testing in a three-dimensional nonuniform system. Given the limitations of the traditional analytical solution methodology, a new approach for the analysis of well-test data is considered in this work. The approach considered here is based on the idea of combining the spatial discretization used in a conventional numerical model with the Laplace transform in time used in conventional analytical models. A solution to this hybrid numerical model is obtained in Laplace space using standard techniques of matrix algebra. A set of solutions

in Laplace space is then back transformed to real space, producing a solution in real space that can be formulated in a continuous manner over a range of times. In the following discussion, the theoretical basis of this approach is explored and its implementation in this work is described.

A Time-continuous Numerical Method

Approximate numerical methods such as the finite difference (FE) or finite element (FE) approaches have been widely used in groundwater studies for applications where analytical solutions are not feasible. These numerical approaches involve both spatial and temporal discretization of the governing equations, with the quality of the approximation dependent on the discretization strategy. The size of the time increment is varied during the course of a simulation in order to improve computational efficiency. However, selection of the proper time increment may present difficulties when model output is required at particular points in time. In groundwater flow and transport applications, problems often arise with conventional numerical approaches when a comparison between model output and measured data is desired for the specific times at which the measurements were made. This is especially true when working with data from hydraulic or tracer tests, where the density of the data in time may be quite large.

In order to avoid some of the problems associated with temporal discretization, a hybrid method, which combines spatial discretization with a Laplace transform in time, is employed here. The spatial discretization scheme is the same as that in a conventional finite-difference model. The resultant spatially discretized system of algebraic equations in complex space is solved using complex arithmetic for the matrix inversion. The Laplace-space solution is then inverted back into real space using an appropriate numerical inversion scheme. This procedure yields a solution that is continuous over a range of times, with the only approximation in the temporal domain being that introduced by the numerical inversion scheme.

This time-continuous method has been employed by a number of workers during the past two decades (e.g., Gurtin, 1965; Javandel and Witherspoon, 1968; Chen and Chen, 1988; Sudicky, 1989; Moridis and Reddell, 1991; Sudicky and McLaren, 1992). The most difficult problem associated with this method has been the inversion of the Laplace-space solution back into real space. Various methods for approximate numerical inversion, all of which involve the evaluation and summation of the transform-space function, have been developed by a number of authors (e.g., Stehfest, 1970; Talbot, 1979; Crump, 1976). One focus of the research of this project is the development of a more efficient inversion algorithm. As noted by Sudicky (1989), De Hoog et al. (1982)

propose a quotient difference algorithm for increasing the rate of convergence of the summation-series approach of Crump (1976). This quotient-difference algorithm has been shown to have a significant computational advantage over other algorithms in decreasing the computations required for the analysis of well-test data (Liu and Butler, 1991). The computational savings are such that this method appears to hold considerable promise for use as a practical tool for analysis of well tests in fully three-dimensional systems. The following section describes a discrete-in-space, continuous-in-time model that has been developed for the analysis of well tests in systems where conventional analytical approaches are not viable.

The Three-Dimensional Finite Difference Time-continuous Model (3DFDTC)

The time-continuous approach can be used only if Laplace transforms exist for the governing equation together with all boundary and initial conditions. Thus, the approach described here only strictly applies to confined flow systems. The cylindrical-coordinate form of the governing equation for three-dimensional flow in a confined system is

$$\frac{1}{r}\frac{\partial}{\partial r}(rK_r\frac{\partial h}{\partial r}) + \frac{1}{r^2}\frac{\partial}{\partial\theta}(K_\theta\frac{\partial h}{\partial\theta}) + \frac{\partial}{\partial z}(K_z\frac{\partial h}{\partial z}) = S_s\frac{\partial h}{\partial t} \tag{1}$$

where

h = drawdown, [L];

S_s = specific yield, [1/L];

K_r, K_θ, K_z = hydraulic conductivity in the radial, angular, and vertical direction, respectively, [L/T];

t = time, [T];

r = radial distance, [L];

θ = angular position, in radians;

z = vertical depth from the top of the aquifer, [L].

For the case of a pumping test in a layered aquifer, the initial and boundary conditions are defined as

$$h(r,0) = h_a, r < \infty \tag{2}$$

$$h(\infty, t) = h_a, t \geq 0 \tag{3}$$

$$2\pi \sum_{j=1}^{J} K_{rj} m_j \left(r \frac{\partial h}{\partial r} \right)_{r-r_v} = -\sum_{i=1}^{NP} q_i \square_i (t) \tag{4}$$

where

$$\square_i (t) = box\ car\ function = \begin{cases} 1, & if\ t_{1i} \le t \le t_{2i}, & i=1,2,\cdots,NP \\ 0, & elsewhere \end{cases}$$

h_a = initial head in the aquifer, [L];

NP = number of pumping periods;

t_{1i} = starting time for pumping period i, [T];

t_{2i} = ending time for pumping period i, [T];

r_w = radius of pumping well, [L];

q_i = pumpage for pumping period i, [L^3/T];

J = total number of screened layers in the well bore;

K_{rj} = conductivity in radial direction for layer j;

m_j = depth of layer j.

The application of the Laplace transformation to equations (1) and (4), in conjunction with (2), results in:

$$\frac{1}{r} \frac{\partial}{\partial r} (r K_r \frac{\partial h}{\partial r}) + \frac{1}{r^2} \frac{\partial}{\partial \theta} (K_\theta \frac{\partial h}{\partial \theta}) + \frac{\partial}{\partial z} (K_z \frac{\partial h}{\partial z}) = S_s (\overline{h} p - h_a) \tag{5}$$

$$2\pi \sum_{j=1}^{J} K_{rj} m_j \left(r \frac{\partial \overline{h}}{\partial r} \right)_{r-r_v} = -\sum_{i=1}^{NP} q_i \frac{e^{t_{1i} p} - e^{-t_{2i} p}}{p} \tag{6}$$

where

p = Laplace transform variable;

$\overline{h}$ = head in Laplace space.

In order to improve the ease of radial discretization, the derivatives in the radial direction can be rewritten in a logarithmic form using the transformation $\overline{r} = \log_e (\frac{r}{r_w})$.

This approach allows a discretization in the radial direction which increases exponentially when using $\Delta \overline{r}$. Thus, the form of equations (5) and (6) employed for the discretization is

$$\frac{1}{r^2} \frac{\partial}{\partial \overline{r}} (K_r \frac{\partial h}{\partial \overline{r}}) + \frac{1}{r^2} \frac{\partial}{\partial \theta} (K_\theta \frac{\partial h}{\partial \theta}) + \frac{\partial}{\partial z} (K_z \frac{\partial h}{\partial z}) = S_s (\overline{h} p - h_a) \tag{7}$$

II.A.4

$$2\pi \sum_{j=1}^{J} K_{rj} m_j \left(\frac{\partial \bar{h}}{\partial \bar{r}}\right)_{\bar{r}=0} = -\sum_{i=1}^{NP} q_i \frac{e^{t_{1i}P} - e^{-t_{2i}P}}{P} \tag{8}$$

Unlike many analytical and numerical models, which assume the radius of the well to be infinitely small, the model developed here allows the influence of well bore storage to be taken into consideration. As noted by Papadopulos and Cooper (1967), effects of well-bore storage on drawdown can be significant during early times when the majority of the water is being removed from storage inside the well bore. As time increases, the influence of well- bore storage will gradually diminish, eventually reaching a point at which the infinitely small well-bore assumption is viable.

The implementation of the well-bore storage option in the three-dimensional finite difference, time-continuous model (3DFDTC) is based on earlier work of Settari and Aziz (1974), Rushton and Chan (1977), and Butler (1986). As described by Butler (1986), the approach is based on rewriting the classical pipe flow equation (Vennard and Street, 1975) in a Darcy Law-like formulation and defining a term (involving the friction factor, the cross-sectional area of the well bore, and distance along the well bore) analogous to hydraulic conductivity. This approach allows flow inside the well bore to be governed by the porous media flow equation given by (7). Note that the initial implementation of this approach for this project produces an approximation of well-bore behavior that is equivalent to the hydrostatic head assumption employed in most analytical representations of the well bore (e.g., Papadopulos and Cooper, 1967; Cooper et al., 1967).

In the three-dimensional representation employed here, the portion of the well bore passing through the modelled unit consists of several grid cells in the vertical. The storage coefficient is assumed to be one for the top cell of the well bore, while the storage coefficients for the remaining nodes in the well bore are set equal to the compressibility of water or zero (assuming water is incompressible). Since the radial-discretization scheme employed in the model uses logarithmic increments, the minimum radial location (r_{min}) of the first radial node inside the well bore must be larger than zero (i.e. $0.0 < r_{min} < r_w$). This produces a well bore in the shape of an annular ring rather than a circle. The storage coefficient of the well-bore cells must therefore be adjusted

(by a factor of $\dfrac{r_w^2}{r_w^2 - r_{min}^2}$) to account for the decrease in well-bore cross-sectional area produced by the annular ring representation of the well bore. In addition, the traditional

boundary condition at the well bore (8), which is based on the definition of radial flow along the well screen, is not used in this approach. Instead, a boundary condition at the top node of the well bore, based on the definition of the total flow out of the screened portion of the well, is employed. This flow boundary condition is written as

$$
\pi K_{r,J} m_J \left(\frac{\partial h}{\partial r} \right)_{\bar{r} = \log_e \left(\frac{r_{min}}{r_w} \right)} = -\sum_{i=1}^{NP} q_i \frac{e_1 i p - e_2 i p}{p}
$$
(9)

where m_J is the height of the top grid cell. Note that no-flow conditions in the radial direction are assumed at $r = r_{min}$ for the remaining nodes in the well bore. The use of (9) as a boundary condition makes this approach very useful for analyzing well tests in layered systems where the tested well may be screened in more than one layer (as in (4) with $J > 1$). Instead of having to define in advance the amount of water withdrawn from each layer, the model will implicitly calculate the flow out of each layer given the total flow out of the system defined by (9).

Since the representation of the well bore employed here is equivalent to the conventional hydrostatic head assumption, the hydraulic conductivity of the well bore must be defined such that the heads for all the nodes in the well bore are approximately equal. All three components of well-bore hydraulic conductivity must be at least five orders of magnitude larger than the aquifer conductivity in order to ensure negligible head loss along the well bore. In order to ensure that the majority of water will be drawn from the well bore at early times, the ratio of vertical well-bore hydraulic conductivity over its angular and radial counterparts must be large. An extensive set of experiments indicates that a ratio larger than 100 will ensure that all water will initially be drawn out of well-bore storage.

The 3DFDTC model is developed by applying a conventional central difference scheme to (7), which now represents conditions within both the aquifer and the well bore. After incorporating (9) and the Laplace transform of (3) into the finite difference scheme, the system of algebraic equations for 3DFDTC can be expressed in matrix form as

$$
([A] + p[B])[\bar{h}] = -[C] h_a + \sum_{i=1}^{NP} q_i \frac{e^{-t_0 p} - e^{-t_1 p}}{p} [D]
$$
(10)

where A, B, C, and D are matrices of constant coefficients and $\bar{h}$ is a vector of unknown heads. For the sake of conciseness, (10) is rewritten in the following form:

$$[G] \ [\overline{h}] = [W] \tag{11}$$

Both the left-hand side coefficient matrix G and the right-hand side matrix W of (11) involve the Laplace variable p, for which a value must be given before a solution in Laplace space can be obtained. The resultant solution in Laplace space can then be inverted back into real space using numerical inversion schemes such as those of Stehfest (1970) or Crump (1976). A detailed discussion of inversion algorithms with an emphasis on the method of Crump (1976) can be found in Appendix A.

The Crump algorithm approximates the inversion of a Laplace space function by means of a Fourier series that involve both sine and cosine functions. This method has a smaller error than that of a similar method presented by Dubner and Abate (1968). If the value of h at node j is desired, h_j is found using the following equation developed by Crump [1976]:

$$h_j(t) \approx \frac{e^{p_0 t}}{Tmax} \{ \frac{\overline{h_j}(p_0)}{2} +$$

$$\sum_{k=1}^{2N+1} [RE(\overline{h_j}(p_k)) \cos(\frac{k\pi t}{Tmax}) - IM(\overline{h_j}(p_k)) \sin(\frac{k\pi t}{Tmax})] \} \tag{12}$$

where

$\overline{h}_j(p_k)$ = solution from (11) at node j for $p = p_k$;

2Tmax = the period of the Fourier series approximating the inverse function on the interval [0, 2Tmax];

RE($\overline{h}$) = real part of $\overline{h}$;

IM($\overline{h}$) = imaginary par of $\overline{h}$;

Er = minimum relative error;

$p_k = p_0 + ik\pi/Tmax$;

$p_0 = \mu - \ln(Er/2Tmax)$, the real part of p_k;

μ = maximum real value of all the singularity points of the function in Laplace space;

$i = (-1)^{1/2}.$

Equation (12) shows that the time variable t appears only in the sine, cosine, and exponential functions. Since p_k is independent of time, we can perform the inversion

over a range of times based on one set of solutions of $\overline{h}$ for one specific Tmax. The solution is thus continuous in time because once a set of $\overline{h}$ values is calculated from (11), (12) will give the desired result at any time within the range of [0, 2Tmax].

If the summation is performed as in (12), hundreds of terms (i.e. solutions of (11)) may be needed in order to obtain a solution that satisfies a given convergence criterion. Since the computational effort required for the calculation of each p-space solution of (11) is at least equal to that required for one time step in a conventional numerical model, considerable attention is paid to the convergence of the summation series given in (12). An algorithm developed by De Hoog et al. (1982) has been found to significantly accelerate the convergence of the summation series and has therefore been incorporated into the 3DFDTC model. The acceleration of the summation series is great enough that the continuous-in-time approach is often the most computationally efficient approach for the analysis of well tests in heterogeneous formations. A detailed explanation of the De Hoog algorithm is given in Appendix A.

Discussion and Model Validation

The 3DFDTC model is considerably more flexible than its conventional analytical or numerical counterparts. Since no time-discretization scheme is employed, stability issues related to the time-stepping scheme can be ignored and a solution can be obtained directly for any specific time. Boundary conditions can also be changed easily to adapt to different patterns of stress being placed on the test well. For example, by simply setting $q_i = 0.0$ and changing h_n to H_0 in (10) for nodes located inside the well bore, 3DFDTC can be used to simulate a slug test with an initial head of H_0. If necessary, partial penetration and well skin effects can be accounted for by specifying the vertical position of the well screen and the radius of the skin, respectively. Unequal spacing in both the angular and vertical direction is allowed in order to model spatial variations in flow properties. If there exists a symmetry in heads in either the angular or vertical direction, 3DFDTC will simulate only part of the aquifer system by assuming a no-flow condition along the plane of symmetry. Note also that 3DFDTC can be used in a one- or two-dimensional mode if heads can be assumed equal in the angular and/or vertical directions. In such cases, only one node should be used in the direction of equal heads.

In order to validate the implementation of the time-continuous approach and the well-bore approximation, 3DFDTC has been checked against many analytical solutions for both pumping and slug tests. In all cases, a comparison between the analytical results and those of 3DFDTC revealed very small differences. Three typical examples are chosen here to demonstrate the viability of the 3DFDTC model.

The first example was designed to assess the viability of the well-bore approximation employed in the model. Drawdown produced by pumping at a constant rate from a well of finite radius in a uniform aquifer is simulated. In Figure II.A.1, the simulated results for drawdown within the pumping well are compared with the analytical results of Papadopulos and Cooper (1967) for the same case. The results produced by the two approaches essentially fall on top of one another throughout the duration of the simulation. The small difference in the computed drawdown is attributed mainly to the error caused by the spatial discretization scheme employed in 3DFDTC. Further simulations have shown that by increasing the number of nodes in the radial direction, the difference between the analytical and 3DFDTC results will gradually disappear. Note that in addition to the two curves depicting well-bore storage effects, a third curve, depicting drawdown calculated by 3DFDTC when well-bore storage effects are not included, is plotted on Figure II.A.1 to illustrate the period when well-bore storage effects are important.

In the initial phases of this project, there was considerable concern about numerical problems that might accompany the well-bore approximation as a result of the dramatic change in hydraulic conductivities between the aquifer and the well bore that is required by the approach. The second example is thus chosen to illustrate the performance of 3DFDTC when adjacent hydraulic conductivities differ by many orders of magnitude. A slug test in a well surrounded by a low permeability well skin of finite radius was simulated in order to assess model performance when a permeability contrast of ten orders of magnitude is employed. The configuration consisted of three distinct zones of differing properties: a very high permeability well bore ($K = 10^7$), a low permeability skin ($K = 10^{-3}$), and an aquifer of moderate permeability ($K = 1$). The well was assumed screened throughout the aquifer. Figure II.A.2 illustrates a comparison of the heads simulated by 3DFDTC with the results from the analytical solution of Moench and Hsieh (1985) for a slug test in a well with a skin of finite radius. The solid line in Figure II.A.2 depicts the head at the slugged well simulated by 3DFDTC, while the dashed line displays the results of the analytical solution. As with Figure II.A.1, the two lines essentially fall on top of one another. The differences between the two curves are again mainly due to the error introduced by spatial discretization, since only a total of six nodes are placed inside the well bore and the skin.

The last example is selected to illustrate model performance when there is a strong component of vertical flow, such as might occur in multilevel slug tests. A slug test is simulated in a well that is screened for only a portion of the aquifer thickness. The aquifer is assumed to be homogeneous and isotropic with respect to flow properties.

Figure II.A.3 displays a comparison of the normalized head (H/H_0) simulated by 3DFDTC with the results of the analytical solution of McElwee et al. (1990) for a slug test in a well partially penetrating the aquifer. The solid line in Figure II.A.3 depicts the head at the slugged well simulated by 3DFDTC, while the dashed line displays the results of the analytical solution. The inset provides details of the specific configuration employed for this example. As with the previous examples, 3DFDTC yields results that are essentially indistinguishable from those of the analytical solution.

Given the closeness of the match between the simulation results from 3DFDTC and those from the analytical solutions, it is clear that 3DFDTC can be a very useful tool for the design and analysis of well tests performed under conditions not readily represented by conventional analytical approaches. Therefore, in the succeeding sections of this report, 3DFDTC is used to examine the viability of multilevel slug tests in layered systems. The purpose of this numerical examination of multilevel slug tests in layered systems is to gain insight into how such tests might be designed in order to get more accurate information concerning vertical variations in the flow properties of a unit.
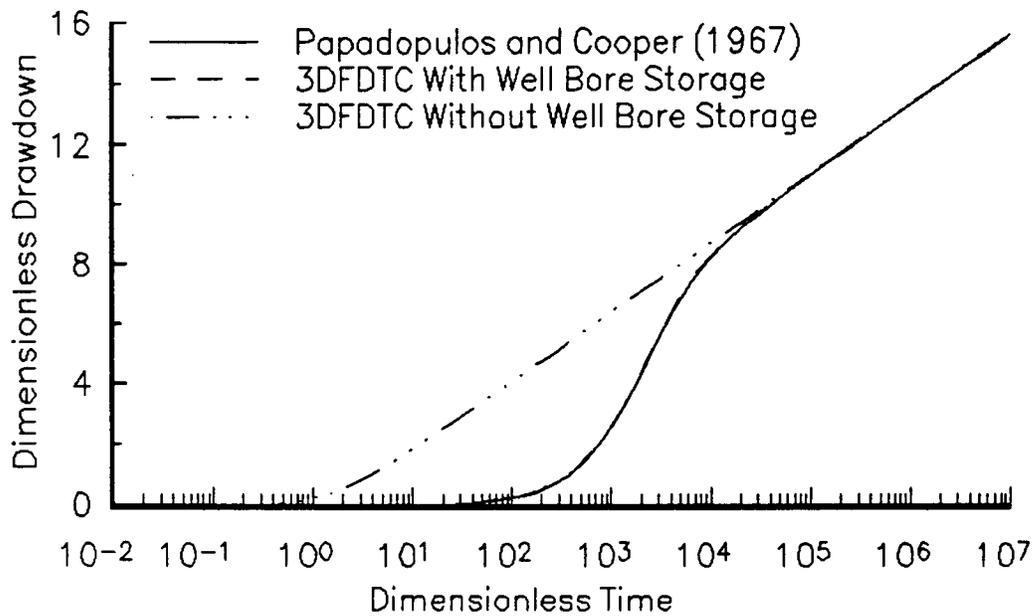
Figure II.A.1 Dimensionless drawdown $(4\pi Ts/Q)$ versus time $(4Tt/Sr^2)$ plot comparing the Papadopulos and Cooper (1967) solution with 3DFDTC results. (Observation well is located at $r=4.6$; $r_w=0.167$, $T=1$ and $S=10^{-5}$; 3DFDTC discretization: 3 radial nodes inside well bore, 39 nodes in the radial from r_w to 37364.15 meters and 5 nodes in vertical).
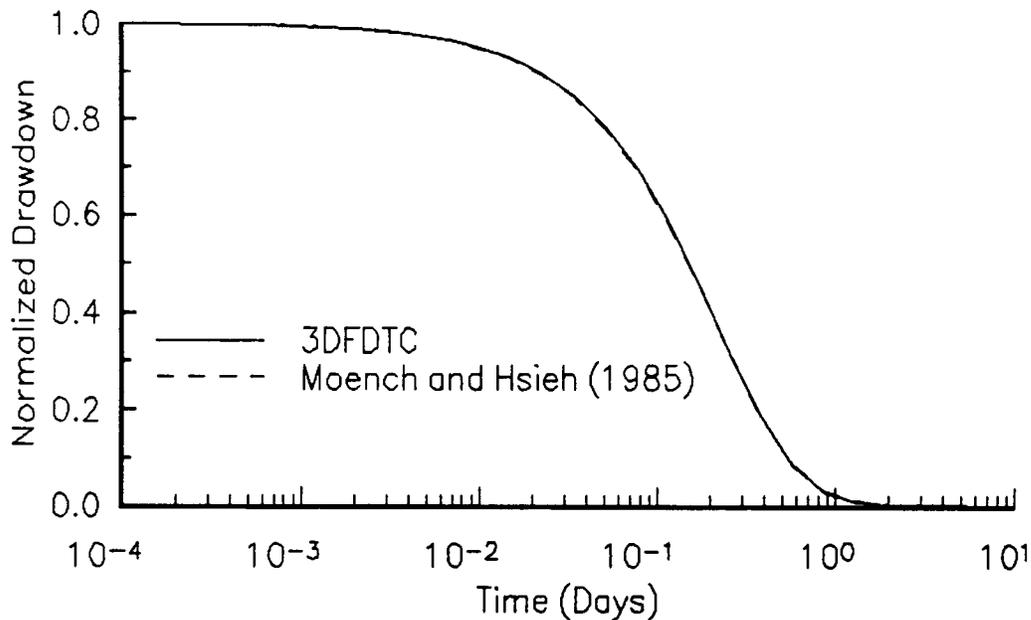

Figure II.A.2 Normalized drawdown (H/H_0) versus time plot comparing Moench and Hsieh (1985) solution with 3DFDTC results. $(r_w=0.167$, $r_{skin}=0.333$, $T_{skin}=10^{-3}$, $S_{skin}=10^{-3}$, $T_{aquifer}=1$, $S_{aquifer}=10^{-5}$; discretization as in Figure II.A.1 except that 3 of the 39 radial nodes are placed between r_w and r_{skin}).
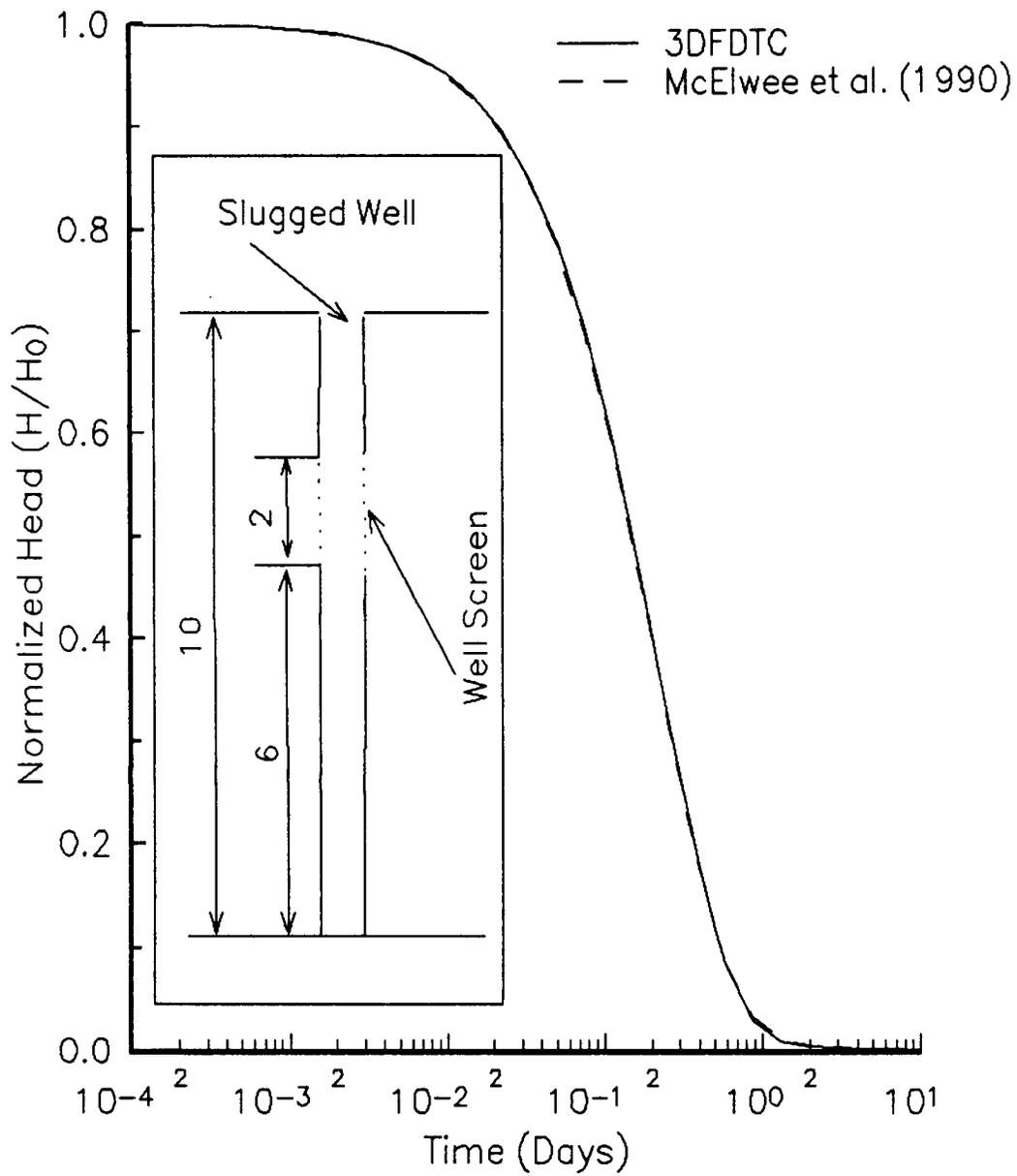
Figure II.A.3 Normalized head (H/H_0) versus time plot comparing McElwee et al. (1990) solution with 3DFDTC results. ($r_w=0.167$, $K=0.1$, $S_s=10^{-6}$; discretization as in Figure II.A.1).

B. THE USE OF SLUG TESTS TO DESCRIBE VERTICAL VARIATIONS IN HYDRAULIC CONDUCTIVITY

Introduction

The slug test has become one of the more commonly employed techniques in applied hydrogeology. This test, which is quite simple in practice, consists of measuring the rate of recovery in a well after a near instantaneous change of water level at that well. One of the primary objectives of the first year of this project was to explore the potential of slug tests to provide information about vertical variations in hydraulic conductivity. Specifically, the aim was to assess if a series of multilevel slug tests in a well that is fully screened across the unit of interest could provide useful information about vertical variations in flow properties. In this section, results of a series of numerical experiments performed to assess the theoretical viability of slug tests for the purpose of describing vertical variations in conductivity are reported. In a later section (III.B), results of a program of field testing at GEMS are described.

Model Configuration

In order to assess the potential of slug tests for identifying vertical variations in horizontal hydraulic conductivity, an early version of the 3DFDTC model described previously was used to generate synthetic slug-test results under a number of test scenarios. The initial set of simulations was carried out using four different hypothetical cases: 1) a uniform, isotropic aquifer; 2) a uniform, anisotropic aquifer; 3) a layered, isotropic aquifer; and 4) a layered, anisotropic aquifer. The layered aquifers consist of alternating high and low conductivity layers, with the following radial (r) and vertical (z) conductivity values (units are meters/day):

	anisotropic case	isotropic case
low conductivity layer	$K_r=1.; K_z=0.1$	$K_r=K_z=1.$
high conductivity layer	$K_r=10; K_z=1.$	$K_r=K_z=10.$

The uniform aquifers are assigned the properties of the low conductivity layer. In all cases, the aquifer is 25 meters thick (with one node per meter in the vertical). The aquifer is bounded above and below by impermeable boundaries. Twenty nodes (equal log spacing) are used in the radial direction resulting in an outer radius (constant head

boundary) of 37364 m. Other model parameters are as follows:

    S_s = specific storage = 1.0×10^{-5} m^{-1};

    H_0 = initial head in well = 1.0 m;

    r_w = well radius = 0.4 m.

Vertical Averaging in Fully Penetrating Slug Tests

One issue of considerable interest to hydrogeologists is the way in which aquifer properties are averaged in various types of hydraulic tests in heterogeneous systems (e.g., Butler and Liu, 1991; Desbarats, 1992). In the initial phase of this work, the manner in which vertical variations in hydraulic conductivity are averaged in a slug test performed over the entire screened interval in a fully penetrating well (fully penetrating slug test) was explored. Figure II.B.1 displays the results of several simulations of slug tests in aquifers with the same thickness-weighted average of layer conductivities, but with different patterns of conductivity variations. Results are shown for the analytical solution of Cooper, Bredehoeft, and Papadopulos (CBP) (Cooper et al., 1967) for a slug test in a uniform, isotropic aquifer with K_r = 4.6, and for four numerical simulations. The numerical simulations include a uniform, anisotropic aquifer case with K_r=4.6, K_z=0.46, and three other simulations of layered aquifers with alternating bands of the properties K_{low} and K_{high} (anisotropic case of table on previous page). The layering schemes are shown in Figure II.B.2. All three layering schemes have a thickness weighted average K_r of 4.6 (15 units of K_r=1.0 and 10 units of K_r=10.0) and a thickness weighted average K_z of 0.46 (15 units of K_z=0.1 and 10 units of K_z=1.0).

As shown in Figure II.B.1A, the numerically simulated heads at the slugged well are essentially identical in the uniform and all three layered cases. All four plots of the numerically simulated heads fall just slightly below the heads computed from the analytical solution as a result of the discretization error discussed in the previous section. Clearly, slug tests over the entire screened interval in fully penetrating wells can provide little information about vertical variations in conductivity when the slugged well is the measurement location. In all cases, the computed conductivity will be a thickness-weighted average of the horizontal conductivities of the individual layers. Figure II.B.1B shows the responses at an observation well in the same set of slug-test simulations. The observation well is screened opposite vertical node 13 (the middle of the aquifer) at a radial distance of 3.7 meters from the center of the slugged well. Note than even though the observation well occurs in a low-conductivity zone in all three layering schemes, the observation-well responses are different in all three cases. Thus, the response at partially penetrating observation wells is a function of the particular layering scheme in the tested

unit. This result clearly demonstrates the potential of observation wells to provide information about conductivity variations using fully penetrating slug tests. In a later section of this report (II.E), the general issue of the use of observation wells in slug tests is explored in more detail.

Although fully penetrating slug tests can provide some information about vertical variations in conductivity when observation wells are employed, the need for observation wells somewhat limits the applicability of the technique. Another approach for gaining information about vertical variations in flow properties is the multilevel slug test (e.g., Dagan, 1978; Braester and Thunvik, 1984; Hayashi et al., 1987; Melville et al., 1991), in which a series of slug tests are performed at different levels in the screened interval in a single well while using packers to isolate the test zone. An extensive series of numerical simulations was performed in this work in order to assess the potential of multilevel slug tests for providing information about vertical variations in hydraulic conductivity.

Multilevel Slug Tests

The simulations of multilevel slug tests performed here all employ a well fully screened in the aquifer with the slug tests being carried out in a limited interval that is isolated by packers above and below the test zone (straddle packer arrangement). A separate packer above the screened section prevents movement of water from the cased region of the well into screened intervals other than the test zone. Note that this configuration is the same as that used in the KGS multilevel slug test system employed in the field testing discussed in a later section (III.A). The nodes representing the slugged interval are assigned an initial head of 1.0, while the remaining nodes in the model (including those in the screened section of the well outside the straddle packer) are assigned an initial head of 0. The slugged interval is assigned a specific storage equal to the inverse of its length, so that the storage coefficient for the slugged interval equals 1.0. The open sections of the wellbore outside the straddle packer are assigned a value for specific storage that corresponds to the compressibility of water. A number of experimental simulations revealed that the simulated slug-test results are fairly insensitive to the length of the individual packers in the straddle packer, a finding similar to that of Braester and Thunvik (1984) in their examination of constant-head packer tests. The following results were therefore obtained using packers both above and below the slugged interval that are two meters in length.

An initial series of simulations was performed in order to assess the dependence of slug-test results on the length of the slugged interval and on proximity to the upper

II.B.3

and lower impermeable boundaries. For this initial set of simulations, the results were analyzed using the CBP analytical solution incorporated in an automated well-test analysis package (Bohling and McElwee, 1992) that utilizes a nonlinear least squares fitting scheme. Figure II.B.3 presents the results of a series of simulations investigating the effects of the length of the test interval on slug tests in the uniform aquifers described earlier (Figure II.B.3A) and in the layered aquifers represented by the middle case of Figure II.B.2 (Figure II.B.3B). In these simulations, the slugged interval is centered on vertical node 13 and the length of the interval is gradually increased symmetrically about that node. Results are presented in terms of the vertical position of the top node of the slugged interval. Note that the conductivity values determined using the automated analysis package can only be considered apparent conductivities, since the true flow field contains a significant vertical flow component, while the CBP analytical solution assumes strictly horizontal flow. Results in Figure II.B.3 are presented in terms of a ratio of apparent K_r to true K_r, so that uniform and layered cases may be readily compared. In this investigation, the true K_r is taken to be the thickness-weighted average of the model K_r values over the length of the slugged interval.

Figure II.B.3 clearly demonstrates that the analysis of multilevel slug tests under the assumption of negligible vertical flow can result in a significant overestimation of the horizontal hydraulic conductivity. The vertical component of flow allows the effect of the pressure disturbance at the slugged well to be dissipated more rapidly than it would be under purely horizontal flow conditions. Figure II.B.3 also demonstrates that the apparent K_r approaches the thickness-weighted average of the true K_r values as the length of the slugged interval approaches the thickness of the aquifer. However, there is a slight discrepancy between the true and apparent values even for the fully penetrating case. Additional simulations have shown that this difference is due to the discretization error resulting from the fairly coarse discretization scheme employed in the radial direction. Note that the overestimation of K_r is worse under isotropic conditions than under anisotropic conditions as a result of the flow being increasingly constrained to the horizontal plane as the ratio of vertical to hydraulic conductivity decreases.

Figure II.B.4 presents the results of simulations designed to examine the effects of impermeable boundaries on slug-test results. A series of simulations was performed in the uniform aquifer configurations described earlier using a three-node slugged interval (Figure II.B.4A) and a one-node slugged interval (Figure II.B.4B), with the center node of the slugged interval being progressively moved from node 2 (in the three-node slugged interval case) or node 1 (in the one-node interval case) to node 13. The difference in magnitude in apparent K_r between the two plots is a result of the increased importance

of vertical flow in the shorter slugged interval. In both cases, the boundary effects are fairly similar. As the slugged interval approaches the boundary, the vertical flow out of the slugged interval is constrained, resulting in a smaller overestimation of K_r.

Figure II.B.5 presents the results from a series of simulations similar to those shown in Figure II.B.4 performed in layered aquifers. Note that, as shown earlier, a greater overestimation of K_r occurs in the isotropic case than in the anisotropic case. Although use of a one-node slugged interval results in a greater overestimation of K_r, it does allow for clearer definition of the boundaries between layers of contrasting conductivity.

Up to this point, the simulated slug-test data have been analyzed using the CBP model, which is clearly an overly simplified representation of the flow system. Two issues of some importance are 1) will the nature of the fit of the CBP model to the data indicate that an inappropriate model is being employed, and 2) will different divergences from the model assumptions produce different types of model misfits. Figure II.B.6 presents the observed and CBP best-fit head values for four of the simulations included in Figure II.B.5. Figure II.B.6A shows the results for a three-node slugged interval centered at vertical nodes 7 and 12 in the layered, anisotropic aquifer, while Figure II.B.6B shows the results for a one-node slugged interval at the same nodes. The CBP model heads consistently fall below the observed heads early in the test and above the observed heads later in the test. This systematic lack of fit is the result of neglecting the vertical component of flow. Unfortunately, a very similar lack of fit results from the presence of a positive well skin (low conductivity zone surrounding the well) in a homogeneous aquifer (McElwee et al., 1990). Thus, skin effects and the effects of partial penetration may be difficult to discriminate in practice.

Given that analyses of slug-test responses using the CBP model do provide at least a gross picture of vertical variations in conductivity, it is reasonable to assume that analyzing the slug-test data with a more appropriate model, i.e. one that accounts for the partial penetration effects seen with multilevel slug tests, would reduce or remove the problem of overestimation of K_r due to neglect of the vertical component of flow. Two other models were considered here for use in the analysis of multilevel slug-test data. McElwee et al. (1990) have developed an analytical solution for slug tests in partially penetrating wells with well skins, which can be readily configured to analyze data from multilevel slug tests in homogeneous, anisotropic aquifers. Unfortunately, this solution, which is based on the application of both Fourier and Laplace transforms, is so computationally intensive that it cannot presently be used for the analysis of large amounts of field data. Ongoing work is directed at improving the computational

efficiency of this model.

Hvorslev (1951) developed a model for the analysis of slug tests performed in a screened interval of finite length in a uniform, vertically unbounded, medium with a vertical to horizontal anisotropy in hydraulic conductivity. A major assumption of the Hvorslev approach is that the specific storage of the aquifer can be ignored. McElwee et al. (1989), in a theoretical analysis of slug tests in confined aquifers, have shown that the head response at the slugged well is relatively insensitive to the specific storage of the unit, indicating that the assumption of Hvorslev may be acceptable for some cases. Figure II.B.7 shows the results of Hvorslev analyses of the same simulated multilevel slug tests employed in Figure II.B.5. Note that the Hvorslev model requires the use of a "shape factor", which is related to the geometry of the well intake region. The shape factor used here is that for Case 8 described in Hvorslev (1951). The Hvorslev function for this case is in the form of a two-parameter (K_r and anisotropy ratio) model. Unfortunately, the two parameters are perfectly correlated, so they cannot be estimated independently (Bohling et al., 1990). For the analyses presented in Figure II.B.7, three different values of anisotropy ratio are employed. The true value of the ratio of horizontal to vertical conductivity is 10. As shown in Figure II.B.7, the resulting overestimation or underestimation of K_r is not strongly influenced by the improper specification of the anisotropy ratio. The correlation between the two parameters is also apparent, since the estimated hydraulic conductivity changes by a multiplicative constant for all analyses as a result of using a different value for the anisotropy ratio.

Figure II.B.8 displays the Hvorslev model fits for the same intervals as shown in Figure II.B.6 for the CBP analyses. The plots are for the case in which the true anisotropy ratio is used. The fitted results, however, would be essentially identical for all values of anisotropy ratio, due to the perfect correlation between the model parameters. Specifying a different anisotropy ratio would result in the same optimal fit (measured in terms of the sum of squared head deviations) for a different value of K_r. Comparing Figures II.B.7 and II.B.8 to Figures II.B.5 and II.B.6 reveals that, in this case, use of the Hvorslev model improves the estimates of K_r and provides a better fit to the observed data. The improved fit is attributed to the fact that the Hvorslev model accounts for the vertical flow component, while the CBP model does not. The Hvorslev model, however, must be used with caution due to its neglect of storage effects on slug-test responses (Chirlin, 1989) and its poor performance in the presence of a well skin (McElwee et al., 1990). Note that the Hvorslev analyses were not performed in the conventional fashion in this work. The optimal conductivity was determined here using a nonlinear regression algorithm to minimize the sum of the squared differences between

the actual observed heads and the model-predicted heads. A conventional Hvorslev analysis is performed by minimizing the sum squared deviation between log-transformed head values, using that portion of the data that appear to fall on a straight line on a log-head versus arithmetic-time plot. The conclusions of this work, however, are not dependent on the fitting criterion. Given the closeness of the Hvorslev calculated parameters to the actual model values, the Hvorslev model was used for the analysis of simulated slug-test data for the remainder of this work.

Dependence of Multilevel Slug Test Results on Layer Thickness and Skin Permeability

The simulations described above showed that multilevel slug tests will indicate the existence of layers of differing conductivity to some degree and that the Hvorslev model is the most appropriate model at present for the analysis of the test data. Further work, however, is needed to explore the dependence of multilevel slug-test results on layer thickness and to assess how a well skin will influence test results. A series of simulations designed to address these issues is described here.

For this series of simulations, the configuration consisted of an aquifer made up of layers of two distinct materials (denoted here as A and B). The model parameters are as follows:

$$S_{SA} = S_{SB} = 1 \times 10^{-5} \text{ m}^{-1};$$
$$H_0 = 1.0 \text{ m};$$
$$r_w = 0.05 \text{ m};$$
$$K_A = 2 \times 10^{-5} \text{ m/sec};$$
$$K_B = 2 \times 10^{-4} \text{ m/sec}.$$

In this case, a model grid of 20 nodes in the radial and 40 nodes in the vertical directions was employed. Equality of heads in the angular direction was assumed, so no additional nodes in the angular direction were required.

The initial scenario examined in this series of simulations (see Table II.B.1 for details of all scenarios examined in these simulations) consisted of an isotropic aquifer of material A in the center of which is located a single isotropic layer of material B. The purpose of this first set of simulations was to examine how layer thickness impacts the conductivity calculated from a slug test. Seven different thicknesses were used for the B layer, which, in all cases, was symmetrically located about the center of the aquifer (total thickness of 50 meters in all cases). Note that a test interval of four meters was assumed.

Figure II.B.9 displays plots of conductivity versus depth to the top of the test

interval for each of the different thicknesses of layer B. An important point to note is that even when the test interval lies completely within layer B (layer thicknesses 4, 6, and 10), the calculated conductivity will underestimate the layer conductivity as a result of the influence of the lower conductivity material adjoining layer B. Only in very thick layers (i.e. layer thicknesses of 20 and 30) is the influence of adjacent material negligible. Note that conductivities calculated for intervals in which layer B was thinner than the slugged interval (layer thicknesses 1 and 2) underestimated layer conductivity as a result of the vertical averaging discussed previously.

The results depicted in Figure II.B.9 were determined for the ideal case in which formation layering extends to the well screen. Often, however, well drilling and development creates a near-well zone (well skin) of properties differing from those of the portion of the formation in which the well is screened. If the well skin is less permeable than the formation, the vertical flow out of the test interval will be suppressed as shown by McElwee et al. (1990). In addition, the calculated conductivity will be a function of both skin conductivity and formation conductivity. As discussed by McElwee et al. (1990), this function is heavily weighted towards the skin conductivity when a low conductivity skin exists and the Hvorslev model is used for the data analysis. Thus, a low conductivity skin will cause the magnitude of the vertical variations in conductivity to be underestimated. If the skin conductivity is significantly less than that of the formation, little to no variation in conductivity will be seen in the vertical.

A well skin may be of higher permeability than the formation as a result of voids forming along the well screen during well emplacement or of well development activities. A high conductivity skin can serve as a conduit for additional vertical flow. A second set of simulations was run using a configuration similar to that used in Figure II.B.9 except that a well skin of .11 m in radius with a conductivity of 5×10^{-4} m/sec was added to the system. The skin was assumed isotropic and to have the same specific storage as the formation as a whole. Figure II.B.10 displays the results of this series of simulations for five of the seven layering schemes examined in Figure II.B.9. Note that in all cases the existence of a high conductivity skin causes the calculated conductivities to increase as a result of the increased vertical flow. The increase is greatest for the thicker layers since the vertical flow moving along the well skin will be in contact with the higher conductivity layer for a longer time. Thus, the spread between the conductivities calculated for the different layers increases with the addition of a high permeability well skin. An additional set of simulations was performed to examine the effect of increasing skin conductivity an order of magnitude to 5×10^{-3} m/sec. Although not shown here, the results of these simulations indicate that the calculated conductivities continue to increase

in a manner similar to the pattern shown in Figure II.B.10. In none of the simulations of this series was the magnitude of the vertical variations in conductivity greatly decreased by the existence of a high conductivity skin.

Two additional series of simulations were performed in configurations similar to that employed in Figure II.B.9 in order to examine the effects of formation anisotropy and a lower specific storage. The addition of anisotropy into the configuration produced results similar to those described previously, i.e. vertical flow was suppressed causing a decrease in the calculated conductivity. In addition, the suppression of vertical flow caused the influence of adjoining lower conductivity layers to be diminished, resulting in the layer B conductivities calculated for the different layering configurations to be more similar. A lower specific storage, on the other hand, resulted in the pressure disturbance induced by the slug test to spread out more rapidly in all directions, thus causing the influence of adjoining lower conductivity layers to be increased. This increased influence of adjoining lower conductivity layers produced considerably lower values for the calculated conductivity. Thus, the specific storage can have a considerable influence on the calculated conductivity in layered systems. This is in contrast to the work of McElwee et al. (1989) for slug tests in homogeneous systems, which showed that specific storage had relatively little influence on head responses at the slugged well.

An important objective of this theoretical analysis was to assess under what conditions vertical variations in conductivity will be suppressed or completely hidden during multilevel slug tests. As discussed earlier, the existence of a low conductivity skin can cause the effect of layering to be suppressed. Additional simulations were performed here to assess other conditions under which vertical variations may be suppressed.

It was shown previously that fully penetrating slug tests in a layered aquifer will yield a conductivity that is a thickness-weighted average of the layer conductivities. No indication of layering will be evident from the head response at the slugged well. An obvious question of importance for multilevel slug tests is how much will layering be suppressed when the screen length is larger than the average layer thickness. Figure II.B.11 displays the results of a series of simulations of slug tests in a layered aquifer consisting of alternating layers of A and B. Each layer is 2.5 m. in thickness. The screen length used in the simulation is 5.0 m. As shown in Figure II.B.11, the vertical variations in conductivity are strongly suppressed in this case. The difference between the calculated layer conductivities is 11% of the actual difference. Additional simulations indicated that vertical variations are less strongly suppressed as the screen decreases in length. This is due to the greater influence of vertical flow at either end of the well

screen as the well screen decreases in length. McElwee et al. (1990) describe how a decrease in aspect ratio (screen length/r_w) promotes the partial penetration effect, i.e. vertical flow out either end of the well screen. Those authors show that for the well radius used in this simulation, partial penetration effects should be rather small for screens greater than about 5 meters in length, a result that is in agreement with Figure II.B.11. Even when partial penetration effects are greater, however, relatively little information about vertical variations in conductivity can be gained when the screen length is several times larger than layer thickness. Thus, if one is interested in characterizing the detailed nature of the conductivity variations in a formation with multilevel slug tests, the screen length must be on the order of the layer thickness or less.

Even when the screen length is on the order of the layer thickness or less, there is still the possibility that other effects could serve to dampen the variations observed through multilevel slug tests. A very extensive set of simulations was performed to assess whether layer thickness and/or a high conductivity skin would serve to dampen the conductivity variations. Results from a small subset of these simulations are described here (see Table II.B.2 for a summary of results from all of the simulations).

Figure II.B.12 displays results for a series of multilevel slug tests performed using a 2.5 m. screen in a layered aquifer consisting of alternating layers (each 2.5 m. in thickness) of A and B. Note that the calculated conductivity for layer B is less than the actual conductivity due to the suppression of vertical flow by the adjoining layers of material A in a manner similar to that seen in Figure II.B.9. This results in the conductivity variations being somewhat dampened (difference between the calculated layer conductivities is 85% of the actual conductivity difference). Figure II.B.13 displays analogous results for the case of layers of .15 m. in thickness and a screen of .15 m. in length. In this case, the effect of the adjoining lower conductivity layers is even greater (calculated conductivity difference is 42% of actual) as a result of the greater proportion of vertical flow that occurs as the aspect ratio decreases. Note that although the addition of anisotropy ($K_r > K_z$) to this configuration does serve to decrease the amount of vertical flow, further simulation results show that calculated conductivity variations change by only a small amount.

Although the simulation results displayed in Figure II.B.10 do not indicate that vertical variations in conductivity are dampened by the existence of a high conductivity skin, a further series of simulations was performed to assess the role of a high permeability skin in the configurations employed in Figures II.B.12 and II.B.13. Figure II.B.14 displays the results of simulations in which a high conductivity skin ($K = 1 \times 10^3$ m/sec) of .11 m. in radius is added to the configuration employed in Figure II.B.12. As

in Figure II.B.10, the addition of a highly conductive skin causes an increase in the calculated conductivities. In this case, the difference between the conductivities calculated for the two layers is somewhat larger than the actual difference (calculated difference is 116% of actual difference). As layer thickness decreases, the effect of a high conductivity skin changes. Figure II.B.15 displays the results of simulations in which the same high conductivity skin is added to the configuration employed in Figure II.B.13. In this case, the layers are thin enough that when the screen is opposite a layer of material A, vertical flow occurs along the well skin and into the layers of material B. This results in a great increase in the conductivity calculated for layers of material A and a dramatic decrease in the calculated difference between layer conductivities (calculated difference is 18% of actual difference). Thus, a highly conductive skin in an aquifer consisting of thin layers can cause multilevel slug tests to be of rather limited effectiveness in describing the vertical variations in hydraulic conductivity.

As stated earlier, the Hvorslev model was employed to calculate K_r values from simulated slug-test data. One final issue to be addressed is that of the quality of the fits of the Hvorslev model to the simulated data. Figure II.B.16 displays a typical plot from the last series of simulations reported on here. As shown in the figure, the Hvorslev model provides a relatively good fit to the simulated data. This was characteristic of all the cases examined here.

The results discussed in this section are taken from a subset of all the simulations performed for this project. Table II.B.1 summarize all the scenarios examined here. Butler et al. (in preparation) provide a detailed discussion of the results for all cases.

Summary

The results of this modeling investigation of the viability of slug tests for the purpose of describing vertical variations in hydraulic conductivity can be summarized as follows:

1) Slug tests performed in a screened interval that passes through the entire aquifer will yield a thickness weighted average of layer conductivities. The response at the slugged well will show no indication of layering. Observation wells must be employed if fully penetrating slug tests are going to provide any information about vertical variations in hydraulic conductivity;

2) In multilevel slug tests, when the screen length is considerably greater than the layer thickness and the aspect ratio (screen length/r_w) is greater than about 100, a slug test will yield a thickness weighted average of the layers intersecting the screen. As the

aspect ratio decreases, the properties of layers outside of the screened interval will influence the calculated conductivity as a result of the increased vertical flow;

3) Experimental simulations showed that model results are relatively insensitive to the length of the individual packer elements of the straddle packer as long as vertical flow is prevented in the borehole;

4) Analysis of multilevel slug-test data with the CBP model (Cooper et al., 1967) can lead to a considerable overestimation of the radial hydraulic conductivity and also produces a systematic lack of fit between predicted and observed responses;

5) The model of Hvorslev (1951) appears to be the best present approach for analyzing multilevel slug-test data. This approach provides more reasonable estimates and a much better fit than the CBP model;

6) A low conductivity skin will make it difficult to describe vertical variations in hydraulic conductivity because the conductivity calculated from the slug-test data will be heavily weighted by the conductivity of the skin;

7) A high conductivity skin will make it difficult to describe vertical variations in hydraulic conductivity when the screened interval and the layer thickness are both small. In this case, a large amount of vertical flow can occur along the skin, making it difficult to detect the existence of layers of low conductivity;

8) Even when the screened interval is less than the layer thickness, considerable error can be introduced into the description of vertical variations in hydraulic conductivity as a result of the influence of layers adjoining the tested layer. The magnitude of the influence of the adjoining layers will depend on the layer conductivities, the specific storage and anisotropy ratio of the tested layer, skin conductivity, and the aspect ratio.

In summary, multilevel slug tests can provide considerable information about vertical variations in hydraulic conductivity under the right conditions. However, well skins and screens of small aspect ratios can dramatically decrease the effectiveness of the approach.

Note that the discussions of this section were based on a series of simulations performed in perfectly stratified aquifers, i.e. layering is continuous throughout the entire model domain. Many aquifers, however, consist of a series of discontinuous layers. Further work is required to assess the effect of layer discontinuity on the results described here.
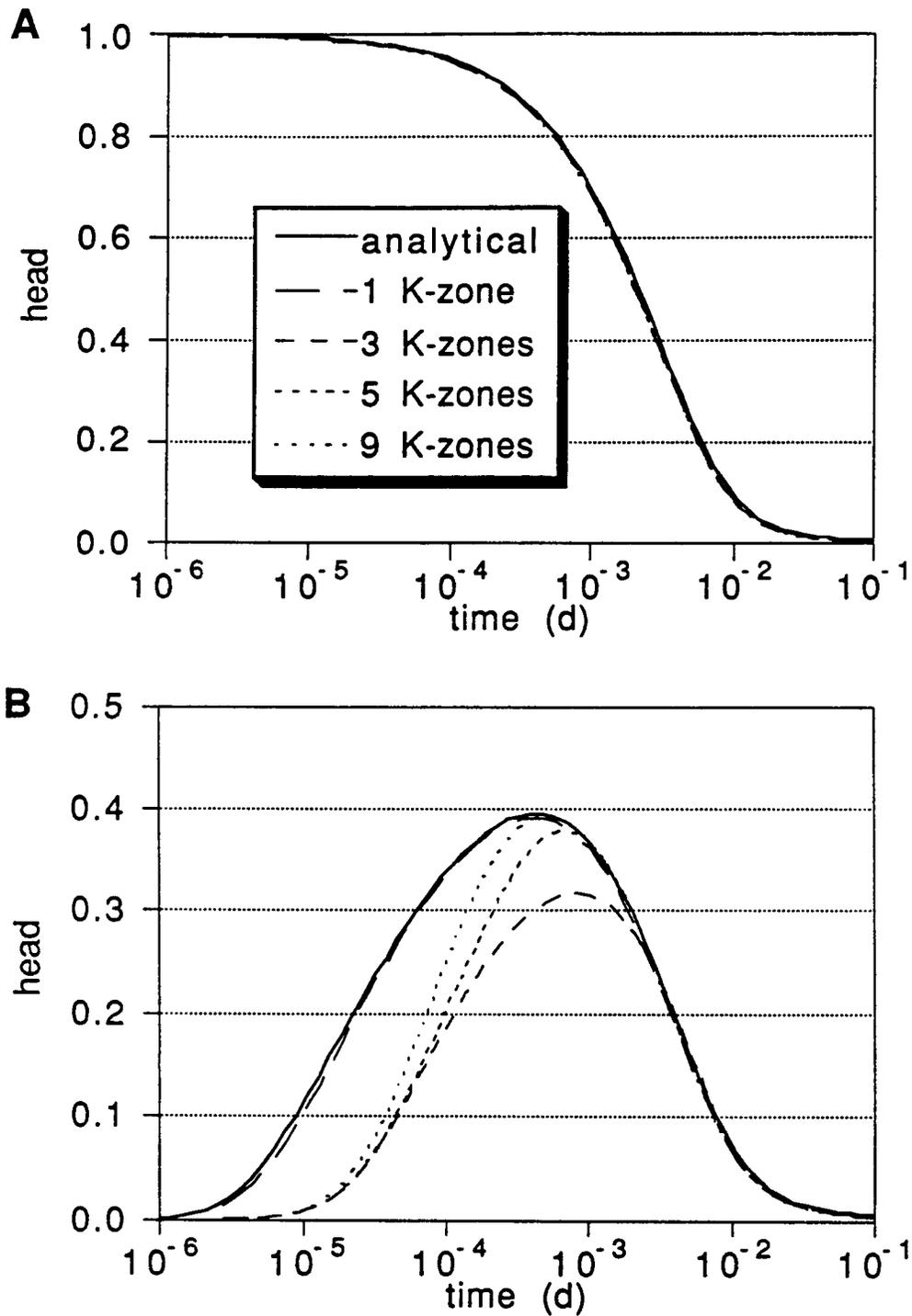
Figure II.B.1: Effects of variable layering on fully-penetrating slug test results at (A) the slugged well and (B) an observation well located at vertical node 13 and 3.7 meters radial distance from the slugged well. Layering schemes are shown in Figure II.B.2.
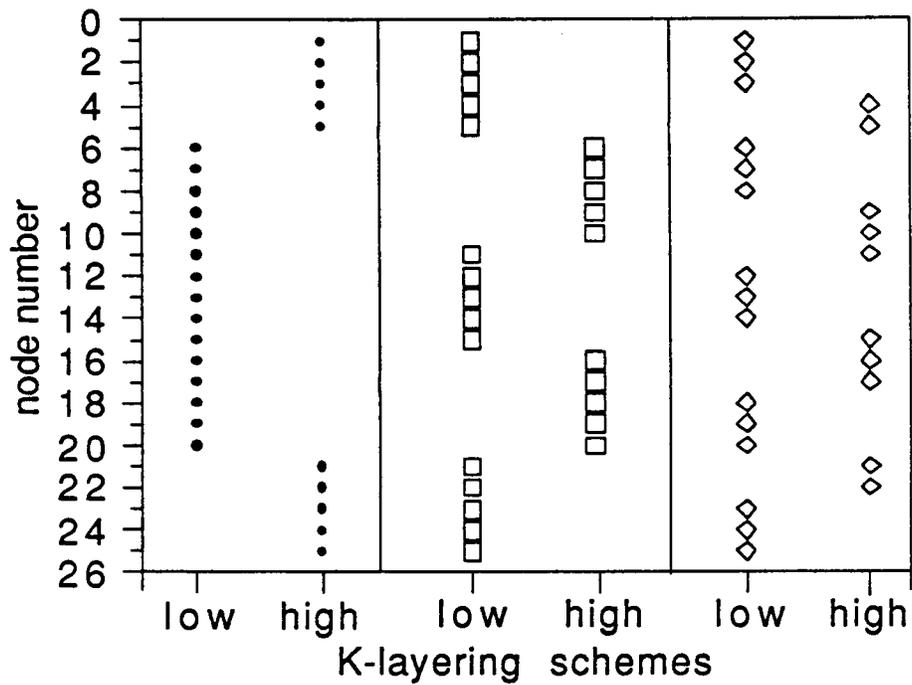
Figure II.B.2: Layering schemes employed for results shown in Figure II.B.1. Low and high hydraulic conductivities are those for the layered, anisotropic aquifer.
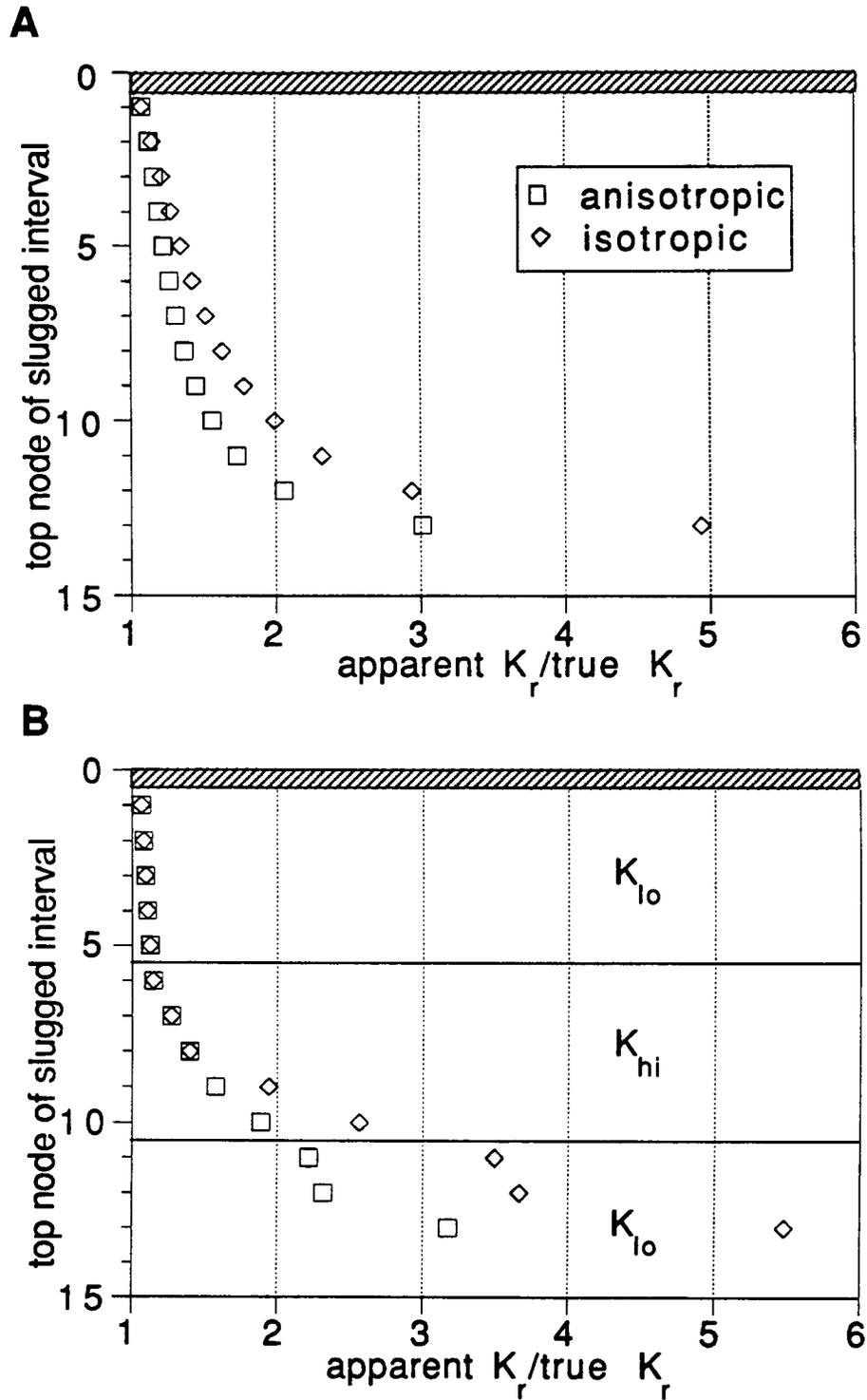
Figure II.B.3: Effects of slugged interval length in the uniform (A) and the layered (B) aquifers. Slugged interval is centered at vertical node 13 and its length increases symmetrically up to the full thickness of the aquifer (25 nodes). Note that the K-configurations are also symmetric about node 13.
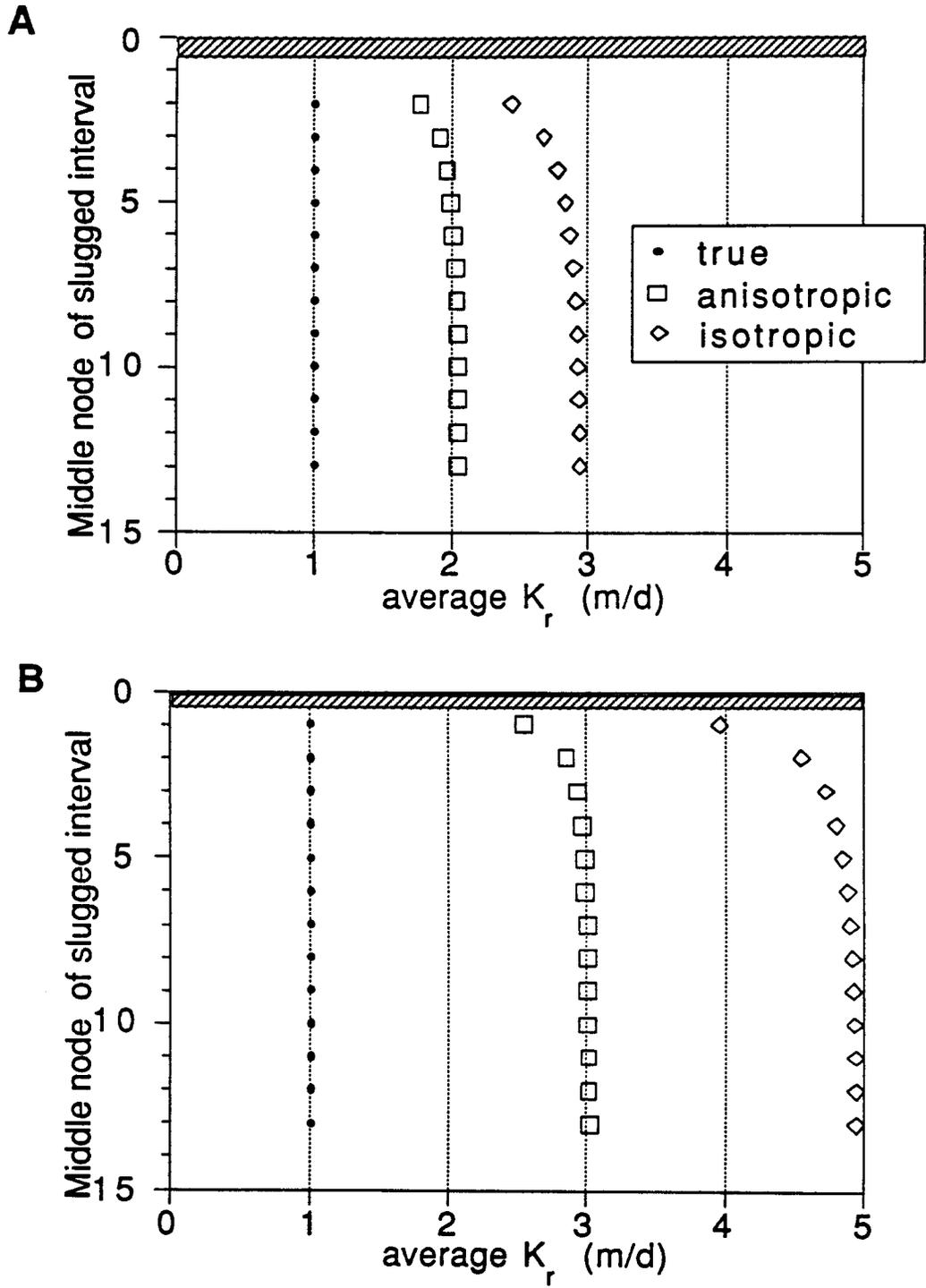
Figure II.B.4: Boundary effects in the uniform aquifers using (A) a three-node slugged interval and (B) a one-node slugged interval.
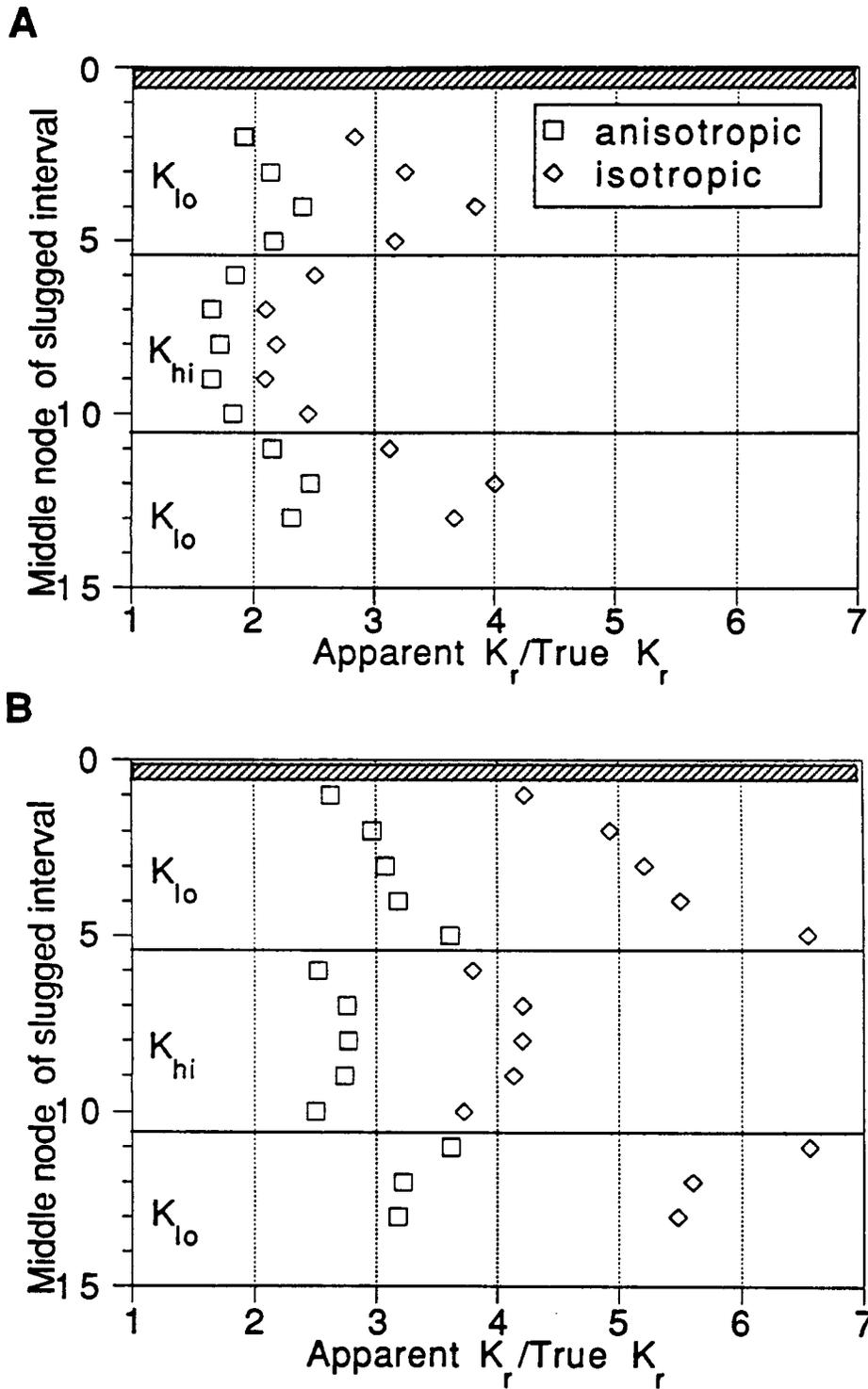
Figure II.B.5: Results of CBP analyses of multilevel slug test results using (A) a three-node slugged interval and (B) a one-node slugged interval in the layered aquifers.
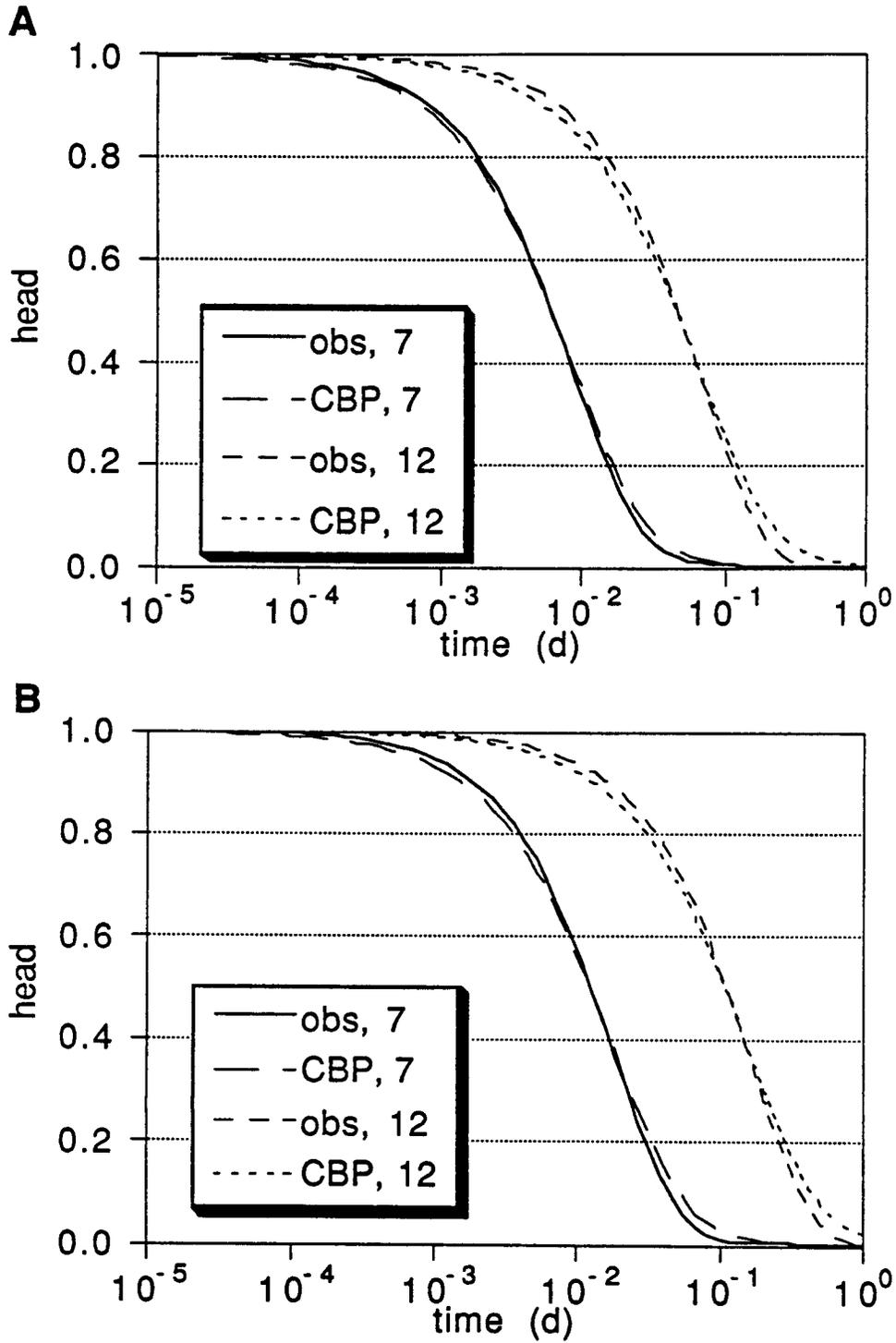
Figure II.B.6: Observed (obs) and CBP best-fit heads at vertical nodes 7 and 12 of layered, anisotropic aquifer using (A) a three-node slugged interval and (B) a one-node slugged interval.
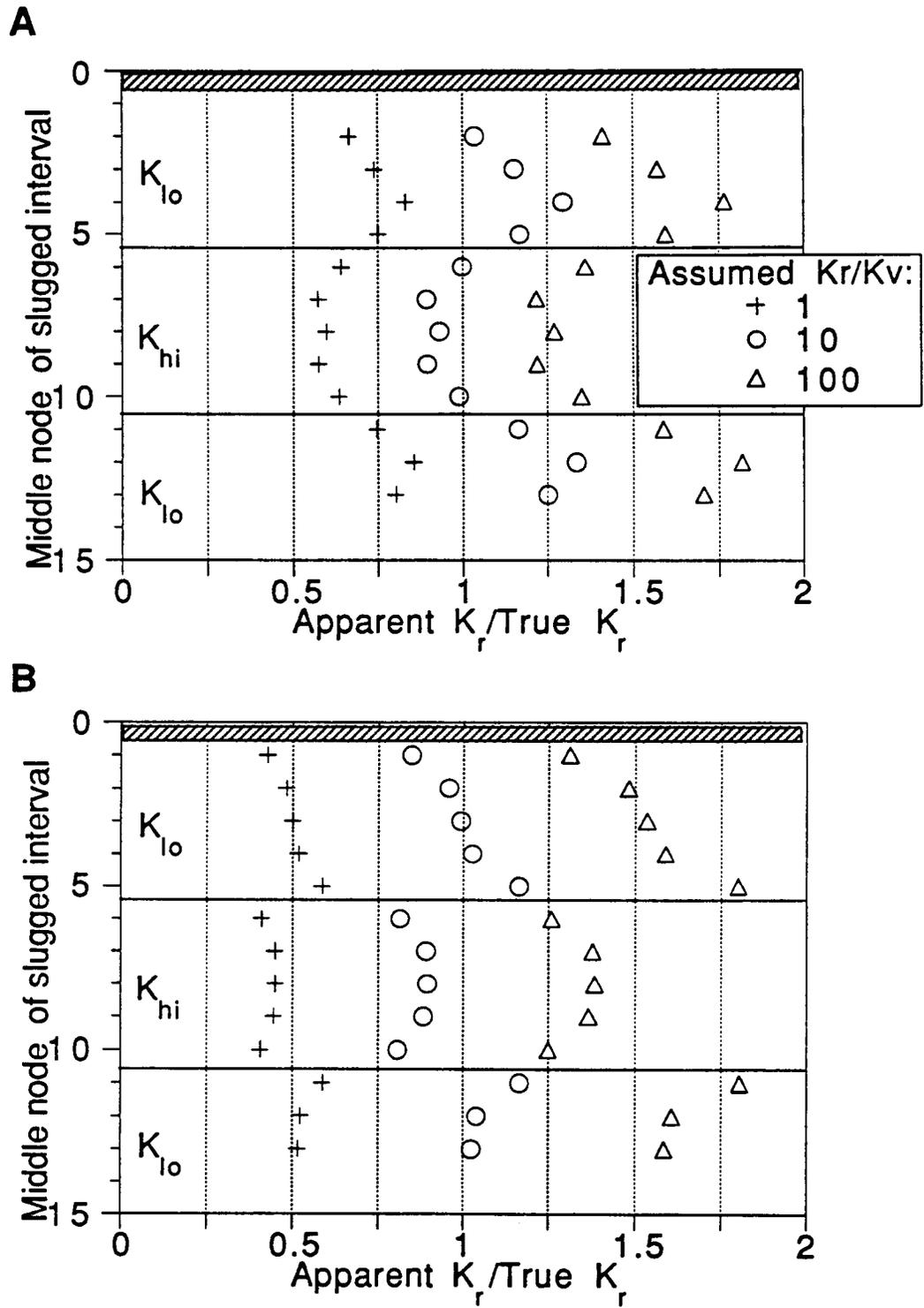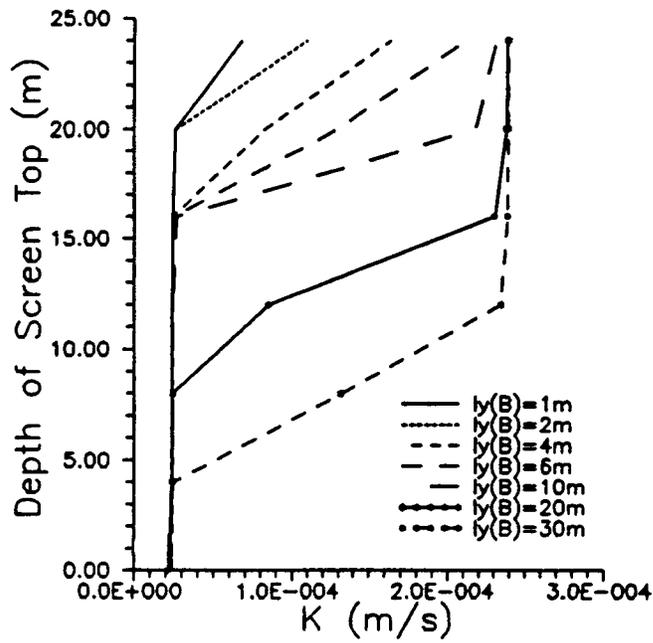
Figure II.B.7: Results of Hvorslev analyses of multilevel slug tests using (A) a three-node slugged interval and (B) a one-node slugged interval in the layered aquifers.
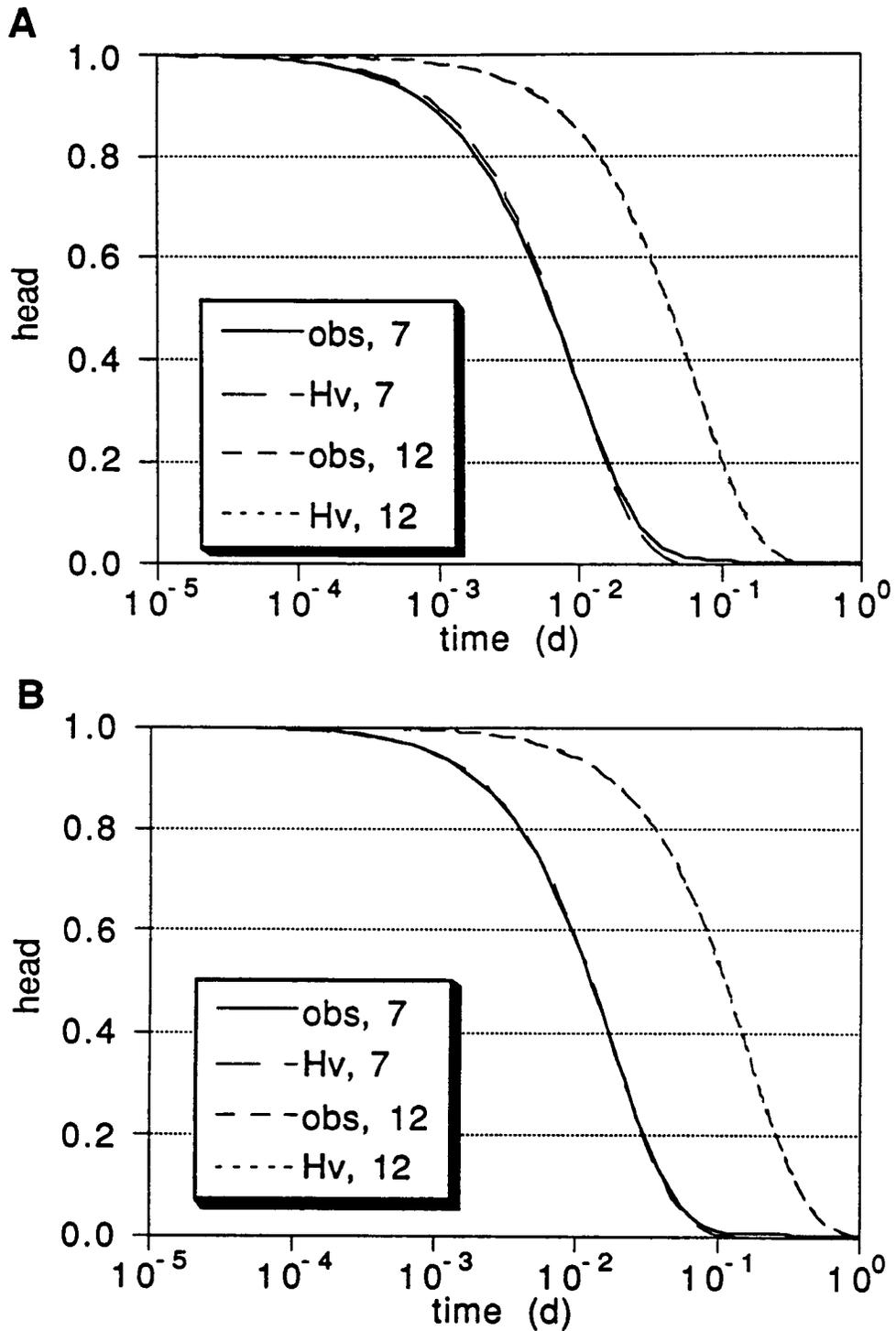
Figure II.B.8: Observed (obs) and Hvorslev (Hv) best-fit heads at vertical nodes 7 and 12 of layered, anisotropic aquifer using (A) a three-node slugged interval and (B) a one-node slugged interval.

Figure II.B.9. Conductivity versus depth plot for Scenario 1 of Table II.B.1 (ly(B) = thickness of layer B)
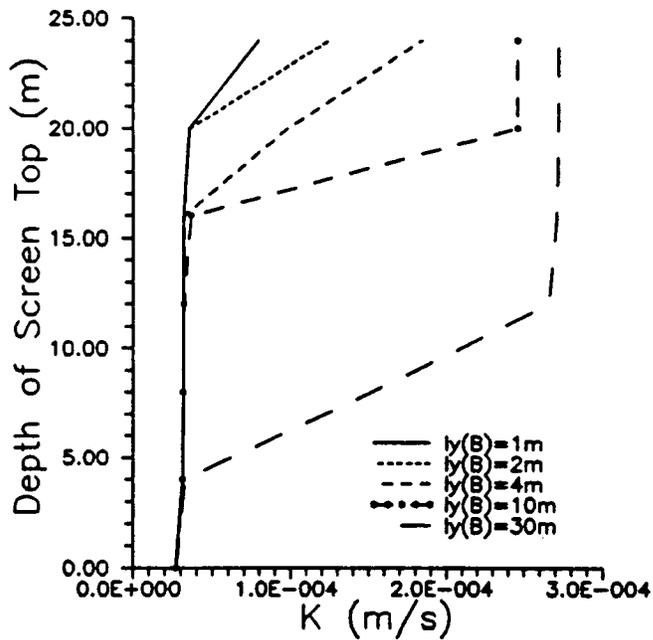
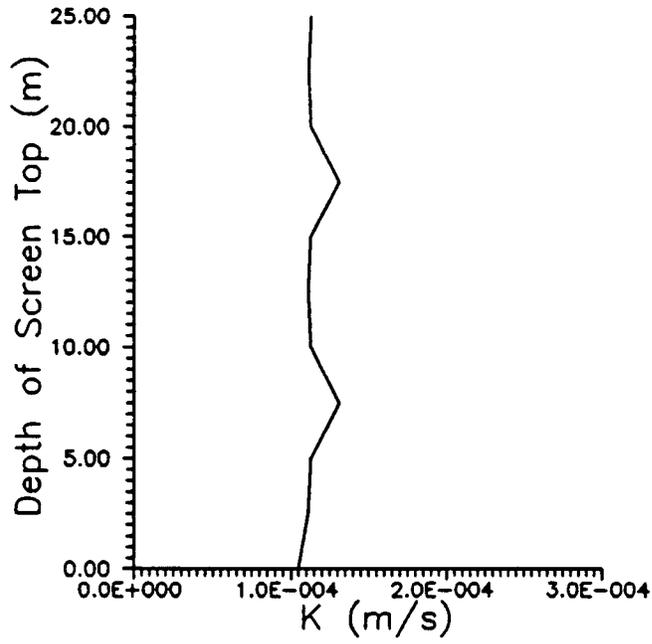Figure II.B.10. Conductivity versus depth plot for Scenario 1A of Table II.B.1 (ly(B) = thickness of layer B)

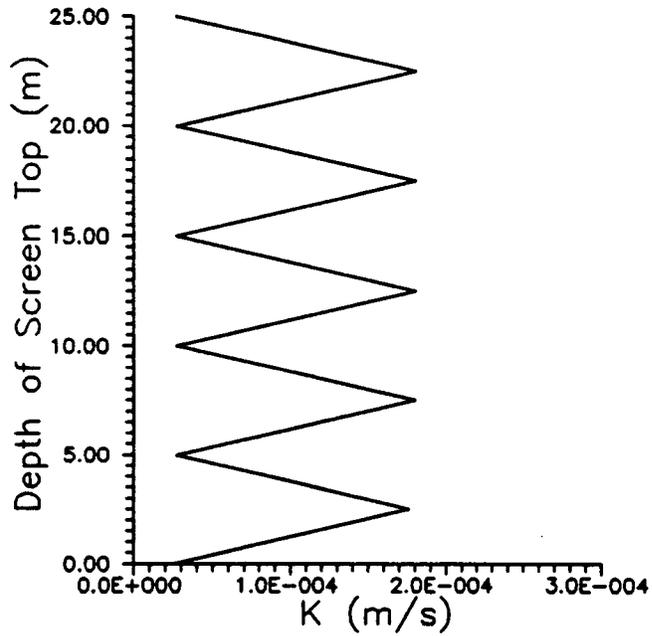Figure II.B.11. Conductivity versus depth plot for Scenario 2 of Table II.B.1

Figure II.B.12 - Conductivity versus depth plot for Scenario 3 of Table II.B.1
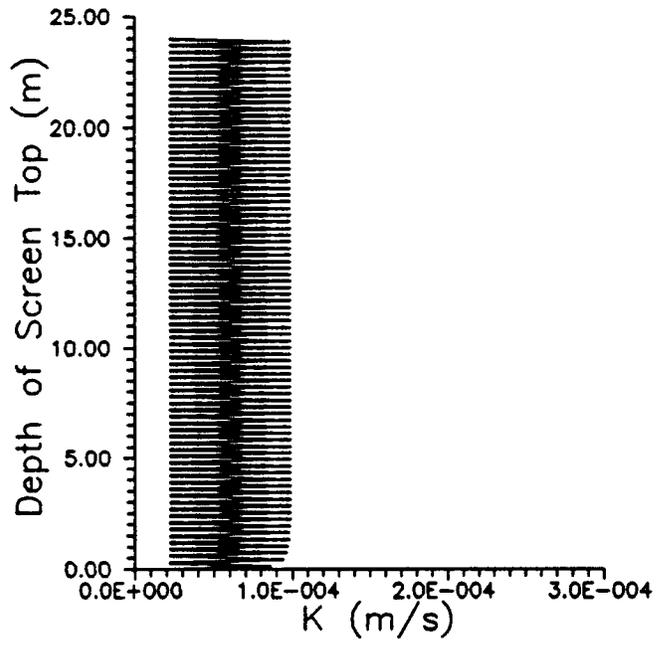
Figure II.B.13 - Conductivity versus depth plot for Scenario 7 of Table II.B.1
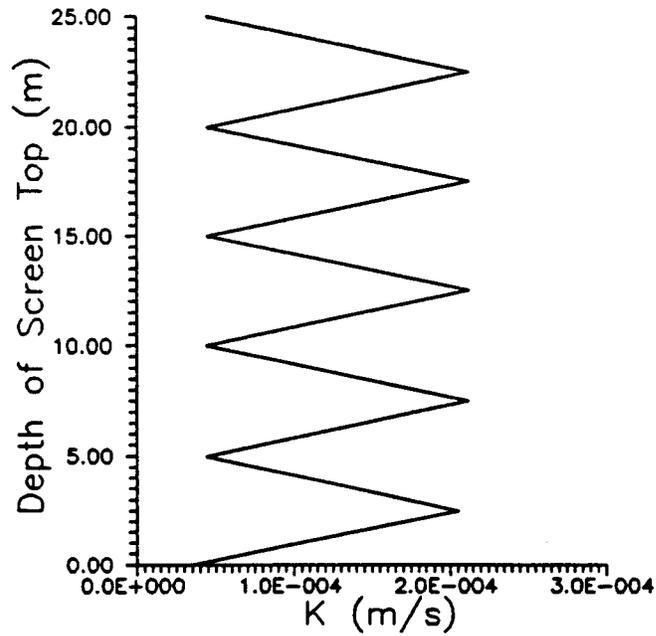

Figure II.B.14 - Conductivity versus depth plot for Scenario 3A of Table II.B.1
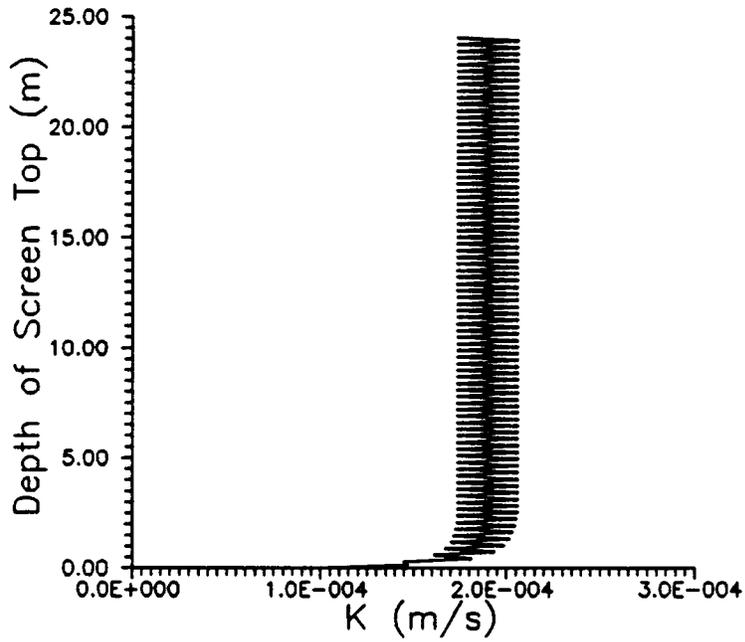
Figure II.B.15 - Conductivity versus depth plot for Scenario 7A of Table II.B.1
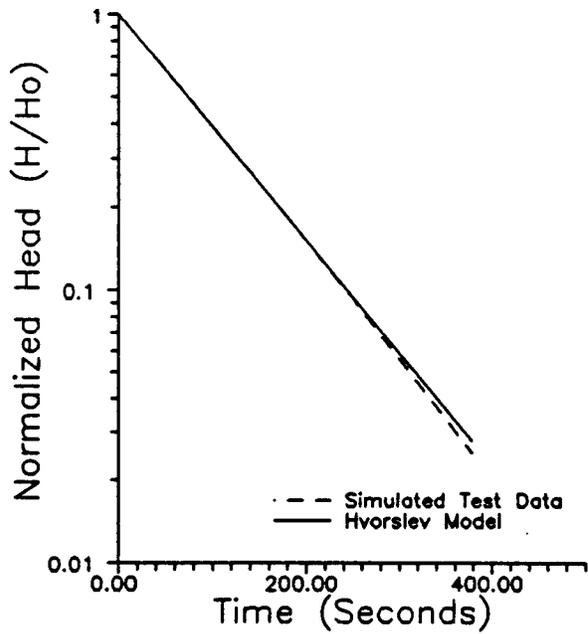

Figure II.B.16 - Plot showing the results of the Hvorslev analysis applied to simulated test data from Scenario 7A

II.B.24

Scenario	K_S (10^{-3}m/s)	K_H/K_V	r_s (m)	l_s (m)	l_y (m)	Note
1	-	1	-	4	1*	1*
1A	0.5	1	0.11	4	1A*	1A*
1B	5	1	0.11	4	1B*	1B*
1C	-	1	-	4	1C*	1C*
2	-	1	-	5	2.5	2*
2A	-	1	-	0.6	0.30	2*
3	-	1	-	2.5	2.5	2*
3A	1	1	0.11	2.5	2.5	2*
3B	-	2	-	2.5	2.5	2*
4	-	1	-	1.25	2.5	2*
4A	1	1	0.11	1.25	2.5	2*
4B	-	2	-	1.25	2.5	2*
4C	1	1	0.11	1.25	2.5	2*
4D	-	1	-	1.25	2.5	2*,3*
5	-	1	-	1.25	1.25	2*
5A	1	1	0.11	1.25	1.25	2*
6	-	1	-	0.3	0.3	2*
6A	1	1	0.11	0.3	0.3	2*
6B	1	1	0.22	0.3	0.3	2*
7	-	1	-	0.15	0.15	2*
7A	1	1	0.11	0.15	0.15	2*
7B	-	2	-	0.15	0.15	2*

Note: Specific storage is 1×10^{-5} m^{-1} if not specified otherwise. $K_A = 2 \times 10^{-5}$ m/s and $K_B = 2 \times 10^{-4}$ m/s for all scenarios. r_s=radius of skin, l_s=length of screen, and l_y=layer thickness.

1*:   Single layers of B located symmetrically about the center of aquifer A. Simulations performed for B layers of 1, 2, 4, 6, 10, 20, and 30 m in thickness.

1A*:   Scenario same as 1 with skin.

1B*:   Scenario same as 1 with higher permeability skin.

1C*:   Scenario same as 1 with lower specific storage (1×10^{-7} m^{-1}).

2*:   Alternating layers of A and B.

3*:   Initial Head is 10 m.

Table II.B.1 - Summary of layered-aquifer slug-test scenarios.

Scenario	Computed difference between layer A and B conductivities (10^{-4} m/s)	% of actual difference (actual difference = 1.8×10^{-4} m/s)
2	0.202	11.22
2A	0.242	13.44
3	1.535	85.28
3A	2.080	115.56
3B	1.475	81.94
4	1.572	87.33
4A	1.770	98.33
4B	1.470	81.67
4C	1.860	103.33
4D	1.572	87.33
5	1.390	77.22
5A	1.510	83.89
6	1.030	57.22
6A	0.750	41.67
6B	0.360	20.00
7	0.760	42.22
7A	0.325	18.06
7B	0.690	38.33

Table II.B.2 - Summary of slug-test simulations in configuration consisting of alternating layers of A and B. Results are given in terms of the difference between the computed conductivities for the two layers.

C. IMPROVEMENTS TO SUPRPUMP

Work on improving the well test analysis program SUPRPUMP continued throughout this grant period. In the March-April 1992 issue of *Ground Water*, a paper on the program (Bohling and McElwee, 1992) was published. Also, the program and user's manual (Bohling et al., 1990) are being published as a Kansas Geological Survey Ground Water Series volume. The development of this program has been an ongoing project for several years.

Over the year several well functions were added to the program, including radially-dependent versions of two important slug test functions, that for a finite radius well fully penetrating a confined aquifer (Cooper et al, 1967) and that for a finite radius well with a finite radius well skin (Moench and Hsieh, 1985). These two functions allow an investigator to analyze well test responses not only in the slugged well, but also in nearby observation wells. This greatly enhances the ability to define the storage coefficient of the aquifer (McElwee et al, 1991). Other functions developed and added to the program included a function describing the response in a finite-radius slugged well with a finite radius well skin partially penetrating a confined aquifer, a version of the Hvorslev function incorporating a more general expression for the shape factor (and thus a wider range of well geometries), and a nonlinear version of the Hvorslev function (see section III.C) accounting for frictional losses across the well screen.

Other ongoing work on the program includes the development of a Microsoft Windows graphical user interface and program revisions which will allow for easier addition of new well functions to the existing library and also enhance program maintainability and portability. The latter modifications include the development of a batch (non-interactive) version of the code. Some of the well functions are quite computationally intensive and several hours of computer time are required to analyze even moderate-sized data sets. Implementation of these functions is not really practical without the ability to submit an analysis job in batch on a multitasking system. Also, it is easier to attach different interactive front-ends to a batch mode program than it is to a program that already includes its own interactive input and output routines. Front-end programs can be written to manage the contents of the input and output files for a batch mode program without having to be concerned with the internal workings of that program.

D. SENSITIVITY ANALYSIS

SUPRPUMP has been built so that sensitivity analysis can be easily performed on all the included well functions for all their respective parameters. The next two sections are specific examples of this kind of analysis. We present a brief overview of the formalism here so that it does not have to be repeated in the following sections.

Normalized Variables

The solutions can be expressed more conveniently for a range of parameters by using normalized variables.

$$h = H \ / \ H_0$$
$$R = r \ / \ r_w \quad \text{or} \quad R = r \ / \ r_s$$
$$\beta = \frac{T}{r_w^2} t \quad \text{or} \quad \beta = \frac{T t}{r_c^2} \tag{II.D.1}$$

where H_0 is the original height of water in the well, H is the height at any time and place, R is the relative radius measured in units of the well radius (r_w) or the screen radius (r_s), and b is the dimensionless time defined using the transmissivity (T) and well or casing radius (r_w or r_c).

Sensitivity Coefficients

We apply first order sensitivity analysis (McElwee, 1987) to the problem. The first order Taylor expansion for the head is (assuming three parameters of interest)

$$H^* \cong H^m + U_{P_1}^m \Delta P_1^m + U_{P_2}^m \Delta P_2^m + U_{P_3}^m \Delta P_3^m \tag{II.D.2}$$

The P's represent parameters such as transmissivity (T), storage (S), initial head (H_0), skin radius (R_s), or any other parameter of interest. H^* is the vector of heads based on true parameters P_1^*, P_2^*, P_3^*, while H^m is the vector of heads based on current estimates P_1^m, P_2^m, P_3^m.

$$U_{P_1}^m = \frac{\partial H^m}{\partial P_1^m}, U_{P_2}^m = \frac{\partial H^m}{\partial P_2^m}, U_{P_3}^m = \frac{\partial H^m}{\partial P_3^m} \tag{II.D.3}$$

are the sensitivities to P_1^m, P_2^m, P_3^m, and $\Delta P_1^m, \Delta P_2^m, \Delta P_3^m$ are unknown perturbations in the parameters.

Normalized Sensitivities to Relative Head

The normalized sensitivity to relative head (u_{P_1}') is defined as follows,

$$U_{P_1}' = P_1 \frac{\partial H}{\partial P_1} = H_0 P_1 \frac{\partial h}{\partial P_1} = H_0 u_{P_1}' \qquad \text{(II.D.4)}$$

$$u_{P_1}' = P_1 \frac{\partial h}{\partial P_1} \qquad \text{(II.D.5)}$$

A similar normalized sensitivity can be defined for all parameters of interest, and they are all functions of space, time and the physical parameters. An examination of this dependence can be very useful.

Parameter Estimation

The objective is to minimize $E = \sum_i \left[H_i^e - H_i \right]^2$, where H_i^e = observed head at index point i and H_i = calculated head at index point i. Assume that $H^e = H^* + \varepsilon$, where ε = an error vector. Thus,

$$H^e - H^m = U_{T_1}^m \Delta T_1^m + U_{T_2}^m \Delta T_2^m + U_{R_s}^m \Delta R_s^m + \varepsilon \qquad \text{(II.D.6)}$$

Now we must solve for new parameter estimates

$$P_1^{m+1} = P_1^m + \Delta P_1^m \quad P_2^{m+1} = P_2^m + \Delta P_2^m \quad P_3^{m+1} = P_3^m + \Delta P_3^m. \qquad \text{(II.D.7)}$$

An iterative process now occurs until the changes in the parameters are minimal; at that point we assume the correct parameters have been found.

Sensitivity Design Matrix

The sensitivity design matrix [A] defined here is a sum over time and space of products for any two sensitivity coefficients.

$$a_{ij} = [A]_{ij} = \sum_{r,t} U_i(r,t)U_j(r,t)$$

(II.D.8)

$$i, \; j = P_1, P_2, P_3$$

If we are fitting three parameters P_1, P_2, and P_3 then the sensitivity design matrix is 3 x 3 (in general it could be any size). The least squares solution for the delta parameter changes can be expressed in terms of the inverse of [A]. In general, the solution is well behaved if the diagonal elements are large and nearly equal and the off-diagonal elements are small. This will be the case if the sensitivity coefficients are large and do not have similar shapes over the measurement times and locations.

Sensitivity Correlation Matrix

One way to measure the similarity of the sensitivity coefficients is to define the sensitivity correlation matrix as shown here; it will have ones on the diagonal and the off-diagonal terms will vary between ± 1.

$$c_{ij} = [C]_{ij} = \frac{a_{ij}}{\sqrt{a_{ii}a_{jj}}}$$

(II.D.9)

If any of the off-diagonal terms are exactly one, the inverse of [A] does not exist and the inverse problem can not be solved for aquifer parameters. From a practical standpoint, anytime the off-diagonal elements of the correlation matrix get above .9 the [A] matrix becomes ill-conditioned rather rapidly and the inverse solution becomes more unreliable.

Parameter Covariance Matrix

The parameter covariance matrix is defined as

$$COV(P) = [B] = [A]^{-1}\sigma^2$$

(II.D.10)

where σ^2 = head variance and the estimated standard error of parameter i is given by $\sqrt{b_{ii}}$. As long as an inverse of [A] can be found, the reliability of the parameter estimates can be assessed by looking at the parameter covariance matrix defined here. The form shown here results from some simplifying assumptions about the errors in head such as additive, zero mean, noncorrelated and constant variance. With these assumptions the estimated standard errors of the parameters are given by the square roots of the diagonal elements of the parameter covariance matrix.

E. SLUG TESTS IN THE PRESENCE OF A WELL SKIN

Introduction

Slug tests are frequently used to characterize the transmissivity of an aquifer. However, in the presence of heterogeneity it is uncertain how the slug test is averaging the aquifer properties. In this paper, we look at the effect of one kind of heterogeneity: a well skin. A well skin can be created by the process of establishing the well, and may have a transmissivity value (T1) greater or less than that of the aquifer transmissivity (T2). We have investigated this problem using sensitivity analysis and an automated well-test analysis program we have developed. The sensitivity coefficients for T1 and T2 are similar in shape but shifted slightly in time. Thus, it is difficult to obtain good estimates for both T1 and T2 due to correlation. The maximum amplitude of the sensitivities is inversely proportional to transmissivity. Varying the skin radius shifts the head response curve along the dimensionless time axis. When fitted to the Cooper-Bredehoeft-Papadopulas (C-B-P) model, the data show a systematic lack of fit, however, it is not large. The effective transmissivity obtained from the C-B-P fit is a weighted average of T1 and T2 and can be predicted with a simple empirical formula. The effective transmissivity is highly weighted by the smallest transmissivity and is a weak function of the skin radius. Addition of observation wells makes little difference in the C-B-P fit results. The value of the effective transmissivity does not depend on the initial slug height. If one attempts a three parameter fit using T1, T2, and the skin radius (Rs), it is found that T1 and Rs are usually very highly correlated leading to a nonunique situation. If Rs is assumed known and one tries to solve for T1 and T2, the situation is better, but the fit is still difficult and depends on the initial estimates and the quality of the data. Having copious amounts of accurate data and multiple observation wells is the best situation for obtaining an accurate fit.

Model for Slug Tests With Skin

The physical situation is shown schematically in Figure 1. Mathematically the model is given by the following equations (Moench and Hsieh, 1985):

$$\frac{\partial^2 H_1}{\partial r^2} + \frac{1}{r}\frac{\partial H_1}{\partial r} = \frac{S_1}{T_1}\frac{\partial H_1}{\partial t} \qquad r_w \leq r \leq R_s \qquad \text{(II.E.1)}$$

$$\frac{\partial^2 H_2}{\partial r^2} + \frac{1}{r}\frac{\partial H_2}{\partial r} = \frac{S_2}{T_2}\frac{\partial H_2}{\partial t} \qquad r \geq R_s \qquad \text{(II.E.2)}$$

At the well bore

$$\pi r_c^2 \left(\frac{\partial H_1}{\partial t} \right)_{r_w} = \left(2\pi r T_1 \frac{\partial H_1}{\partial r} \right)_{r_w} \quad r_c \equiv \text{casing radius} \tag{II.E.3}$$

Initial conditions:

$$H_1 = H_2 = 0 \quad at\ t = 0\ for\ r > r_w$$
$$H_1 = H_0 \quad at\ t = 0\ for\ r = r_w \tag{II.E.4}$$

The boundary conditions between the skin and aquifer are

$$H_1 = H_2\ at\ r = R,$$
$$T_1 \frac{\partial H_1}{\partial r} = T_2 \frac{\partial H_2}{\partial r} \quad at\ r = R, \tag{II.E.5}$$

Far away from the slugged well

$$H_2 = 0 \quad at\ r = \infty \tag{II.E.6}$$

Sensitivities for T_1 and T_2

The sensitivities for T_1 and T_2 are very similar in shape as shown in Figure 2. However, the sensitivity for T_2 is shifted slightly to larger time values. Figure 2 shows the sensitivity to the skin region when it has the same value for transmissivity as the aquifer. Figure 3 shows the sensitivities when the skin transmissivity is an order of magnitude smaller. Note that the maximum amplitude of the sensitivity is inversely proportional to the transmissivity. The lower sensitivity for T_2 coupled with the similarity in shape (meaning correlation is high) indicates that it is going to be very difficult to get accurate estimates for T_2 . Away from the slugged well there is some difference in shape between sensitivities for T_1 and T_2 , however, the amplitude decays rapidly making it difficult to utilize these differences.

Effect of Varying the Skin Radius

Varying the skin radius shifts the head response curve along the dimensionless time axis for both the slugged well and observation wells. Figure 4 shows the normalized head in the slugged well for various skin radii. Figure 5 is a similar plot for an observation well located at 100 well radii away from the slugged well. Increasing the skin radius shifts the head response curve to larger dimensionless time (beta) when $T_1 \ll T_2$. This is true for both the slugged well and the observation well. However, the response in the observation well declines with increasing skin radius for $T_1 \ll T_2$.

Fitting Well Skin Data to the C-B-P Model

Many times the C-B-P model (Cooper et al., 1967) is used to fit slug test data. The obvious question is: What is the effective transmissivity when a well skin is present? Figure 6 shows a resulting fit with SUPRPUMP (Bohling and McElwee, 1992). The fitted data show a systematic deviation which may be diagnostic. The skin data is greater than the C-B-P model for early time and less than the C-B-P model for larger times, when $T_1 \ll T_2$. In general, the effective transmissivity resulting from the application of the C-B-P model to well skin data is an average of the skin and aquifer transmissivities. We have found that a good empirical equation for the effective transmissivity is

$$\frac{1}{T_{\text{eff}}} = \left[\frac{\ln(R_s / r_w)}{T_1} + \frac{\ln(r_{\text{eff}} / r_w) - \ln(R_s / r_w)}{T_2} \right] \qquad \text{(II.E.7)}$$

r_{eff} = effective radius influenced by the slug test.

$$r_{\text{eff}} / r_w = [C / S]^{1/2} \qquad 1 \le C \le 2 \qquad \text{(II.E.8)}$$

S = storage coefficient.

The result given by this equation is highly weighted by T_1 and has a weak dependence on the skin radius when $T_1 \ll T_2$. In general, the lowest value of transmissivity (whether it is the aquifer or the skin) will be the dominant factor in determining the effective transmissivity. Table 1 gives some typical results for effective transmissivity for varying skin radii and transmissivity distributions. As one might expect the effective transmissivity is independent of initial slug height.

Table 1
Effective Transmissivities in the Presence of a Skin

T_1	T_2	R_s/r_w	T_{eff} C-B-P	C (emp.)	T_{eff} (emp.
0.1	1.0	5	.205	2	.208
0.1	1.0	10	.155	2	.155
0.1	1.0	20	.126	2	.124
1.0	0.1	5	.175	1	.172
1.0	0.1	10	.260	1	.250
1.0	0.1	20	.456	1	.456

The storage coefficient was 10^{-3} for all the above simulations and an observation well was used at $100\ r_w$.

Parameter Estimation with the Well Skin Model

The well skin model of Moench and Hsieh has been implemented in SUPRPUMP and can be used to look at sensitivities and to fit the data. Figure 7 is a plot of the sensitivities to T_1 and R_s. The sensitivity to R_s is smaller than to T_1 and is of opposite sign. However, the shape of the two sensitivities in Figure 7 is almost identical and very high correlation is the general rule. Away from the slugged well there is some difference in shape between sensitivities for T_1 and R_s , however, the amplitude decays rapidly making it difficult to utilize these differences. Therefore, it is extremely difficult to obtain good estimates for both T_1 and R_s. Usually there will be many pairs of values of T_1 and R_s that will give equally good results. In tests we have run, the high correlation persists even if observation wells are available and used. In some cases the approximate value for the skin radius may be known from the diameter of the hole made by the drilling equipment; in this case one can try holding R_s constant and just fitting T_1 and T_2

.

Three Parameter Fit

Table 2 shows the output from the SUPRPUMP package used in design mode for the three parameter fit (T_1, T_2, and R_s) of the Moench and Hsieh well skin solution. Four observation wells were used at r/r_w of 1, 25, 50 and 100 for 56 time measurements between .01 and 1000. units of dimensionless time (BETA). The 95% confidence limits

show that T_1 and T_2 could be determined within about $\pm$ 40%, however, the skin radius (R_s) is very poorly determined. The root causes of these results can be seen by looking at the matrix of normalized sensitivities, the sensitivity correlation matrix, and the parameter correlation matrix in Table 2. The diagonal elements of the matrix of normalized sensitivities shows that T_1 has the highest sensitivity by far. The sensitivity correlation matrix and the parameter correlation matrix shows that the correlation between T_1 and R_s is greater than .99 . These results are for perfect model data with an assumed accuracy of $\pm$ .025 Ho. In the real world things are likely to be much worse.

Alluvial Aquifer Example

Figures 8 and 9 show a real example of a slug test performed in the Kansas River valley near Lawrence, Ks. Figure 8 shows the fit of the data to the C-B-P model. There is a systematic deviation present and we thought it might be explained by a skin effect. Figure 9 shows the same data fit to the Moench and Hsieh model. The fit is much better, but it was difficult to obtain and is very sensitive to the number of parameters fit and the initial estimates for those parameters. Many of the analyses did not converge. Consequently, even though the fit is much better, we do not believe very much accuracy can be ascribed to the estimated aquifer conductivity. On the other hand, the effective conductivity from the C-B-P model and the skin conductivity from the Moench and Hsieh model agree fairly well and can probably be used with some confidence. Unfortunately, it is the aquifer conductivity that is of greatest interest.

Summary

We have investigated the problem of a slugged well having a well skin using sensitivity analysis and an automated well-test analysis program we have developed. The sensitivity coefficients for T_1 and T_2 are similar is shape but shifted slightly in time. Thus, it is difficult to obtain good estimates for both T_1 and T_2 due to correlation. The maximum amplitude of the sensitivities is inversely proportional to transmissivity. Varying the skin radius shifts the head response curve along the dimensionless time axis. When fitted to the Cooper-Bredehoeft-Papadopulas (C-B-P) model, the data show a systematic lack of fit, however, it is not large. The effective transmissivity obtained from the C-B-P fit is a weighted average of T_1 and T_2 and can be predicted with a simple empirical formula. The effective transmissivity is highly weighted by the smallest transmissivity and is a weak function of the skin radius. If one attempts a three parameter fit using T_1, T_2, and the skin radius (R_s), it is found that T_1 and R_s are usually very highly correlated leading to a nonunique situation. If R_s is assumed known and one tries

to solve for T_1 and T_2, the situation is better, but the fit is still difficult and depends on the initial estimates and the quality of the data. Having copious amounts of accurate data and multiple observation wells is the best situation for obtaining an accurate fit.

TABLE 2
SUPRPUMP OUTPUT
THREE PARAMETER FIT

The estimated root-mean-squared residual is .2500E-01

The parameter values with approximate 95% confidence intervals are:

Parameter	Value	Lower Bound	Upper Bound
TRANSMISS. OF AQUIFER	1.000	.6227	1.377
TRANSMISS. OF SKIN	.1000	.5668E-01	.1433
SKIN RADIUS	10.00	-1.459	21.46

For the following arrays:
Col-Row 1 represents TRANSMISSIVITY OF AQUIFER (T2)
Col-Row 2 represents TRANSMISSIVITY OF SKIN (T1)
Col-Row 3 represents SKIN RADIUS (Rs)

Raw crossproducts matrix of normalized sensitivities:

	1	2	3	
1	.2357E-01	.8306E-01	-.3155E-01	I This matrix shows that
2	.8306E-01	1.093	-.4113	I T1 has the highest
3	-.3155E-01	-.4113	.1566	I sensitivity by far.

The reciprocal condition number of the
sensitivity crossproducts matrix is .1079E-02

Sensitivity correlation matrix:

	1	2	3	
1	1.000	.5174	-.5192	
2	.5174	1.000	-.9940	-------Very high correlation
3	-.5192	-.9940	1.000	between T1 and Rs.

Covariance matrix of normalized parameter variations:

	1	2	3
1	.3630E-01	-.6035E-03	.5727E-02
2	-.6035E-03	.4787E-01	.1256
3	.5727E-02	.1256	.3349

Parameter correlation matrix:

	1	2	3	
1	1.000	-.1448E-01	.5194E-01	
2	-.1448E-01	1.000	.9918	--------Very high correlation
3	.5194E-01	.9918	1.000	between T1 and Rs.

Figure 1. Schematic of a slug test in a well with a skin.

Figure 2.
Variation of u'ₜ With Time at the Slugged Well

$T_1 = T_2 = 1.0$

$r/r_w = 1$

u'_{T_2}

u'_{T_1}

$BETA = T_1 t/r_w^2$

NORMALIZED SENSITIVITY

DIMENSIONLESS TIME (BETA)

Figure 3.
Variation of u'ₜ With Time at the Slugged Well

$T_1 = 0.1, T_2 = 1.0$

u'_{T_2}

$r/r_w = 1$

u'_{T_1}

$BETA = T_2 t/r_w^2$

NORMALIZED SENSITIVITY

DIMENSIONLESS TIME (BETA)
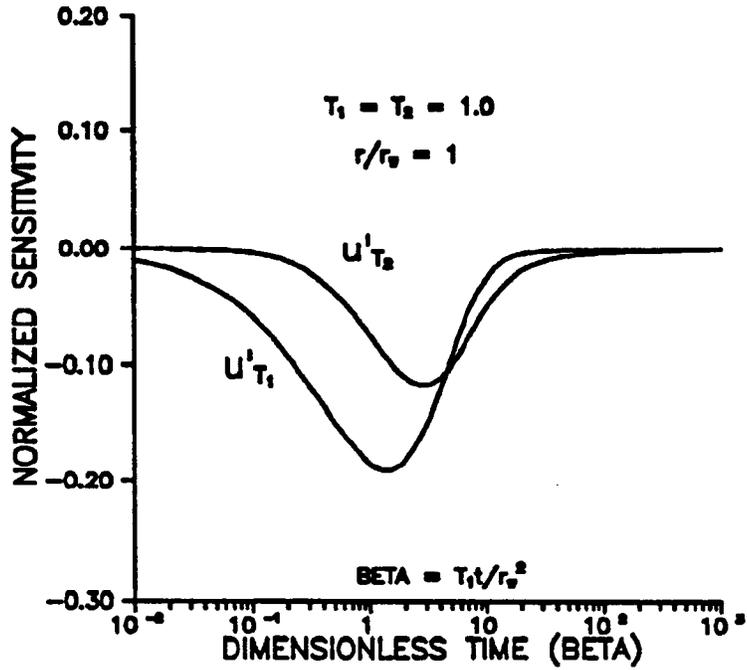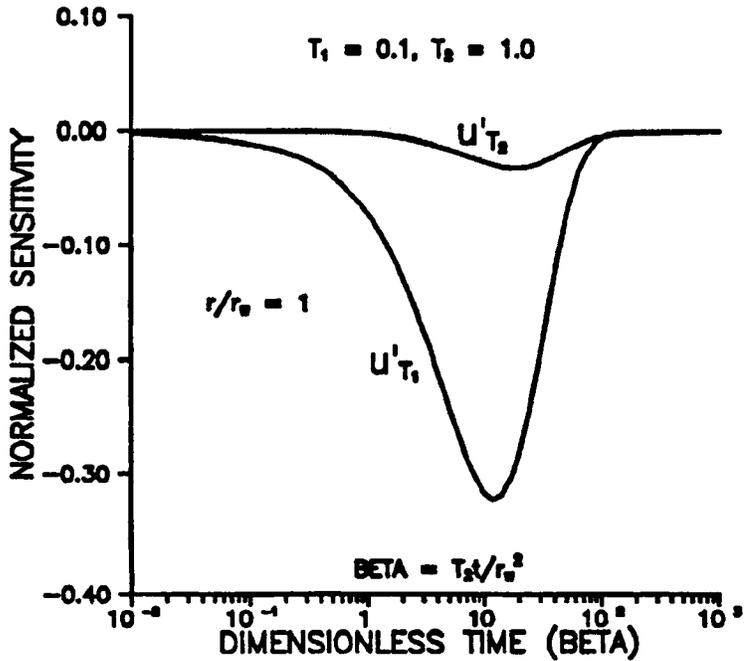
Figure 4.
Variation of Head in Slugged Well With Skin Radius

$T_1 = 0.1$, $T_2 = 1.0$

$r/r_w = 1$

5.0
10.0
20.0 $= R_s/r_w$
50.0.

$BETA = T_2 t/r_w^2$

NORMALIZED HEAD

DIMENSIONLESS TIME (BETA)
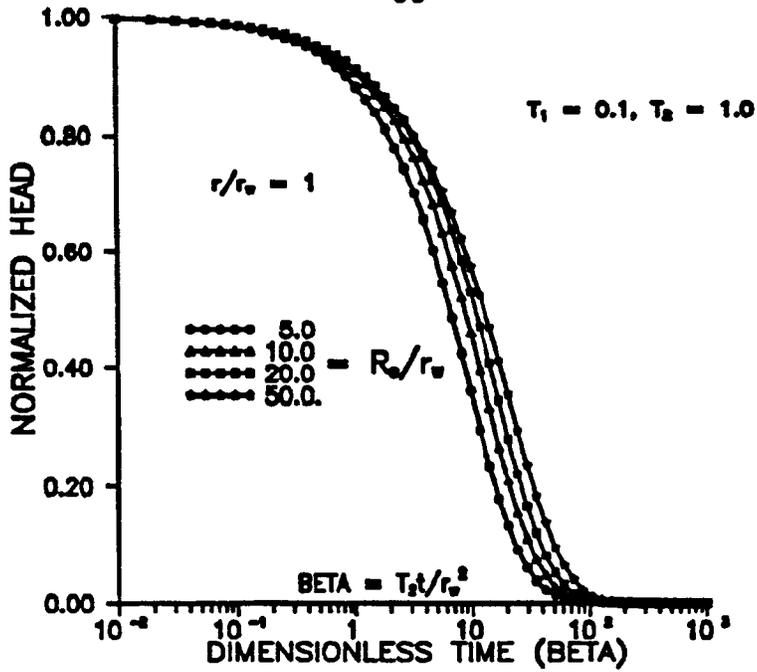
Figure 5.
Variation of Head in Obs. Well With Skin Radius

$r/r_w = 100$ $T_1 = 0.1$, $T_2 = 1.0$

5.0
10.0
20.0 $= R_s/r_w$
50.0.

$BETA = T_2 t/r_w^2$

NORMALIZED HEAD

DIMENSIONLESS TIME (BETA)

II.E.10
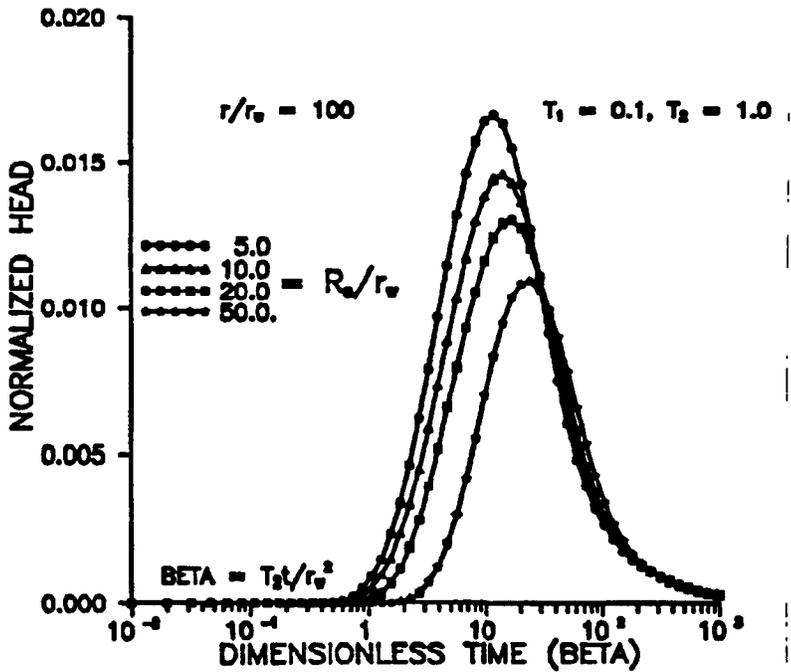
Figure 6.
Fit of Well Skin Data to the C-B-P Model

$T_1 = 0.1$, $T_2 = 1.0$

$r/r_w = 1$

•••• Well Skin Data
▲▲▲▲ C-B-P Model

BETA = $T_2 t/r_w^2$
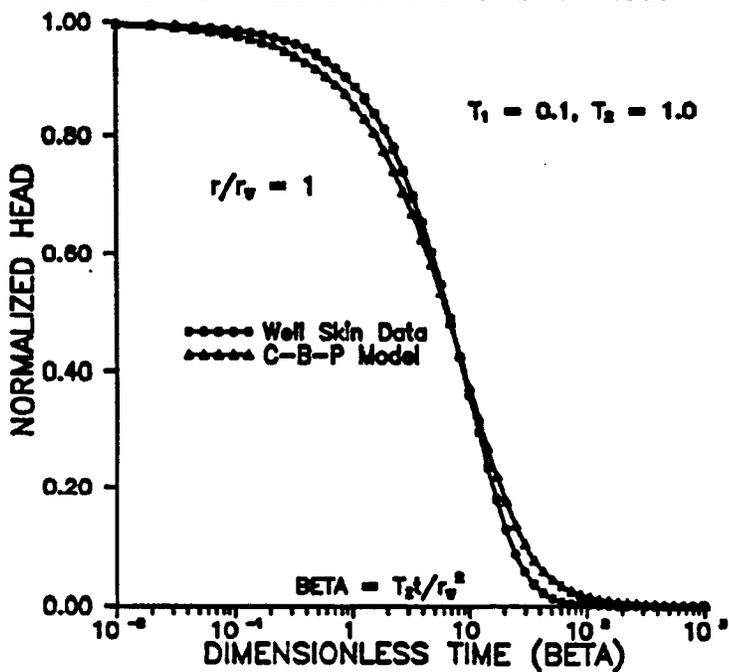
Figure 7.
Comparison of u'_{T_1} and u'_{R_s} at the Slugged Well

$T_1 = 0.1$, $T_2 = 1.0$

u'_{R_s}

u'_{T_1}

$r/r_w = 1$

BETA = $T_2 t/r_w^2$

II.E.11
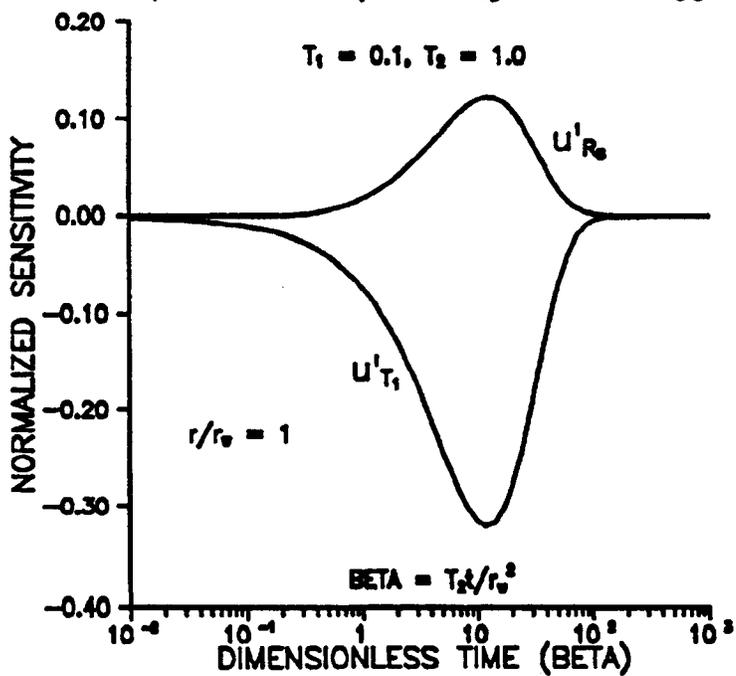
Figure 8.
Analysis of an Alluvial Aquifer Slug Test With the C-B-P Model

GEMS 7/10/91 Slug Test # 7- Well #4

—— Measured Data
--- Fitted C-B-P Model

K = 1.3 ft/day
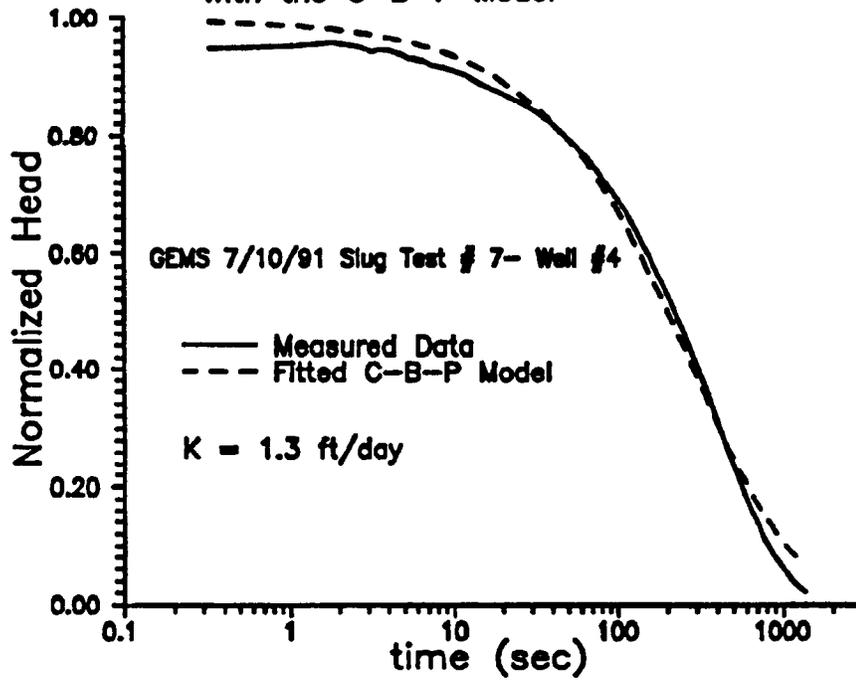
Figure 9.
Analysis of an Alluvial Aquifer Slug Test With the Skin Model

GEMS 7/10/91 Slug Test # 7- Well #4

—— Measured Data
--- Fitted Moench-Hsieh Model

K_2 = 3.7 ft/day
K_1 = 1.6 ft/day

II.E.12
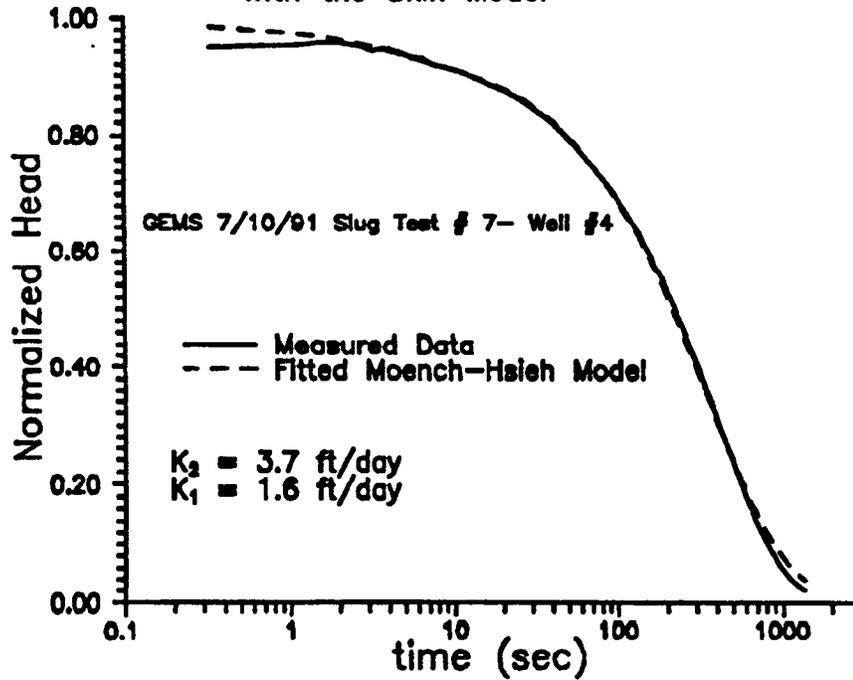
F. SLUG TESTS WITH OBSERVATION WELLS

Introduction

Slug tests are commonly used for site characterization. An earlier paper (McElwee et al., 1989) dealt with the use of sensitivity analysis to design a test which would give reasonably accurate estimates of the aquifer parameters by an informed choice of the number and times of measurements. Most practitioners know that slug tests are not very sensitive to the storage coefficient, as explained in the earlier paper. An investigation of the radial dependence of the Cooper et al. (1967) analytical slug test solution shows that the use of one or more observation wells can vastly improve the parameter estimates, particularly the estimate for storage.

Cooper - Bredehoeft - Papadopulos Analytical Solution for Slug Tests

The solution given by Cooper et al. (1967) is

$$H\left(\alpha, \beta, H_o, \frac{r}{r_s}\right) = \frac{2H_o}{\pi} \int_0^\infty \frac{e^{-\beta u^2/\alpha}}{\Delta(u)} F\left(u, \alpha, \frac{r}{r_s}\right) du \qquad \text{(II.F.1)}$$

where

$$F\left(u, \alpha, \frac{r}{r_s}\right) = \left\{ J_0\left(u\frac{r}{r_s}\right) \cdot [uY_0(u) - 2\alpha Y_1(u)] \right.$$

$$\left. - Y_0\left(u\frac{r}{r_s}\right) \cdot [uJ_0(u) - 2\alpha J_1(u)] \right\}, \qquad \text{(II.F.2)}$$

$$\Delta(u) = [uJ_0(u) - 2\alpha J_1(u)]^2 + [uY_0(u) - 2\alpha Y_1(u)]^2, \qquad \text{(II.F.3)}$$

$$\beta = \frac{Tt}{r_c^2}, \qquad \text{(II.F.4)}$$

J, and Y are Bessel Functions,

$$\alpha = \frac{r_s^2}{r_c^2} S, \qquad \text{(II.F.5)}$$

r_s and r_c are screen and casing radii,

$$\frac{H}{H_0} = h \equiv \text{relative head, and} \quad H_0 \equiv \text{initial head displacement} \qquad \text{(II.F.6)}$$

Slug-test responses can be expressed as a function of four parameters: alpha, a parameter related to screen and casing radii and the storage coefficient; beta, a dimensionless time involving transmissivity and the casing radius; H_0, the initial head displacement; and r/r_s, the distance to an observation well divided by the screen radius.

Relative Head or Sensitivity to H_0

Figure 1 shows the relative head or sensitivity to H_0 versus dimensionless time for various radii. The maximum occurs for $r = r_s$ (Figures 1 and 3), and decreases with time and distance. Figure 3 shows that the area of influence spreads with time. Figure 1 shows that an observation well will respond in time with a bell shaped curve whose maximum amplitude decays with distance from the slugged well. At about $175r_s$ the response has fallen to about .01 H_0 at a dimensionless time of 10 for $\alpha = 10^{-3}$ (Figures 1 and 2). Smaller $\alpha' s$ result in larger responses in space and time as shown in Figures 2 and 4.

Sensitivity to Transmissivity

Figures 5-8 illustrate the dependence of the sensitivity to transmissivity on time, distance, and alpha. u_T' has positive and negative lobes except for $r = r_s$ (Figures 5 and 7). Figure 7 shows that the maximum sensitivity to transmissivity occurs at the well. A given observation well will be sensitive to the transmissivity over a definite time interval (Figure 5), and the sensitivity decays rapidly with increasing r. Figures 6 and 8 illustrate the dependence on the storage coefficient (alpha). The maximum amplitude of the sensitivity seems to vary inversely with alpha (Figure 6), while the amplitude at $r = r_s$ does not seem to have a strong dependence on alpha (Figure 8). As noted previously, we need a smaller alpha (storage coefficient) for sensitivities to propagate farther from the slugged wells (Figure 8).

Sensitivity to Storage

Figures 9-12 illustrate the dependence of the sensitivity to storage on α, β, and r. The maximum sensitivity does not occur at $r = r_s$ (Figures 9 and 11), but rather at a distance of about $5r_s$ for $\alpha = 10^{-3}$. Figure 11 shows that the shape of u_s' moves out to larger distances while widening and decaying with increasing time. The dependence on alpha shown in Figure 12 reveals that the signal propagates much farther from the well

for smaller values of α. Figure 10 shows that, for a chosen r, the maximum amplitude of the sensitivity is inversely proportional to α and occurs at earlier times for smaller α's.

Correlation of u_T' and u_s'

Figure 13 shows that the shape of the sensitivities with respect to transmissivity and storage at $r = r_s$ are extremely similar except for amplitude. This means that data from a slugged well are much more sensitive to T than S and that there will be high correlation between these two parameters. Figure 14 shows the two sensitivities at $r = 10r_s$ and reveals that they have considerably different shapes and nearly the same maximum amplitude. This means that data from the observation well is much more sensitive to storage than data from the slugged well and that the correlation between T and S is dramatically reduced by the use of an observation well.

Simulation for an Alluvial Field Site

We have developed an alluvial field site for hydraulic testing. It consists of about 35 feet of coarse sand and gravel overlain by about 35 feet of silt and clay. The following is a simulation of expected results at this site. From earlier laboratory work and pumping tests we know some average values for K, T and S.

$$K \approx 300 \text{ ft/day} = .208 \text{ ft/min}$$
$$T \approx (.208 \text{ ft/min}) (35 \text{ feet}) = 7.28 \text{ ft}^2/\text{min}$$
$$S \approx .00063$$

We simulate the results for the slugged well and two observation wells at 5 and 10 feet away, taking data over a three minute interval (slug tests have very short duration in this media). It is assumed the slugged well is 4 inches in diameter and all wells are fully screened. The simulated data is rounded to the nearest tenth of a foot and then analyzed in an inverse program (SUPRPUMP).

Alluvial Field Site Results

	Slugged Well Only	Slugged Well + Obs. Well	Slugged Well + 2 Obs. Wells
Range of T (ft^2./min)	7.11 - 8.00	7.22 - 7.37	7.24 - 7.38
Range of S	$(.178 - .722) \times 10^{-3}$	$(.616 - .666) \times 10^{-3}$	$(.609 - .648) \times 10^{-3}$
Corr.	.98	.54	.44
rms Dev.	.026	.026	.025
Remarks	Trouble Converging	Converged rapidly	Converged Rapidly

Results From Dakota Aquifer, Lincoln County, Kansas

As part of a regional study of the Dakota aquifer in Kansas a number of pumping and slug tests have been performed. One site in Lincoln County was slug tested with an observation well (21.2 ft. from slugged well). The following are details of the two wells:

	Slugged Well	Observ. Well
Depth	98.4 feet	94.4 feet
Dia.	4 inches	2 inches
Screen	78-98 feet	84-94 feet

The test was analyzed three ways:

	Slugged Well	Obser. Well	Slugged Well + Obser. Well
T (ft^2/sec)	$.896 \times 10^{-3}$	1.0005×10^{-2}	1.029×10^{-2}
S	$.2 \times 10^{-3}$	$.514 \times 10^{-4}$	$.520 \times 10^{-4}$
Corr.	.99	.269	.49
rms Dev	.0024	.0030	.0040

It is clear that the use of an observation well greatly improves the estimate for S and makes the inverse problem much better conditioned. Figure 15 shows the field measurements and the fitted data.

Conclusion

While it would usually not be practical to install an observation well solely for use in a slug test, many times nearby wells are available. Generally, the observation well must be fairly close (a few tens of feet or less) to the slugged well to be effective. The storage coefficient must be small in order to see the effect of the slug at greater distances from the slugged well. Since the temporal and spatial dependence of the sensitivities for transmissivity and storage are considerably different, the addition of one or more observation wells will substantially reduce the correlation between these two parameters, and result in much better estimates than usually obtained in slug tests. These ideas have been illustrated using typical data from our research sites.

Figure 1.
Variation of u'_{H_o} With Time For Various r/r_o

Figure 1. Variation of u'_{H_o} With Time For Various r/r_o

Figure 2.
Variation of u'_{H_o} With Time For Various Alpha

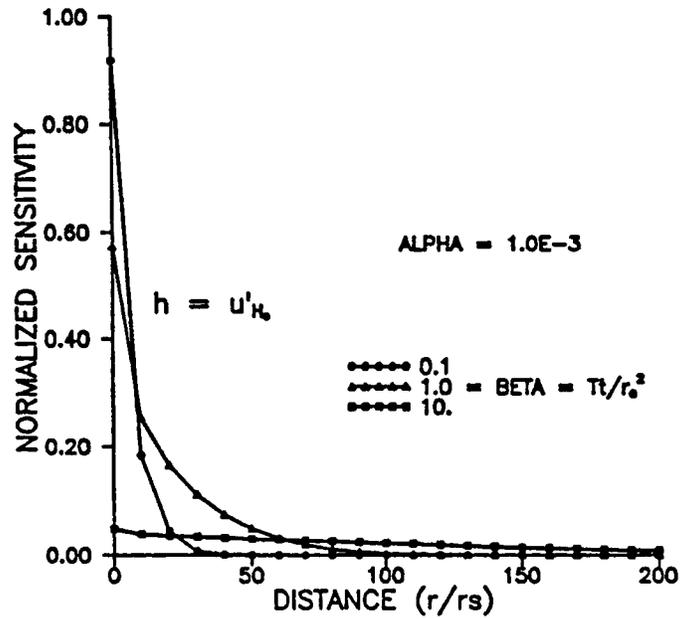Figure 2. Variation of u'_{H_o} With Time For Various Alpha

II.F.6
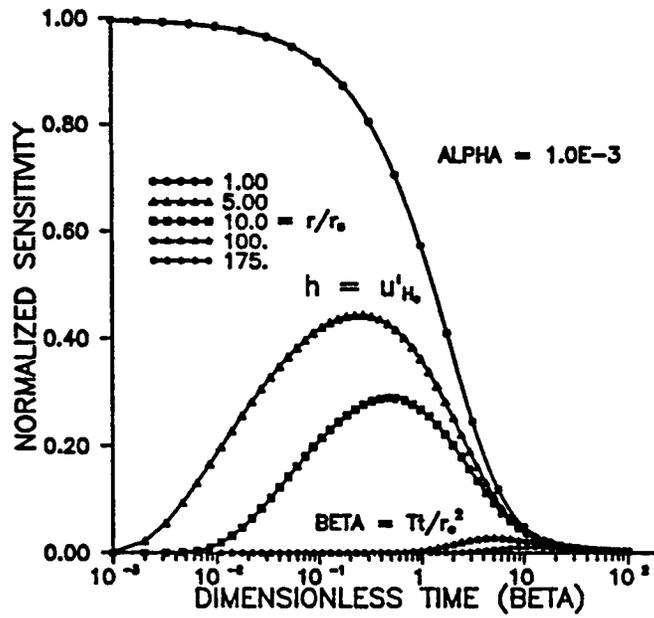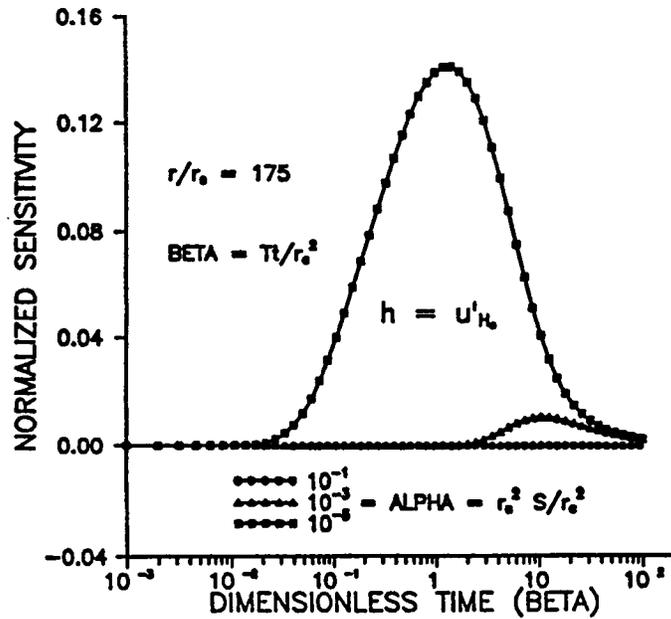
Figure 3.
Variation of u'_{H_o} With Distance For Various Times
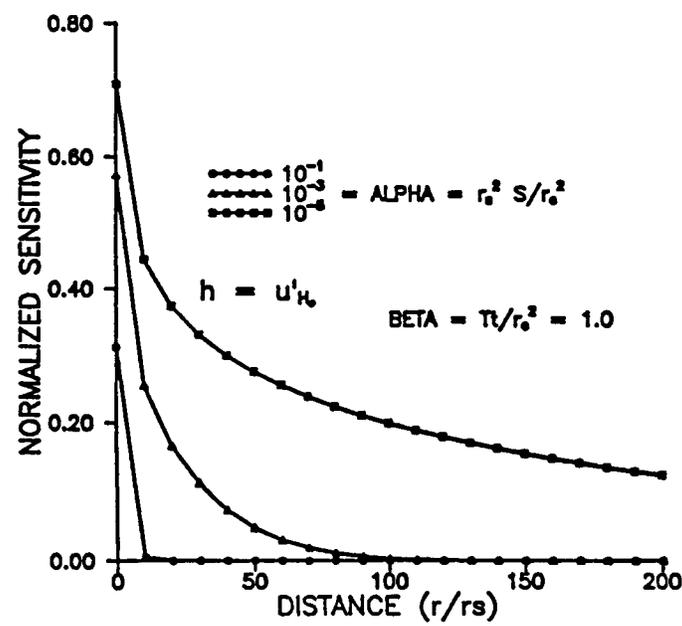

Figure 4.
Variation of u'_{H_o} With Distance For Various Alpha

II.F.7

Figure 5.
Variation of u'$_T$ With Time For Various r/r$_e$
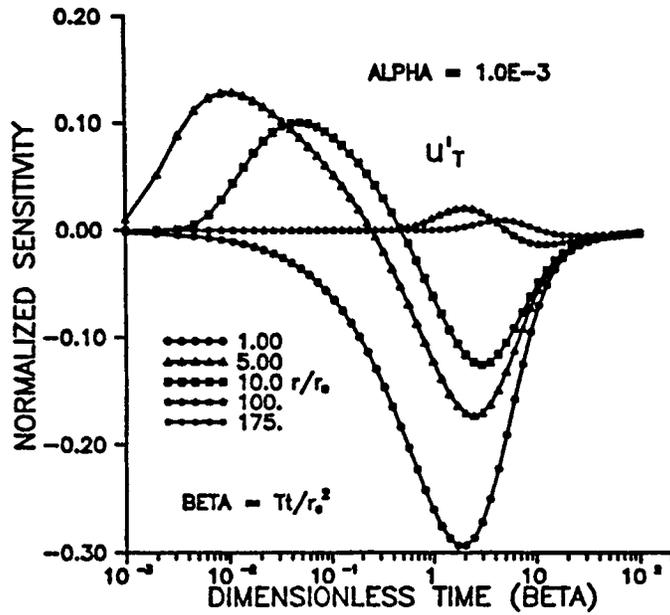
Figure 6.
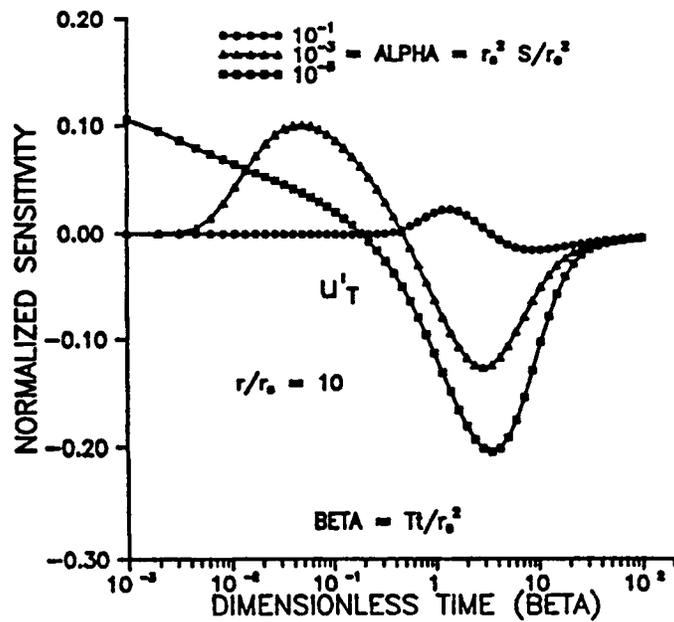Variation of u'$_T$ With Time For Various Alpha

Figure 7.
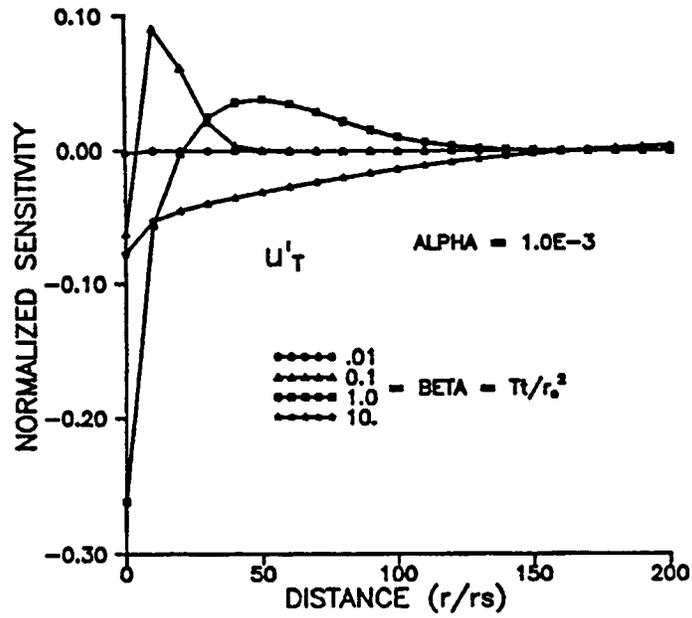Variation of u'_T With Distance For Various Times

Figure 8.
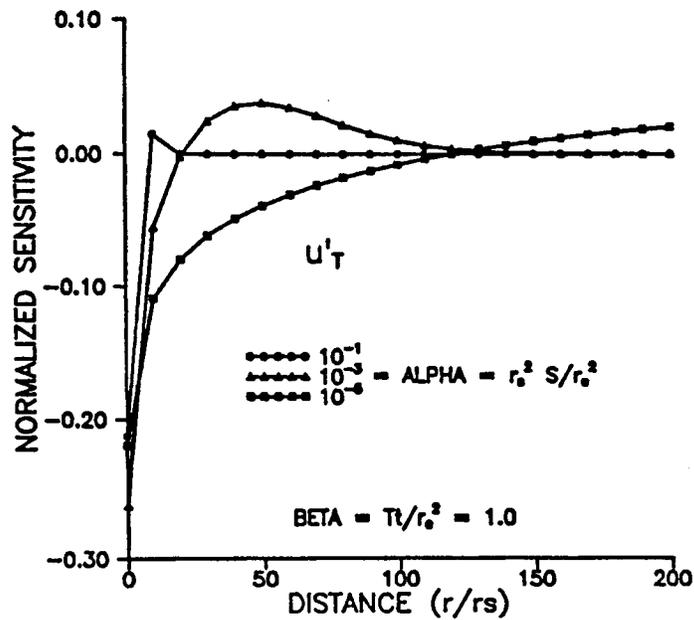Variation of u'_T With Distance For Various Alpha

Figure 9.
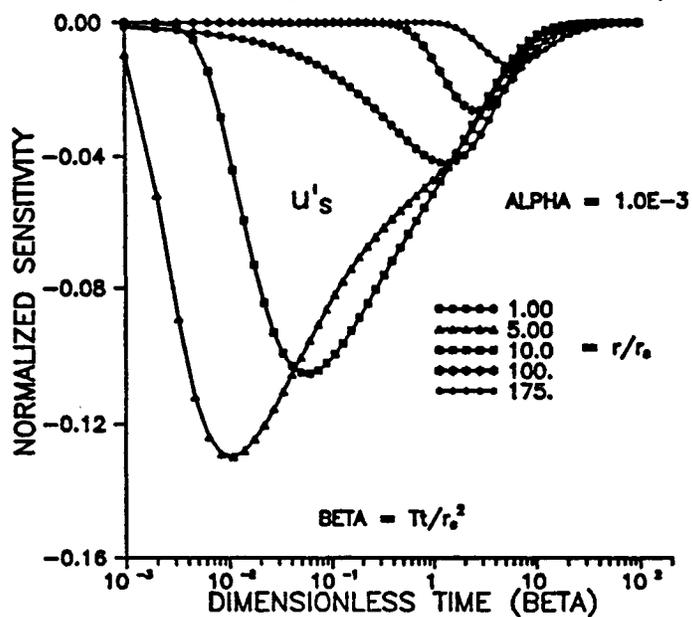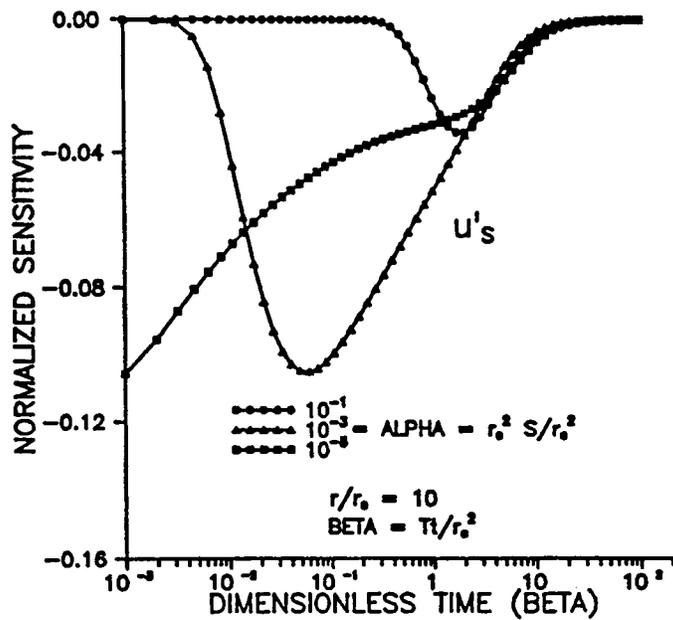## Variation of u'$_s$ With Time For Various r/r$_e$

NORMALIZED SENSITIVITY

u'$_s$

ALPHA = 1.0E-3

1.00
5.00
10.0   = r/r$_e$
100.
175.

BETA = Tt/r$_e^2$

DIMENSIONLESS TIME (BETA)

Figure 10.
Variation of u'$_s$ With Time For Various Alpha

NORMALIZED SENSITIVITY

u'$_s$

10^{-1}
10^{-3} = ALPHA = r$_e^2$ S/r$_e^2$
10^{-5}

r/r$_e$ = 10
BETA = Tt/r$_e^2$

DIMENSIONLESS TIME (BETA)

Figure 11.
Variation of u's With Distance For Various Times

ALPHA = 1.0E-3

u'$_s$

- •••••• .01
- •••••• 0.1   = BETA = Tt/r_s^2
- •••••• 1.0
- •••••• 10.

NORMALIZED SENSITIVITY
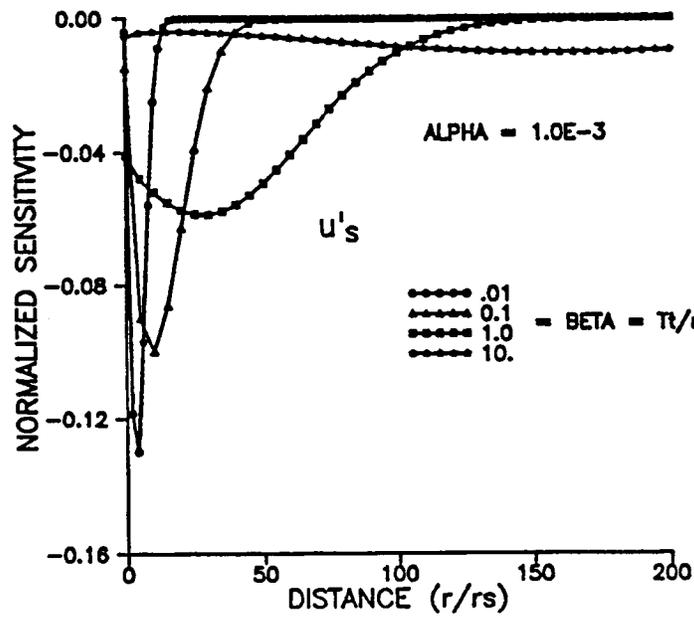
DISTANCE (r/rs)

Figure 12.
Variation of u's With Distance For Various Alpha

- •••••• 10^{-1}
- •••••• 10^{-3} = ALPHA = r_s^2 S/r_s^2
- •••••• 10^{-5}

u'$_s$

BETA = Tt/r_s^2 = 1.0

NORMALIZED SENSITIVITY

DISTANCE (r/rs)
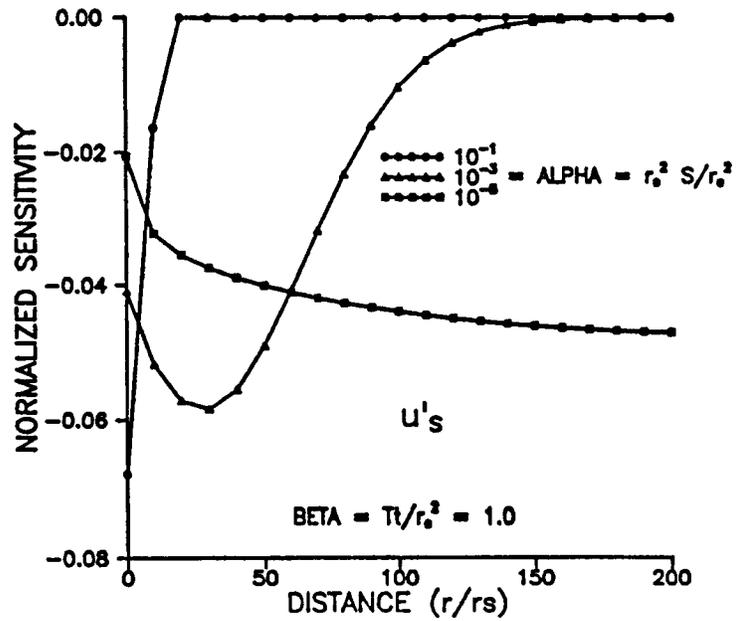
Figure 13.
Comparison of Sensitivities at the Screen Radius

$ALPHA = 1.0E-3$

$r/r_\circ = 1$

$BETA = Tt/r_e^2$
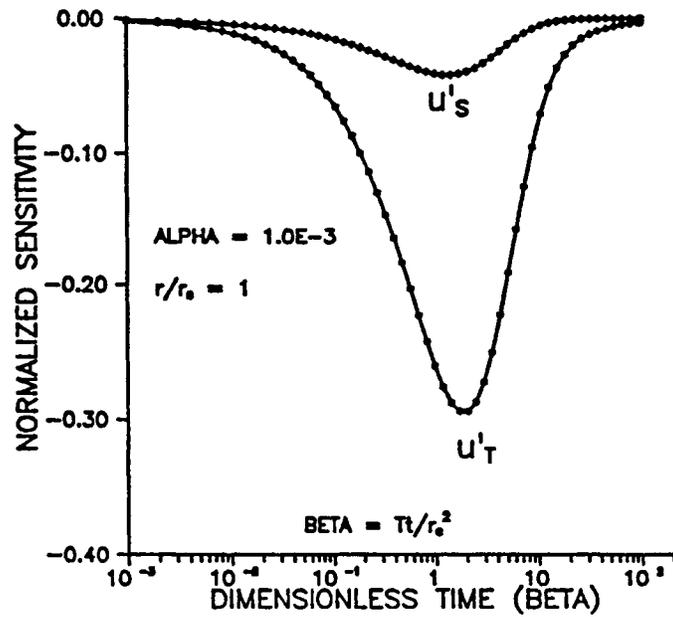
Figure 14.
Comparison of Sensitivities at 10 Screen Radii

$ALPHA = 1.0E-3$

$r/r_\circ = 10$
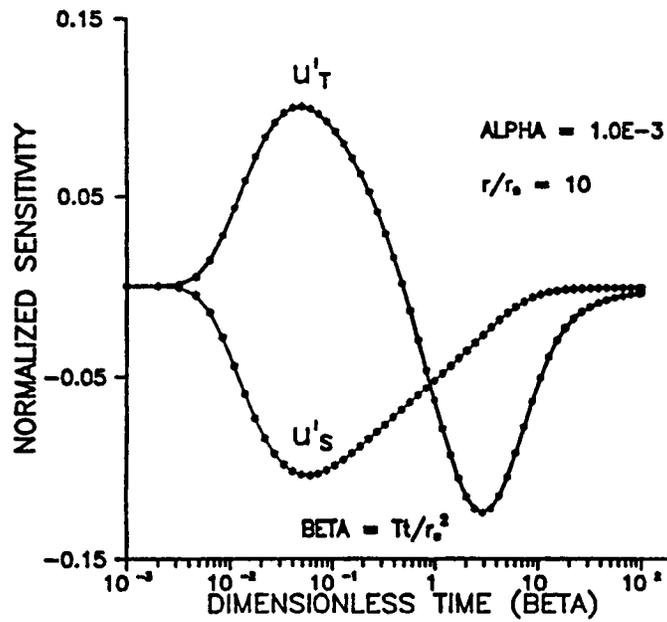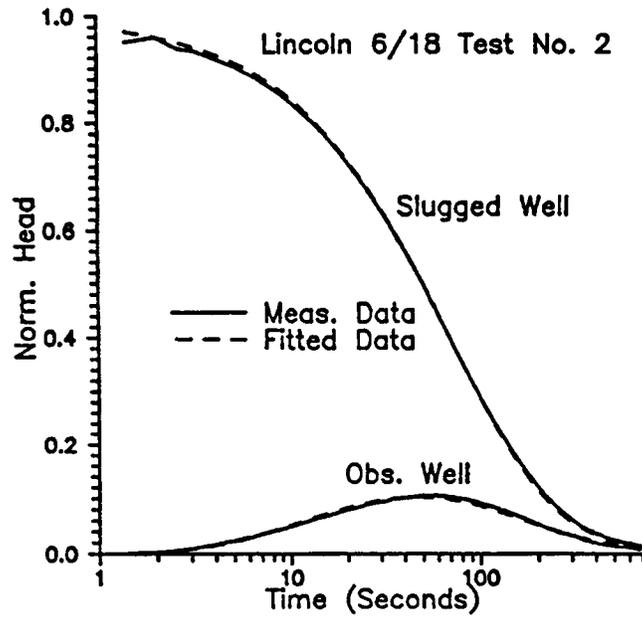
$BETA = Tt/r_\circ^2$

II.F.12

Figure 15.
Dakota Aquifer Test, Lincoln County Kansas

II.F.13

III. FIELD INVESTIGATIONS OF MULTILEVEL SLUG TESTS

A. KGS MULTILEVEL SLUG-TEST SYSTEM

In 1989, a slug-test system was developed at the KGS for the purpose of performing slug tests in wells of small diameters (.05 m ID) located in highly permeable alluvial units (McElwee and Butler, 1989). This equipment served as the basis of a multilevel slug test system that is being developed for the research described in this report. A prototype straddle-packer system for multilevel slug tests has been constructed at the KGS. The prototype system consists of two packers (each approx. .67 m in length when fully inflated) that are used to seal off the test interval from the adjacent screen. A section of .025 m ID PVC (SCH 40) pipe is connected to the central flow-through pipe of the top packer of the pair. A series of sections of the .025 m ID PVC pipe runs to a third packer located above the top of the screened interval. This pipe allows the pressure pulse initiating a slug test to be confined to the straddle-packer interval. The central flow-through pipe of the middle packer is closed off prior to testing. A slug test is initiated by adding or removing water to the casing above the third packer and then opening the central flow-through pipe in the middle packer. As with the original KGS slug-test system (McElwee and Butler, 1989), the central flow-through pipe is opened by the mechanical lowering of a plug attached to pump rods. Although the test interval can be up to several meters in length, it cannot be less than .29 m in the present configuration.

After the completion of testing at one level, the packers are deflated and the string of packers and pipes is moved until the straddle-packer interval is opposite the next zone to be tested. The string can be moved until the top of the third packer is raised above the static water level or lowered below the top of the screen. At that point, a section of PVC pipe must be either removed or added, respectively, to the pipe string connecting the straddle packer to the top packer before testing can be continued. In this manner, a series of multilevel slug tests can be readily performed across the entire screened interval of a well in a relatively short period of time. At shallow depths the string of packers and pipes can be lifted manually, while at deeper depths a special tripod and winch arrangement that was constructed during the first year of this project is employed. Note that the packers used in this system were designed and constructed at the KGS. Commercially available packers for use in .05 m ID wells have central flow-through

pipes that are .0125 m ID or smaller. Packers with larger flow-through pipes (.025 m and .019 m) were designed in an effort to ensure that the parameters estimated from the response data would be reflective of properties in the aquifer, and not the diameter of the flow-through pipe.

As stated above, slug tests are initiated by adding or removing water from the cased section of the well above the third packer. In all cases, pressure transducers (PS7000 and PS9000 series, Instrumentation Northwest, Inc.) placed above the third packer are employed to measure water-level recoveries in the slugged well. During the field season, the transducers are calibrated in the laboratory on a monthly to bimonthly basis as described in section IV.E. Between laboratory calibrations, transducer functioning is checked in the field by measuring the height of the column of water above the transducer using an electric tape (Model 101 flat tape water meter, Solinst Canada Ltd.). The transducers are connected to one of two types of data acquisition devices: a datalogger (21X datalogger, Campbell Scientific, Inc.), or a data acquisition card (WB-FAI-B high speed interface card, Omega Engineering, Inc.). Note that the data-acquisition card has been placed in the expansion chassis of a 12 MHZ laptop computer (Supersport 286 Portable Computer, Zenith Data Systems Corp.).

In the following section, the use of this equipment in an initial series of multilevel slug tests at GEMS is described.

B. MULTILEVEL SLUG TESTS AT GEMS

Multilevel Tests at GEMS 2-5

The prototype KGS multilevel slug-test system was employed in a series of multilevel slug tests at GEMS. GEMS well 2-5 (depth = 20.67 m, screen length = 9.14 m), which is screened essentially through the entire sand and gravel section at the site, was used for these tests. An initial series of tests was run in which the slug consisted of the volume of water required to raise water levels 3.07 meters in the cased section of the well (H_0=3.07 m). As shown in Figure III.B.1, the slug-test responses measured at the different depths were very similar. Note that Table III.B.1 lists the depths corresponding to each test interval. Although the variation in the hydraulic conductivity values calculated from the core samples taken from GEMS 2-5 at these same depths was also small (Butler et al., 1991), the decision was made to repeat the series of slug tests using H_0's of different magnitudes to see if greater discrimination between test zones would be possible using a different H_0. Figure III.B.2 shows a plot for slug tests over the same intervals as Figure III.B.1 using a H_0 of approximately 1.65 m. A comparison of the two figures shows that, although there is little difference between tests using the same H_0, there is a considerable difference between tests using different H_0's. Normalized plots of the slug-test responses from a series of tests with differing H_0's in the third test interval are presented in Figure III.B.3. Note the dramatic dependence of the slug-test responses on magnitude of H_0. Dependence relationships of this form were seen in all the tested intervals. Table III.B.1 summarizes the parameters calculated from the slug-test responses for a subset of the tested intervals. In all cases, the higher the H_0, the lower the calculated conductivity. The inverse relationship between the magnitude of H_0 and the calculated conductivity does not appear to require a threshold value for H_0. Experiments have shown that differences in H_0 as small as .03 meters will still produce conductivity differences in the direction predicted from this relationship. Thus, the small difference in H_0 that exist between the slug tests shown on Figure III.B.1 or Figure III.B.2 could easily explain the differences displayed on those plots. Note that when special care was taken to ensure that the same volume was used for the slug in repeat tests at a given interval, the plots of the responses for the repeat tests coincided.

It is important to note that the theory from which the conventional methodology used for slug-test analysis (e.g., the CBP or Hvorslev models) was developed holds that

the slug-test responses should be independent of H_0. In other words, plots of slug-test responses from tests using differing H_0 normalized by the H_0 used in each test should coincide. Clearly, the multilevel slug tests at GEMS are being affected by processes not considered in the standard theory.

The dependence of slug-test responses on H_0 was not the only anomalous behavior observed during the multilevel slug testing at GEMS. Figures III.B.1 - III.B.3 are plots of slug-test responses given in the format of the Hvorslev method (log heads versus arithmetic time). Note the concave downward form of the curves. Conventional theory dictates that these plots should be concave upward or straight lines (Chirlin, 1989; McElwee et al., 1990). Nothing in the conventional theory would allow for concave downward plots. Additional indications that the multilevel slug tests at GEMS are being affected by processes not considered in the standard theory are seen in Figures III.B.4 and III.B.5, where the slug-test data are fitted using conventional approaches (CBP and Hvorslev techniques). The systematic deviation displayed on these plots between the fitted model and the data are characteristic of the behavior observed in every multilevel slug test performed in GEMS well 2-5.

Clearly, the processes that are producing these anomalous responses need to be explained before much useful information can be obtained from multilevel slug tests at GEMS. The decision was made to suspend multilevel slug testing and to concentrate on trying to explain the observed behavior. The objective of the work in the first year of this project thus shifted to the definition of the underlying mechanisms causing the anomalous behavior and the incorporation of these mechanisms into a general theory that can be the basis of new techniques for slug-test analysis. In the following sections, a series of field experiments, which were performed in an attempt to define the relevant processes, are described. These experiments led to the development of a nonlinear flow model that is described in a later section.

Field Experiments to Explain Anomalous Behavior

A series of field experiments were designed to assess the role of several possible factors in explaining the observed behavior. Factors that could be important in explaining the observed behavior include the following: 1) Frictional flow losses - these could occur in the cased region of the well above the top packer, within the PVC pipe

connecting the straddle packer to the top packer, within the packer flow-through pipes, and within the well screen; 2) Non-Darcian flow within the aquifer in the vicinity of the well screen; 3) Aquifer heterogeneities; and 4) Measured pressure not reflective of water level position - the transducers used in the field tests are measuring pressure, which may not always equate to the position of the water level.

The first of the above factors was considered the most likely, although there was no reason to immediately rule out the possibility of non-Darcian flow. Simulations that were performed as part of the theoretical work described in section II.B (scenario 4D of Table II.B.1) indicated that the third factor (aquifer heterogeneities) is not going to produce a dependence on H_0 in perfectly stratified systems. Even in a system of discontinuous layers, one would not expect that aquifer heterogeneities would always produce the inverse relationship between H_0 and slug-test parameters that is seen in all tests at GEMS. The fourth factor may be important in the initial period of a test (e.g., the first one or two seconds of the data shown in Figure III.B.4 displays some oscillations in pressure that we suspect are due to water hammer effects and not actual movement of the water column), but should not affect data in the middle and latter portions of a test.

A series of field experiments was designed to test the possibility of frictional flow losses in each of the components of the system listed above. In order to simplify the testing procedure, the multilevel slug-test system was not used for these experiments. Instead, all experiments were carried out using a single packer inflated in the cased region of a well with a short screened interval. This configuration allows for a long length of well casing between the top of the packer and the static water level.

GEMS well 10-1 (depth = 17.25 m, screen length = .76 m) was selected for the initial series of tests. The packer was placed just above the screened region and two transducers were placed in the well above the packer. One transducer was placed immediately above the packer (7.59 m below static water level) and one was placed slightly below the static water level (.58 m below static water level). Thus, there was 7.01 m of casing separating the two transducers. If there are significant flow losses within the casing, normalized plots of the transducer data should differ. Figure III.B.6 displays data from two tests of this series: Test 1, which employed an H_0 of 1.07 m, and Test 6, which employed an H_0 of 6.83 m. Note that on both plots the early-time data display pressure oscillations that are attributed to the water hammer effects accompanying the opening of the flow-through pipe in the packer. In both plots, the transducer closest

III.B.3

to the packer displays the largest early-time pressure oscillation, consistent with a water hammer explanation (Parmakian, 1963). After the early-time pressure transients have passed, there is little to no difference between the normalized pressure measurements from the transducers. Thus, frictional flow losses within the cased region of the well do not appear to be an important mechanism for these tests. Note that Figure III.B.6 clearly indicates that the dependence of slug-test responses on H_0 is seen with the single packer setup. Note also that a Hvorslev plot of the tests of Figure III.B.6 will display a marked concave downward curvature. Thus, the same behavior was observed in the single packer tests as in the multilevel packer tests. This would imply that the PVC pipe employed in the multilevel system is not primarily responsible for the observed behavior.

The next series of field tests was designed to assess whether frictional losses within the flow-through pipe of the packer could be an explanation for the observed behavior. In order to test the importance of this mechanism, a transducer must be placed below the packer and isolated from the region above the packer. Unfortunately, there is not enough room in a .05 m ID well to place such a transducer-packer arrangement. Therefore, work was shifted to GEMS well 0-6 (depth = 24.69 m, screen length = 1.52 m, radius = .127 m), which is currently the only large-diameter observation well at the site. Unfortunately, GEMS 0-6 is screened in the bedrock underlying the alluvial deposits, so the velocity of the slug-test induced flows is considerably lower than in the wells sited in the sand and gravel section of the alluvium. Preliminary testing, however, did reveal that the slug-test responses at this well displayed a similar dependence on H_0. In addition, a slight downward curvature was seen on Hvorslev plots of tests when a very large H_0 (7.39 m) was employed. Thus, even a well sited in material of lower permeability displayed much of the same anomalous behavior.

A simple transducer-packer arrangement was constructed at the KGS for this set of experiments. The transducer cable was run through the central flow-through pipe of the packer until the bottom of the packer, a short distance above the location of the plug used to initiate the slug tests, at which point it passes out of the flow-through pipe at a T connection. A compression fitting was placed on the cable at the T connection to ensure that no water leaked into the flow-through pipe along the transducer cable. This setup enabled the transducer sensor to be placed below the packer, isolated from the region above the packer. A series of experiments was performed in the field and laboratory to ensure a watertight seal was obtained with the compression fitting and that the transducer was truly isolated from the cased region above the packer. Neither in

III.B.4

these experiments nor in any of the following tests was there any indication of leakage in this system.

Figure III.B.7 displays the head data from a test (H_0 = 6.88 m) in the first series using the transducer-packer arrangement. The upper transducer is located above the packer, .46 m below the static water level. The lower transducer is located below the packer, 11.88 m below the static water level (total distance between the two transducers is 11.42 m). The plotted data show that there are differences between the two transducers in the early portions of the test. These differences, however, become negligible later in the test. Some flow losses do seem to occur within the packer flow-through pipe, but, since the differences do not extend through the entire test, they are probably not the primary reason for the observed anomalous behavior. A comparison of Figures III.B.6 and III.B.7 shows that recovery to the static water level in the bedrock well takes much longer than in the wells sited in the sand and gravel section. The velocities in the flow-through pipe in the wells in the sand and gravel section are clearly much greater than in the bedrock well and thus the effect of frictional losses in the flow-through pipe should be larger. However, given that a similar dependence on H_0 is observed in the bedrock and alluvial wells, frictional losses in the flow-through pipe are probably still not the primary mechanism producing the anomalous responses.

In order to further assess the possible role of the packer in the production of the observed behavior, an additional series of experiments was run in which the packer arrangement was not employed. Instead, PVC pipes (.06 m OD) of differing lengths (1.60 and 3.10 m), which had been filled with sand and sealed at both ends, were used to perform the slug tests. A slug test was initiated by rapidly lowering a PVC pipe below the static water level, causing a rise in water levels. Pipes of different lengths cause the H_0's to be different (H_0 = .36 m for short pipe and = .69 m for large pipe). Figure III.B.8 displays the results from two tests of this series. As with tests using the packer, a dependence on H_0 is observed. Thus, flow losses in the central flow-through pipe in the packer do not appear to be the primary mechanism producing the observed dependence on H_0.

Frictional losses in the well screen appear to be the most likely source of the observed behavior. Unfortunately, there is not an easy way of testing the importance of this mechanism in the field. An initial attempt at assessing the importance of frictional losses in the well screen was made using the transducer-packer arrangement discussed earlier. In this case, a piece of well screen (1.52 m in length) was screwed on to the

bottom end of the flow-through pipe. The transducer situated below the packer was located outside this section of screen. The idea was to mount a piece of screen whose slot size was smaller than that used in the well screen at GEMS 0-6. The screen with the smallest slot size should be the feature with the most resistance to flow in the system. If frictional losses in this screen are important, measurements from the transducer located below the packer outside the mounted screen should differ from the measurements from transducers above the packer. A series of experiments with screens of two different slot sizes were performed. In all cases, the responses were similar to those of Figure III.B.7. There were no additional losses of any significance. We suspect, however, that this result may be more of a function of experimental design (i.e. slot sizes of mounted screen are too large, slots of screen in well are encrusted with mud, etc.), so further tests are planned both in the laboratory and field in an attempt to better assess the importance of this mechanism.

Summary

An initial series of multilevel slug tests was performed at a well sited in the sand and gravel section at GEMS. The data from this series of tests indicated that the slug-test responses at this well were being affected by mechanisms not accounted for in the conventional theory. An inverse relationship between the magnitude of the induced slug (H_0) and the estimated conductivity, a concave downward curvature to data plotted in the Hvorslev format, and systematic deviations between the test data and the best-fit conventional models were the most obvious indications of these mechanisms. Additional experiments indicated that some of these processes also affect slug-test responses in a well in the less permeable bedrock underlying the alluvial section at GEMS.

A large number of field experiments were performed in an attempt to identify the relevant mechanisms producing the observed behavior. The results of these experiments indicated that frictional flow losses in the well casing, in the PVC pipe string used in the multilevel slug-test system, and in the flow-through pipe in the packer were not the primary mechanisms producing the observed responses. Experiments to assess the importance of frictional flow losses within the well screen produced ambiguous results. Further work is needed to assess the role of flow losses within the well screen and possible non-Darcian flow in the aquifer.

Although the work described here is ongoing, an important recommendation can be made about the performance and analysis of slug tests. A series of slug tests at a well

should always be performed using at least two different H_0's (preferably differing by at least .5 m). If plots of the response data normalized by the corresponding H_0 all coincide, then one can feel confident that some variant of the conventional approach for analysis of slug-test data can be employed. As shown in the experiments described in this section, the use of only one H_0 in a series of slug tests could lead to considerable error in the estimated parameters. It is important to note that the behavior described here has, to the best knowledge of the authors, never been reported on in the literature. This is not especially surprising due to the fact that H_0 is almost never varied during a program of slug testing and that most slug tests are performed and analyzed in a rather approximate fashion. However, if our ability to predict contaminant movement in the subsurface is to be improved, it is essential that the error being introduced into the modeling analyses by the use of incorrect parameter values be diminished.

Although field experiments directed at defining the relevant mechanisms producing the anomalous behavior have not yet been completed, work has already begun on the development of a theory to account for some of the observed behavior. In the next section of this report, a theory based on the incorporation of a nonlinear flow term into the Hvorslev model is described and examples of application of the theory to data from wells at GEMS are presented.
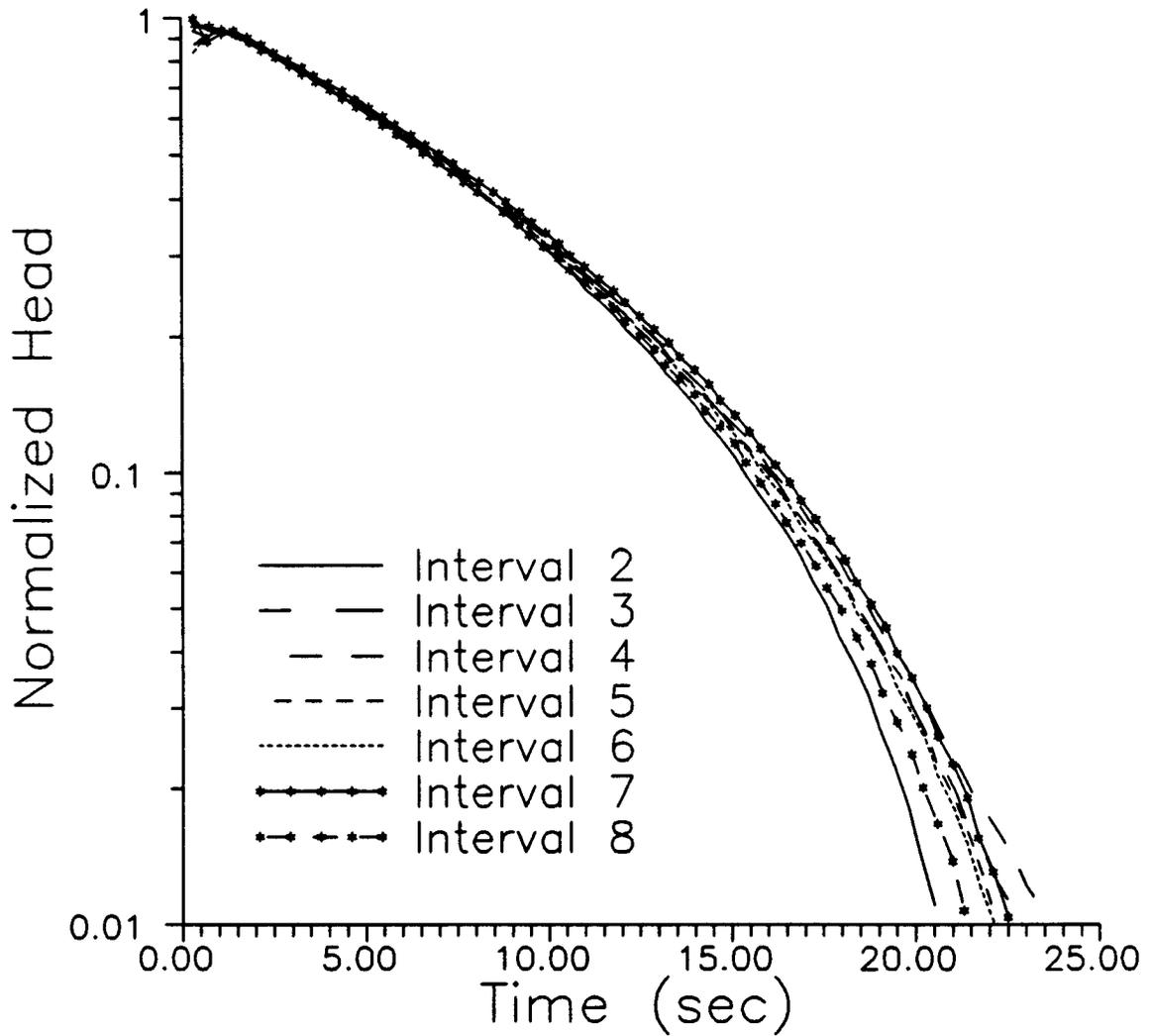
Figure III.B.1 - Normalized head (H/H_0) versus time plots for slug tests in seven intervals of GEMS well 2-5 $(H_0 = 3.07 \text{ m})$. See Table III.B.1 for depths corresponding to each interval.
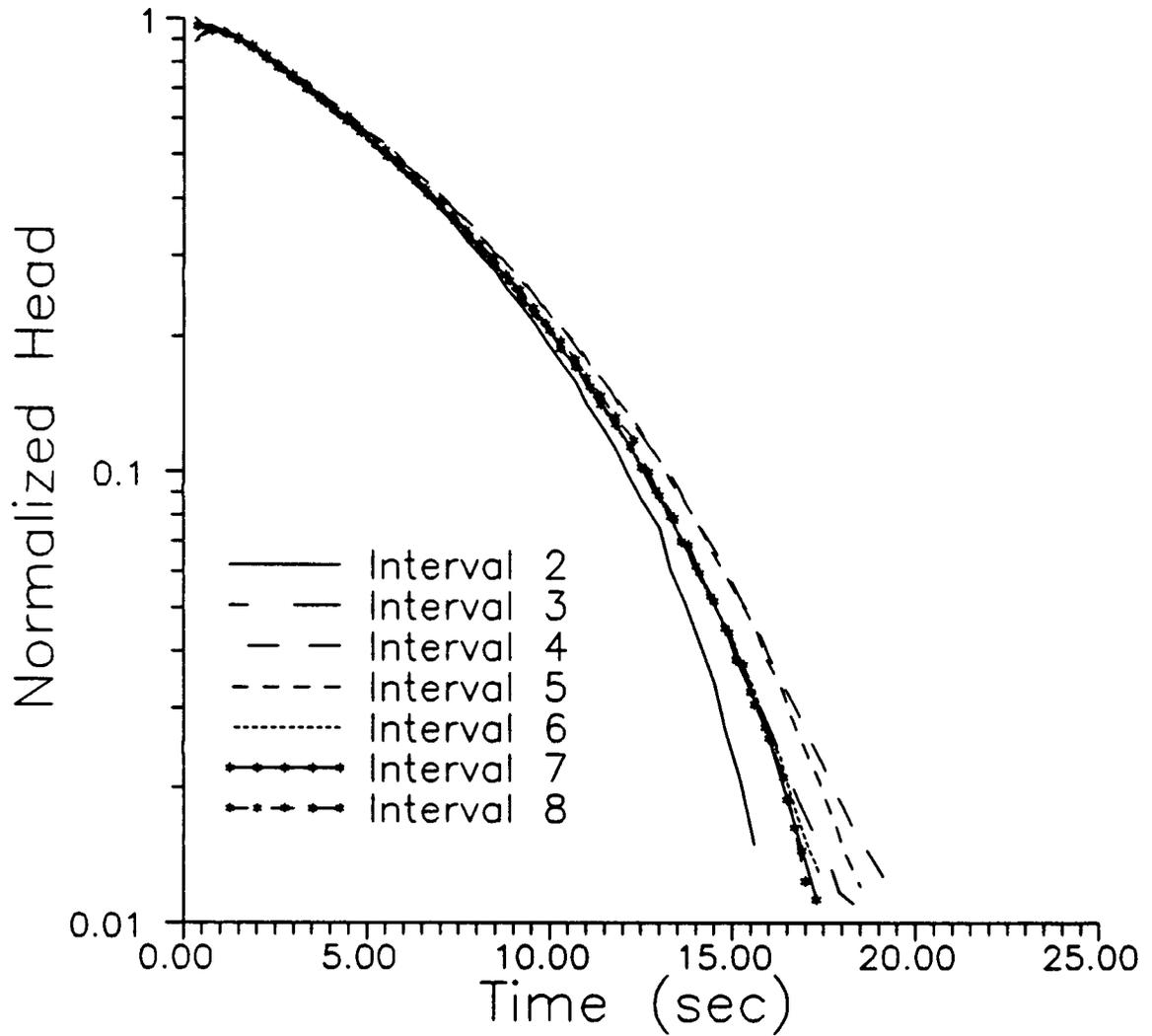
Figure III.B.2 - Normalized head (H/H$_0$) versus time plots for slug tests in seven intervals of GEMS well 2-5 (H$_0$ = 1.65 m). See Table III.B.1 for depths corresponding to each interval.
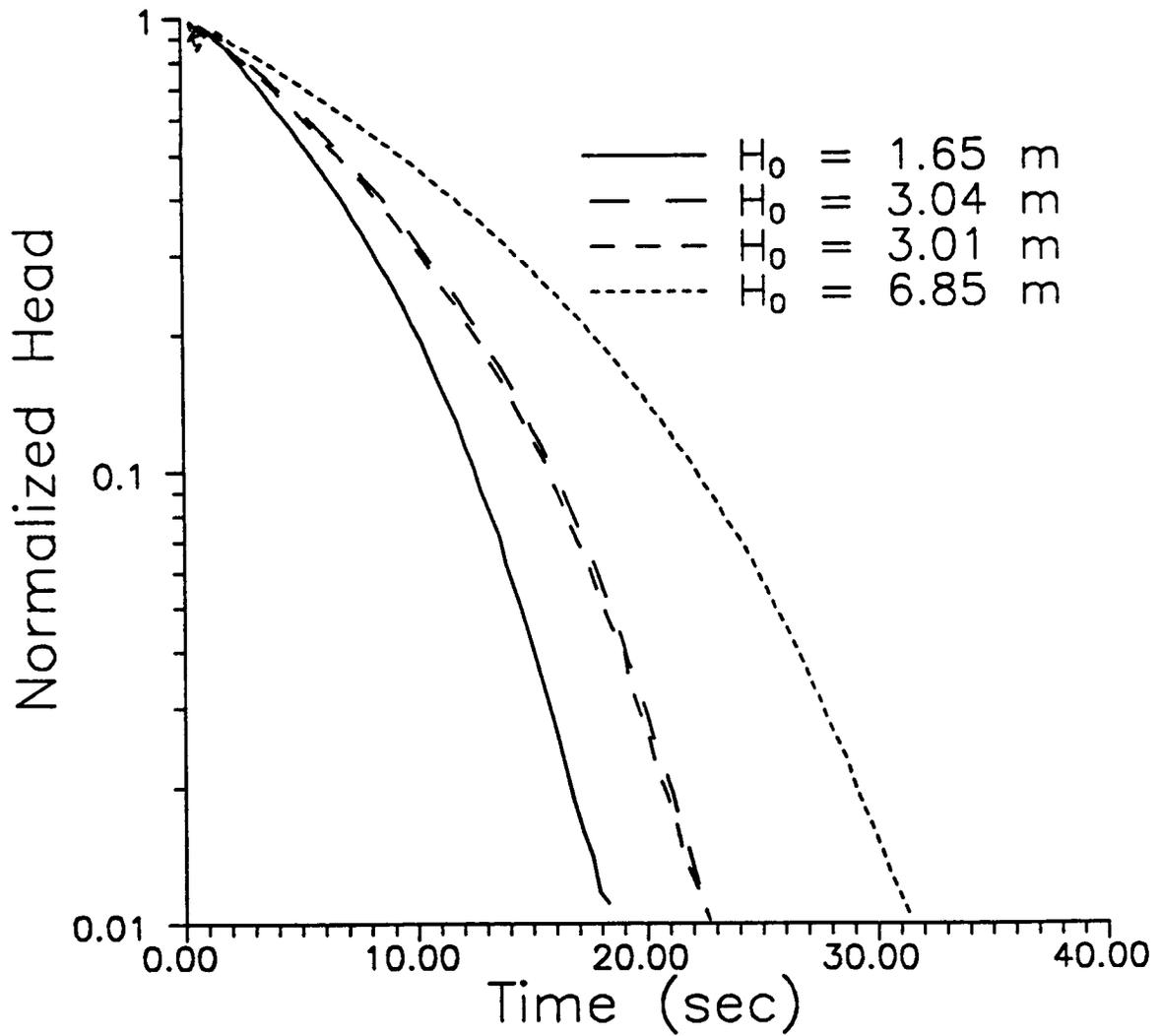
Figure III.B.3 - Normalized head (H/H$_0$) versus time plots for slug tests in the third interval (19.77-20.05 m) of GEMS well 2-5 using H$_0$'s of different magnitudes.
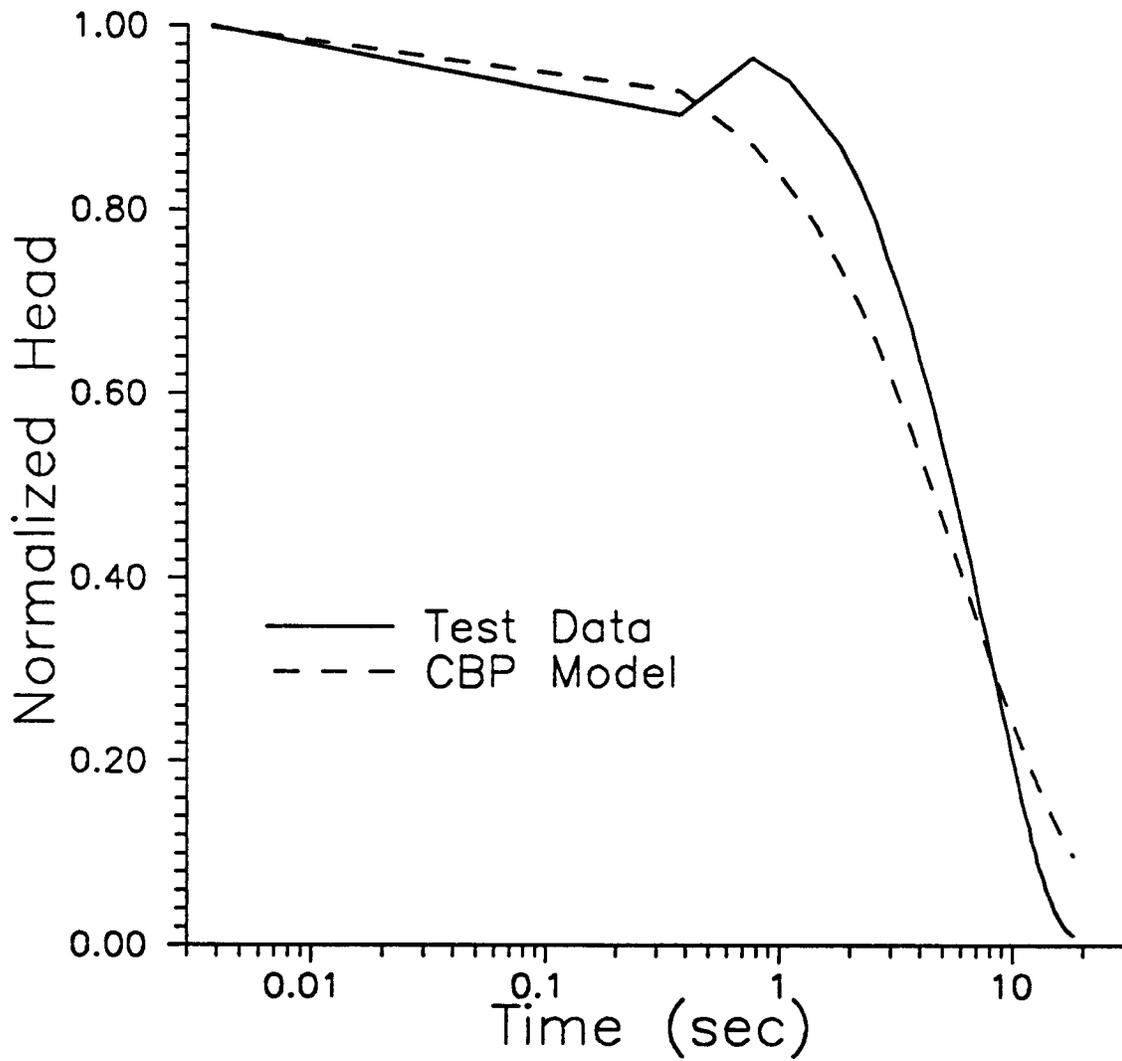
Figure III.B.4 - Normalized head (H/H_0) versus time plots of slug-test data from interval 3 (19.77-20.05 m) of GEMS well 2-5 and the best-fit CBP model.
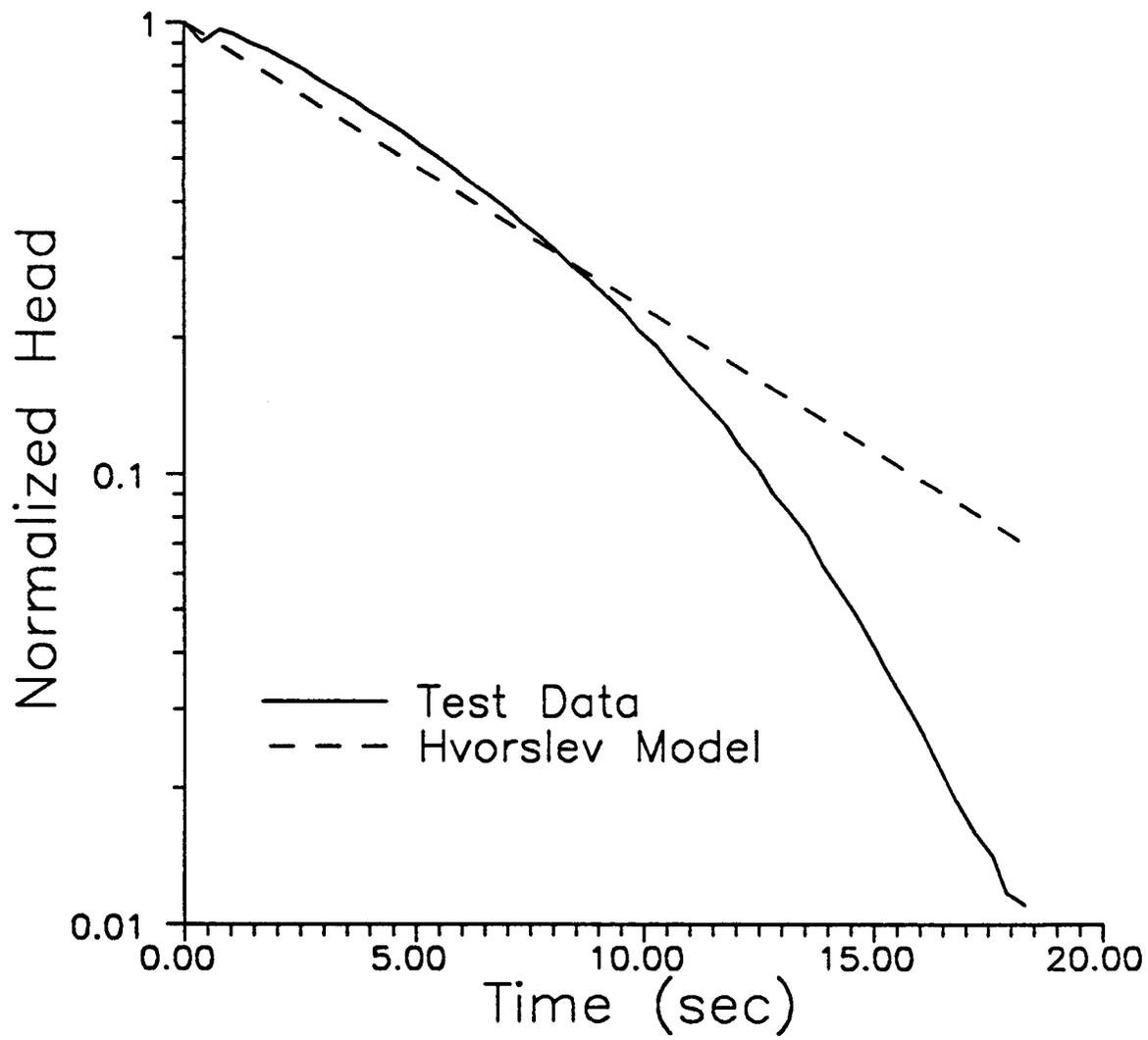
Figure III.B.5 - Normalized head (H/H$_0$) versus time plots of slug-test data from interval 3 (19.77-20.05 m) of GEMS well 2-5 and the best-fit Hvorslev model.
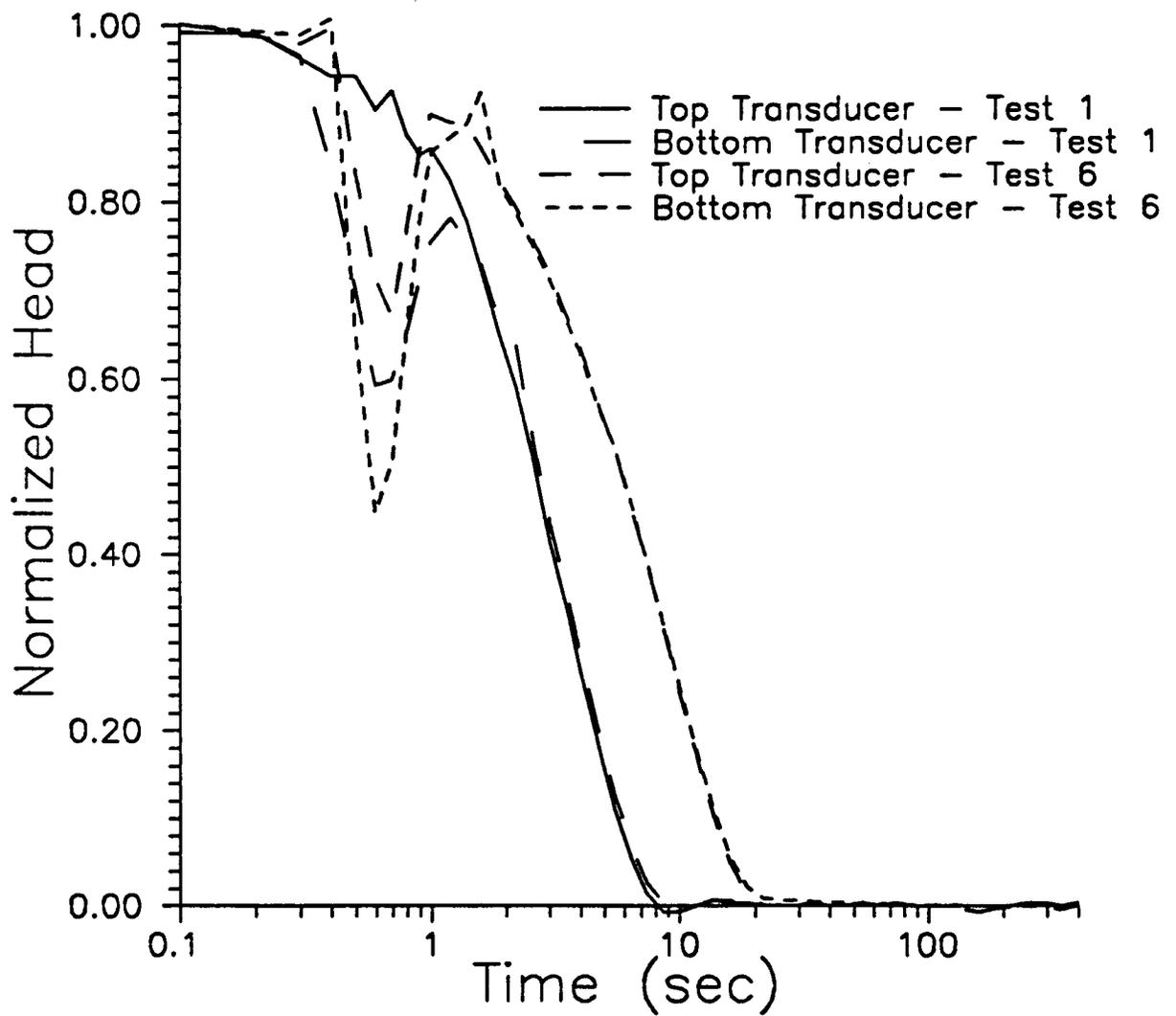
Figure III.B.6 - Normalized head (H/H_0) versus time plots for two slug tests at GEMS well 10-1 (H_{01} = 1.07 m; H_{06} = 6.83 m). Note that two transducers were used in each test.
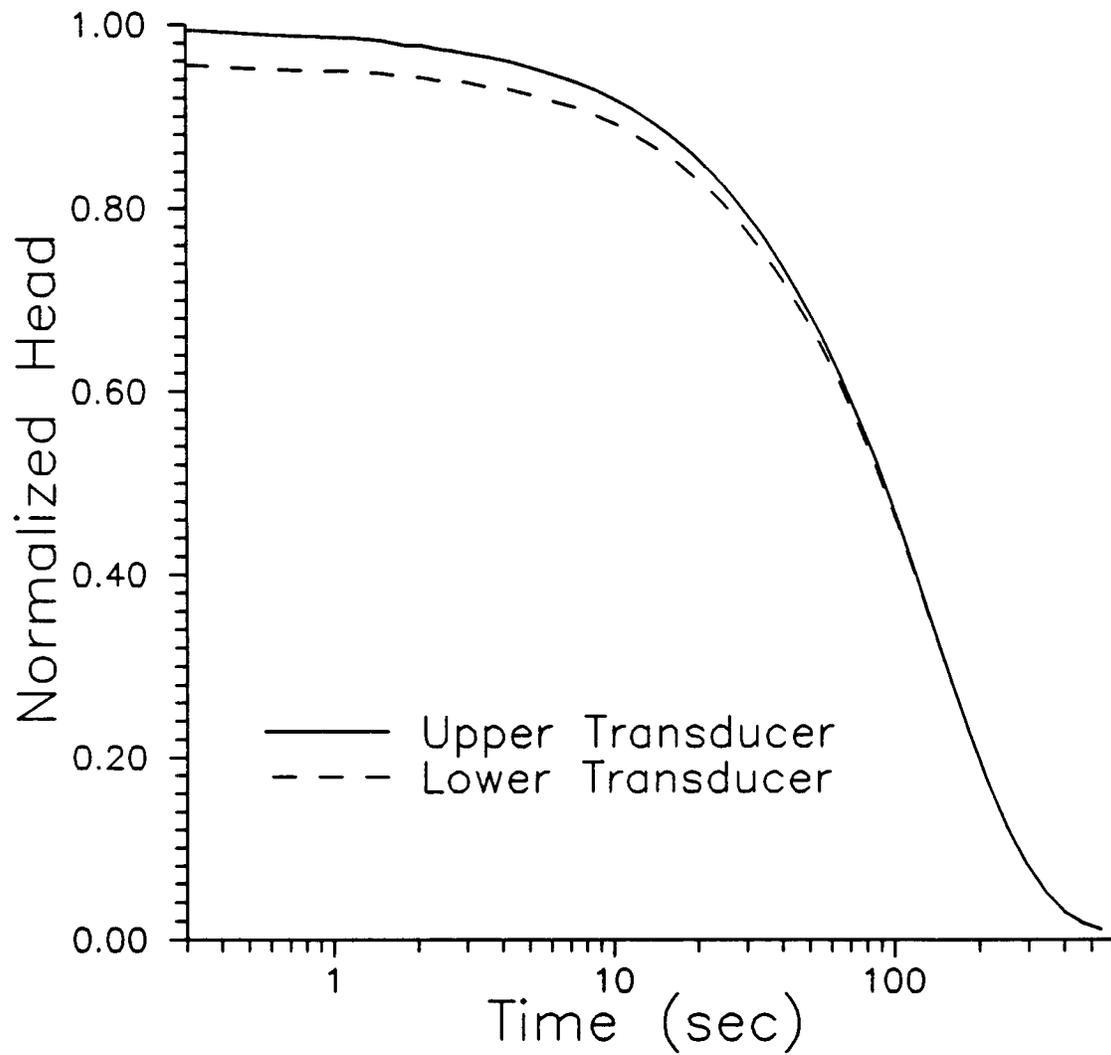
Figure III.B.7 - Normalized head (H/H₀) versus time plots for slug test at GEMS well
0-6 (H_0 = 6.88 m). Note that the transducer-packer arrangement described in the text
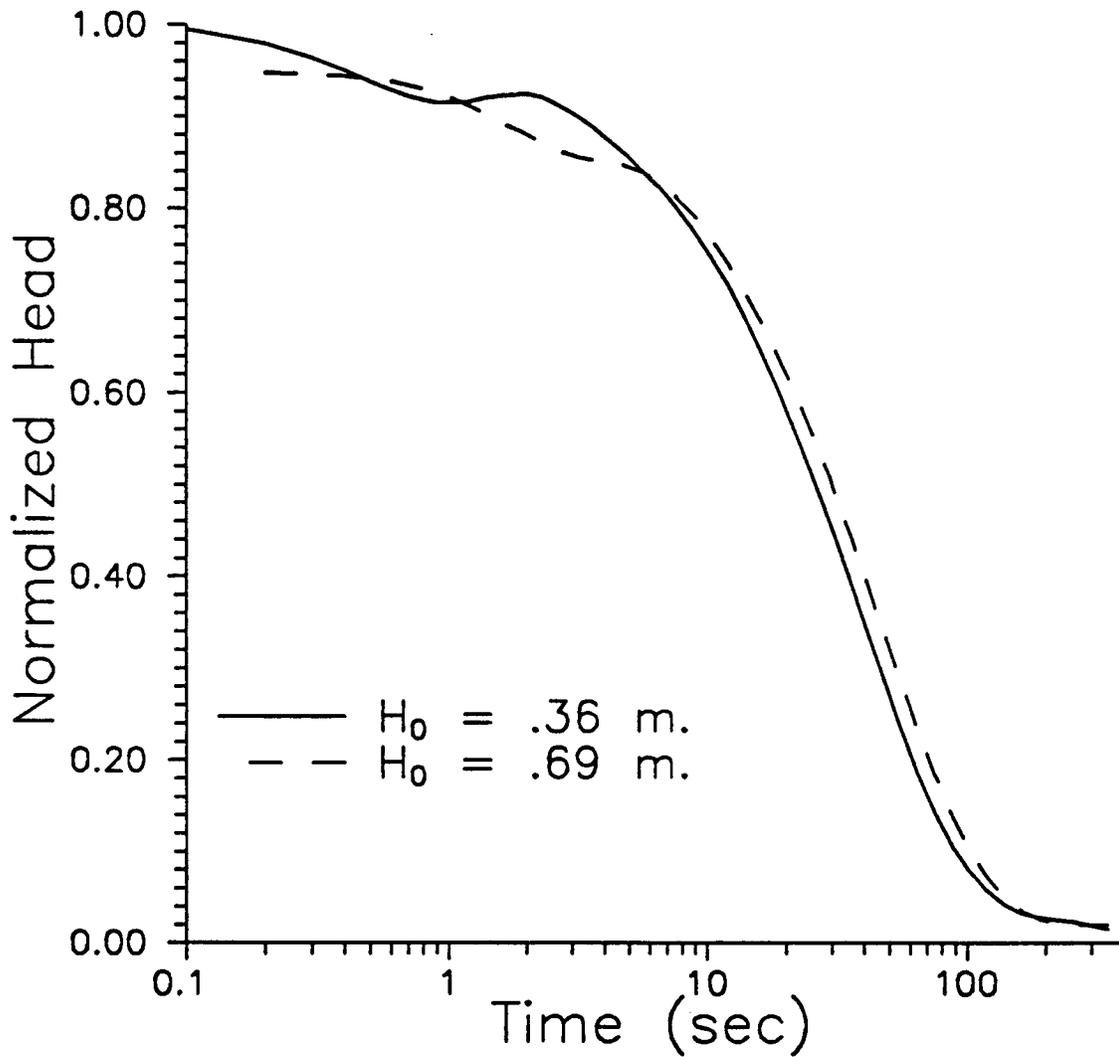was used in this test.

Figure III.B.8 - Normalized head (H/H_0) versus time plots for two slug tests at GEMS well 0-6 (H_{01} = 0.36 m; H_{02} = 0.69 m). Note that these slug tests were initiated using the PVC pipes described in the text.

Interval (m)	K_{HV} (10^{-3} m/s)	K_{CBP} (10^{-3} m/s)	H_0 (m)
20.07 - 20.36	0.2105	0.0682	6.88
20.07 - 20.36	0.2136	0.0693	6.86
20.07 - 20.36	0.3499	0.1124	1.66
20.07 - 20.36	0.2856	0.0921	3.06
20.07 - 20.36	0.2960	0.0956	3.12
19.77 - 20.05	0.3499	0.1135	1.65
19.77 - 20.05	0.2785	0.0904	3.04
19.77 - 20.05	0.2881	0.0938	3.01
19.77 - 20.05	0.2045	0.0664	6.85
19.46 - 19.74	0.3377	0.1098	1.74
19.46 - 19.74	0.2797	0.0911	3.05
19.46 - 19.74	0.2805	0.0913	3.03
19.46 - 19.74	0.2074	0.0676	6.86
19.15 - 19.43	0.3347	0.1085	1.62
19.15 - 19.43	0.2823	0.0917	3.04
19.15 - 19.43	0.2673	0.0864	3.28
19.15 - 19.43	0.2011	0.0652	6.85
18.83 - 19.12	0.3539	0.1177	1.58
18.83 - 19.12	0.2839	0.0922	3.03
18.83 - 19.12	0.2777	0.0900	3.19
18.83 - 19.12	0.2031	0.0660	6.87
18.52 - 18.81	0.3481	0.1124	1.60
18.52 - 18.81	0.2723	0.0882	3.23
18.52 - 18.81	0.2908	0.0943	2.94
18.52 - 18.81	0.2068	0.0672	6.90
18.22 - 18.50	0.3441	0.1111	1.69
18.22 - 18.50	0.2868	0.0929	3.01
18.22 - 18.50	0.2941	0.0955	2.99
18.22 - 18.50	0.2117	0.0688	6.92

Table III.B.1 - Results of Hvorslev (K_{HV}) and CBP (K_{CBP}) analyses for the multilevel slug tests using different initial heads (H_0). Interval nos. increase down table (top is no.2).

III.B.16

C. DEVELOPMENT OF A NONLINEAR MODEL FOR ANALYSIS OF SLUG-TEST DATA

Introduction

As described in the previous section and in section IV.A, slug-test response data from wells in the sand and gravel aquifer at GEMS are being affected by mechanisms not accounted for in the conventional theory on which the standard methods for data analysis are based. One possible mechanism that could be producing the anomalous observed behavior is friction between the water and the casing walls or screen slots. In this section, an additional term is incorporated into the Hvorslev model to account for frictional losses within the well screen. The initial model that is developed will assume that frictional losses in the well screen are independent of water velocity. However, since frictional effects are generally proportional to some power of the velocity, the final model developed here will assume a dependence of frictional losses on velocity. This velocity dependence will lead to a model of a nonlinear form. Following model development, several example applications of the new model to data from slug tests at GEMS are given.

Incorporation of Frictional Flow Losses into the Hvorslev Model

Constant Resistance

The conventional Hvorslev equation is

$$Q(t) = \pi r_c^2 \frac{\partial H(t)}{\partial t} = -FK \cdot h(t) \qquad \text{(III.C.1)}$$

where

Q(t) = flow into/out of the well in response to induced slug;

H(t) = height of water in well at time t;

h(t) = head of water in the aquifer just outside the screen;

K = hydraulic conductivity;

F = Hvorslev geometric factor;

r_c = casing radius.

If there is a loss in head across the screen due to wall or slot friction, H(t) and h(t) will not be the same. This results in

$$Q(t) = -\left(\frac{H(t) - h(t)}{R}\right)$$ (III.C.2)

where R is the resistance factor. In this first case, we consider R a constant and see what are the consequences. Replacing h(t) in equation (III.C.1) with equation (III.C.2) and eliminating Q(t) gives

$$\pi r_c^2 \frac{\partial H(t)}{\partial t} = -FK \cdot (Q(t)R + H(t))$$ (III.C.3a)

$$\frac{\partial H(t)}{\partial t} = \frac{-FK}{\pi r_c^2(1 + FKR)} \cdot H(t)$$ (III.C.3b)

Equation (III.C.3b) is easily solved to give the solution

$$Ln(H(t)) = \frac{-FK}{\pi r_c^2(1 + FKR)} t + const.$$ (III.C.4)

Clearly, this equation will plot as a straight line on a log-linear plot just as the traditional Hvorslev method, the only difference being that the slope is modified by the resistance factor (R). Equation (III.C.4) shows that a constant resistance can not give the concave downward behavior or the dependence on initial head that we observe in the slug-test data from GEMS.

Resistance Proportional to a Power of the Velocity

The more realistic assumption is that the resistance is proportional to some power of the velocity. For simplicity, usually only the first or second power of velocity is considered. If we assume R is proportional to the first power of the water velocity in the well casing, we obtain

$$R = A \cdot |V| = A \left|\frac{dH(t)}{dt}\right|$$ (III.C.5)

III.C.2

where A is an assumed constant of proportionality. Using equation (III.C.5) for R and substituting into equation (III.C.3a) gives

$$\pi r_c^2 \frac{dH(t)}{dt} = -FK\left[H(t) + Q(t)A \left| \frac{dH(t)}{dt} \right| \right].$$ (III.C.6a)

Using equation (III.C.1) to eliminate Q(t) gives the result

$$\frac{dH(t)}{dt} \left[1 + FKA \left| \frac{dH(t)}{dt} \right| \right] = -\frac{FK}{\pi r_c^2} H(t)$$ (III.C.6b)

The generalization of equation (III.C.5) for any power (N) of the velocity is

$$R = A \cdot |V|^N = A \left| \frac{dH(t)}{dt} \right|^N.$$ (III.C.7)

Similarly, the generalization of equation (III.C.6) is

$$\frac{dH(t)}{dt} \left[1 + FKA \left| \frac{dH(t)}{dt} \right|^N \right] = -\frac{FK}{\pi r_c^2} H(t).$$ (III.C.8)

Numerical Solution

Equation (III.C.8) is nonlinear in the variable H(t) and in general can not be solved in closed form. However, it does yield to standard numerical solution techniques. We have tried several possibilities. One form that has worked well is explored here. Solving equation (III.C.8) for the time derivative of H(t) results in the following

$$\frac{dH(t)}{dt} = \frac{-\dfrac{FK}{\pi r_c^2} H(t)}{\left[1 + FKA \left|\dfrac{dH(t)}{dt}\right|^N\right]} \qquad \text{(III.C.9)}$$

The time derivatives in equation (III.C.9) can be evaluated numerically by the central difference rule.

$$\left[\frac{\partial H(t)}{\partial t}\right]^{n+1/2} = \frac{H^{n+1} - H^n}{\Delta t} \qquad \text{(III.C.10)}$$

where H^n is the value of H(t) at time n and Dt is the time step between times n+1 and n. Evaluating equation (III.C.9) at time n+1/2 and using equation (III.C.10) along with the Crank-Nicolson approximation

$$H^{n+1/2} = \left(H^{n+1} + H^n\right)/2$$

gives the following numerical approximation

$$H^{n+1} = H^n - \frac{\dfrac{\Delta t \cdot FK}{2\pi r_c^2}\left(H^{n+1} + H^n\right)}{\left[1 + FKA\left|\dfrac{H^{n+1} - H^n}{\Delta t}\right|^N\right]}. \qquad \text{(III.C.11)}$$

However, equation (III.C.11) still can not be solved directly since H^{n+1} appears on both sides of the equation. Therefore, we must resort to an iterative scheme by adding another superscript to be the interactive index. $H^{n(m)}$ is the m th iteration value at the nth time level. Rewriting equation (III.C.11) with iteration indices results in the following form

$$H^{n+1(m+1)} = H^n - \frac{\frac{\Delta t}{2t_0}\left(H^{n+1(m)} + H^n\right)}{\left[1 + FKA\left|\frac{H^{n+1(m)} - H^n}{\Delta t}\right|^N\right]} \qquad \text{(III.C.12)}$$

where we have also used the standard definition of the Hvorslev time lag

$$t_0 = \frac{\pi r_c^2}{FK} \qquad \text{(III.C.13)}$$

Equation (III.C.12) must be iterated until there is relatively little difference in the H(t) for consecutive iterations. At that point one can move on to another time step and repeat the iteration procedure. In this way the complete time dependence of H(t) can be generated numerically. We have implemented this scheme with N=2 in the automated well-test analysis program SUPRPUMP (Bohling and McElwee, 1992). Note that when N=2 is employed, the simulated data does display a pronounced downward curvature on the standard log-linear Hvorslev plot. Also, examination of (III.C.12) shows that this model will produce a dependence on initial head. Thus, the two major anomalous features seen in the GEMS data can be reproduced by this model.

Application of Nonlinear Model to GEMS Data

The nonlinear model was applied to data from a series of slug tests at GEMS. Figures III.C.1-III.C.3 are representative of the fits that were obtained. In all cases, when slug-test data from a well sited in the sand and gravel section of GEMS were analyzed with this model, very good fits were obtained.

Although the fits were dramatically improved by use of this approach (compare Fig. III.C.3 with Figs. III.B.4-III.B.5), the conductivity estimates indicate that we still have not incorporated all the relevant mechanisms into the model. This is clearly shown by Figures III.C.1-III.C.2, which display slug-test response data from two tests done at the same well using different initial heads. The conductivities estimated from these data using the nonlinear Hvorslev model are .000984 m/s and .000641 m/s for the low and high initial head cases, respectively. Thus, there still seems to be an inverse dependence of estimated conductivity on the magnitude of the initial head. Further work is being carried out in an attempt to explain this continued dependence on initial head.
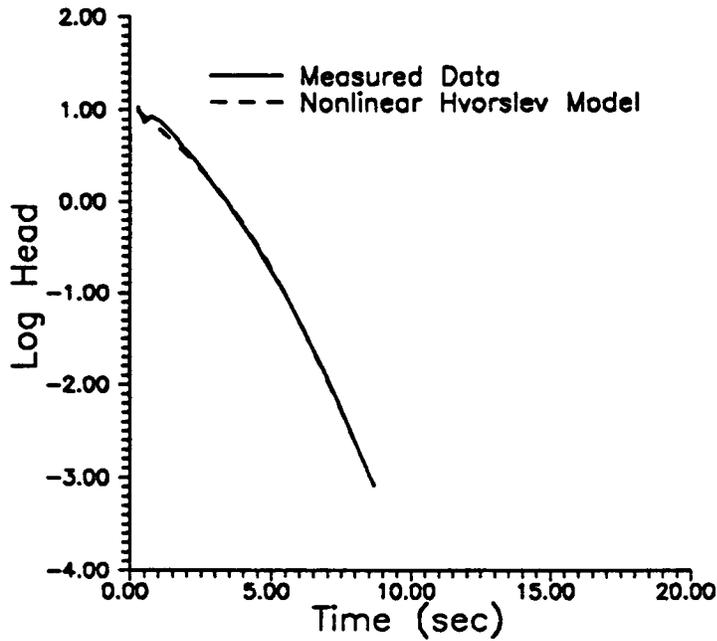
Figure III.C.1 - Natural logarithm of head versus time plots of slug-test data from GEMS well 0-2 (H_0=.88 m) and the best-fit nonlinear Hvorslev model
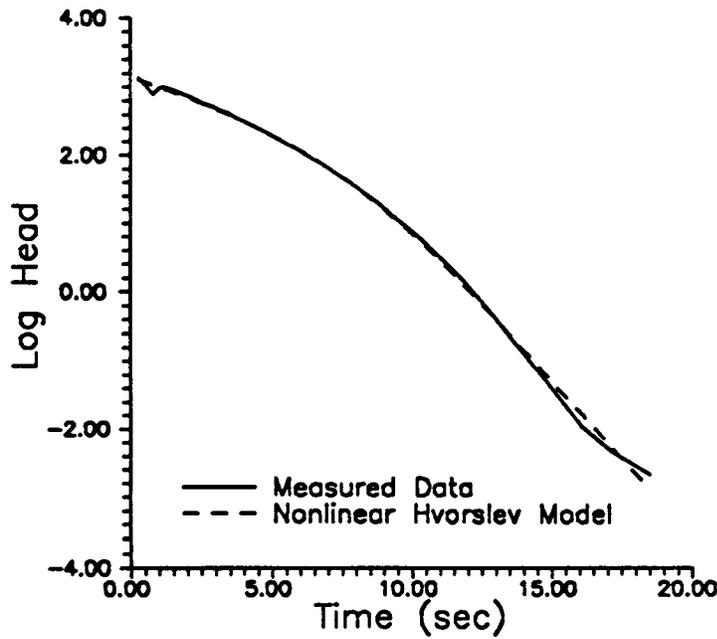

Figure III.C.2 - Natural logarithm of head versus time plots of slug-test data from GEMS well 0-2 (H_0=7.05 m) and the best-fit nonlinear Hvorslev model

V. CONSTRUCTION PROJECTS AND EQUIPMENT PURCHASES

Additional Bladder Sampler

Considerable construction and assembly of equipment has taken place during this first year. An additional complete bladder sampler was constructed to allow uninterrupted sampling in case the first one should sustain damage (which it did). We traveled to Otis Air Force Base on Cape Cod, Mass. to demonstrate our bladder sampler to the USGS, June 9-14, 1991. The sampler performed well there and has received a lot of attention nationally. The continued consistent performance of our bladder sampler is very significant in that we can reliably obtain the samples needed for the characterization of the hydraulic conductivity distribution in coarse sand and gravel.

Laboratory Equipment

A laboratory pressure standard was constructed to calibrate all pressure transducers (both field and laboratory) and establish their accuracy. A laboratory grade power supply was obtained to supply voltage to pressure transducers and other laboratory equipment. Three new laboratory pressure transducers were acquired to replace some older ones that have or will fail. Miscellaneous small hand tools were also acquired so that tools were not shared between field and laboratory activities. A vacuum pump was obtained to help in sample resaturation (accurate determination of hydraulic conductivity requires that the samples be as free of air as possible). The laboratory apparatus for measuring hydraulic conductivity on cores has been upgraded for greater accuracy by adding digital temperature measurement and a caliper for measuring water levels in the manometers. There is a carryover of $5-6000. in the equipment category that has been earmarked for low permeability equipment. This equipment will allow us to measure the hydraulic conductivity of silt and clay samples. We were not able to complete the purchase this first year of the grant. We wanted to evaluate this equipment before purchasing it and were not able to attend a one day seminar with hands on training until late in this grant period. Consequently, our state fiscal year end procedures prevented us from making the purchases this grant period.

Field Equipment

A portable field trailer (commercial travel trailer) is in the process of being outfitted to handle our equipment for all standard field work. This will take the place of the field laboratory structure that was originally proposed. We feel this portable field unit will give much more flexibility. A new highly accurate and flexible IEEE-488 bus-based

data acquisition system (including hardware and software) has been obtained and an interface has been constructed for our pressure transducers. This system is much more interactive with the user through a personal computer and should make our data acquisition easier and more efficient. As mentioned in the section on drilling and sampling, we believe the air driven jackhammer is the preferred method of driving the sampler, so we have obtained a used air compressor and jackhammer for all future sampling.

Pumping and developing two inch wells is a difficult operation without the correct equipment. Until recently, few methods were available except air lifting, jet pumps (with their inherent difficulty in priming), hand bailers, and surge blocks. We have obtained two relatively new items that make this work much easier. The first is a PVC hand pump capable of yielding a few gallons per minute. It comes in five foot sections and can be screwed together for whatever depth is needed. The second item is a Grundfos submersible pump which will go down a two inch well and pump at up to nine gallons per minute at shallow depths. It is powered by a converter which runs on 220 AC volts. The converter produces variable frequency voltage to power the pump which means the pump can be run at variable rates. We have found the pump to be very valuable at GEMS; it produces its full rated flow at maximum rpm and can be adjusted to lower rates at will.

Several additional pieces of field equipment have been constructed for special purposes. One of these is a portable grout machine for making a water impermeable seal between the well casing and the wall of the hole. This grouting is necessary for two reasons. First, most state regulations require it to prevent surface contamination of the aquifer. Second, the hydraulic tests that we perform require a good seal if we hope to measure the true aquifer permeability and not some permeability of the bore hole. In years past, we have done this grouting with the full drill rig and that has prevented the timely grouting of some wells (they have stood open for up to four weeks). With this new portable system the grouting can be done in less than an hour or two after drilling the hole. Another piece of equipment we have constructed allows slug testing directly through the center of hollow stem auger flights while drilling. We constructed this equipment because it seemed that sometimes a well skin was being developed around the well in the process of drilling and completing it. With this arrangement, a screened section of casing is driven ahead of the auger flights into virgin aquifer material and a slug test performed there. The only disturbance is due to driving the pointed two inch casing into place. This procedure should give us the best chance of testing relatively undisturbed aquifer material in situ. The equipment was constructed but was not tested in

this grant period. Another piece of constructed equipment was a tripod for lowering equipment down a well. The equipment to be lowered typically is a pump or packer on the end of pump rods or cable. The tripod is powered by an electric winch that runs off car batteries and is highly controllable. It was designed to easily raise and lower equipment weighting about three hundred pounds or less (in testing, it could lift around nine hundred pounds at its upper limit). At the GEMS site, where shallow depths are the rule, we will not need this much lifting power except when working with larger pumps in future planned four inch diameter holes.

An additional piece of equipment we have acquired is an ultrasonic level indicator for directly measuring the water level in a well. Currently, we use pressure transducers to infer what the water level is by measuring the pressure. However, when the water column is moving or accelerating the pressure may not give a correct indication of the water level due to inertial effects. In coarse sand and gravel aquifers, such as at GEMS, the water velocity in the well casings during slug tests can be high, so these effects can be pronounced. With this piece of equipment we will have an independent check of the water level which can be compared to the pressure transducers. We believe that this equipment will help us explain some effects that we consistently see in slug tests at GEMS.

Computer Laboratory

A computationally intensive project like this one needs the benefit of state-of-the-art computers. Originally, we had budgeted for two top of the line 386 machines; however, computer technology is advancing very rapidly and prices are continuing to fall at an equally rapid pace. Consequently, we were able to buy four computers for the price originally budgeted for two. Four computers (two 386 machines and two 486 machines) have been purchased on this grant and they are used for both research and teaching. The 486 machines, which are very fast (33Mhz), have large memories (16 Megabytes) and contain large hard disks (200 Megabytes) have greatly aided the research. The 386 machines run at 25Mhz, have 4 megabytes of memory and 70 megabytes of hard disk space. The 386 machines serve dual purposes of research and education. Also an HP Laser Jet III printer has been obtained. This acquisition means that two laser printers are available in the computer laboratory. A network for printer sharing has been set up so that every computer has access to a high quality laser printer. In addition, each computer is connected to our main frame computer (Data General machine). In this way each computer can act as a terminal into the mainframe and information can be shared between

the two systems. Miscellaneous software has been obtained to allow the computers to function efficiently for our specific tasks.

A computer laboratory has been set up to give access to the computers for both research and teaching. The laboratory currently contains five computers (one new 486 machine, two new 386 machines, and two older computers). The computer laboratory is used by our research group and other geohydrology graduate students. The computer laboratory allows hands on computer training to geohydrology graduate students through formal class work. We have taught two classes: Physics 727/Geology 771, Finite Element Methods, spring semester 1992 (7 students), and Physics 727/Geology 771, Finite Difference Methods, fall semester 1991 (7 students). In addition, we have made the laboratory available for other computer oriented classes taught by other hydrogeology faculty members. We expect this computer laboratory to continue to be a valuable asset to our research and graduate education in geohydrology.

VI. PERSONNEL AND PRODUCTIVITY ISSUES

A. PUBLISHED AND PLANNED PAPERS

Published Papers

The following papers were published in this grant period, however, they were not directly supported by this grant due to the long lead time for publication. The material covered is very closely related to the present work and was instrumental in putting together the present project.

McElwee, C.D., Butler, J.J., Jr., and Healey, J.M., 1991, A new sampling system for obtaining relatively undisturbed samples of unconsolidated coarse sand and gravel: *Ground Water Monitoring Review*, v. 11, no. 3, pp. 182-191.

Bohling, G.C. and McElwee, C.D., 1992, SUPRPUMP: An interactive program for well test analysis and design: *Ground Water*, v. 30, no. 2, pp. 262-268.

Butler, J.J., Jr., and W.Z. Liu, 1991, Pumping tests in nonuniform aquifers - the linear strip case, *Journal of Hydrology*, v. 128, pp. 69-99.

Papers Planned or in Preparation

The following papers are planned for future publication in professional journals. Currently they exist as informal Kansas Geological Survey Open File Reports.

McElwee, C.D., Bohling, G.C., and Butler, J.J., Jr., Sensitivity analysis of slug tests: *Ground Water* or *Journal of Hydrology*.

Butler, J.J., Jr., McElwee, C.D., Liu, W.Z., and Bohling, G.C., Effects of partial penetration, anisotropy, boundaries and well skin on slug tests: *Ground Water* or *Journal of Hydrology*.

Bohling, G.C., Hyder, Z., Liu, W.Z., Butler, J.J., Jr., and McElwee, C.D., A numerical model of slug tests in layered geologic systems: *Ground Water* or *Journal of Hydrology*.

McElwee, C.D., Butler, J.J., Jr., Bohling, G.C., and Liu, W.Z., The use of observation wells with slug tests: *Ground Water* or *Journal of Hydrology*.

Liu and Butler, A time-continuous numerical model for well tests in heterogeneous aquifers, *Journal of Hydrology*.

B. LIST OF PARTICIPATING PERSONNEL

McElwee, C.D.- PI, is a Senior Scientist at the Kansas Geological Survey (KGS) in the Mathematical Geology Section and is also an Adjunct Professor in the Geology Department of the University of Kansas (KU).

Butler, J.J. Jr. - Co-PI, is an Assistant Scientist at the KGS in the Geohydrology Section and is also an Adjunct Assistant Professor in the KU Geology Department.

Bohling, G.C. - Investigator, is a Research Assistant in the Mathematical Geology Section at KGS.

Macpherson, G.L. - Investigator, is an Assistant Professor in the KU Geology Department.

Miller, R.D. - Investigator, is an Assistant Scientist at the KGS and is the Chief of the Exploration Services Section of the KGS.

Liu, W. - is a student Research Assistant in the Geohydrology Section at KGS and is working on a Ph.D. degree in the KU Civil Engineering Department.

Mennicke, C.M. - is a student Research Assistant in the Mathematical Geology Section at KGS and is working on a Ph.D. degree in the KU Geology Department.

Hyder, Z. - is a student Research Assistant in the Mathematical Geology Section at KGS and is working on a Ph.D. degree in the KU Civil Engineering Department.

C. INTERACTIONS WITH OTHER RESEARCH GROUPS
Papers Presented at Professional Meetings

Bohling, G.C., Hyder, Z., Liu, W.Z., Butler, J.J., Jr., and McElwee, C.D., 1991, A numerical model of slug tests in layered geologic systems: *Eos, Trans. Amer. Geophys. Union*, v. 72, no. 44, p. 146. Also KGS Open-File Report no. 91-62, 22 pp.

McElwee, C.D., Butler, J.J., Jr., Bohling, G.C., and Liu, W.Z., 1991, The use of observation wells with slug tests: *Eos, Trans. Amer. Geophys. Union*, v. 72, no. 44, p. 220. Also KGS Open-File Report no. 91-63, 32 pp.

Butler, J.J., Jr., and McElwee, C.D., 1991, Hydrogeologic characterization of hazardous waste sites, 8th Annual Water and the Future of Kansas Conf. Proc., pp. 10-11 (invited talk).

McElwee, C.D. and Butler, J.J., Jr., 1992, Effective transmissivities from slug tests in wells with a skin: *Eos, Trans. Amer. Geophys. Union*, v. 73, no. 14, p. 126.

USGS trip to Otis Air Force Base

Carl McElwee traveled to Otis Air Force Base on Cape Cod, Mass. to demonstrate our bladder sampler to United States Geological Survey (USGS) researchers, June 9-14, 1991. There are a number of pollution problems at the base, our work was involved with a study of a sewage plume (LeBlanc, 1984; Hess and LeBlanc, 1987). Kathryn Hess of the New England District of the USGS Water Resources Division organized and supervised the field tests. Our sampler and the Waterloo sampler were compared in a variety of situations. Our sampler performed well there and has received a lot of attention nationally. At deeper depths, where heaving is a problem and recovery is difficult, our sampler performed consistently. It seems that this bladder sampler can be very useful in a variety of situations where samples are needed to characterize the hydraulic conductivity distribution in coarse sand and gravel.

Trip to University of Nebraska

Jim Butler traveled to the University of Nebraska at Lincoln to give an invited talk and to meet with researchers in hydrogeology, Jan. 31 - Feb. 1, 1992. The talk, entitled "Well testing in heterogeneous formations", was part of the T. Mylan Stout Lecture Series in the Dept. of Geology. Dr. Vitaly Zlotnik was the leader of the research group with whom meetings were held.

VII. SUMMARY OF YEAR ONE RESEARCH AND OUTLOOK FOR YEAR TWO

A. SUMMARY OF RESEARCH IN YEAR ONE

The major focus of the first year of this project was on the use of slug tests to describe spatial variations in hydraulic conductivity. This research on slug tests in heterogeneous formations had both theoretical and field components.

The theoretical work was directed at developing a better understanding of the type of information that can be obtained from slug tests in heterogeneous units. Since traditional modeling techniques are of limited effectiveness for the analysis of slug-test data from wells in heterogeneous formations, a new numerical model, which is continuous in time and employs an approximate representation of flow in the well bore, was developed. This model was then used in a detailed study of slug tests in layered aquifers. The results of this study helped to 1) define the manner in which layer properties are vertically averaged during a slug test, 2) demonstrate that observation wells can provide useful information about vertical variations in formation properties, and 3) delineate conditions when multilevel slug tests can provide little information about vertical variations in hydraulic conductivity within a unit. The technique of sensitivity analysis was then employed to study the form of the effective parameters obtained from slug tests in wells surrounded by a finite-radius zone of low permeability (well skin). These effective parameters are shown to be heavily influenced by the properties of the well skin. Since observation wells were shown to be of use in the analysis of slug tests in layered aquifers, the final component of the theoretical analysis was a detailed examination of slug tests with observation wells. This analysis showed that the use of observation wells in slug tests can significantly improve the reliability of the estimated parameters.

The field component of this study of slug tests in heterogeneous formations mainly concentrated on an assessment of multilevel slug tests in highly permeable alluvium. A prototype multilevel slug-test system, built at the KGS, was tested at GEMS. The results of the multilevel tests indicated that slug tests in the sand and gravel section at GEMS are being affected by mechanisms not accounted for in the conventional theory on which the standard methods for slug-test data analysis are based. The existence of these mechanisms were reflected by a concave downward curvature on log head versus arithmetic time plots, a dependence of slug-test responses on the magnitude of the induced slug (H_0), and systematic deviations between plots of the test data and the best-fit

conventional models. A series of experiments were carried out at GEMS in order to clarify the mechanisms producing the observed behavior. Although these experiments have not yet been completed, friction within the well screen is considered the most likely mechanism producing the observed behavior. A nonlinear term has been added to the model of Hvorslev (1951) in order to account for these frictional losses. The initial form of this new nonlinear Hvorslev model appears to be superior to the conventional approaches for the analysis of slug-test data from the sand and gravel section at GEMS. Further work, however, is still needed to identify all the relevant mechanisms affecting slug-test responses at GEMS and to incorporate these mechanisms into a general model that can be used for the analysis of slug-test data.

In addition to the research on slug tests in heterogeneous formations, a significant amount of the work in the first year of this project was directed at increasing our knowledge of the subsurface at GEMS. This work included hydraulic testing of wells in the aquifer and underlying bedrock at GEMS; a detailed study of the aqueous geochemistry of the alluvium and underlying bedrock; continued drilling and sampling activities; further modifications of the bladder sampler developed at the KGS; continued laboratory analyses of the cores obtained with the bladder sampler; and a detailed seismic survey. These characterization efforts, which will continue throughout this project, are directed towards the development of a detailed picture of the subsurface at GEMS, so that we can better assess the results of the hydraulic and tracer tests that are being performed as part of this research.

A considerable amount of construction and assembly of equipment took place during the first year of this project supporting the research effort. This equipment included an additional bladder sampler, a laboratory calibration system for pressure transducers, a portable field trailer, a tripod and winch system for moving equipment in a well, and interfaces for data acquisition equipment.

B. OUTLOOK FOR RESEARCH IN YEAR TWO

The second year of this project will build upon the progress made in year one. The major task of the early part of year two will be to complete the study of the mechanisms that are producing the anomalous behavior in slug tests at GEMS and to incorporate the relevant mechanisms into a new model for the analysis of slug-test data. Following the completion of the slug-test work, the focus of the research will shift to multidimensional pulse tests. The primary emphasis of the remainder of year two will

be an evaluation of pulse tests for providing information concerning the lateral and vertical variations in hydraulic conductivity between wells. A better assessment of this interwell variation should shed light on how these properties might be averaged to form equivalent parameters for mathematical modeling, and thus should lead to more accurate predictions of contaminant movement in the subsurface. As with year one of this project, a significant component of the work in year two will be efforts directed at continued characterization of the subsurface at GEMS. The detailed information collected in this characterization effort will be of vital importance in the third year of this work when tracer tests will be performed at GEMS.

VIII. REFERENCES

Baker, S.R. and Friedman, G.M., 1969, A non-destructive core analysis technique using x-rays: *Jour. Sed. Petrology*, v. 39, no. 4, pp. 1371-1383.

Barker, J.A., 1982, Laplace transform solutions for solute transport in fissured aquifers: *Adv. Water Resources*, v. 5, pp. 98-104.

Birkelo, B.A., Steeples, D.W., Miller, R.D., and Sophocleous, M.A., 1987, Seismic reflection study of shallow aquifer during a pumping test: *Ground Water*, v. 25, pp. 703-709, Nov.-Dec.

Bohling, G.C. and McElwee, C.D., 1992, SUPRPUMP: An interactive program for well test analysis and design: *Ground Water*, v. 30, no. 2, pp. 262-268.

Bohling, G.C., McElwee, C.D., Butler, J.J., Jr., and Liu, W.Z., 1990, User's guide to well test design and analysis with SUPRPUMP version 1.0: KGS Computer Program Series no. 90-3, 95 pp.

Braester, C., and Thunvik, R., 1984, Determination of formation permeability by double-packer tests: *J. of Hydrology*, v. 72, pp. 375-389.

Butler, J. J., Jr., McElwee, C. D., Bohling, G. C., and Healey, J. M., 1991, Hydrogeologic characterization of hazardous waste sites: Kansas Water Resources Research Inst. Contribution No. 289, 129 pp.

Butler, J.J., Jr., 1986, Pumping Tests in Nonuniform Aquifers: A deterministic and stochastic analysis (Ph.D. dissertation): Stanford Univ., Stanford, CA. 220 pp.

Butler, J.J., Jr., and Liu, W.Z., 1991, Pumping tests in nonuniform aquifers - the linear strip case: *J. of Hydrology*, v. 128, pp. 69-99.

Chen, C., 1985, Analytical and approximate solutions to radial dispersion from an injection well to a geological unit with simultaneous diffusion into adjacent strata: *Water Resources Research*, v. 22, no. 4, pp. 1069-1076.

Chen, C., 1986, Solutions to radionuclide transport from an injection well into a single fissure in a porous formation: *Water Resour. Res.*, v. 22, no. 4, pp. 508-518.

Chen, H.T., and Chen, C.K., 1988, Hybrid Laplace transform/finite element method for two-dimensional heat conduction: *J. Thermophys.*, v. 2, no. 1, pp. 31-36.

Chirlin, G.R., 1989, A critique of the Hvorslev method for slug test analysis: the fully penetrating well: *Ground Water Monitoring Review*, v. 9, no. 2, pp. 130-138.

Cooper, H.H., Bredehoeft, J. D., and Papadopulos, I.S., 1967, Response of a finite-diameter well to an instantaneous charge of water: *Water Resour. Res.*, v. 3, no. 1, pp. 263-269.

Crump, K.S., 1976, Numerical inversion of Laplace transforms using a Fourier series approximation: *J. Assoc. Comput. Mach,* v. 23, no. 1, pp. 89-96.

Dagan, G., 1978, A note on packer, slug, and recovery tests in unconfined aquifers: *Water Resour. Res.* , v. 14, no. 5, pp. 929-934.

De Hoog, F.R., Knight, J.H., and Stokes, A.N., 1982, An improved method for numerical inversion of Laplace transforms: SIAM *J. Sci. Stat. Comput.* , v. 3, no. 3, pp. 357-366.

Desbarats, A.J., 1992, Spatial averaging of transmissivity in heterogeneous fields with flow toward a well: *Water Resour. Res.* v. 28, no. 3, pp. 757-767.

Dubner, H., and Abate, J., 1968, Numerical inversion of Laplace transforms by relating them to the finite Fourier cosine transform: *J. Assoc. Comp. Mach.,* v. 15, no. 1, pp. 115-123.

Environmental Protection Agency, 1984, Test Method--The determination of inorganic anions in water by ion chromatography--Method 300.0: U.S. Environmental Protection Agency, EPA-600/4-84-017, 5 pp.

Fishman, M.J. and Friedman, L. C., eds., 1989, Methods for determination of inorganic substances in water and fluvial sediments: U. S. Geological Survey, *Techniques of Water-Resources Investigations,* Book 5, Chapter A1, 545 pp.

Grantham, R.L., 1990, Feasibility of using seismic reflection to detect gas trapped in alluvial materials: Masters thesis, University of Kansas Department of Geology.

Gurtin, M.E., 1965, Variational principles for initial value problems: *Q. App. Math.,* v. 22, pp. 252-256.

Hackett, G., 1987, Drilling and constructing monitoring wells with hollow-stem augers Part 1: Drilling considerations: *Ground Water Monitoring Review,* v. VII, no. 4, pp. 51-62.

Hayashi, K., Ito, T., and Abe, H., 1987, A new method for the determination of in situ hydraulic properties by pressure pulse tests and application to the Higashi Hachimantai geothermal field: *J. Geophys. Res.,* v. 92, no. B9, pp. 9168-9174.

Healey, J., Anderson, J., Miller, R.D., Keiswetter, D., Steeples, D.W., and Bennett, B., 1991, Improved shallow seismic-reflection source: building a better Buffalo : *Soc. Explor. Geophys. Exp. Abs.,* v. 1, p. 588-591.

Hess, K.M., and LeBlanc, D.R. , 1987, Preliminary measurements of aquifer heterogeneity at a tracer-test site, Cape Cod, Massachusetts: EOS, v. 68, no. 16, p. 299.

Hunter, J.A., Pullan, S.E., Burns, R.A., Gagne, R.M., and Good, R.L., 1984, Shallow seismic-reflection mapping of the overburden-bedrock interface with the engineering seismograph–Some simple techniques: *Geophysics*, v. 49, p. 1381-1385.

Hvorslev, M.J., 1951, Time lag and soil permeability in ground-water observations: Bull. no. 36, Waterways Exp. Sta., Corps of Engrs., U.S. Army. 50 pp.

Javandel, M.S., and Witherspoon, P.A. ,1968, Application of the finite element method to transient flow in porous media: *Soc. Pet. Eng. J.* , v. 8, pp. 241-252.

Jiang, X., 1991, A field and laboratory study of scale dependence of hydraulic conductivity: M.S. thesis, Univ. of Kansas, Lawrence, Ks., 149 pp.

Keely, J.F., and Boateng K., 1987, Monitoring well installation, purging and sampling techniques, Part 1: Conceptualizations: *Ground Water,* v. 25, no. 3, pp. 300-313.

Kipp, K.L., Jr., 1985, Type curve analysis of inertial effects in the response of a well to a slug test: *Water Resources Research.*, v. 21, no. 9, pp. 1397-1408.

LeBlanc, D.R, 1984, Sewage plume in a sand and gravel aquifer, Cape Cod, Massachusetts: U.S. Geological Survey Water-Supply Paper 2218.

Liu, W.Z., and Butler, J.J., Jr., 1991, A time-continuous finite difference approach for flow and transport simulations: Kansas Geol. Survey, Open File Report 91-20, 19 pp.

McElwee, C.D., 1987, Sensitivity analysis of ground-water models, *in* Jacob Bear and M. Yavuz Corapcioglu: *Proceedings of the 1985 NATO Advanced Study Institute on Fundamentals of Transport Phenomena in Porous Media*: Martinus Nijhoff Publishers, Dordrecht, The Netherlands, pp. 751-817.

McElwee, C.D., and Butler, J.J., Jr., 1989, Slug testing in highly permeable aquifers (abstract): GSA 1989 Annual Mtg. Abstract with Program, p. A193.

McElwee, C.D., Bohling, G.C., and Butler, J.J., Jr., 1989, Sensitivity analysis of slug tests: Kansas Geol. Survey, Open-File Report 89-33, 29 pp.

McElwee, C.D., Butler, J.J., Jr., and Healey, J.M., 1991, A new sampling system for obtaining relatively undisturbed samples of unconsolidated coarse sand and gravel: *Ground Water Monitoring Review*, v. 11, no. 3, pp. 182-191.

McElwee, C.D., Butler, J.J., Jr., Bohling, G.C., and Liu, W.Z., 1991, The use of observation wells with slug tests: *Eos, Trans. Amer. Geophys. Union*, v. 72, no. 44, p. 220.

McElwee, C.D., Butler, J.J., Jr., Liu, W.Z., and Bohling, G.C., 1990, Effects of partial penetration, anisotropy, boundaries and well skin on slug tests: *Eos, Trans. Amer. Geophys. Union*, v. 71, no. 17, p. 505.

Melville, J.G., Molz, F.J., Guven, O., and Widdowson, M.A., 1991, Multilevel slug tests with comparisons to tracer data: *Ground Water.* v. 29, no. 6, pp. 897-907.

Merey, C, Miller, R.D., Ticken, E.J., and Lewis, J.S., in press, Hydrogeological characterization using a shallow seismic reflection survey at Fort Ord, California: *Soc. Expl. Geophys. Exp. Abs.*

Miler, R.D., Steeples, D.W., and Brannan, M., 1989, Mapping a bedrock surface under dry alluvium with shallow seismic reflections: *Geophysics*, v. 54, pp. 1528-1534.

Miller, R.D., Steeples, D.W., Hill, R., and Gaddis, B., 1990, Identifying intra-alluvial and bedrock structures shallower than 30 meters using seismic-reflection techniques: Soc. Explor. Geophys. volumes on Geotechnical and Environmental Geophysics, Stan Ward, ed., *Volume 3: Geotechnical,* pp. 89-97.

Minning, R.C. , 1982, Monitoring well design and installation: Proceedings of the Second National Symposium on Aquifer Restoration and Ground Water Monitoring, Columbus, Ohio, pp. 194-197.

Moench, A., and Ogata, A., 1984, Analysis of constant discharge wells by numerical inversion of Laplace transform solutions, in: Rosenshein, J., and Bennett, G.D., ed., Groundwater Hydraulics, *AGU Water Resour. Monogr. 9*, AGU, Washington, DC., pp. 146-170.

Moench, A.F., and Hsieh, P.A., 1985, Analysis of slug test data in a well with finite-thickness skin: in *Memoirs of the 17th Intern. Cong. on the Hydrogeology of Rocks of Low Permeability,* v. 17, pp. 17-29.

Moench, A.F., 1984,. Double porosity models for a fissured groundwater reservoir with fracture skin: *Water Resour. Res.,* v. 10, no. 7, pp. 831-846.

Molz, F.J., Guven, O., and Melville, J.G., 1989, Characterization of the hydrogeologic properties of aquifers: The next step: in: Proc. of the Conf. on New Field Techniques for Quantifying the Physical and Chemical Properties of Heterogeneous Aquifers, National Water Well Association, pp. 407-418.

Moridis, G.J., and Reddell, D.L., 1991, The Laplace transform finite difference method for simulation of flow through porous media: *Water Resour. Res.,* v. 27, no. 8, pp. 1873-1884.

Neitzel, E.B., 1958, Seismic reflection records obtained by dropping a weight: *Geophysics*, v. 34, p. 58-80.

Papadopulos, I.S., 1966, Nonsteady flow to multiaquifer wells: *J. Geophys. Research*, v. 71, no. 20, pp. 4791-4797.

Papadopulos, I.S., and Cooper, H.H., Jr., 1967, Drawdown in a well of large diameter: *Water Resour. Res.* , v. 3, no. 1, pp. 241-244.

Parkhurst, D. L., Thorstenson, D. C., and Plummer, L. N., 1980, PHREEQE--A computer program for geochemical calculations: U. S. Geological Survey, *Water-Resources Investigations* , 80-96, 195 pp.

Parmakian, J., 1963, *Waterhammer Analysis* : Dover Pub., New York, 161pp.

Perry, C.A. and Hart, R.J., 1985, Installation of observation wells on hazardous waste sites in Kansas using a hollow-stem auger: *Ground Water Monitoring Review,* v. V, no. 4, pp. 70-73.

Prijambodo, R., Raghavan, R., and Reynolds, A.C., 1985. Well test analysis for wells producing layered reservoirs with crossflow: *Soc. Pet. Eng. J.* , pp. 380-396.

Raghavan, R., 1989, Behavior of wells completed in multiple producing zones: SPE Formation Evaluation, v. 4, no. 2, pp. 219-230.

Riggs, C.O., 1983, Soil sampling in the vadose zone: in: Proc. of NWWA/EPA Conf. on Characterization and Monitoring of the Vadose (Unsaturated) Zone, Las Vegas, Nv., pp. 611-622.

Rushton, K.R., and Chan, Y.K., 1977, Numerical pumping test analysis in unconfined aquifers: *J. Irrigation and Drainage Div.* , v. 103(IR1), pp. 1-12.

Russell, D.G., and Prats, M., 1962, Performance of layered reservoirs with crossflow-single-compressible-fluid case: *Soc. of Petr. Eng. J.* (Dec., 1962), pp. 53-67.

Settari, A., and Aziz, K., 1974, A conputer model for two-phase coning simulation: *Society of Petroleum Eng.* , v. 14, no. 3, pp. 221-236.

Steeples, D.W., and Miller, R.D., 1990, Seismic-reflection methods applied to engineering, environmental, and ground-water problems: Soc. Explor. Geophys. volumes on Geotechnical and Environmental Geophysics, Stan Ward, ed., *Volume 1: Review and Tutorial*, pp. 1-30.

Steeples, D.W., Miller, R.D., and Knapp, R.W., 1987, Downhole .50-caliber rifle—an advance in high-resolution seismic sources: *Soc. Explor. Geophys., Exp. Abs.*, 57th Ann. Mtg., pp. 76-78.

Stehfest, H., 1970, Numerical inversion of Laplace transforms: *Commun. ACM.*, v. 13, no. 1, pp. 47-49.

Sudicky, E.A., 1989, The Laplace transform Galerkin technique: A time-continuous finite element theory and application to mass transport in groundwater: *Water Resour. Res.*, v. 25, no. 8, pp. 1833-1846.

Sudicky, E.A., and McLaren, R.G., 1992, The Laplace transform Galerkin technique for large-scale simulation of mass transport in discretely fractured porous media: *Water Resour. Res.*, v. 28, no. 2, pp. 499-514.

Talbot, A., 1979, The accurate numerical inversion of Laplace transforms: *J. Inst. Math. Appl..*, v. 23, pp. 97-120.

Vennard, J.K., and Street, R.L., 1975, *Elementary Fluid Mechanics*: Wiley and Sons, New York, 740pp.

Zapico, M.M., 1987, Aquifer evaluation procedures-core acquisition and an assessment of slug tests: M.Sc. Thesis, University of Waterloo.

Zapico, M.M., Vales, S. and Cherry, J.A., 1987, A wireline piston core barrel for sampling cohesionless sand and gravel below the water table: *Ground Water Monitoring Review*, v. VII, no. 3, pp. 74-82.

IX. APPENDICES

Appendix A
Numerical Laplace Transforms

This appendix begins by briefly discussing three commonly used numerical methods for the back transformation of Laplace-space functions into real space. The Crump (1976) method is the focus of the remainder of the appendix and the algorithm of De Hoog et al. (1982) is introduced as an approach for accelerating the convergence of the summation series employed in the Crump method.

The inversion step, i.e. the back transformation of the Laplace-space function into real space, is probably the most difficult step of a problem involving the Laplace transformation. Many methods for the numerical inversion of Laplace-space solutions have been employed in the groundwater literature. The most commonly used methods are those of Stehfest (1970), Talbot (1979), and Crump (1976). The numerical inversion scheme of Stehfest produces a solution for one specific time. At least 10 or more Laplace solutions (i.e. 10 p_k values) are usually required for the inversion in order to obtain a solution of acceptable accuracy. The maximum number of Laplace solutions (K) that can be used in the Stehfest algorithm is related to the largest number the computer can manipulate. Generally, K should be assigned a value as large as possible for a given machine in order to minimize the error of the inversion. Once the value of K is selected, the accuracy of the inversion is fixed.

The Talbot inversion algorithm also produces a solution for one specific time. In this case, however, there is no limit on the value of K and thus on the accuracy of the inversion. Computations are terminated when a summation series converges to a prespecified criterion by comparing inversion results obtained using two successive p_k values.

The Crump method differs from both of the preceding methods in that a single set of p_k solutions can be employed to perform the inversion for a range of times. The accuracy of the inversion in this case is determined by both the number of terms in the summation and the values of summation-series parameters.

Previous work (e.g., Barker, 1982; Moench and Ogata, 1984; Moench, 1984; Chen, 1985, 1986; Kipp, 1985;) has shown that all three of the above methods can be used in groundwater flow and transport applications with high accuracy. The selection of an inversion method should therefore be based on the specific requirements of the problem being addressed. If solutions are required at only a few points in time, then the Talbot or Stehfest algorithms are the most appropriate approaches. If, as is often the

case in well-test applications, there are a large number of points in time, the method of Crump (1976) is the most efficient method. Although 3DFDTC enables the user to select either the Stehfest or Crump algorithms, the algorithm of Crump will undoubtedly be the most commonly used approach for well testing applications and thus is the focus of the remainder of this discussion.

Crump (1976) found that a series transformation may be incorporated into (12) of section II.A to speed up the rate of convergence and, at the same time, reduce the truncation error. This approach, known as the epsilon algorithm, produces, without exception, much faster series convergence than a conventional summation. The number of Laplace-space solutions required in the summation series is reduced from hundreds to tens. The epsilon algorithm involves the approximation of the summation series of (12) of II.A by a sequence of partial sums that are calculated using a recursive equation. De Hoog et al. (1982) presents a quotient difference algorithm that dramatically improves on the speed of convergence of the epsilon algorithm. Liu and Butler (1991) provide a detailed description of the De Hoog algorithm, a summary of which is given here.

In the De Hoog algorithm, the summation series inside the brackets of (12) of II.A is rewritten as the real value of the following equation,

$$S_{2N} = \sum_{k=0}^{2N} a_k z^k, \text{ where } z = e^{\frac{i\pi t}{Tmax}} \tag{1A}$$

where

$$z = e^{\frac{i\pi t}{Tmax}};$$

$$a_k = \overline{s_j}(p_k)$$

This summation can be approximated by

$$S_{2N} \approx v(z, 2N) = d_0 / (1 + d_1 z / (1 + \cdots + d_{2N} z)) \tag{2A}$$

where $d_j, \cdots, j=1, 2N$ are called the continued fraction coefficients

and are defined as $d_0 = a_0$, $d_{2n-1} = -q_n^{(0)}$, $d_{2n} = -e_n^{(0)}$, $n=1, \cdots, N$. The initial $e_r^{(i)}$

and $q_r^{(i)}$ terms are defined as:

$e_0^{(i)} = 0$, for $i=0, 1, \cdots, 2N$, and $q_1^{(i)} = \dfrac{a_{i+1}}{a_i}$, for $i=0, 1, \cdots, 2N-1$.

An array of q and e coefficients can be formed using the following relationships

$$\text{for } r = 1, \cdots, 2N, \quad e_r^{(i)} = q_r^{(i+1)} - q_r^{(i)} + e_{r-1}^{(i+1)}, \quad i = 0, \cdots, 2N-2r \quad (3A)$$

$$\text{and for } r = 2, \cdots, N, \quad q_r^{(i)} = q_{r-1}^{(i+1)} e_{r-1}^{(i+1)} / e_{r-1}^{(i)}, \quad i = 0, \cdots, 2N-2r-1 \quad (4A)$$

This array can be written out as

$$
\begin{array}{cccc}
q_1^{(0)} & & & \\
e_0^{(1)} & e_1^{(0)} & & \\
& q_1^{(1)} & q_2^{(0)} & \\
e_0^{(2)} & e_1^{(1)} & e_2^{(0)} & \\
& q_1^{(2)} & q_2^{(1)} & \\
e_0^{(3)} & e_1^{(2)} & & \\
& q_1^{(3)} & & \\
e_0^{(4)} & & &
\end{array}
\qquad (5A)
$$

The following recursive equations can then be used to calculate the terms required in the approximate summation of (2A):

$$A_n = A_{n-1} + d_n z A_{n-2}$$
$$\qquad\qquad n = 1, 2, \cdots, 2N \qquad (6A)$$
$$B_n = B_{n-1} + d_n z B_{n-2}$$

with $A_{-1} = 0$, $B_{-1} = 1$, $A_0 = d_0$ and $B_0 = 1$.

Using these recursive equations, (2A) can now be written as $S_{2n} \approx v(z, 2N) = A_{2N}/B_{2N}$. Equation (12) thus becomes:

$$h_j(t) \approx \frac{1}{Tmax} e^{P_0 t} S_{2N} = \frac{1}{Tmax} e^{P_0 t} RE\left[\frac{A_{2N}}{B_{2N}}\right] \qquad (7A)$$

Liu and Butler (1991) show that use of (7A) instead of the epsilon algorithm approach can reduce the number of terms required in the summation by a factor of two or more. Note that as described by Liu and Butler (1991), careful selection of the Tmax parameter is required in order to realize the maximum computational reductions. Those authors provide recommendations on the selection of Tmax and other summation parameters.

Appendix B

Concepts of Seismic Reflection Prospecting

It is the purpose of this short appendix and the attached figures to describe basic principles and features of seismic reflection. The paper is intended primarily for those who have heard of seismic reflection but do not know how it works.

The seismic-reflection method is a powerful technique for underground exploration that has been in use for over 60 years. The revolution in microelectronics during the past ten years has resulted in the construction of new seismographs and microcomputers for data collection and processing that permit the cost-effective use of seismic reflection in a wide variety of applications that were not feasible previously.

Seismic-reflection techniques depend on the existence of discrete velocity and/or density changes in the subsurface. These discrete changes in either mass density or seismic velocity are known as acoustical contrasts. The measure of acoustical contrast is formally known as acoustic impedance, which is simply the product of mass density and the speed of seismic waves traveling within a material. In many cases, the acoustical contrasts occur at boundaries between geologic layers or formations, although man-made boundaries such as tunnels and mines also represent contrasts

Compressional waves, or P-waves, are the most commonly used type of seismic wave for reflection prospecting. P-waves propagating through the earth behave similar to sound waves propagating in air. P-waves generate echoes (reflections) when they come in contact with an acoustical contrast in the air or under the ground. In the underground environment, however, the situation is more complex because energy that comes in contact with a solid acoustical interface can be transmitted across the interface or converted into refractions and/or shear waves as well as reflected waves.

Seismic reflection is sensitive to the physical properties of earth materials and is relatively insensitive to chemical makeup of both the earth materials and their contained fluids. The seismic-reflection technique involves no assumptions about layering or seismic velocity. However, no seismic energy will be reflected back for analysis unless acoustic impedance contrasts are present within the depth range of the equipment and procedures used. This is identical to the observation that sound waves in air do not echo back to an observer unless the sound wave hits something solid that causes an echo. The classic use of seismic reflections involves identifying the boundaries of layered geologic units. It is important to note that the technique can also be used to search for anomalies such as isolated sand or clay lenses and cavities.

The simplest case of seismic reflection is shown in Figure B-1. A source of seismic waves emits energy into the ground, commonly by explosion, mass drop, or

projectile impact. Energy is radiated spherically away from the source. One ray path originating at the source will pass energy to the subsurface layer and return an echo to the receiver at the surface first. In the case of a single flat-lying layer and a flat-topographic surface, the path of least time will be from a reflecting point midway between the source and the receiver with the angle of incidence on the reflecting layer equal to the angle of reflection from the reflecting layer.

The sound receivers at the surface are called geophones and are essentially low-frequency microphones. The signals from the geophones are transmitted by seismic cables to the recording truck which contains a seismograph. The seismograph contains amplifiers that are very much like those on a stereo music system. The sounds from the earth are amplified and then recorded on digital computer tape for later processing and analysis. The purpose of the computer processing is to separate the echo sounds from other sounds, to enhance them, and to display them graphically.

In the real world, there are commonly several layers beneath the earth's surface that are within reach of the seismic-reflection technique. Figure B-2 illustrates that concept. The reader should note that echoes from the various layers arrive at the geophone at different times. The deeper the layer, the longer it takes for the echo to arrive at the geophone. The fact that several layers often contribute echoes to seismograms tends to make the seismic data more complex.

In the case of a multi-channel seismograph, several geophones detect sound waves almost simultaneously. Each channel has one or more geophones connected to it. Reflections from different points in the subsurface are recorded by various geophones. Note in Figure B-3 that the subsurface coverage of the reflection data is exactly half of the surface distance across the geophone spread. Hence, the subsurface sampling interval is exactly half of the geophone interval at the surface. For example, if geophones are spaced at 16-m intervals at the earth's surface, the subsurface reflections will come from locations on the reflector that are centered 8 m apart.

In Figure B-4 we have placed source locations and receiver locations in such a way that path S1–R2 reflects from the same location in the subsurface as path S2–R1. This is variously called a common-reflection point (CRP) or a common-depth point (CDP), depending upon the preference of the author. The power of the CDP method is in the multiplicity of data that come from a particular subsurface location. By gathering common midpoint data together and then adding the traces in a computer, the reflection signal is enhanced. Before this addition can take place, however, the data must be corrected for differences in travel time for the reflected waves caused by the differences in source-to-geophone distance. The degree of multiplicity is called CDP fold. A

seismograph with 24 channels, for example, commonly is used to record 12-fold CDP data.

The seismic-reflection method is used to determine the spatial configuration of underground geological formations. Figure B-5 shows conceptually what we are trying to accomplish with such a survey. Note that the peaks of the seismic reflections have been blackened to assist in the interpretation. This example is a very simple version of typical near-surface geology that depicts a buried sand lens in a river valley. As the sand lens is moved to deeper layers below the surface, it becomes more difficult to detect, but the physical principles remain the same.

In an earlier part of this discussion, we briefly touched on the analogy between a seismograph and a stereo music system. A stereo music system has control knobs to enhance high frequencies (like a flute) or low frequencies (like a bass drum). A seismograph has similar capabilities in choosing the sound frequencies that are recorded. A seismologist selects the frequencies to be enhanced depending on the depth and size of the underground geologic features of interest.

In order to detect small geologic features, it is necessary to use a seismograph that can record and enhance the high-frequency sound waves. The use of high-frequency seismic waves in reflection seismology is known as "high-resolution" seismic exploration. As research and instrumentation developments allow recording higher and higher seismic frequencies, it is becoming possible to prospect for progressively smaller geologic targets.
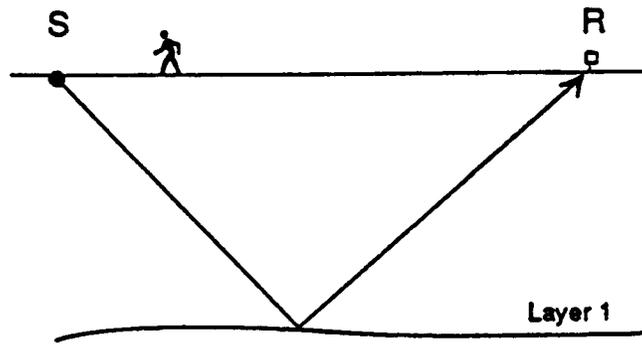
Figure B-1. Reflection from one layer.
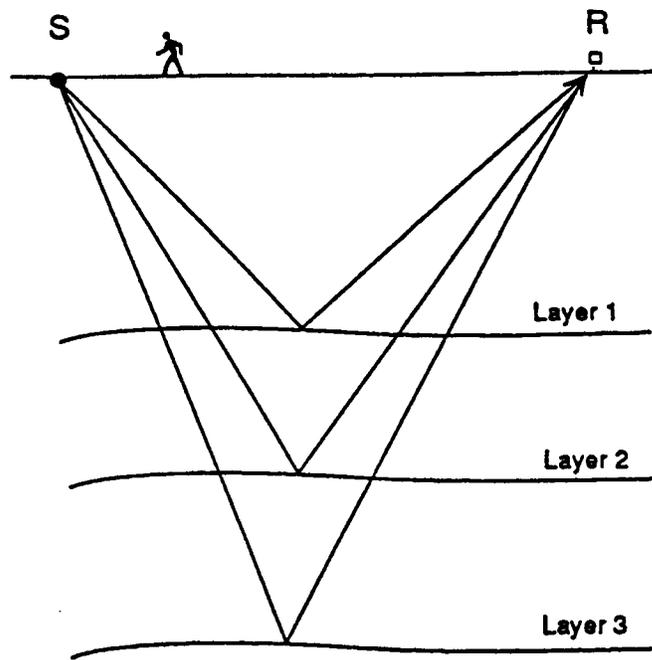
Figure B-2. Reflection from three layers.

Simple Reflection Ray Paths
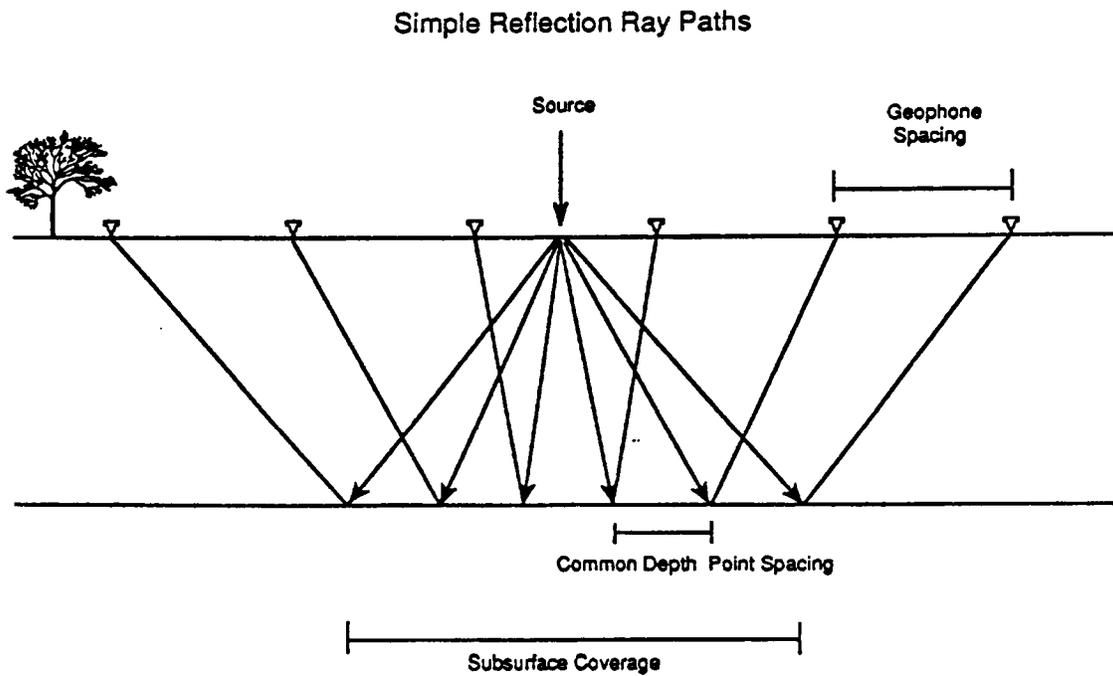
Figure B-3.   Schematic drawing of seismic ray paths for a single shot with a six-channel reflection seismograph.

CDP Concept
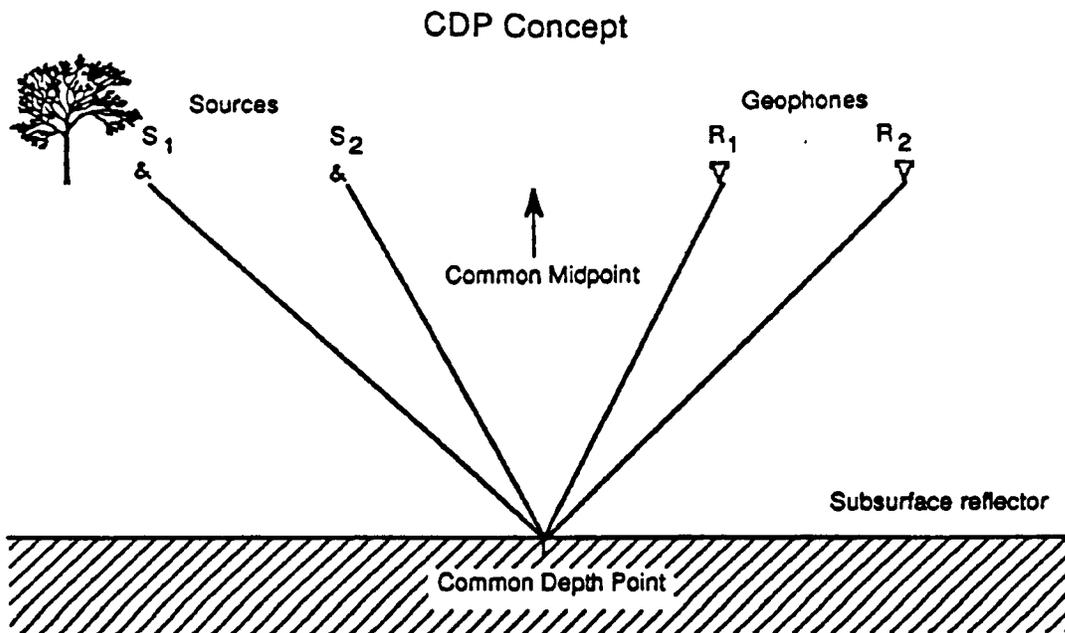
Figure B-4.   The concept of Common Depth Point (CDP). Note that ray paths from two different shots (S1 and S2 reflect from a common point in the subsurface.
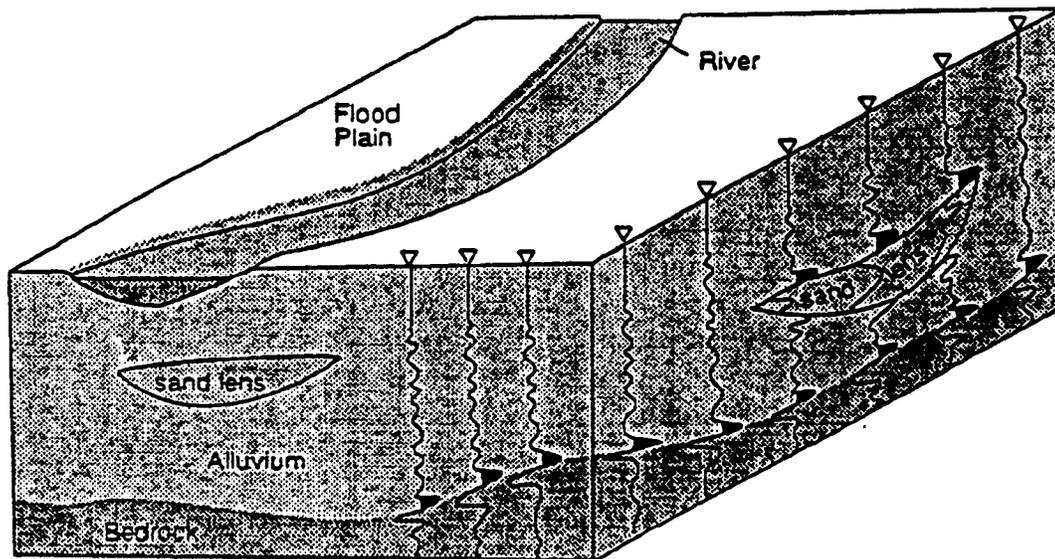
Figure B-5. Schematic showing a seismic section relating to real-world geology.

Appendix C
Approximate Flow Regime Around Bedrock Well

The well test situation is shown schematically in Figure C-1. The well penetrates bedrock, and is screened below the top of the boundary between the bedrock and the alluvium, which is shown as a plane. The well, when pumped causes a cone of depression of the hydraulic head around the well. The maximum radius of this cone of depression is shown as a circle on the plane separating the two units. Also shown schematically are flow lines (arrows) which demonstrate that most flow is horizontal, from the bedrock sandstone into the bedrock well. However, the cone of depression induces downward flow from the alluvium, and this flow moves vertically or obliquely toward the bedrock well.

Assuming the bedrock sandstone is homogeneous and isotropic, it is possible to represent this flow by Figure C-2. This figure shows a vertical slice of Figure A-1 through a vertical plane including the well. The boundary between the bedrock and the alluvium is shown by a heavy horizontal line. The maximum horizontal extent of the cone of depression caused by the pumping test is shown on that boundary as a rectangle. Diagrammatic flow lines are also shown as straight arrows. In fact, the flow lines are probably curved, but for purposes of this exercise they are shown as being straight. The length of the path from the boundary between the alluvium and bedrock increases with increasing distance from the well, with the longest path being from the boundary between the two units starting at the maximum diameter of the cone of depression. The shortest path is that path which is vertical or nearly vertical, closest to the well bore. It is water from the alluvium traveling along this path that will reach the well screen first. Because this path is nearly vertical, it can be treated, as a first approximation, in the same way that column experiments of continuous sources of contaminants are treated. That is, the concentration distribution in the column is described by:

$$D_x \frac{\partial^2 C}{\partial x^2} - v_x \frac{\partial C}{\partial x} = \frac{\partial C}{\partial t}$$

where D_x is the dispersion coefficient in the x direction

C is concentration of a tracer species

x is distance

v_x is flow velocity in the x direction

t is time

Using the boundary and initial conditions that the tracer is a continuous source (or $C(0,t) = C_0$) and that the tracer is not present in the aquifer before the test begins, the above equation is integrated to produce the following solution:

$$C(x,t) = C_0 / 2 \ \text{erfc} \ [\ (x - v \, t) / 2 \ (a_x \, v \, t)^{0.5}]$$

where a_x is the longitudinal dispersivity

erfc is the complementary error function

v is the linear velocity of the water, assumed to be that of the tracer

The longitudinal dispersivity is unknown at GEMS. Assuming it is unity, the equation can be solved for velocity, and, by knowing hydraulic gradient, can be used to estimate hydraulic conductivity.
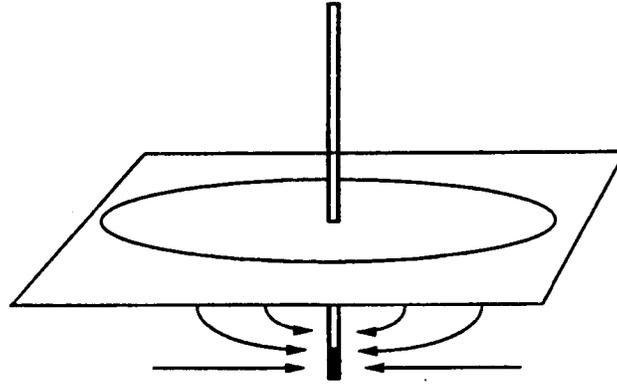
Figure C-1: Schematic diagram of the bedrock well, boundary between the alluvium and bedrock, radius of the cone of depression created during pumping, and possible ground-water flow paths.
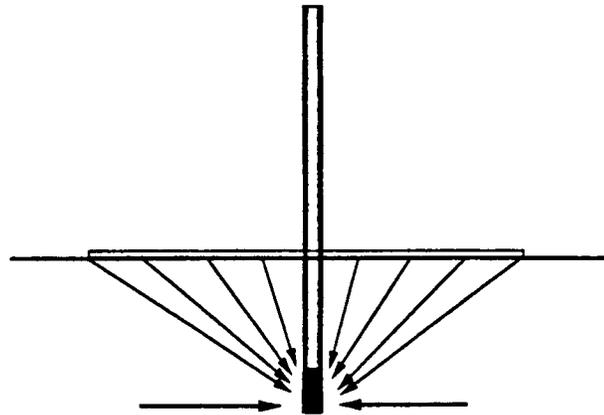
Figure C-2: Vertical cross section through Figure C-1, generalizing ground-water flow paths as straight lines. Note that the flow paths are mostly vertical near the well and increasingly more horizontal with distance from the well.

Appendix D
Walkaway Noise Tests

Preliminary experiments with various parameters and equipment included the 7.3 kg sledge hammer, downhole 30.06 rifle, downhole 50 caliber, 12 gauge auger gun, and 8 gauge auger gun as sources and 50, 100, 140, 200, 280, and 400 Hz analog low cut filters (Figures D1-D28). The direct wave has a strong presence from first arrival to the bottom of the record. The very repetitive nature of this arrival is a direct result of the relatively narrow bandwidth of the wavelet and the high acoustic impedance contrast between the near-surface material and the clay interface at several feet of depth. The high acoustic contrast between the near-surface material and the clay layer channels the energy, creating a standing wave that travels within the low velocity near-surface material. The narrow band nature of the energy makes both analog and digital filtering relatively ineffective. Ground roll is difficult to identify even with no analog low cut filter. This is probably a result of the attenuative nature of the 100 Hz geophones and the near-surface material. Reflections from interfaces deeper than the bedrock surface can be interpreted directly on walkaway displays with analog low cut filters greater than about 100 Hz.

The 96 channel walkaways were recorded by maintaining 48 receiver locations and occupying two different source location separated by 48 ft. This pseudo walkaway recording method resulted in an apparent discontinuity between receiver locations 48 and 49. This signal difference is actually a result of variability in the source locations.

Reflections from the bedrock surface can be identified on most walkaways when the analog low cut filter is in excess of 100 Hz. The dominant frequency and signal-to-noise ratio is significantly higher with the downhole 30.06 than with any other source tested (Figures 2-8). The air-coupled wave and ringy direct and refracted waves represent the most significant obstacles to the recording of high quality reflection events from interfaces shallower than the bedrock surface. The dominant frequency of the bedrock reflection is approximately 200 Hz.

The 70 msec event on most records between 75 and 96 ft offset is interpreted to be the bedrock reflection at this site. The apparent NMO velocity is approximately 3000 ft/sec. The walkaways from the auger guns have slightly more air wave and lower dominant frequency. The 50 cal data as well possess a lower dominant frequency, more air wave, and is sufficiently energetic to overdrive the near offset receivers. The sledge hammer proved an extremely noisy source with significantly more ground roll and air coupled wave. Considering signal quality, dominant frequency, relative source energy, and site preparation the 30.06 represented the ideal source for the site and geologic target.
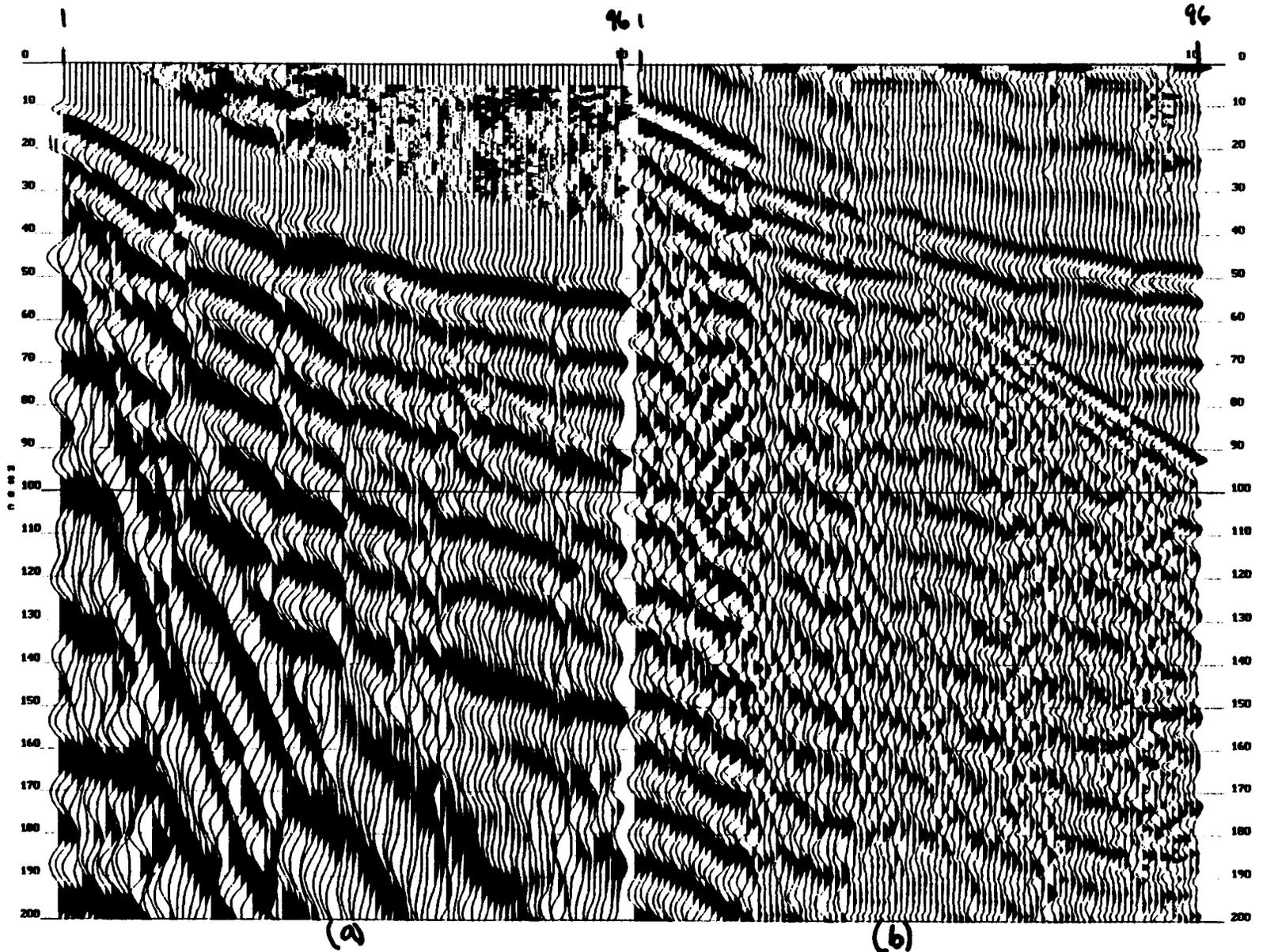
Figures D1.-D7.

Walkaway noise tests with the downhole 30.06 rifle. a) represents the raw field file with a 25 ms AGC scale, b) represents a) with a 100 Hz digital low cut filter.

Figure 1 was recorded with no analog lowcut filters, Figure 2 with analog low cuts at 50 Hz, Figure 3 with analog low cuts at 100 Hz, Figure 4 with analog low cuts at 140 Hz, Figure 5 with analog low cuts at 200 Hz, Figure 6 with analog low cuts at 280 Hz, and Figure 7 with analog low cuts at 400 Hz.

Figures D8.-D14.

Walkaway noise tests with the 12-gauge auger gun. a) represents the raw field file with a 25 ms AGC scale, b) represents a) with a 100 Hz digital low cut filter.

Figure 8 was recorded with no analog lowcut filters, Figure 9 with analog low cuts at 50 Hz, Figure 10 with analog low cuts at 100 Hz, Figure 11 with analog low cuts at 140 Hz, Figure 12 with analog low cuts at 200 Hz, Figure 13 with analog low cuts at 280 Hz, and Figure 14 with analog low cuts at 400 Hz.

Figures D15.-D21.

Walkaway noise tests with the 8-gauge auger gun. a) represents the raw field file with a 25 ms AGC scale, b) represents a) with a 100 Hz digital low cut filter.

Figure 15 was recorded with no analog lowcut filters, Figure 16 with analog low cuts at 50 Hz, Figure 17 with analog low cuts at 100 Hz, Figure 18 with analog low cuts at 140 Hz, Figure 19 with analog low cuts at 200 Hz, Figure 20 with analog low cuts at 280 Hz, and Figure 21 with analog low cuts at 400 Hz.

Figures D22.-D28.

Walkaway noise tests with the downhole 50 cal rifle. a) represents the raw field file with a 25 ms AGC scale, b) represents a) with a 100 Hz digital low cut filter.

Figure 22 was recorded with no analog lowcut filters, Figure 23 with analog low cuts at 50 Hz, Figure 24 with analog low cuts at 100 Hz, Figure 25 with analog low cuts at 140 Hz, Figure 26 with analog low cuts at 200 Hz, Figure 27 with analog low cuts at 280 Hz, and Figure 28 with analog low cuts at 400 Hz.

Figures D1.

Source to Receiver Offset (ft)

IX.D.3

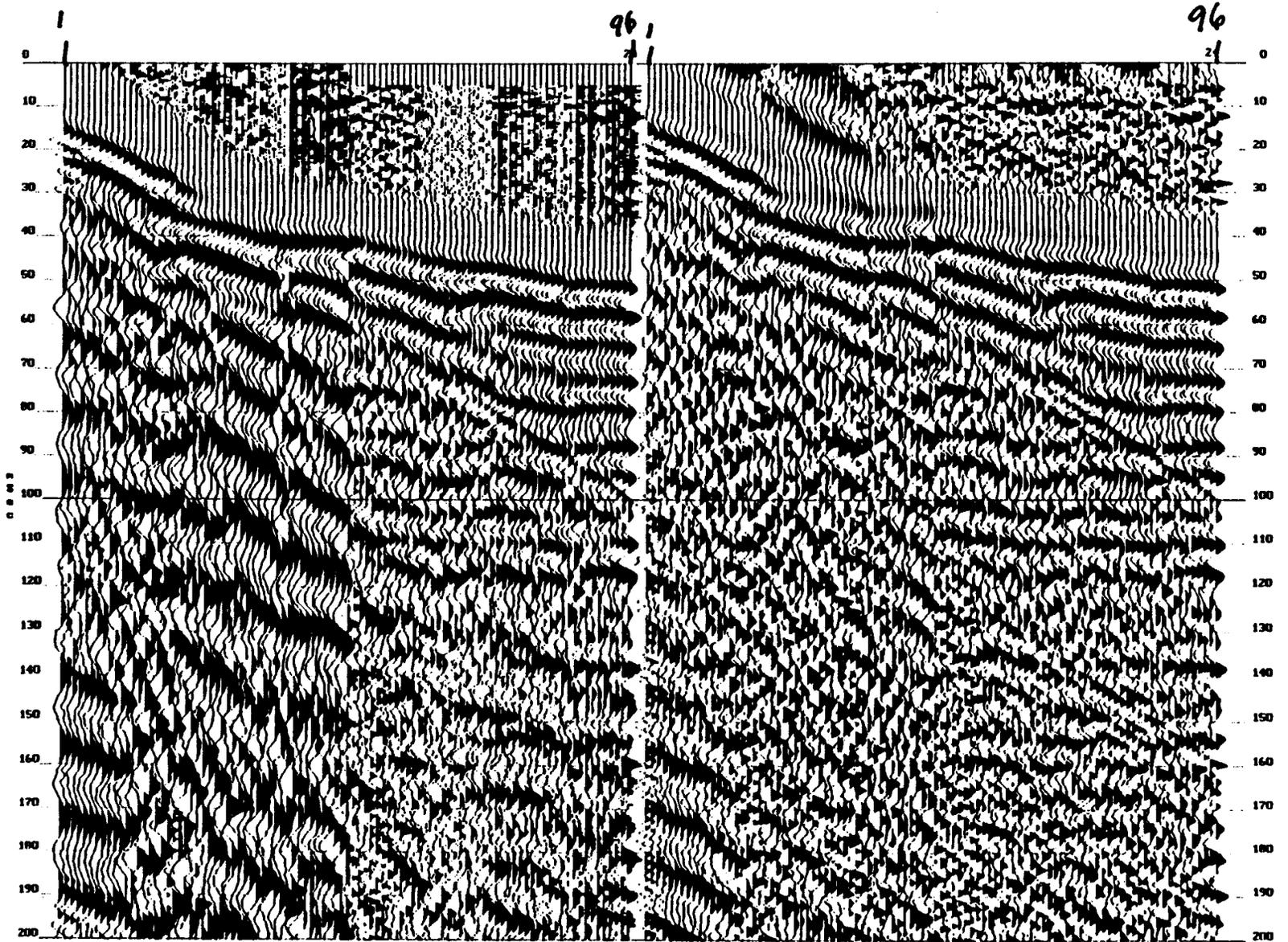(a)   (b)
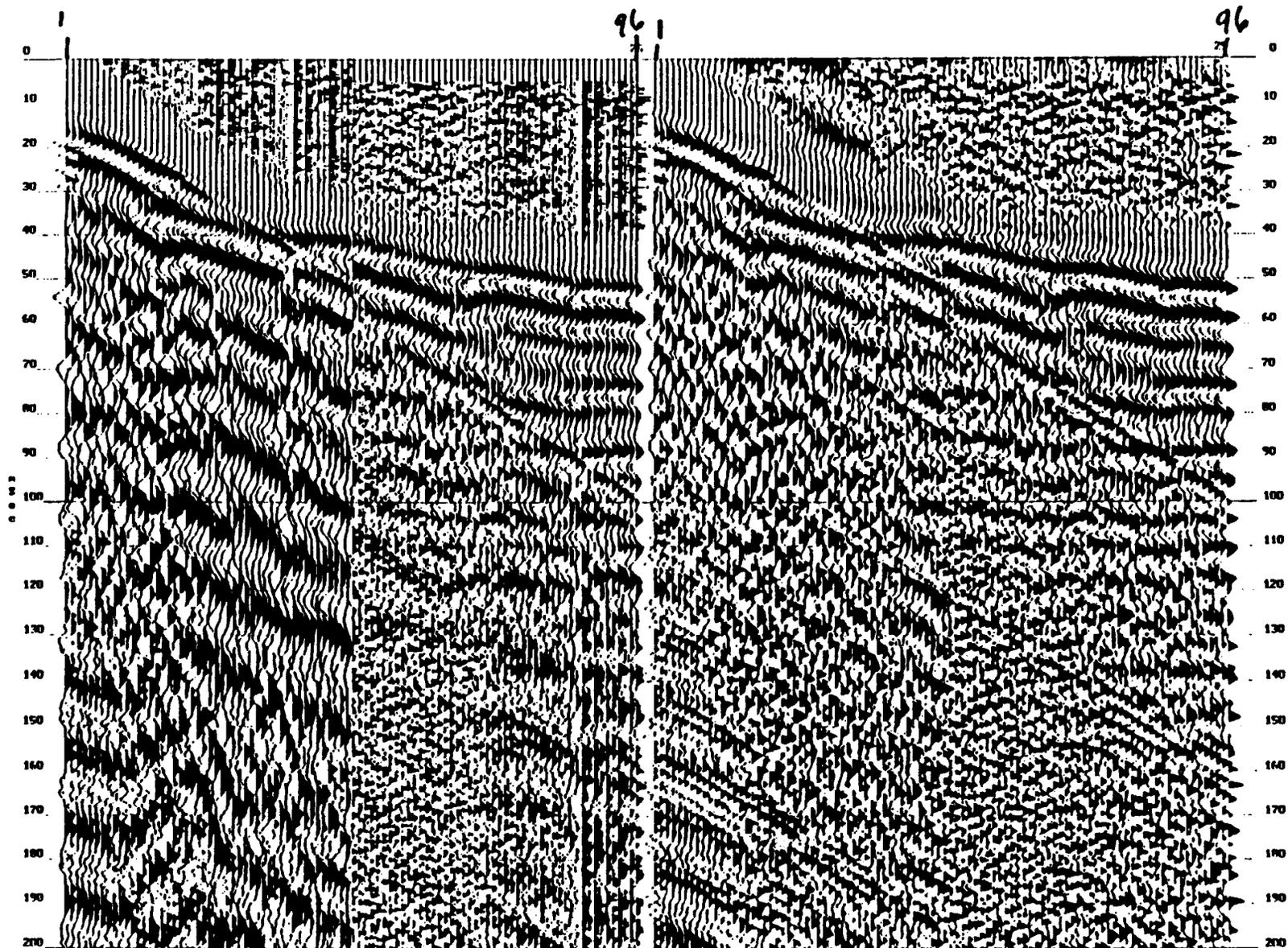
Figures D2.

Source to Receiver Offset (ft)

(a)   (b)
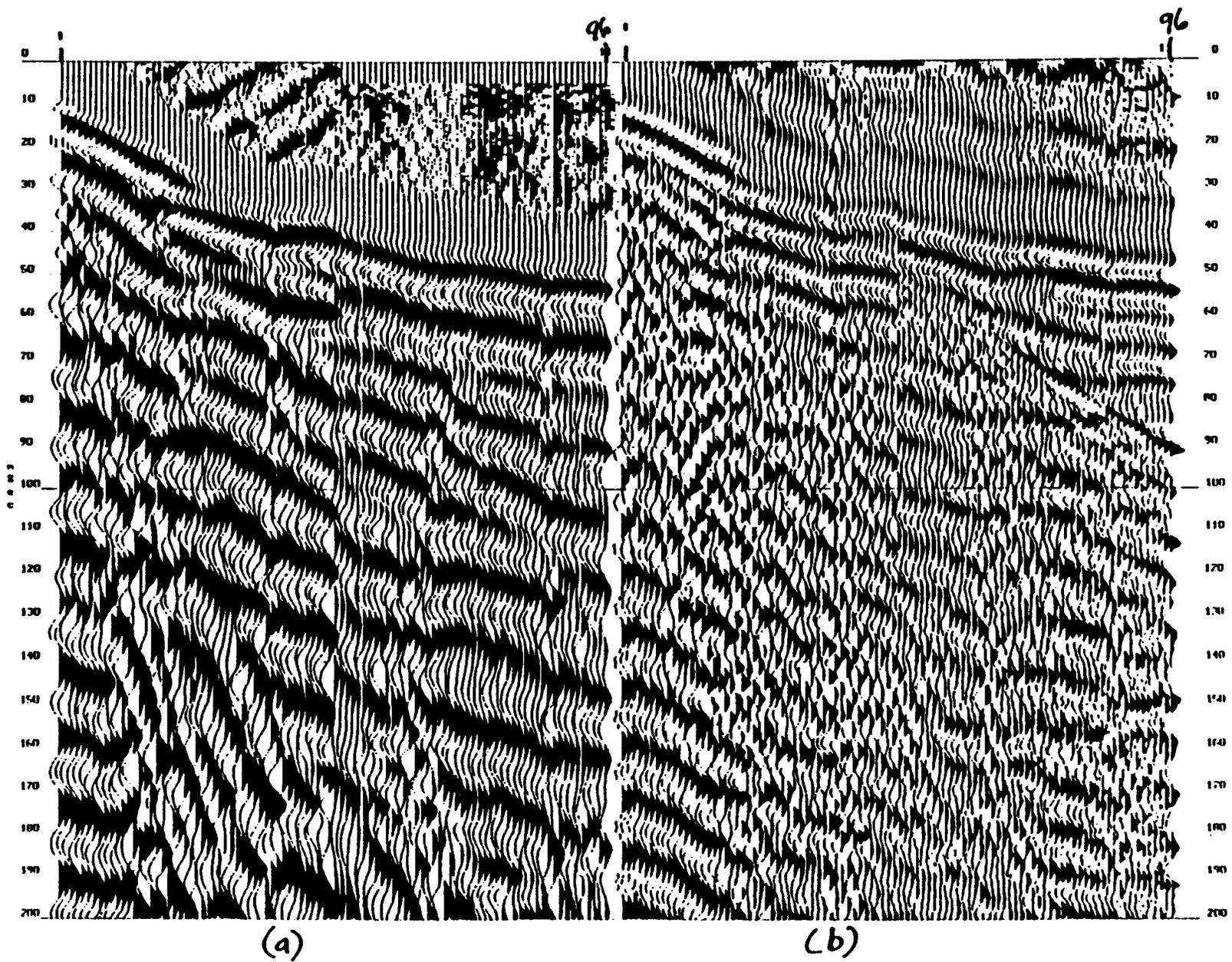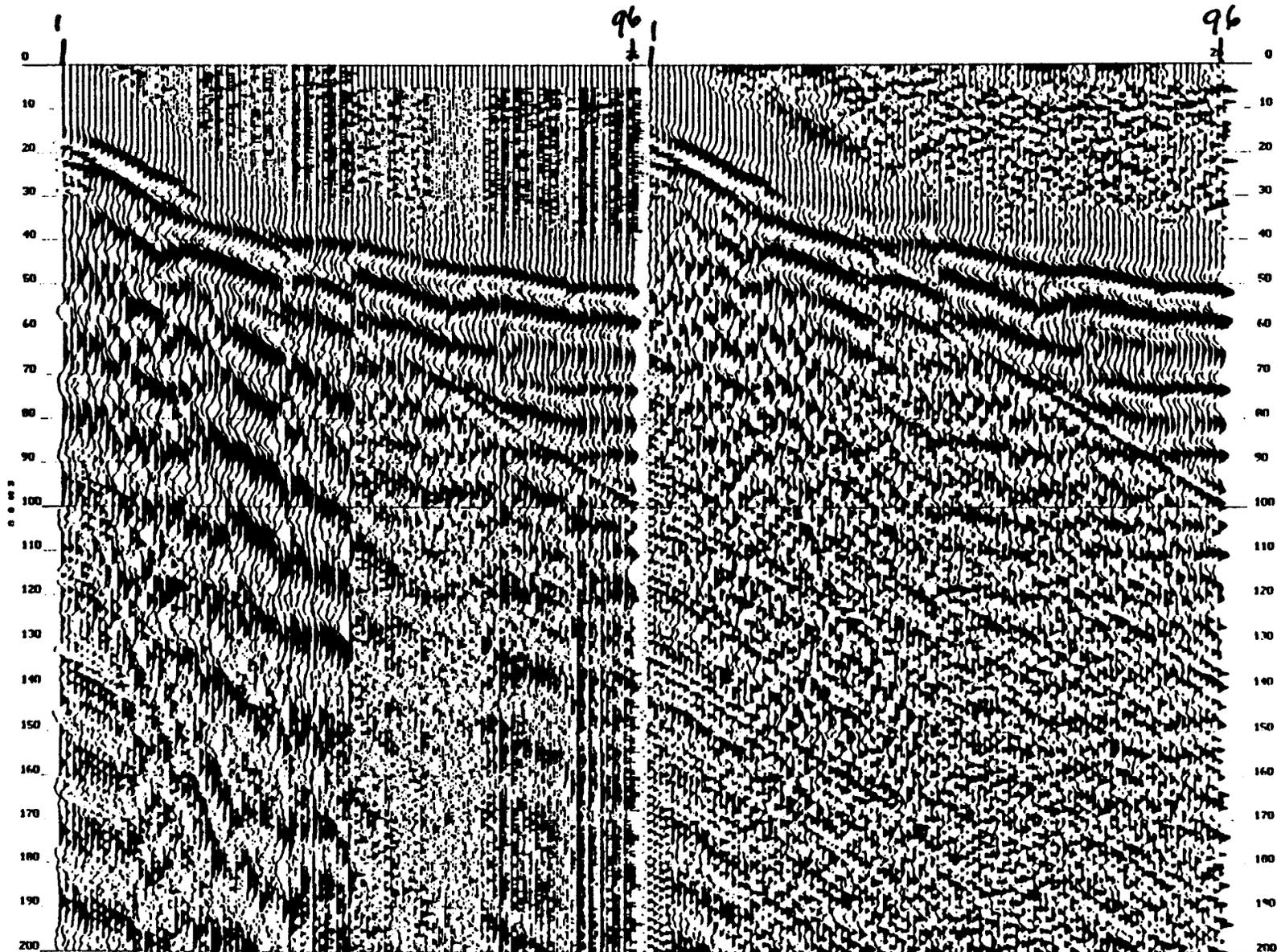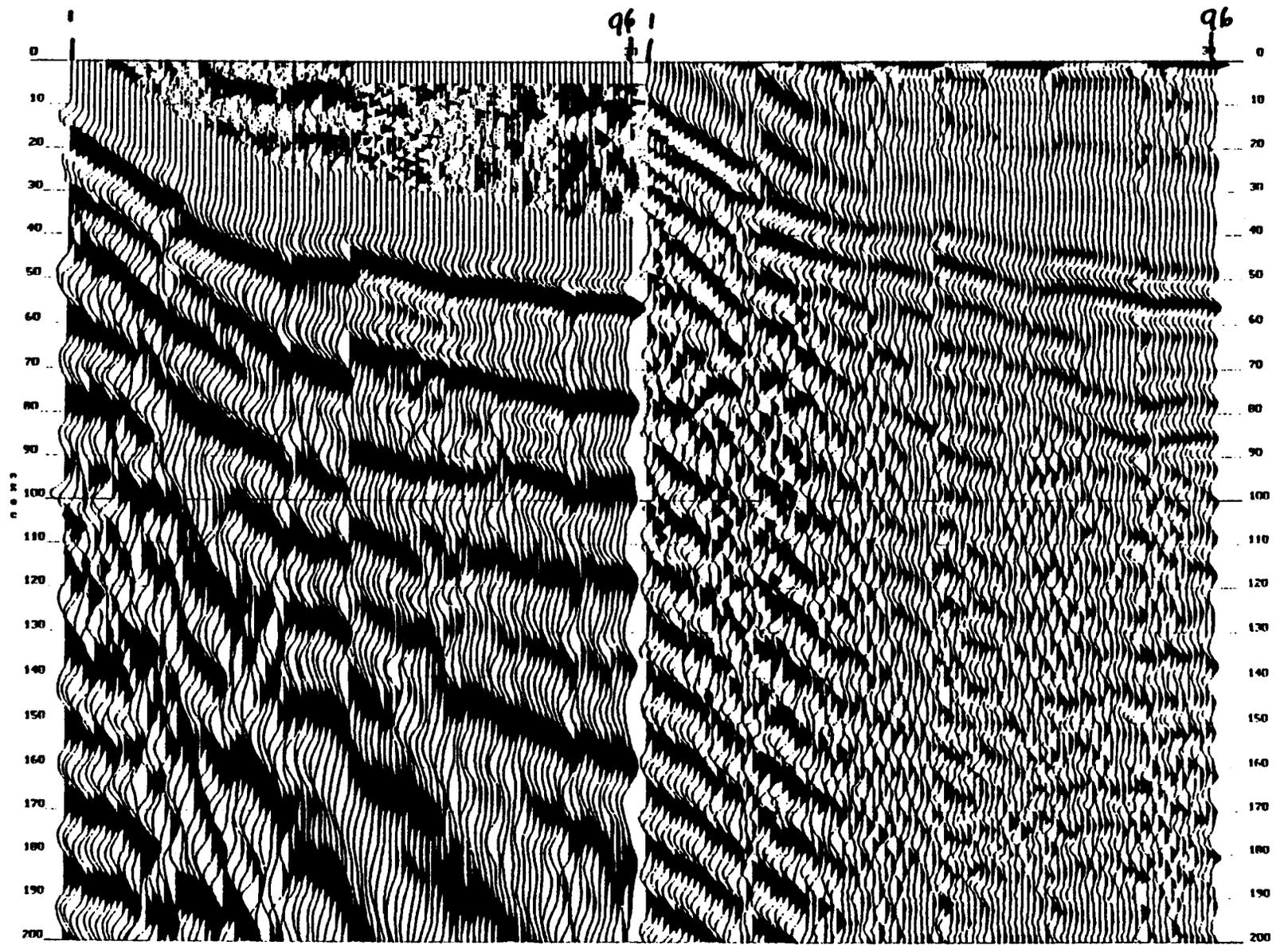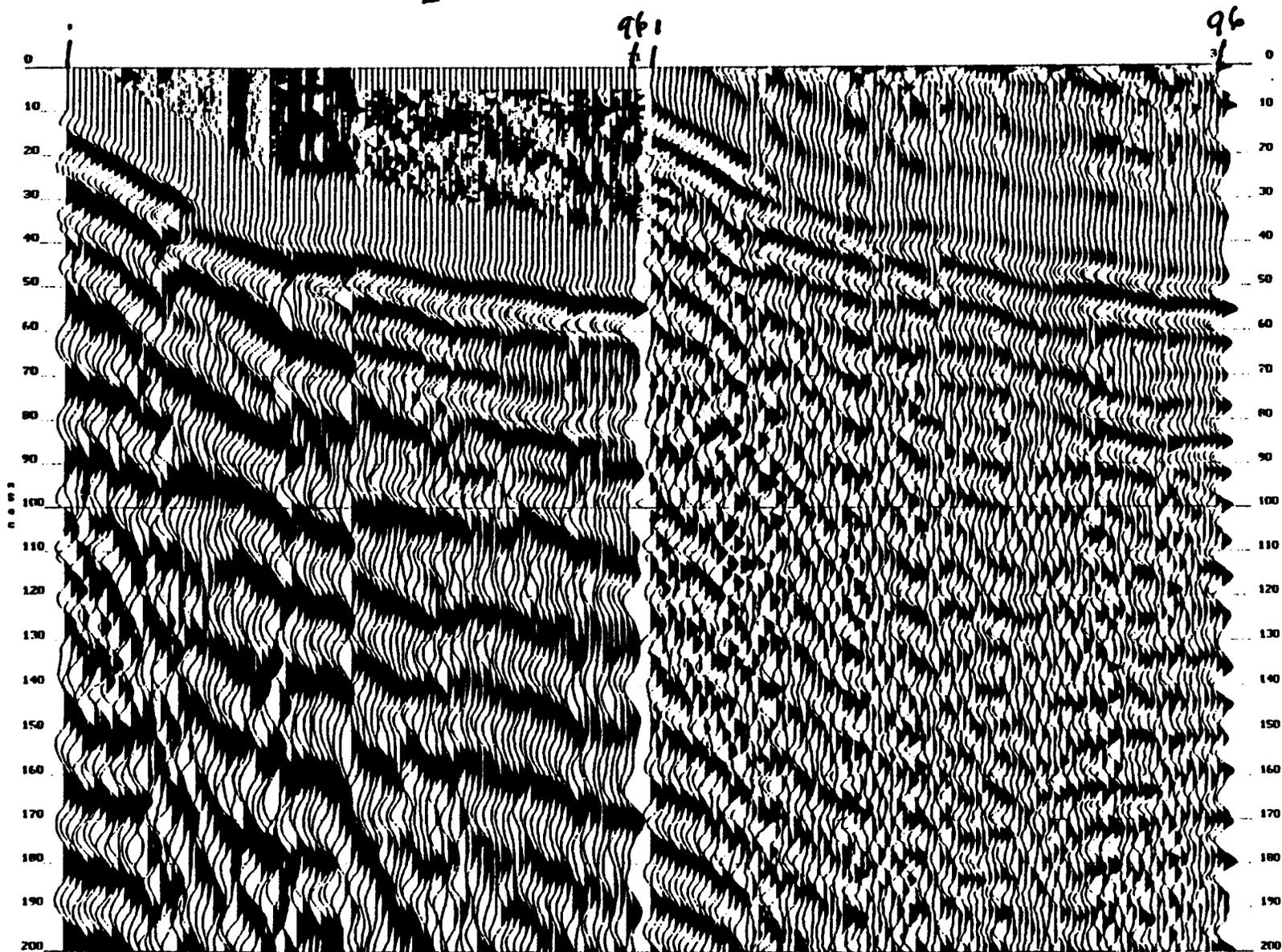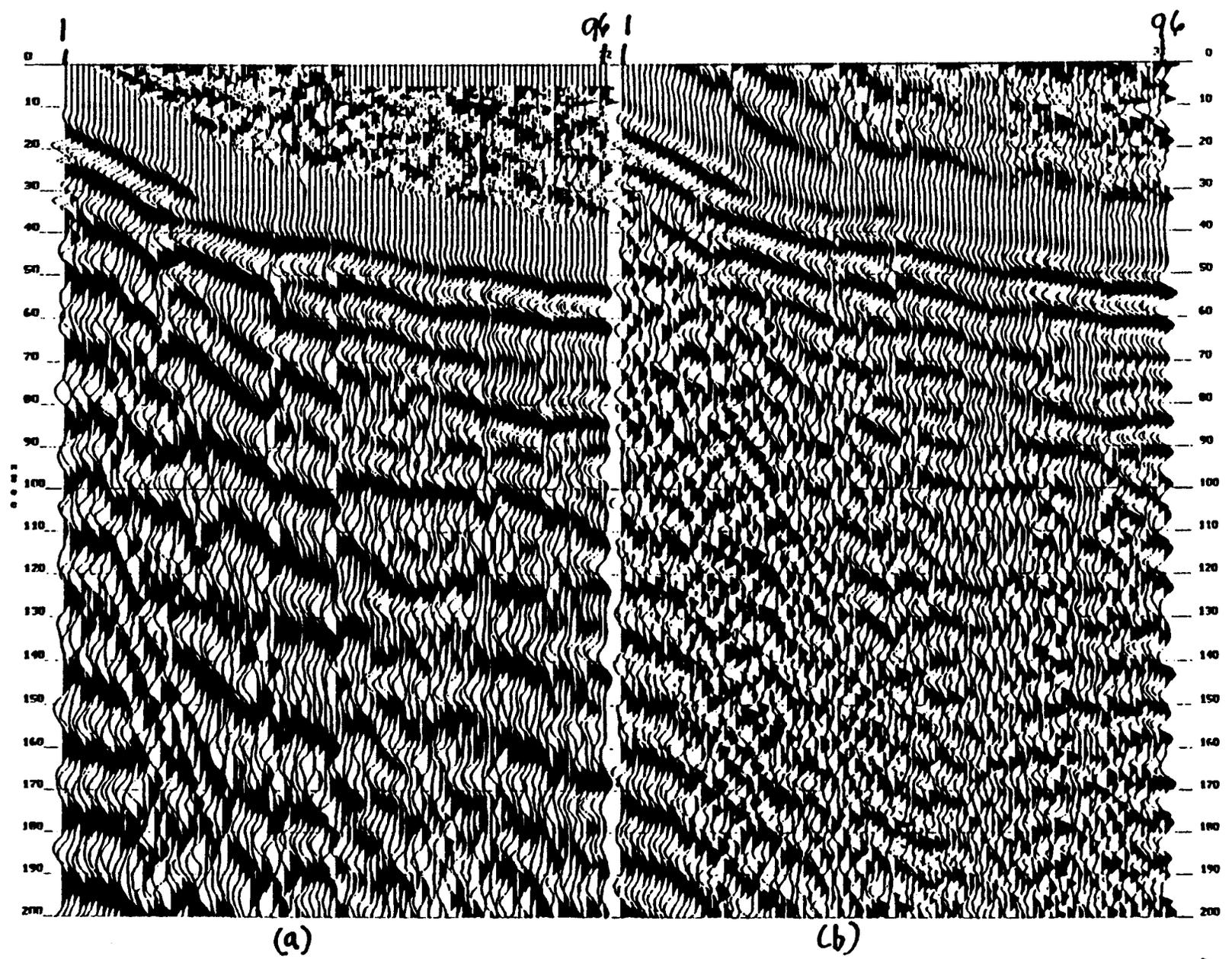
Figures D3.

Source to Receiver Offset (ft)
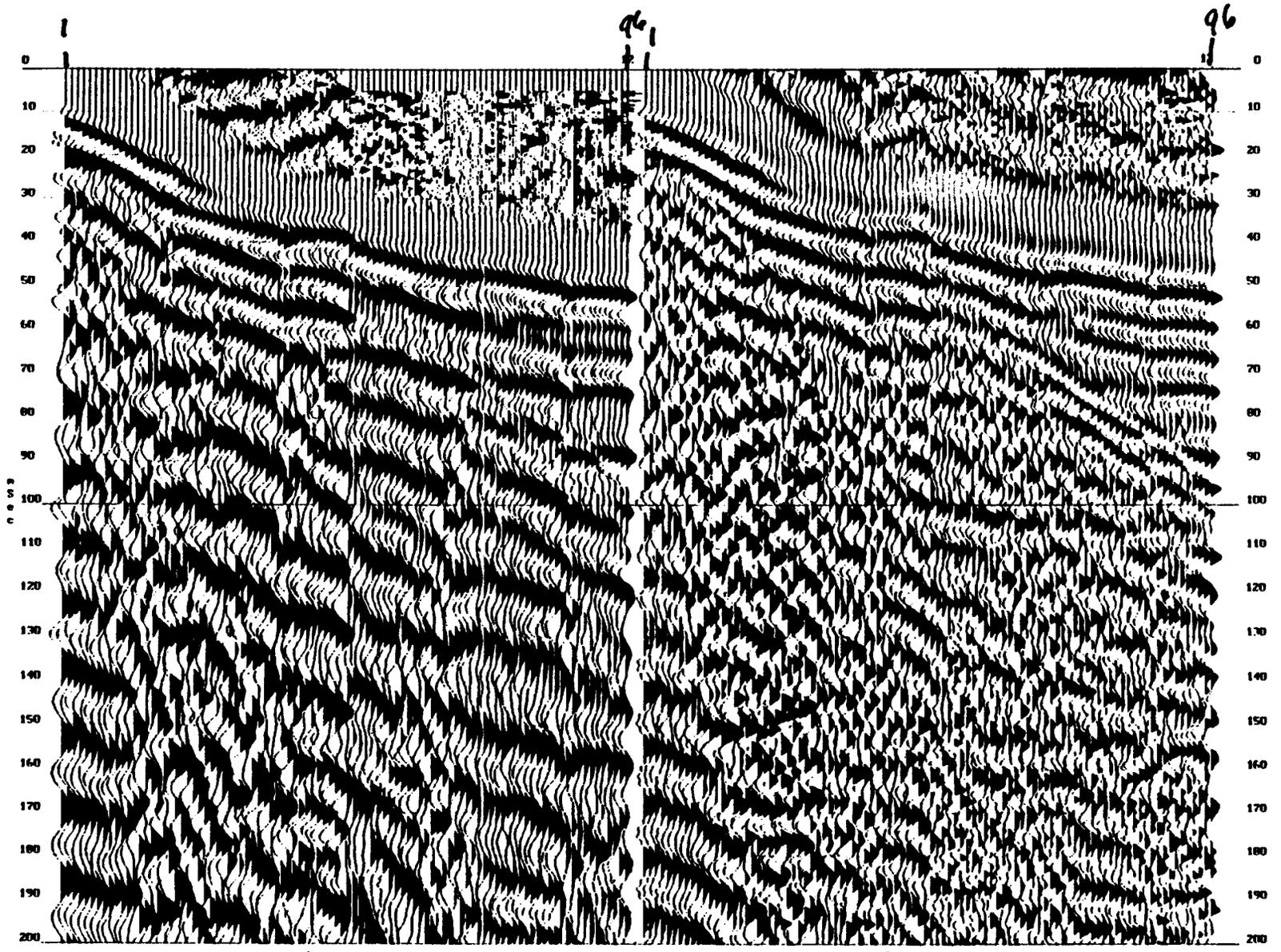
(a)   (b)

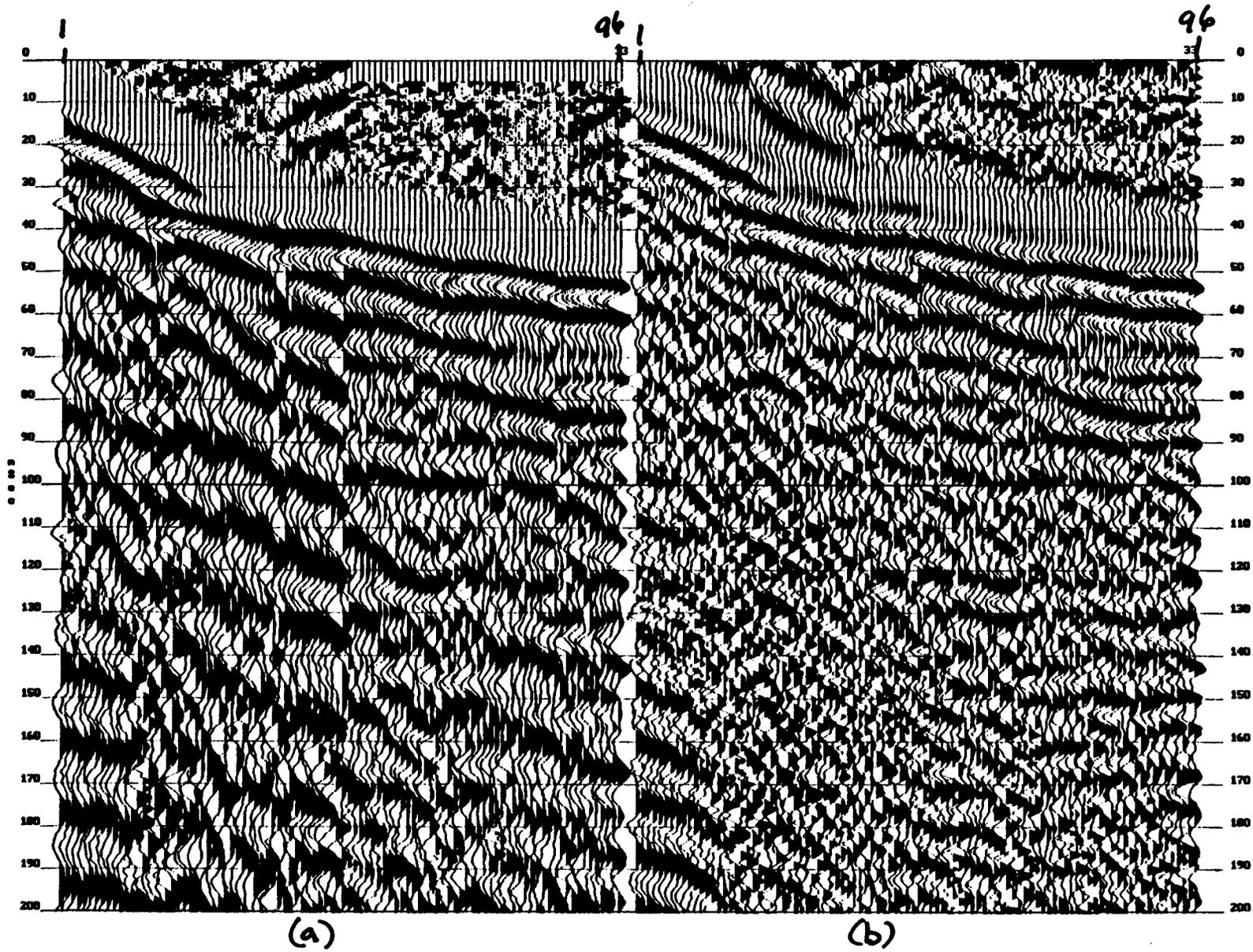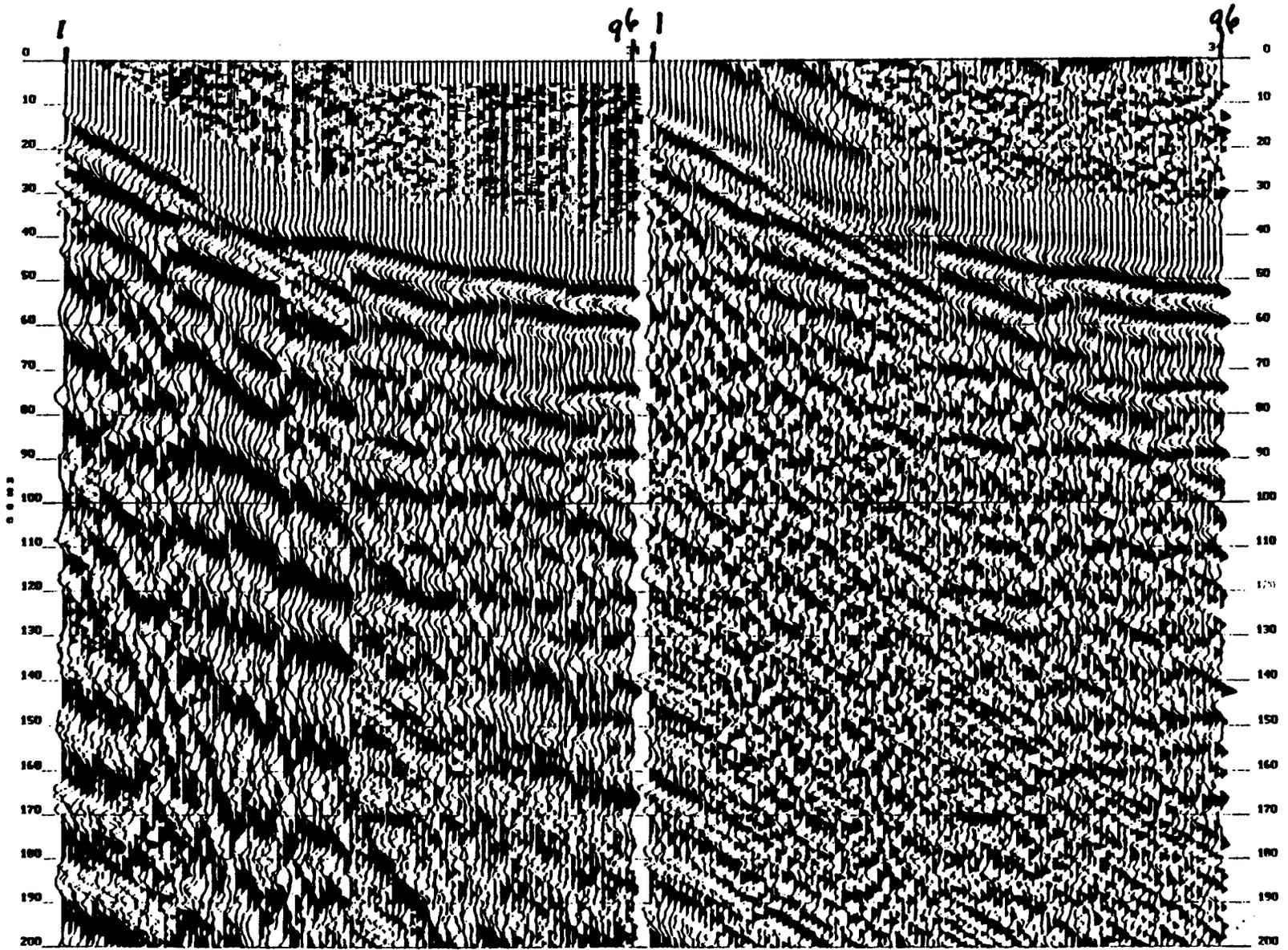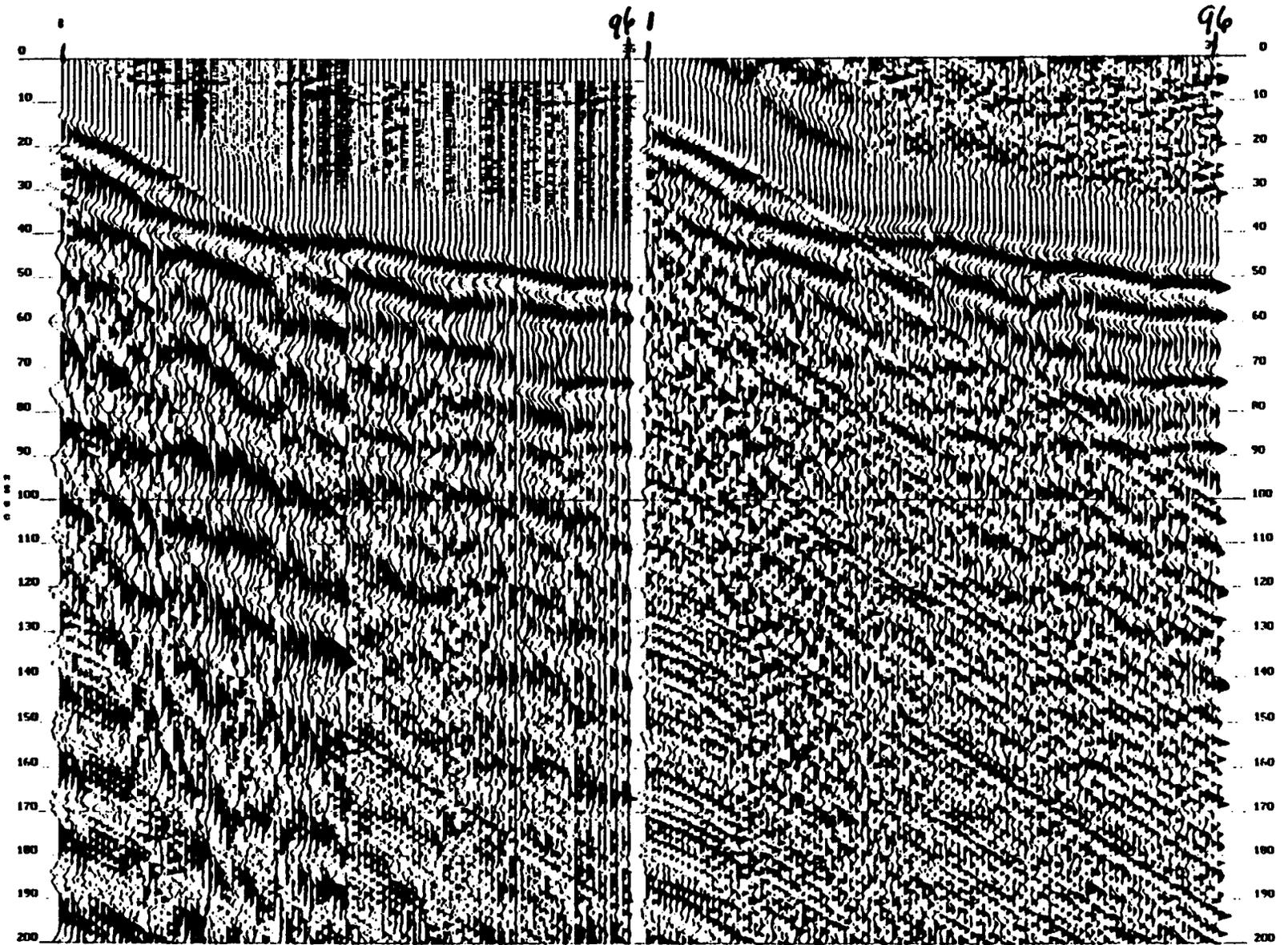Figures D4.

Source to Receiver Offset (ft)

(a)

(b)
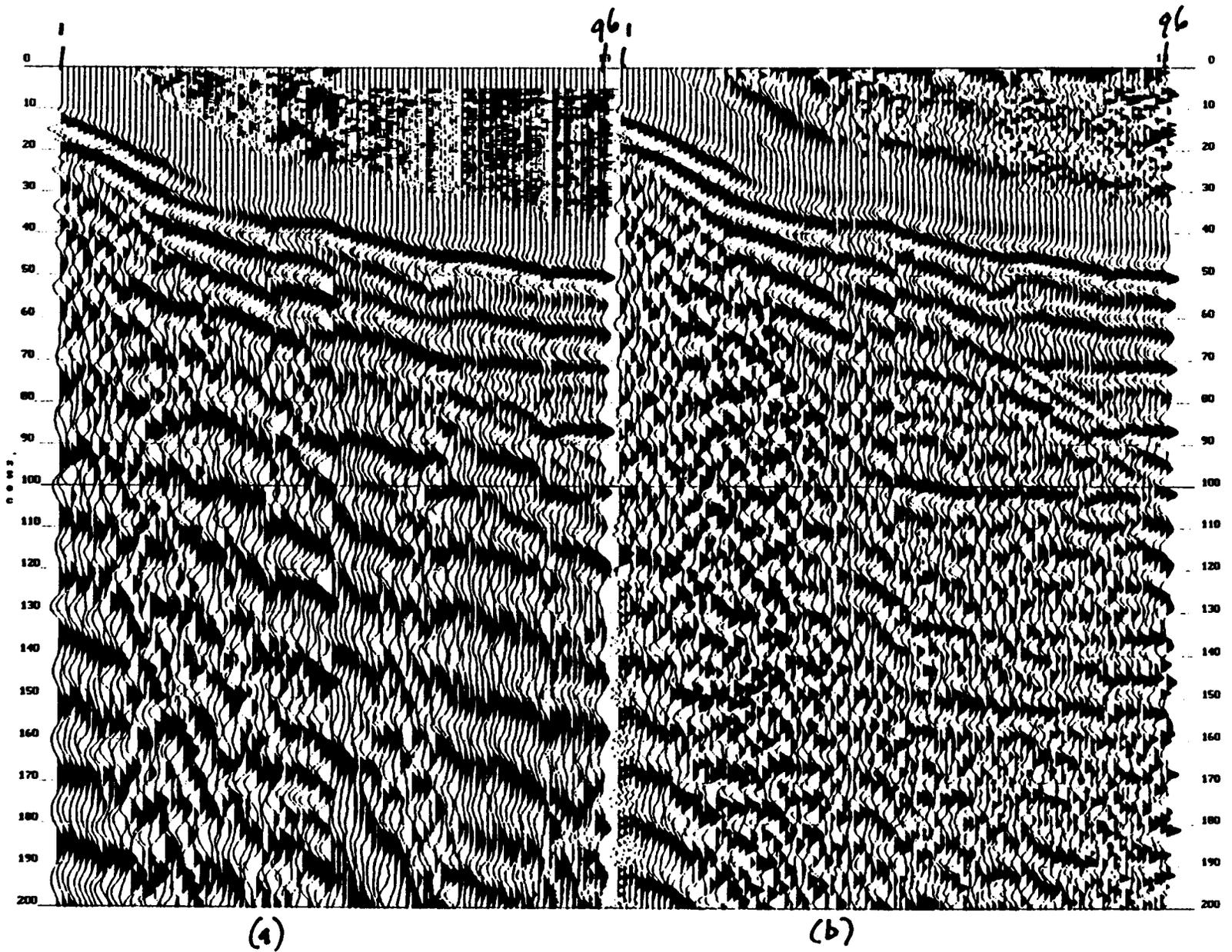
Figures D5.

Source to Receiver Offset (ft)

(a)　　　　　　(b)
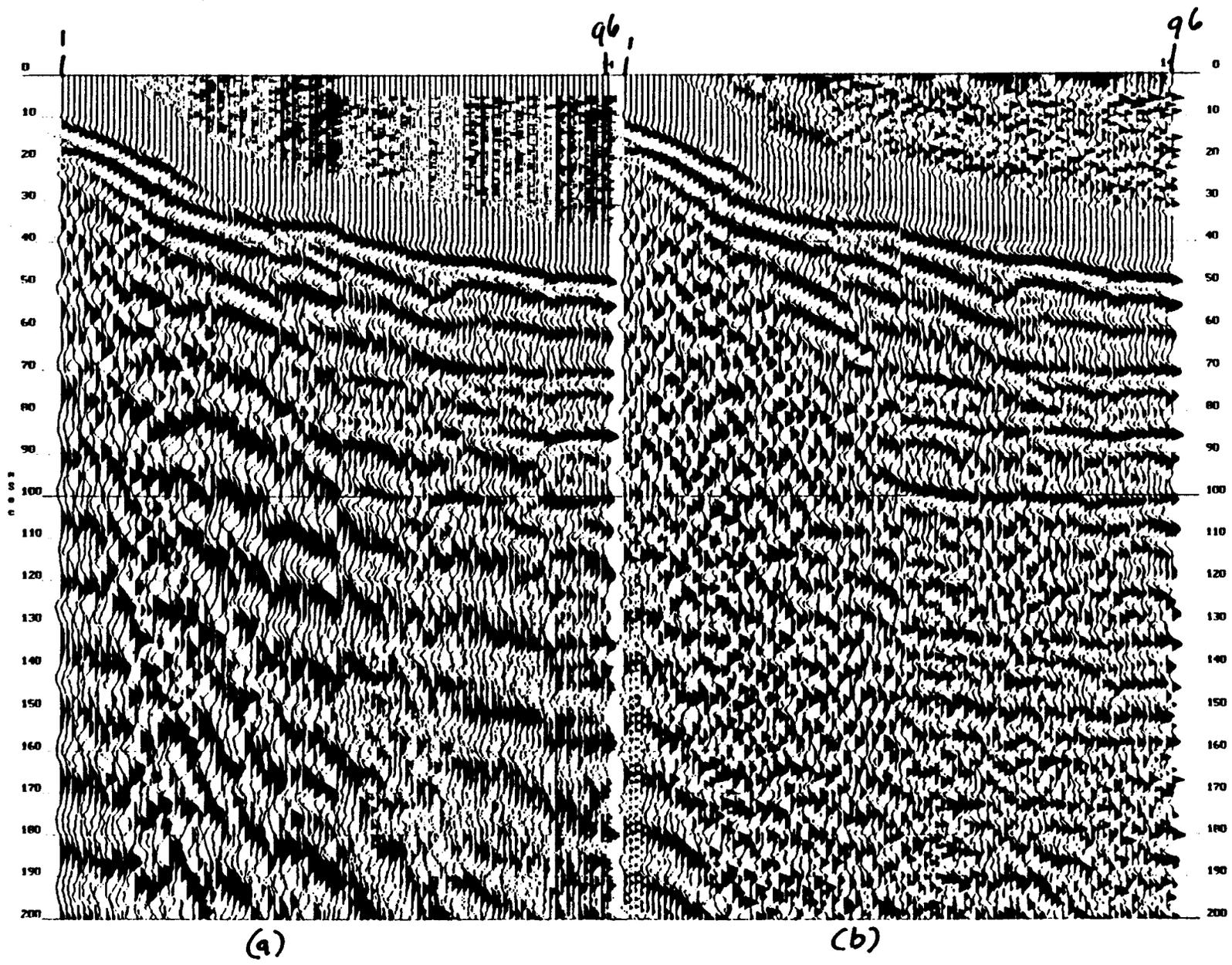
Figures D6.

Source to Receiver Offset (ft)

(a)

(b)

IX.D.8
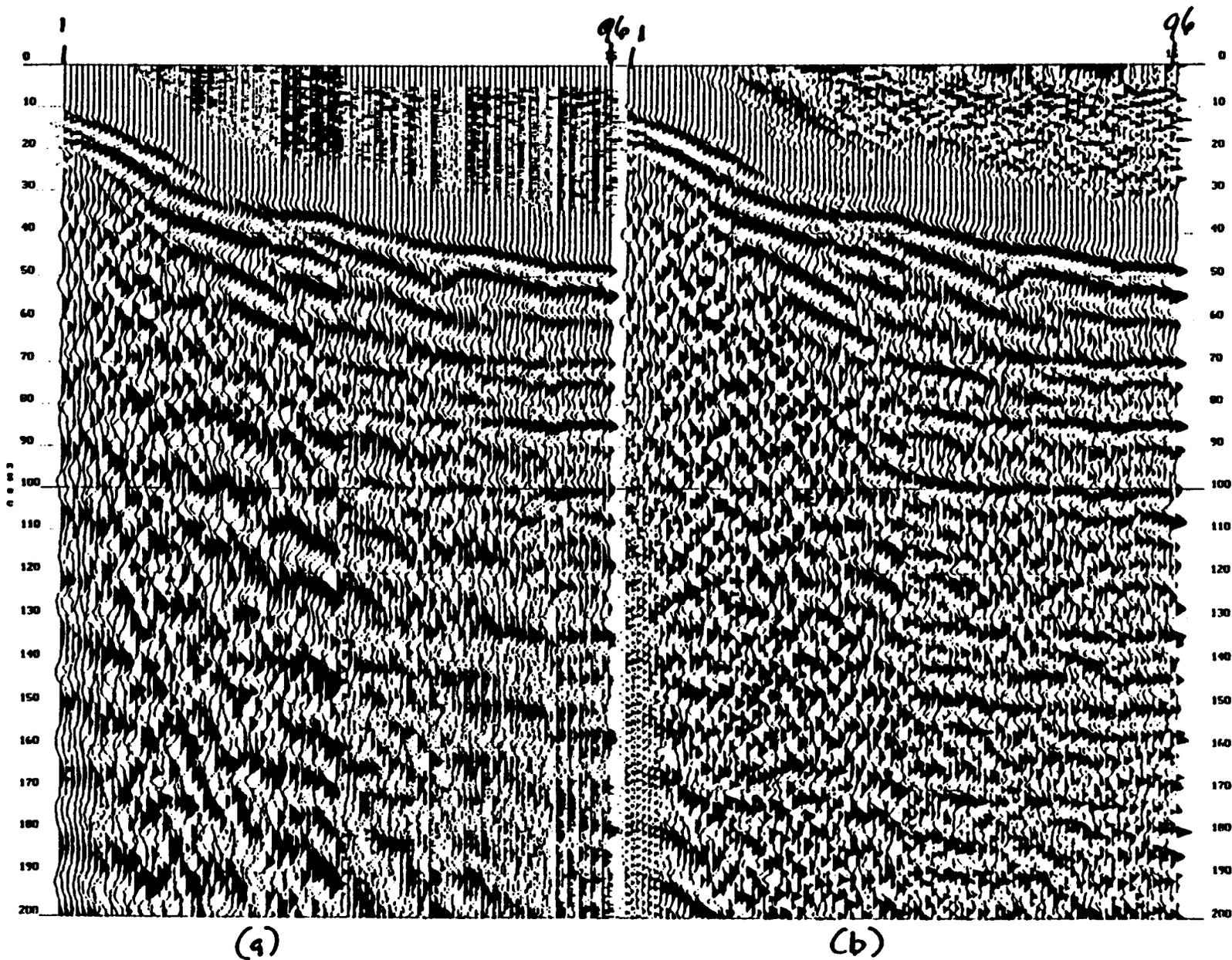
Figures D7.

Source to Receiver Offset (ft)

(a)

(b)

IX.D.9

Source to Receiver Offset (ft)

(a)　　　　　　　　　(b)
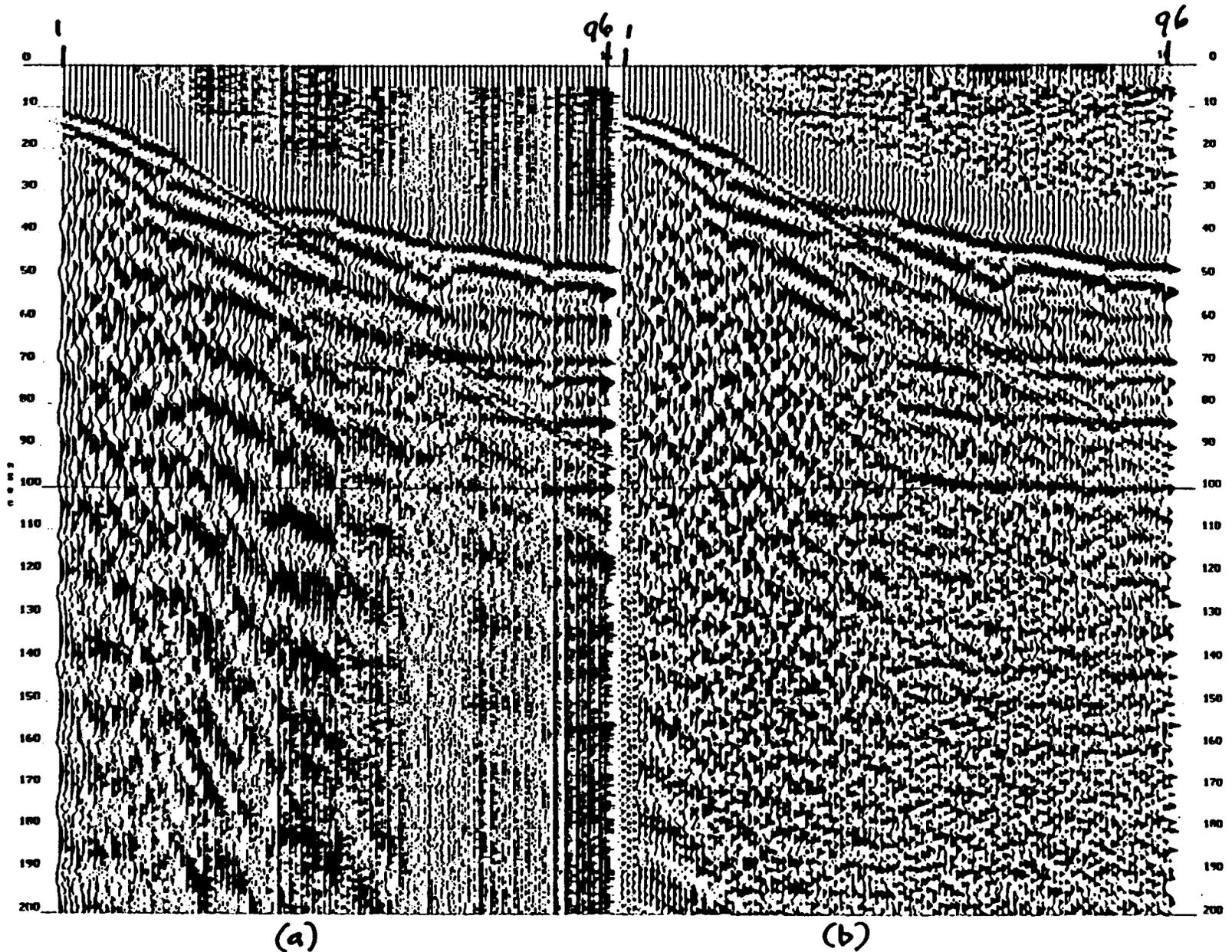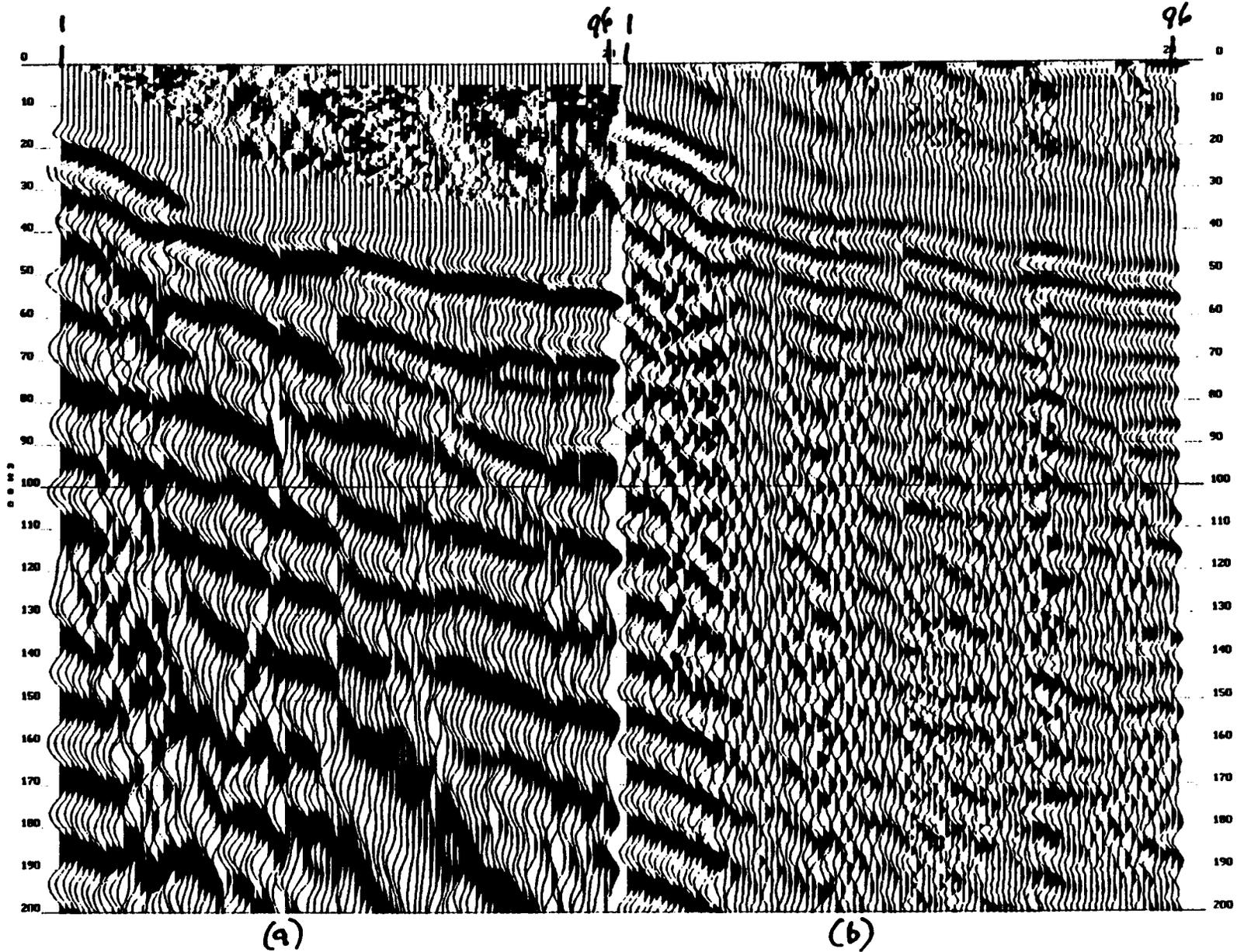
Figures D9

Source to Receiver Offset (ft)

(a)   (b)
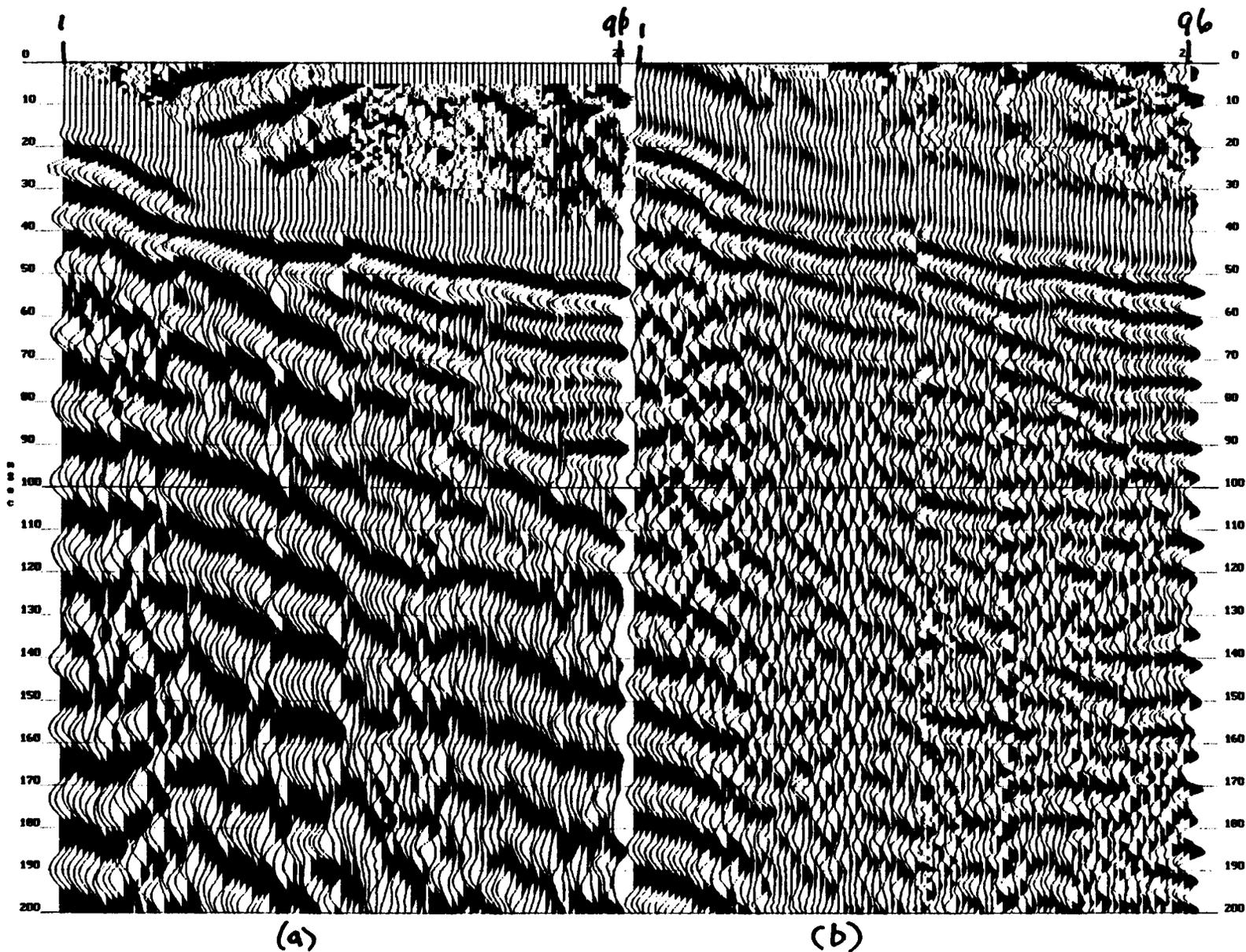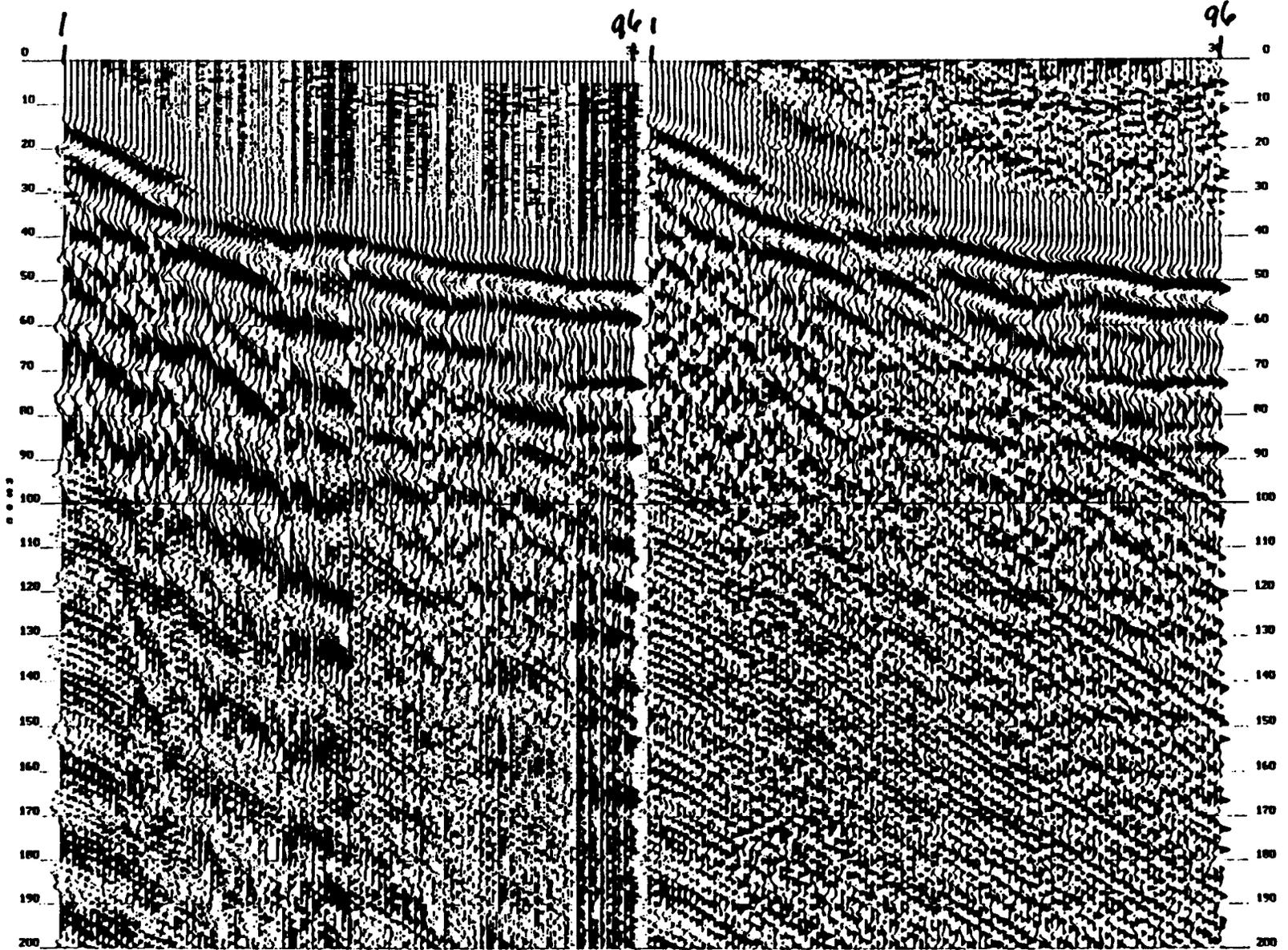
Figures D10.

Source to Receiver Offset (ft)

(a)   (b)
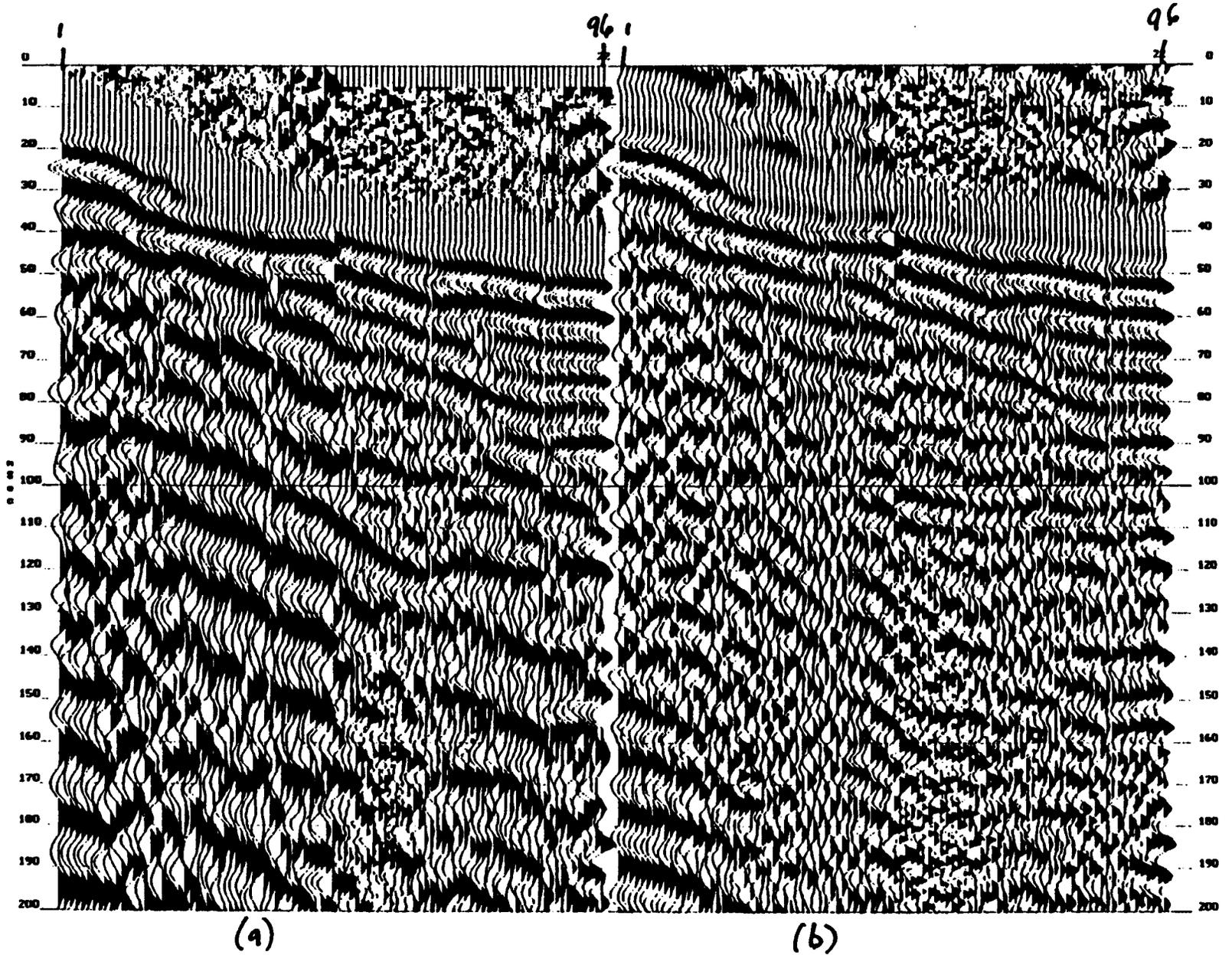
Figures D11.

Source to Receiver Offset (ft)

(a) (b)
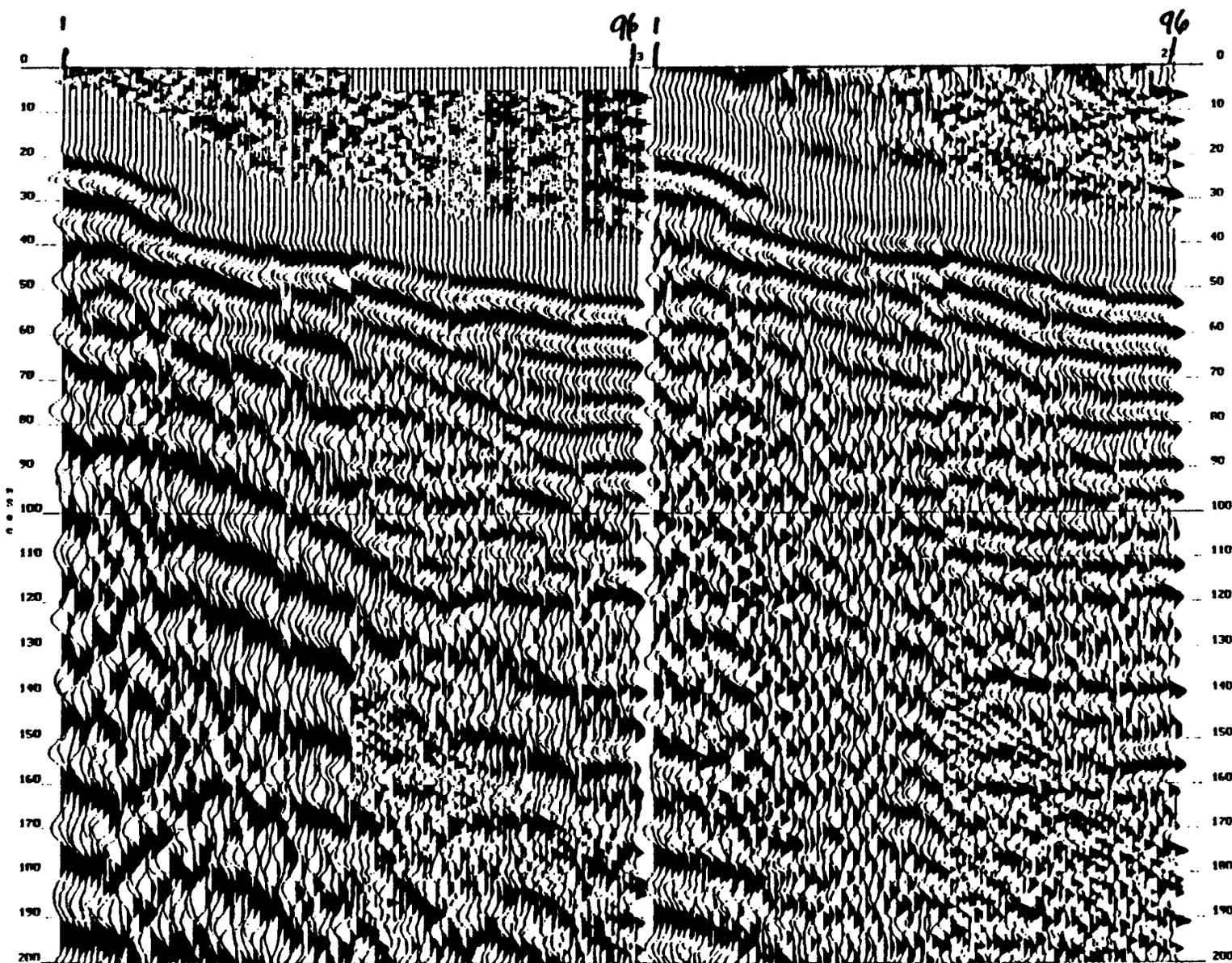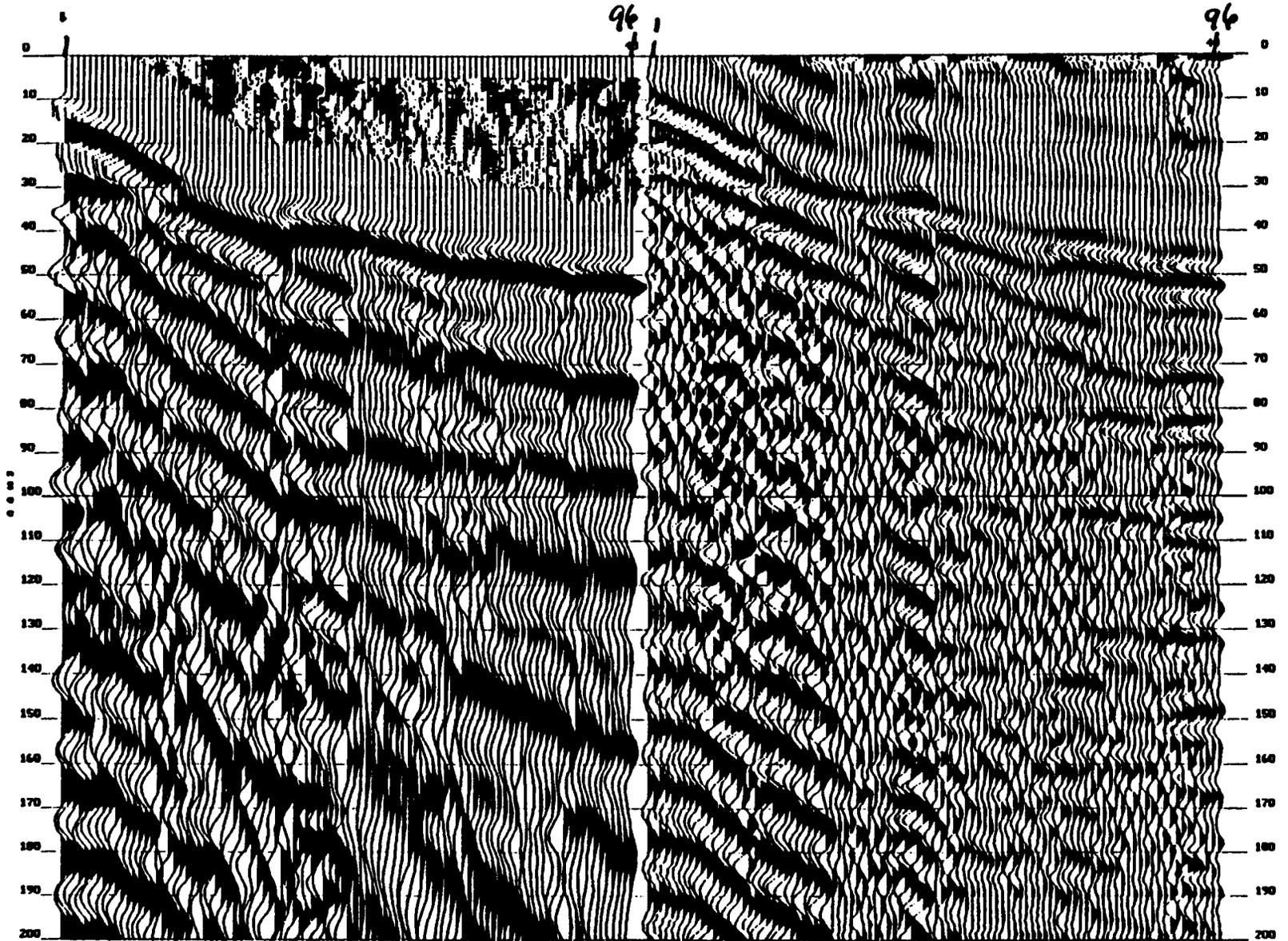
IX.D.13

Figures D12.

Source to Receiver Offset (ft)

(a)   (b)

IX.D.14

Figures D13.

Source to Receiver Offset (ft)

(a)

(b)

Source to Receiver Offset (ft)

(a)   (b)

Figures D15.

Source to Receiver Offset (ft)

(a)   (b)

IX.D.17

Figures D16.

Source to Receiver Offset (ft)

(a)   (b)

IX.D.18

Figures D17.

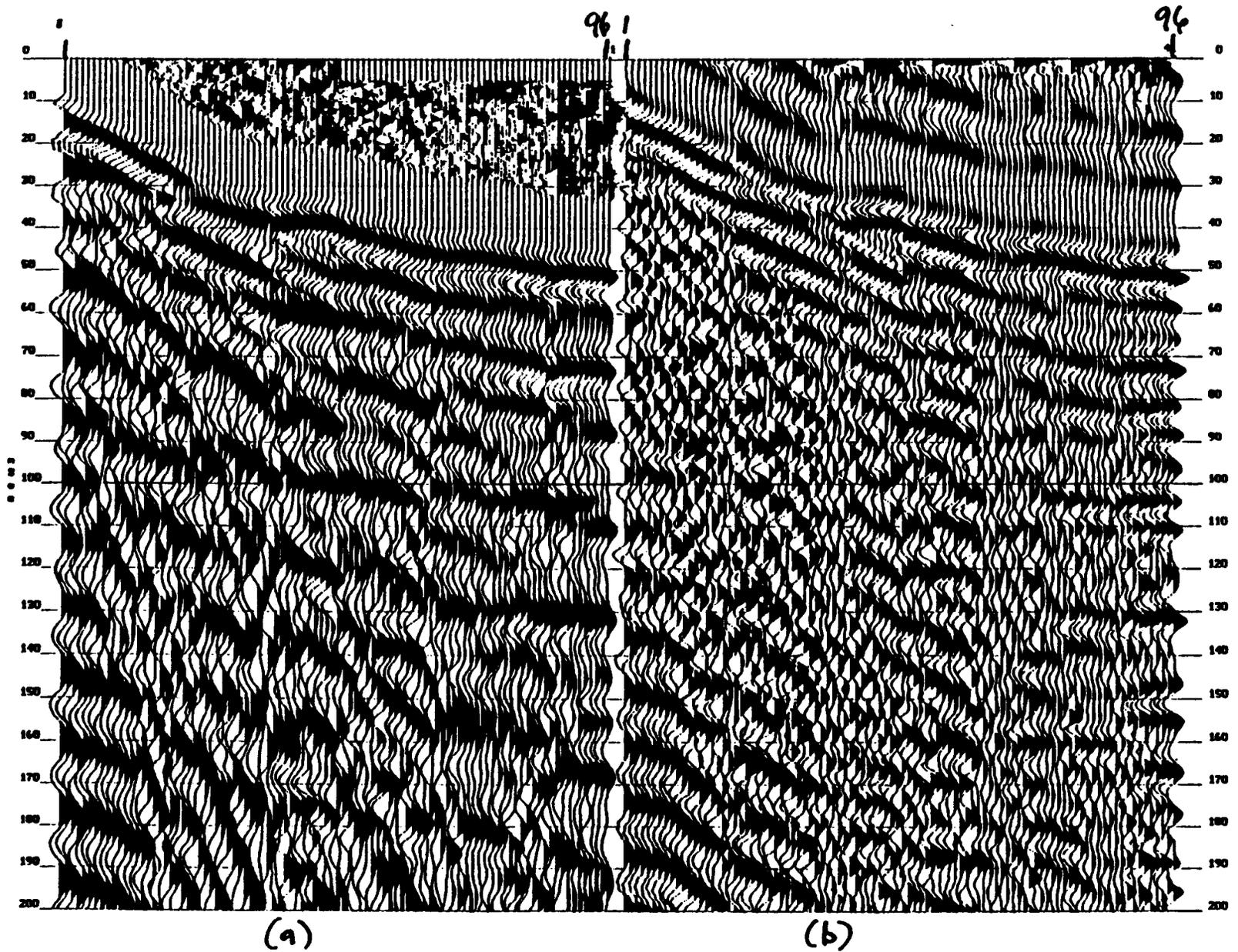Source to Receiver Offset (ft)

(a)　　　(b)

Source to Receiver Offset (ft)

(a)   (b)

Source to Receiver Offset (ft)

(a)　　　　　　(b)

Figures D20 Source to Receiver Offset (ft)

(a) (b)

IX.D.22

Figures D21.

Source to Receiver Offset (ft)

(a)   (b)

Figures D22.

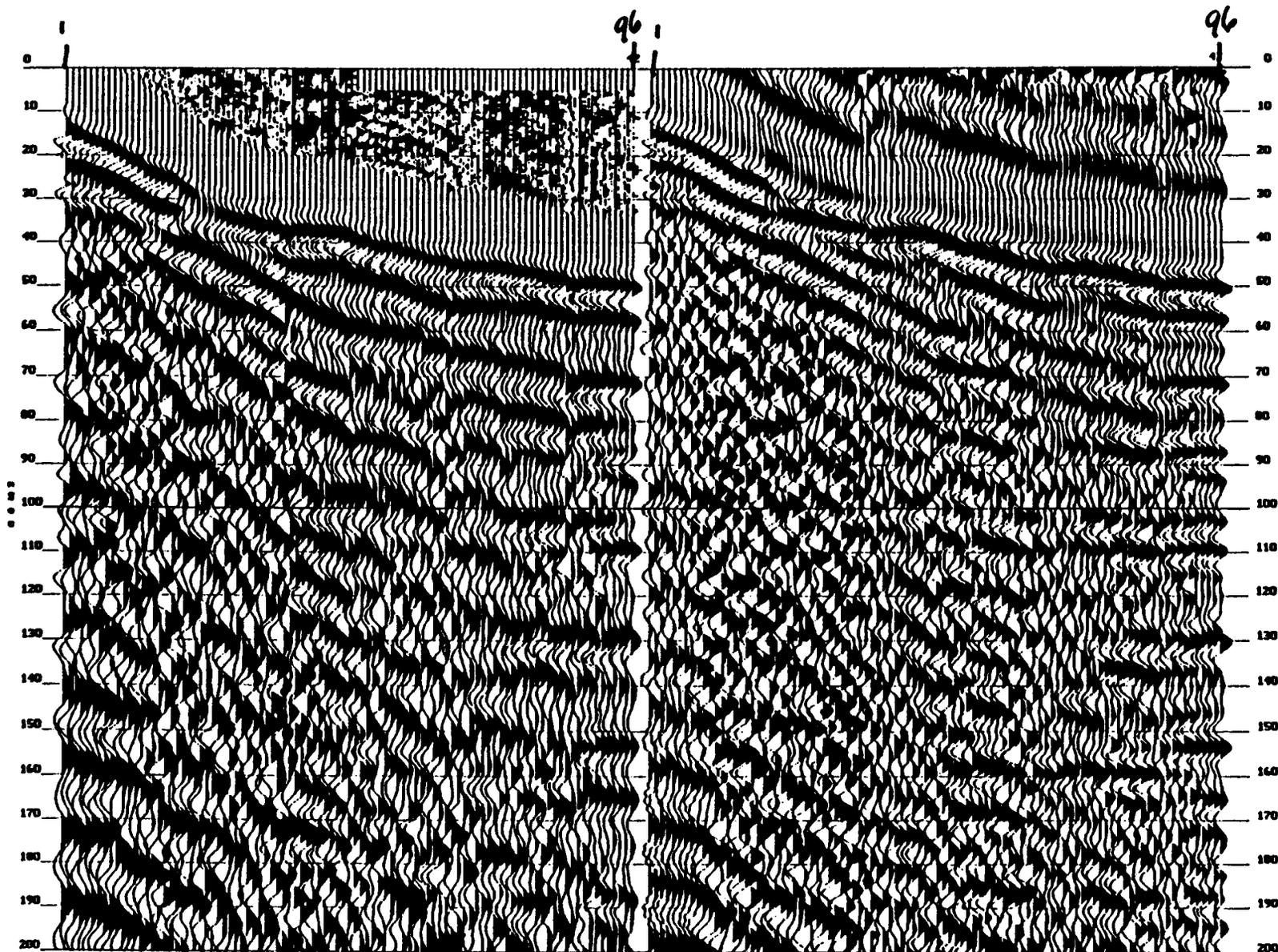Source to Receiver Offset (ft)

(a)

(b)

IX.D.24

Figures D23.

Source to Receiver Offset (ft)

(a)   (b)

Figures D24.
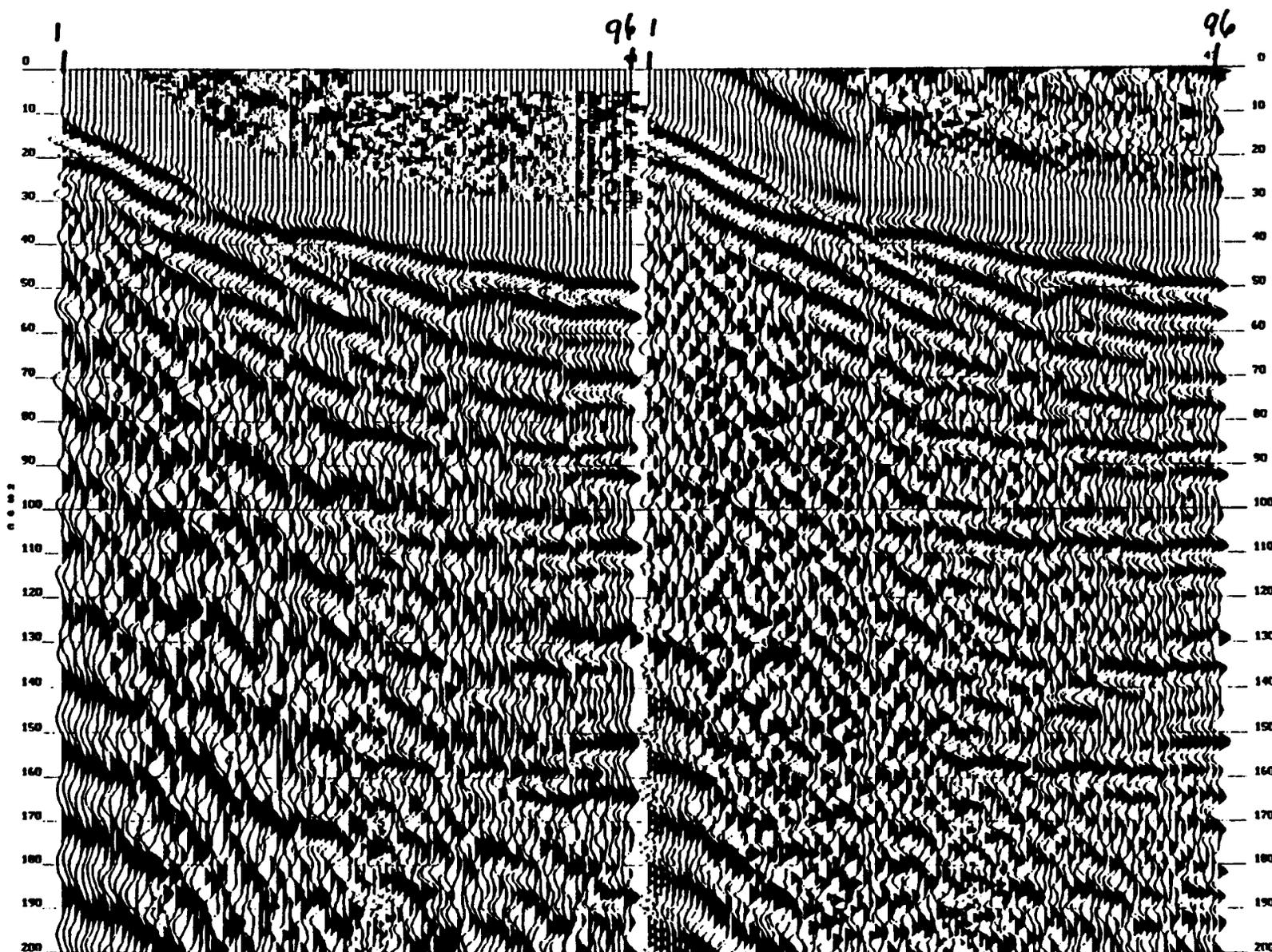
Source to Receiver Offset (ft)

(a)   (b)

IX.D.26

Figures D25.

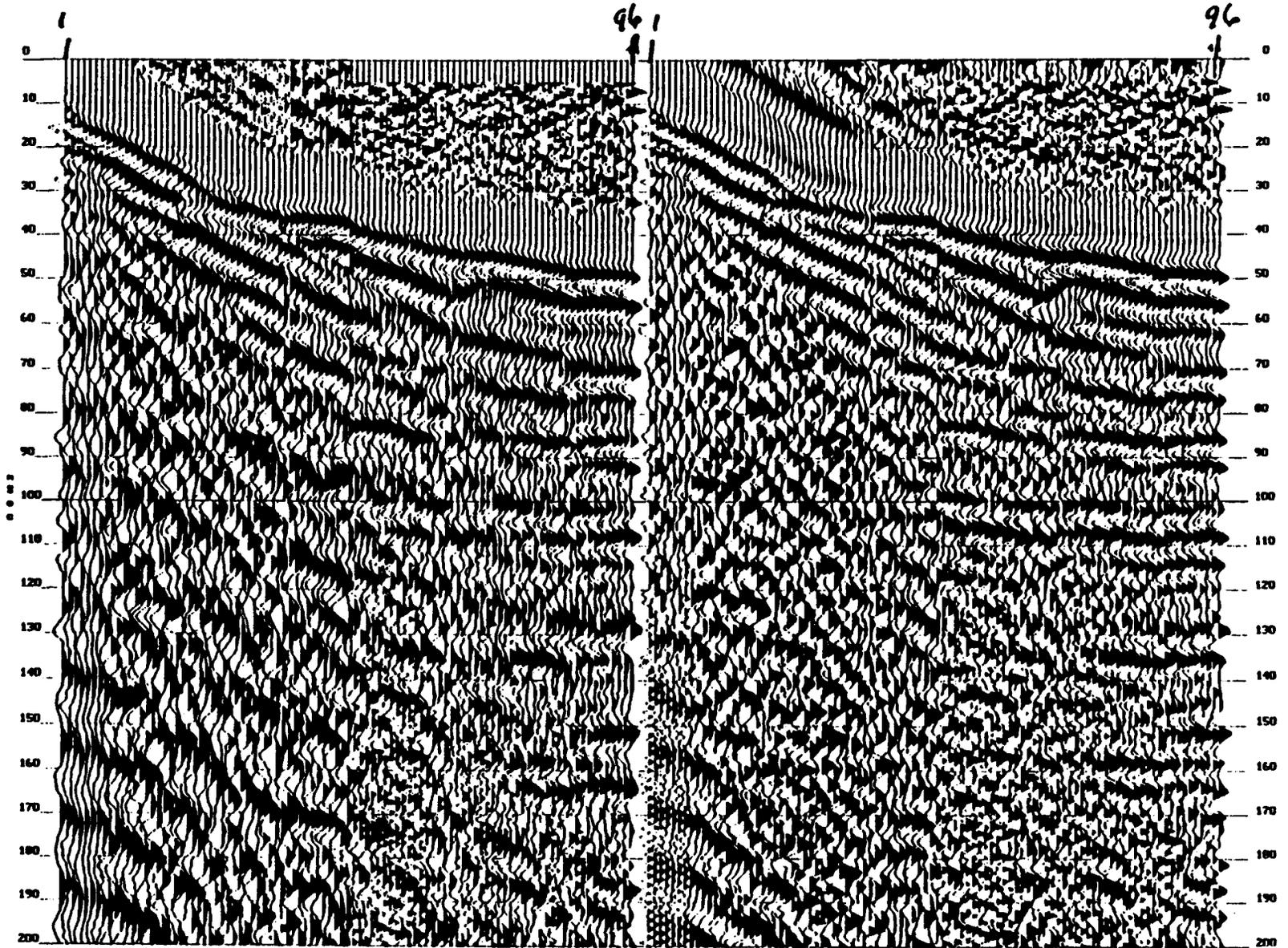Source to Receiver Offset (ft)

(a)   (b)

IX.D.27

Figures D26.

Source to Receiver Offset (ft)

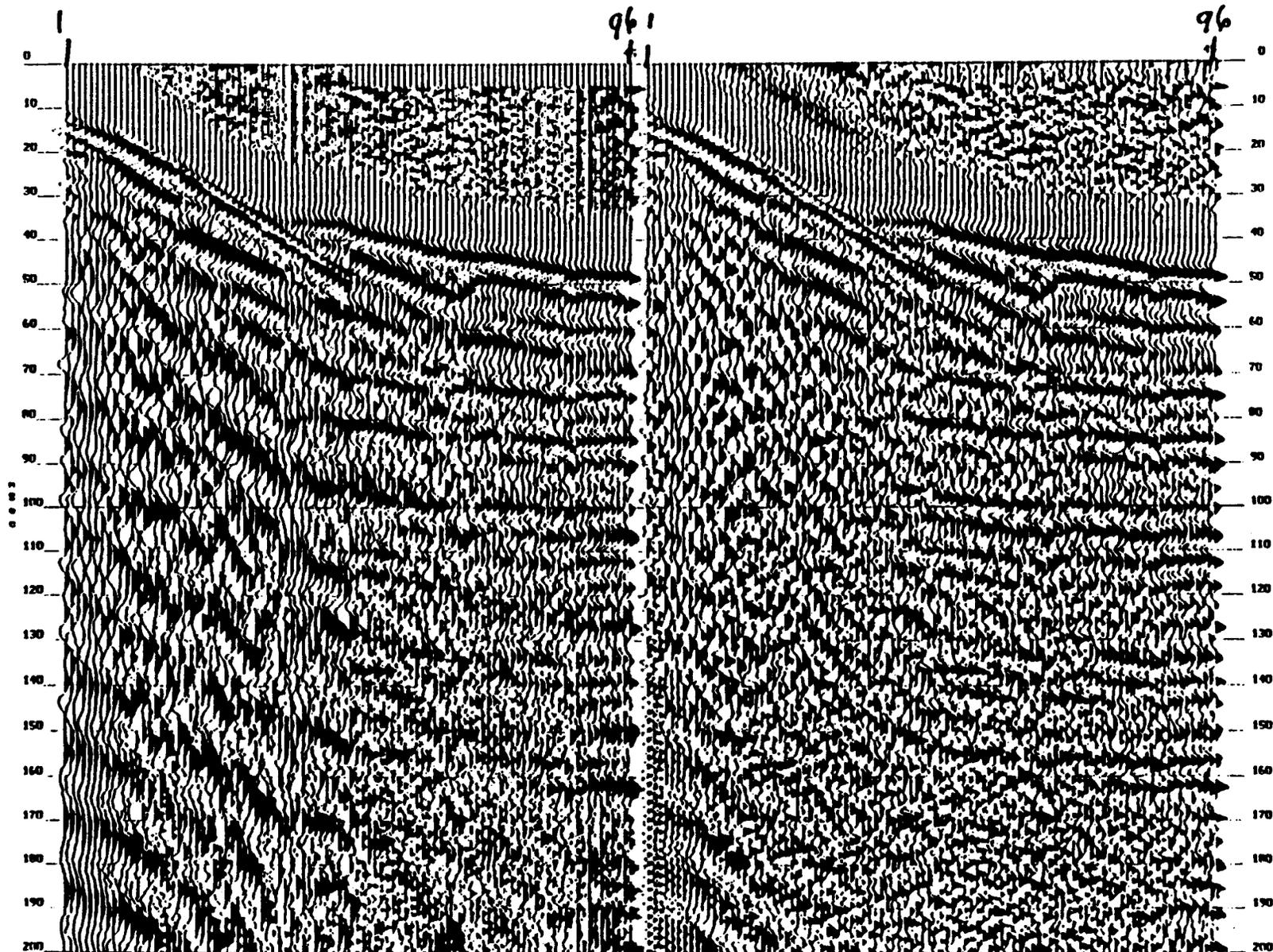(a)   (b)

IX.D.28

Figures D27.

Source to Receiver Offset (ft)
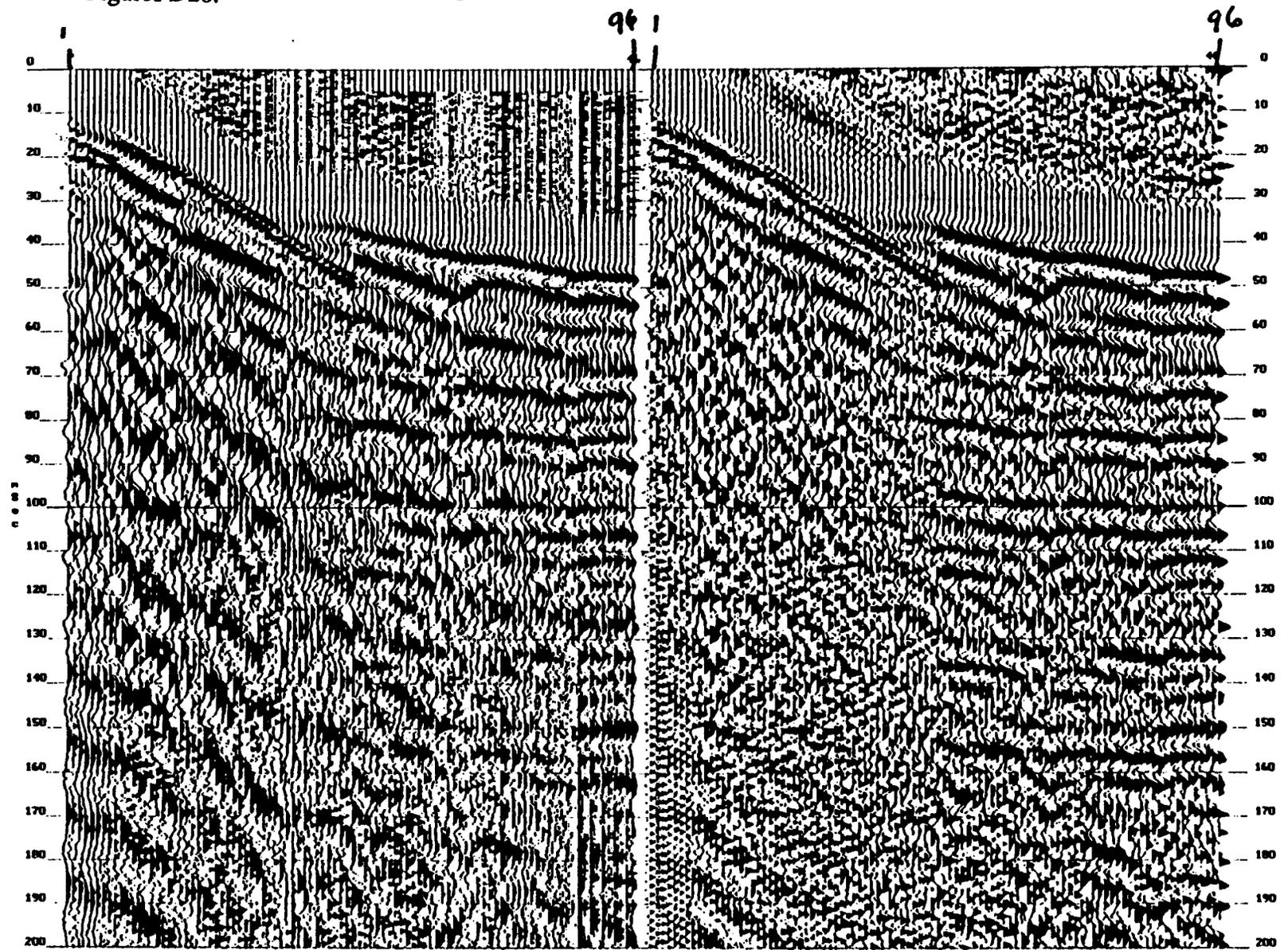
(a) (b)

Figures D28.

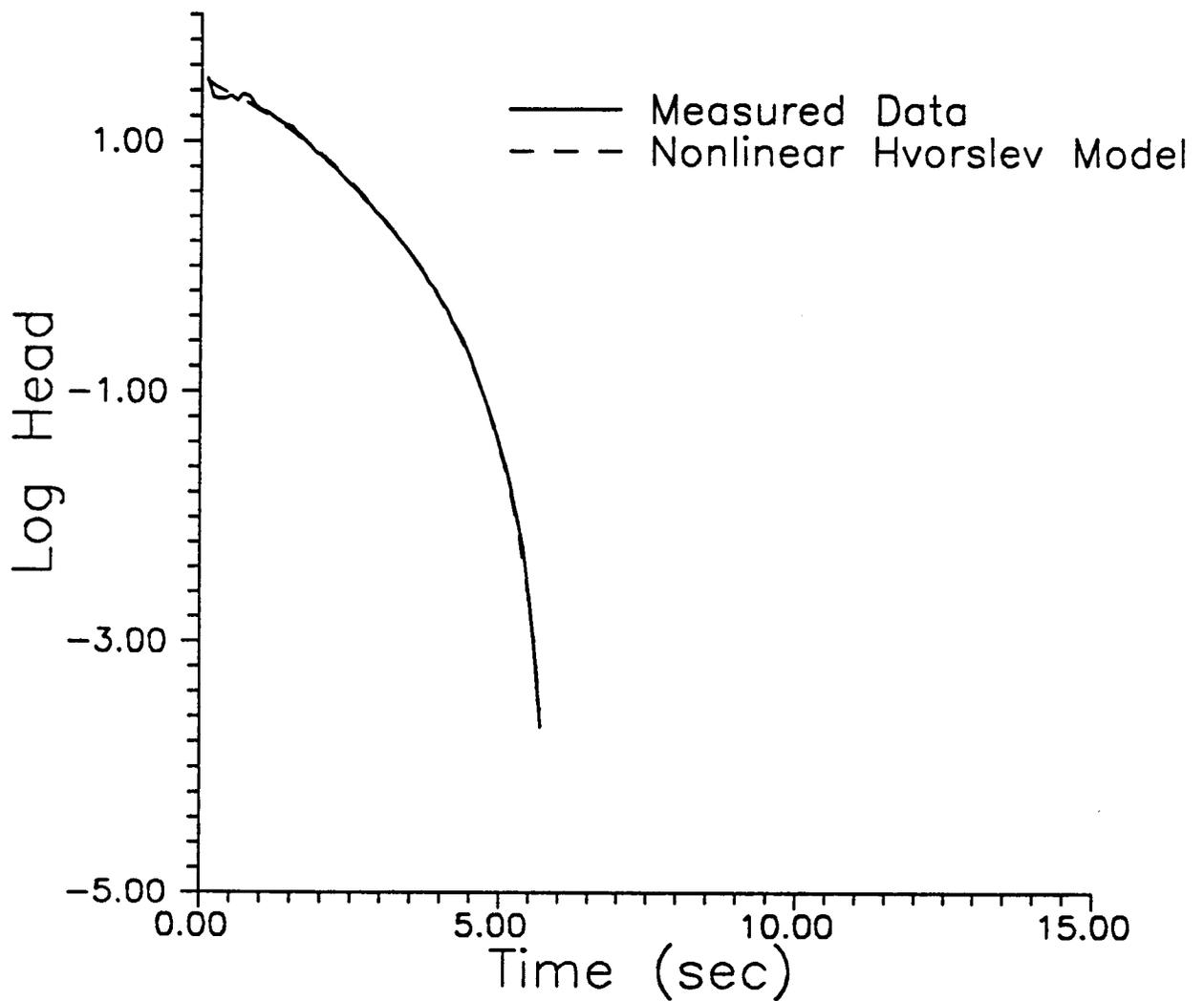Source to Receiver Offset (ft)

(a)   (b)

Figure III.C.3 - Natural logarithm of head versus time plots of slug-test data from a fully penetrating slug test at GEMS well 2-5 (H_0=.79 m) and the best fit nonlinear Hvorslev model.

IV. SITE CHARACTERIZATION ACTIVITIES

A. GEMS SLUG-TEST SURVEY

As part of the effort to describe the spatial variations in hydraulic conductivity in the subsurface at GEMS, slug tests were performed in most of the wells screened in the sand and gravel section. In all cases, the KGS single-packer slug-test system (McElwee and Butler, 1989) was used to perform these tests. As discussed in Section III.B, the slug-test response data from wells at GEMS have displayed anomalous features that prevent ready analysis by conventional methods. In Section III.C, a nonlinear variant of the Hvorslev (1951) model was developed in an attempt to account for the observed phenomena. Although this model does not apparently account for all the mechanisms that are affecting the slug-test data at GEMS, it does seem to do a better job than any other presently existing model. Thus, the data from this series of slug tests were analyzed by the nonlinear Hvorslev model (see Fig. III.C.3 for an example fit using data from this series of tests).

Table IV.A.1 summarizes the estimated parameter values determined from this program of testing. Note that in Sections III.B and III.C considerable attention was given to the issue of the dependence of estimated parameters on the magnitude of H_0. In order to minimize the error that might be introduced by this dependence, a calibrated container of known volume was used to add the water utilized as the slug at each well. Thus, the slug introduced at each well consisted of approximately the same volume of water. The actual H_0 did differ somewhat between wells (H_0 range was .67-.93 m) mainly as a result of the differences in the schedules (thicknesses of pipe wall) of the PVC casing used at wells at the site. The conductivity values listed on Table IV.A.1 are quite high, but they are not surprising given the coarse sand and gravel deposits underlying GEMS. As discussed in Section III.C, the nonlinear Hvorslev model does not fully account for the dependence on H_0. Thus, the values reported in Table IV.A.1 must be considered somewhat approximate. However, by controlling H_0 to within narrow bounds, the error due to the H_0 dependence should be similar between wells. Thus, the variations between the values reported on in Table IV.A.1 should be a reasonable reflection of the actual natural variability within the sand and gravel section at the site. Note that slug tests within the overlying clay and silt deposits and the underlying bedrock yielded conductivity values considerably lower than those of the sand and gravel section.

Well #	A (10^4 sec²/m³)	K (10^{-3} m/sec)	K (m/day)
0-1	1.577	0.893	77.13
0-2	0.676	0.984	84.98
0-5	0.411	0.499	43.11
0-7	2.250	5.19	448.22
1-1	0.527	0.735	63.55
1-5	3.764	1.69	146.21
1-7	3.212	1.84	158.67
2-2	0.142	0.506	43.69
2-5	1.164	0.537	46.43
2-6	4.022	0.730	63.07
2-7	3.124	4.71	406.61

Table IV.A.1 - Summary of estimated values for hydraulic conductivity (K) and the constant of proportionality (A) determined from a program of slug testing at GEMS. Parameters estimated using the nonlinear Hvorslev model described in section III.C.

B. PUMPING TEST OF BEDROCK WELL
Introduction

As part of our continuing effort to characterize the geohydrology of the GEMS site, we performed a pumping test on the 0-6 well (Table 1 of Section IV.D) which is drilled ten feet into bedrock. We decided to do this after earlier well development work at the site showed that the bedrock well was capable of producing 5-10 gallons per minute. Unfortunately, no other wells at the site are currently completed into the bedrock. Therefore, no observation well was available for taking data except the pumping well itself. We knew that typically a data set from a single pumping well was difficult to analyze due to complicating factors such as the presence of the pump and possible well bore storage effects. Also, a sensitivity analysis usually shows that a single pumping well is not very sensitive to some parameters. In particular, the storage coefficient is usually not very well determined for a single pumping well. We decided to perform the test anyway to see what estimates of bedrock parameters could be made and to take samples of the bedrock water over time to look at the geochemistry (next section IV.C).

The Pumping Test

The bedrock pumping test was performed in late April of 1992. We monitored the background water levels in the bedrock well (0-6) and two nearby alluvial wells screened at 65 feet (Well 0-5) and at 55 feet (Well 0-7) for a few days before and after the pumping test to see if there was any significant trend that would need to be subtracted out of the collected pumping test data. Also, we monitored barometric pressure during the same time periods to see if any corrections should be made for changing barometric conditions. The largest deviation observed that could be attributed to either a trend or barometric fluctuation was .11 feet of water. Therefore minimal correction is needed to the data.

During the pumping test we collected data from the three wells (0-6, 0-5, and 0-7) and from a flowmeter that was in the pump discharge line. All of this data set was collected automatically by a data logger and stored in computer readable format on floppy disks for later analysis. The pump was turned on and allowed to pump at 6.01 gpm (average value of flowmeter data) for one hour. At that point, the flow rate was increased to 8.04 gpm (average value of flowmeter data) for one hour. After two hours the pump was shut down and data were taken during recovery. Figure 1 shows a plot of the data collected in the pumping well versus time.

Data Analysis

Attempts to analyze the complete data set shown in Figure 1 with SUPRPUMP in a consistent manner have met with some difficulty. Different segments of the data (first pumping period, second pumping period, and recovery period) seem to indicate different values of the aquifer parameters. Clearly, the real world situation is much more complex than the simple models in SUPRPUMP can handle. It appears that further numerical analysis with the program discussed in section II.A is needed. The bedrock well extends ten feet into the bedrock from the base of the alluvium and is screened for the lower five feet. It would seem likely that the base of the alluvium is acting like a constant head boundary and producing a lot of leakage. This is borne out by the fact that during the pumping test the water levels in the alluvial wells changed by less than .2 ft. Also, partial penetration and well bore storage effects may be important. All of these things can be addressed with further analysis by the numerical model. However for this report, time has only permitted a preliminary analysis of the data with SUPRPUMP.

The first attempt to analyze the data used the Theis well function, which is the simplest well function. Figure 2 shows the data from the first pumping perion (one hour) and the resulting Theis curve fit. Clearly, the data at later time does not fit very well. The actual data flattens out while the Theis curve continues to decline. The obvious thought is that the leakage from the overlying alluvium is causing the data to flatten out due to an approach to steady state. SUPRPUMP allows leakage in one of its well functions, so the leaky well function was used to fit the data as shown in Figure 3. The fit is now fairly good except for a region where the actual data falls a little below the leaky curve. The fitted parameters are:

$$T \text{ (transmissivity)} = 10.94 \text{ ft.}^2/\text{day}$$
$$K \text{ (hydraulic cond.)} = 2.19 \text{ ft./day}$$
$$S \text{ (storage)} = .245$$
$$L \text{ (leakage)} = 1.21 \text{ ft}^{-1}$$

Conclusions

The hydraulic conductivity (about 2 ft./day) determined here is considerably lower than that determined by slug tests. Also, the storage coefficient of .245 is typical of an unconfined situation, not a semi-confined leaky aquifer. As mentioned earlier, later sections of the data give fitted parameters somewhat different from those given here. These difficulties are yet to be resolved. However, one thing seems clear from this data: there is a lot of leakage into the bedrock aquifer from the alluvial auifer. This leakage shows up as a large leakage parameter (L) and a large storage coefficient (S). This idea of leakage from the overlying alluvium is born out by the geochemical analysis of the

next section (IV.C). The need for further analysis of this data with a numerical model seems to be indicated.
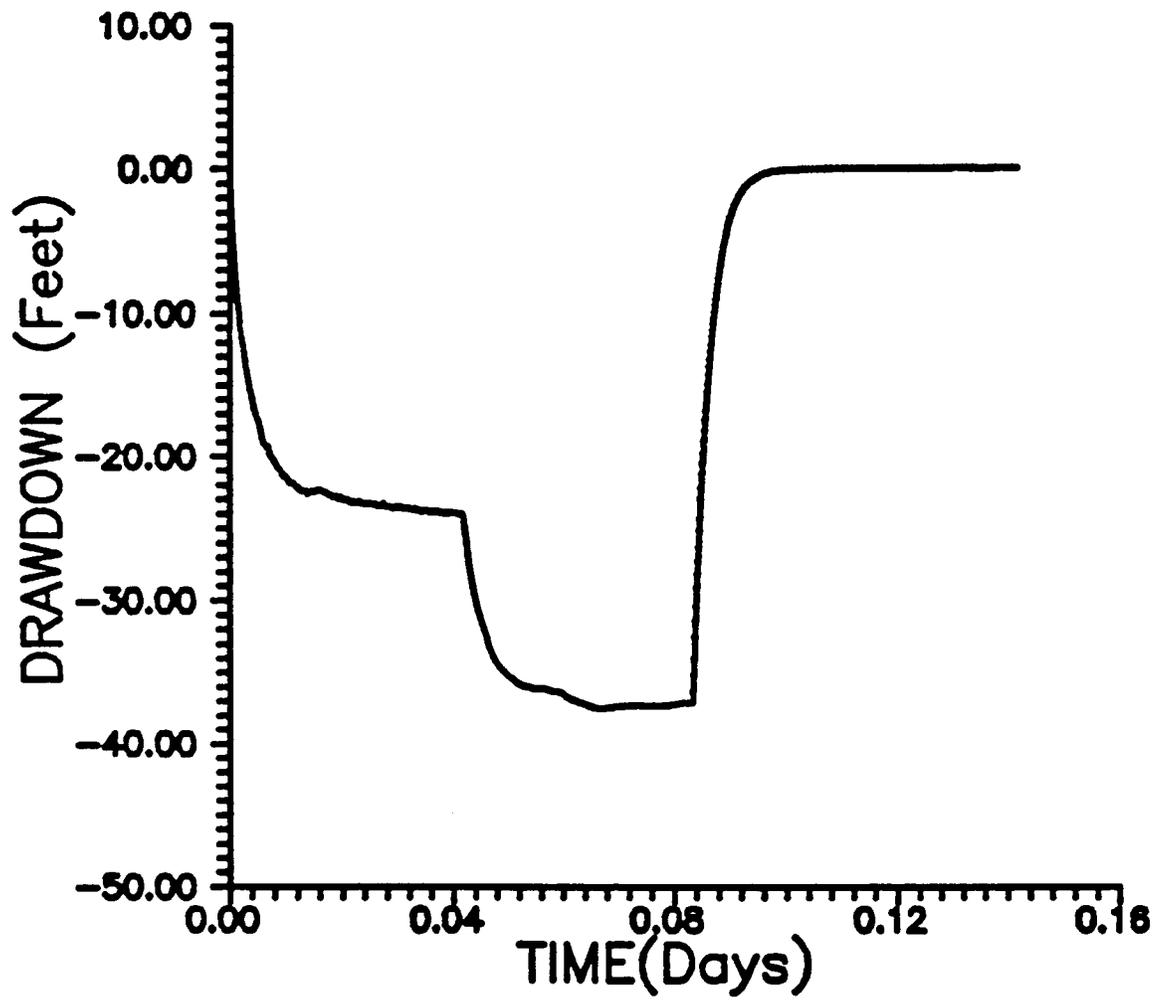
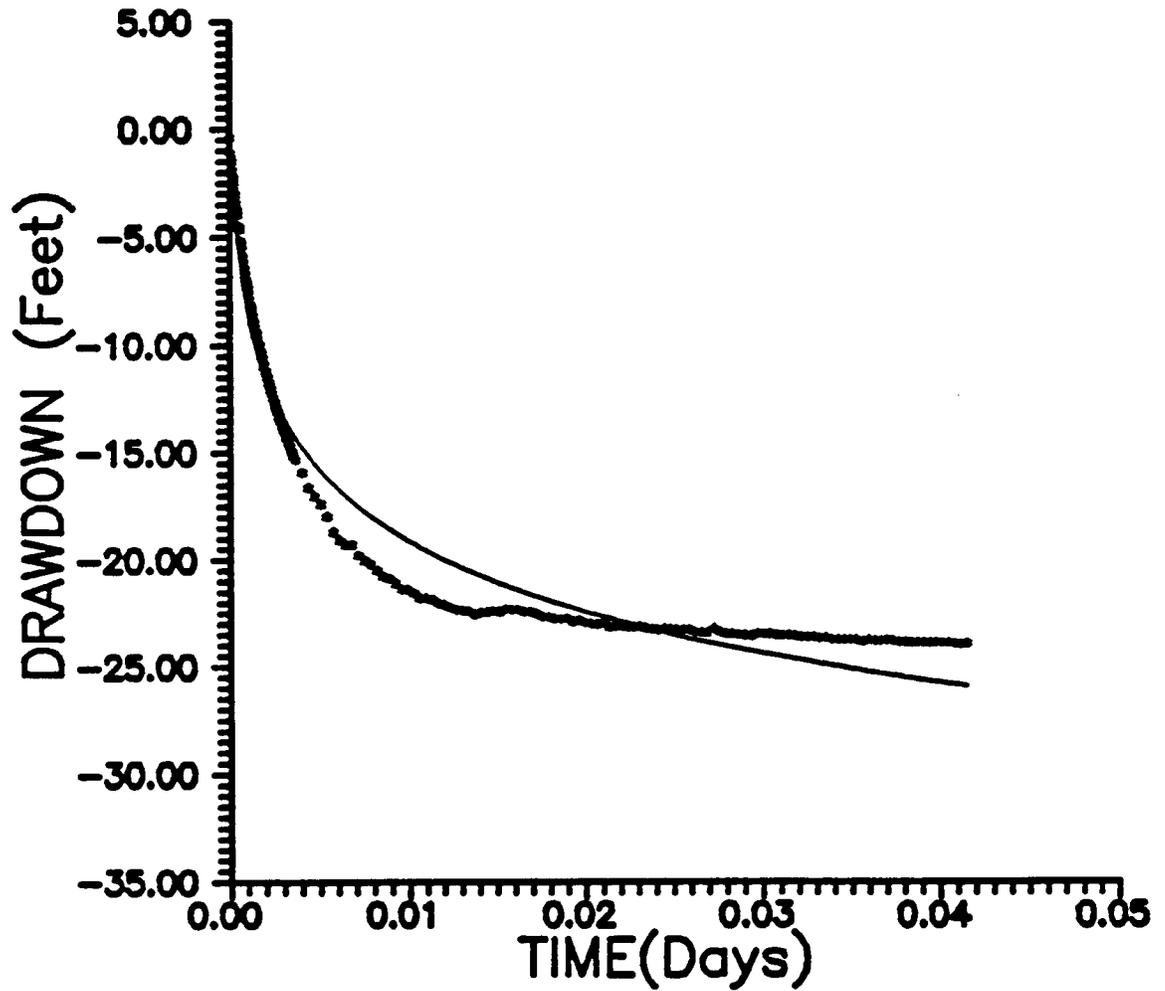Figure 1. Drawdown data from all three periods (two pumping and one recovery).

Figure 2. Fit of first period drawdown data to the Theis well function (solid curve).
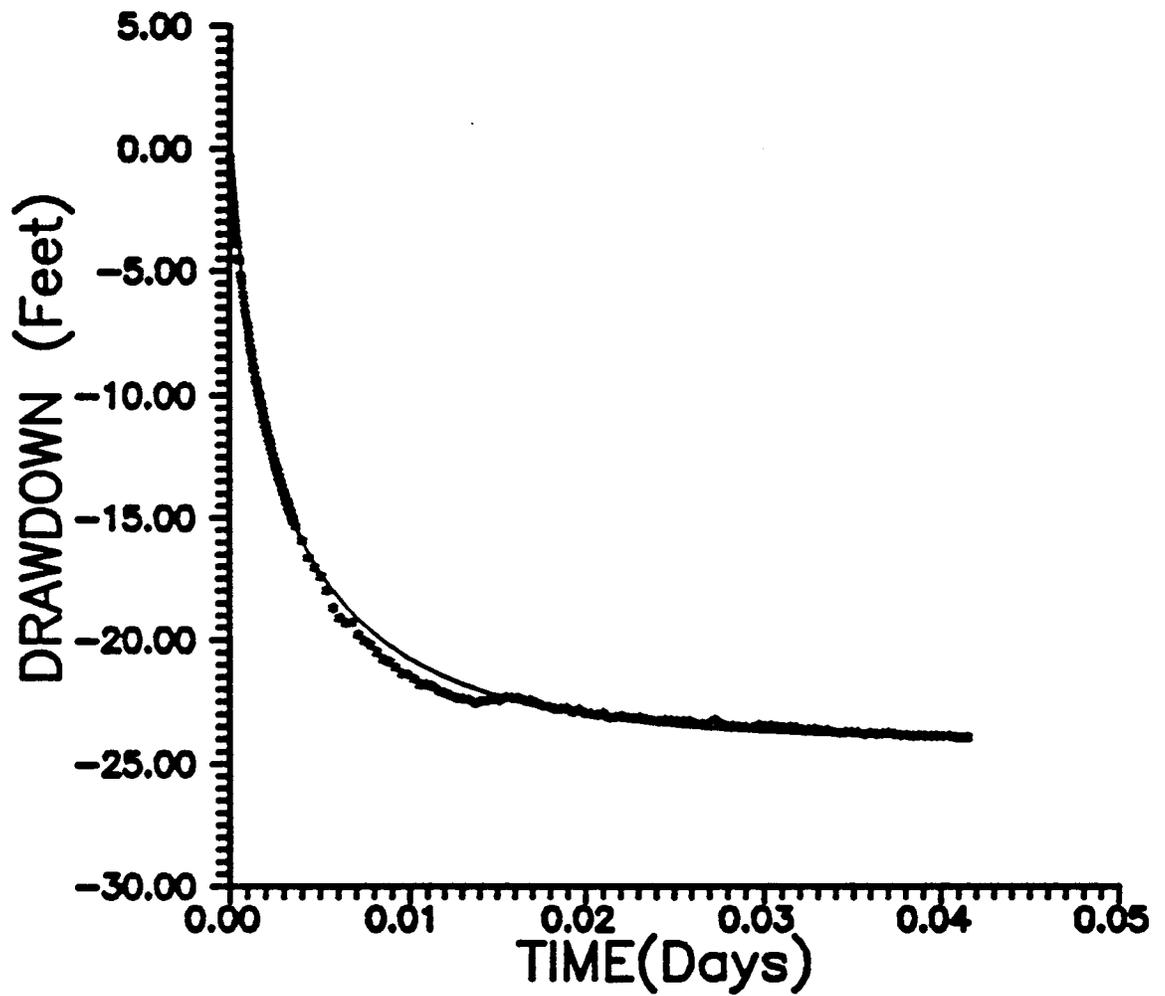
Figure 3. Fit of first period drawdown data to the leaky well function (solid curve).

C. AQUEOUS GEOCHEMISTRY AT GEMS
Introduction

The Geohydrologic Experimental and Monitoring Site (GEMS) near Lawrence, Kansas is instrumented with pumping and observation wells in three well nests. Most wells are screened at different levels of the 21-m thick Kansas River alluvium which underlies the site; one well is completed in the underlying bedrock, which is a Paleozoic sandstone (Shawnee Group). During the summer of 1991, a subset of the wells completed in the alluvium as well as the bedrock well served as preliminary test holes to evaluate geochemical variations in the ground water at the site. Based on the results of chemical analyses of the samples, water samples collected during a pumping test on the bedrock well during the spring of 1992 are here interpreted in terms of cross flow from the alluvial to the bedrock aquifer. In the larger view, this study shows that *in situ* variations in ground water chemistry are useful as tracers of flow, and have potential for quantifying induced cross-formational flow rates.

Methodology
Water Sampling and On-Site Processing

During sampling of wells to characterize geochemical variations at GEMS, two wells (bedrock well and GEMS 01) were pumped until the water temperature stabilized. At this time, approximately 1.5 L of water were collected in a half-gallon polyethylene jug for further processing. The pump was then stopped and temperature and pH measured in a 1000 mL beaker. Two wells were bailed with a Teflon® bailer until nearly dry (less than 0.3 m of water remained) and then allowed to recover for a few hours (NE nest, 35-foot well) or overnight (NE nest, 25-foot well). Approximately 1.5 L of water were bailed and stored in a half-gallon polyethylene jug for further processing. All samples were gravity filtered through 0.45μ filters immediately after collection. A 50-mL aliquot was titrated for total alkalinity using 0.02 N H_2SO_4 while the rest of the sample was filtering. One or two 250-mL low-density polyethylene bottles were filled completely with water, sealed, and stored on ice. One or two more bottles were filled with 250 mL of sample, 5 mL of concentrated HNO_3 immediately added, and the sealed bottles stored on ice.

Procedures for collecting samples during the pumping test are similar to those written above, except that duplicate bottles were collected for the filtered samples, and alkalinity titrations were not done.

Laboratory Methods

The anions F, Cl, SO_4 and NO_3 were determined by ion exclusion chromatography using a Dionex 4000i series ion chromatograph, using an AS4A exchange column, AG4A guard column, and a NG1 guard column. The instrument is equipped with a conductivity detector, and suppression of background conductivity was achieved using an anion micro-membrane suppressor (AMMS-II), continuously regenerated with 25 mN H_2SO_4 at a flow rate of 3 mL/min. The eluent used was 1.8 mM Na_2CO_3 and 1.7 mM $NaHCO_3$ at a flow rate of 2 mL/min. Relative standard deviations (standard deviation/mean) and precisions are shown in Fig 1a-d, and are generally less than 5% except for F and Cl which are strongly affected by the water dip. Spiking the samples with concentrated eluent (EPA, 1984; Test Method 300.0) helped but did not completely eliminate this problem. Tests were also made to assess the linearity of the anion calibration curves below the lower standard used to calibrate the instrument (fig. 2a-d). These tests also show that Cl is difficult to determine at low concentrations (less than 1 mg/L when the lower of two standards is 2 mg/L) either because the water dip results in false positive results or because low levels of Cl are present in the distilled-deionized water used to make up the solutions used in the test.

The cations Ca, Mg, Na, and K were determined by atomic absorption spectrometry using a Perkin-Elmer 2380 Spectrophotometer. Routine methods were used (Fishman and Friedman, 1989). These data are not included in this report, but were used to verify charge balance in the chemical analyses of the ground water samples.

Results

Initial Assessment--Variations in Ground-Water Chemistry at GEMS

Table 1 shows the partial chemical analyses of ground water from the GEMS site. Fig. 3 shows the vertical relationships of these results, illustrating the relatively small change in SO_4 content, the S-shaped curve of NO_3, and the backwards-C shaped curve of Cl distribution. Alkalinity (not shown; see Table 1) shows a steady and dramatic increase with depth. Although the two shallow wells and the bedrock well are screened to sample small intervals, the sand and gravel well (GEMS 01) is screened throughout the entire thickness of the sand and gravel. For this reason, it is not clear whether there is vertical variation within the sand and gravel aquifer. The sediment color (C. Mennicke, personal communication, 1992) suggests that there may be stratification of oxidized and reduced species within the sand and gravel aquifer. Even so, the results of these chemical analyses show that there is sufficient difference in the chemical signature of the sand and

gravel aquifer and the bedrock aquifer to use water chemistry to identify flow into the bedrock well during a pumping test.

Bedrock Pumping Test--Temporal Variations in Ground-Water Chemistry

During a two-hour pumping test of the bedrock well, water samples were collected approximately every 30 minutes to look for changes in water chemistry which would result from induced cross-formational flow from the alluvial aquifer into the bedrock. The first sample was collected eight minutes after pumping started, after temperature and pH of the effluent had stabilized. The well casing was evacuated completely after about nine minutes, according to calculations made using pre-test water level, well depth, casing diameter, and pumping rate, and thus the first sample probably represents mostly ground water which resided within the aquifer before the test. During the test, the pumping rate increased from 6.01 gal/min. to 8.04 gal/min. after 60 minutes of pumping. The chemical data show the same general results whether plotted versus time or versus gallons of water produced.

As shown on time versus concentration plots (fig. 4a-d), the water chemistry begins to change after the second sample. This is especially evident in the plot of NO_3-N (fig. 4a), in which NO_3-N is not detectable initially, but then increases nearly linearly in the last three samples. Cl also shows a linear increase (fig. 4c), although the relative standard deviation is fairly high in the early samples. F concentrations (fig. 4b) are so low that there are difficulties with reproducibility with the methodology used. SO_4 concentrations may have changed slightly during the pumping test, but the differences in SO_4 content of the sand and gravel aquifer and the bedrock aquifer is small enough to make discrimination at this mixing volume (see below) difficult.

Discussion

Origin of Chemical Variation in GEMS Ground Water

The chemical differences in ground water at GEMS have not yet been fully investigated. Geochemical modelling using PHREEQE (Parkhurst *et al.*, 1980) was begun, and preliminary results show that the chemistries are the result of equilibration with calcite under normal, shallow subsurface partial pressures of CO_2; ion exchange on clay minerals; possible dissolution of dolomite; and possible oxidation of pyrite along with introduction of NO_3 from the soil zone. Further modelling will be done to try to clarify and quantify these processes. The differences among the muddy alluvium, sandy alluvium, and bedrock aquifers provide a good opportunity to simulate geochemical processes in this system.

<u>Bedrock Pumping Test</u>

The pumping test showed temporal variations in water chemistry, although slight, did occur. Using NO_3-N as the best indicator of the "end members" (sand and gravel aquifer water having relatively high NO_3-N and the bedrock aquifer have undetectable NO_3-N), it appears that water from the sand and gravel aquifer is produced from the bedrock well after about 38 minutes of pumping. At the end of the test, about 5.6% of the produced water was water from the sand and gravel aquifer and the remaining part from the bedrock aquifer, *if NO_3-N concentrations in the sand and gravel aquifer are represented accurately by the sample from well GEMS 01*. Using NO_3-N content as an indicator of sand and gravel aquifer water, I predicted the concentrations through time of the other anions. These are plotted on figures 4b-d, and show that Cl concentrations are underpredicted, and that other anion concentrations are difficult to predict because of similarities in concentrations in the two aquifers and/or because of analytical difficulties with the element. The underprediction of Cl suggests that there may be chemical stratification within the sand and gravel aquifer, and that the Cl produced from the GEMS 01 well is lower than Cl in the lower part of the sand and gravel aquifer. Alternately, the NO_3-N in the lower part of the sand and gravel aquifer is lower than that produced from the GEMS 01 well, which in turn underpredicted the percentage of sand and gravel water produced from the bedrock well at the end of the pumping test.

In order to better predict the time at which sand and gravel aquifer water was produced from the bedrock well, the samples having detectable NO_3-N were fit to a straight line using linear regression. Figure 5a shows the result of this fit, and shows that leakage from the alluvium began just after the sample collected at 38 minutes after the start of pumping, or at 39.75 minutes as calculated from the equation for the best fit line. When this same calculation is made using the amount of water produced instead of time since pumping began (fig. 5b), the time when NO_3-N should have been detected (using 6.2 gal/min pumping rate) is about 37.8 minutes. Considering the analytical difficulty of detecting NO_3-N concentrations of less than about 0.08 mg/L, the two results are indistinguishable.

Note that the above calculation gives the time at which the mixed waters are produced from the well, not the true travel time of the NO_3-N rich water from the boundary between the alluvium and the bedrock and the screen in the bedrock well. As yet, calculations have not been made for the travel time within the well (from the well screen to the level of the pump) or the travel time within the drop pipe from the pump to the surface.

The flow velocity of leakage along the shortest path (vertical, near the well bore) can be calculated according to the method outlined in Appendix C, using several simplifying assumptions. This calculation will be done in the next year and can be tested with further experiments.

Conclusions and Future Work

The results of this year's work show that ground water in the sand and gravel aquifer, the upper muddy aquifer, and the lower bedrock aquifer are sufficiently different to be useful as "natural" tracers during pumping tests. The NO_3-N content of the alluvium, being investigated under another project, may be the result of over-fertilization of adjoining farmland, but is the best indicator of water sources for this project because it is relatively easy to detect and because the bedrock aquifer does not contain detectable levels.

The pumping test on the bedrock aquifer shows that water from the alluvium leaks into the bedrock aquifer during pumping, and preliminary calculations show that the alluvial aquifer water is produced after about 38 minutes of pumping.

Future goals for completion of this project include the following:

1. Characterize vertical stratification of water chemistry by sampling wells completed at different levels within the sand and gravel alluvium.

2. Repeat bedrock pumping test, but extend the test for a longer period of time to assess the steady-state leakage time. Use this to calculate ground-water velocities and vertical conductivity between the alluvium and bedrock aquifers.

3. Compare the ground-water velocities and conductivities calculated with those calculated from introduced tracers (such as NaBr).

4. If within the scope of the larger project, assess leakage from the upper, muddy alluvium into the lower, sandy alluvium by the same general procedure.
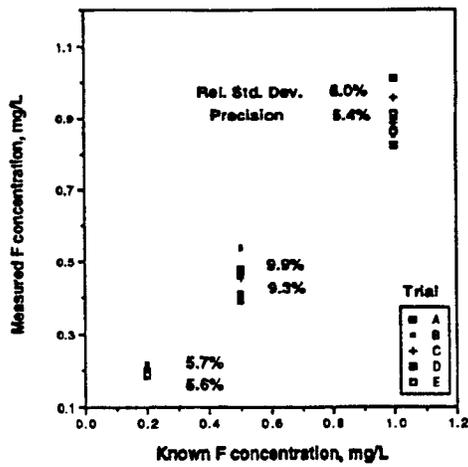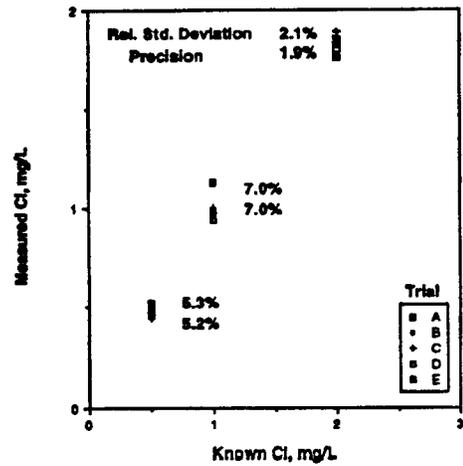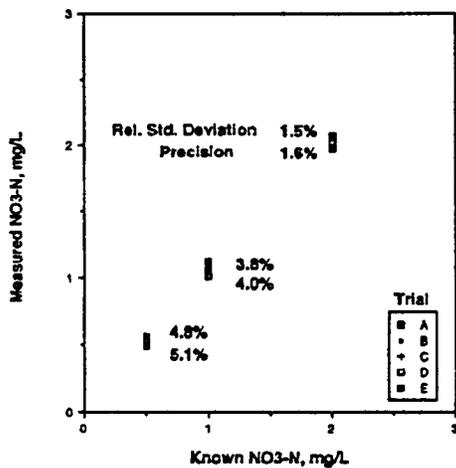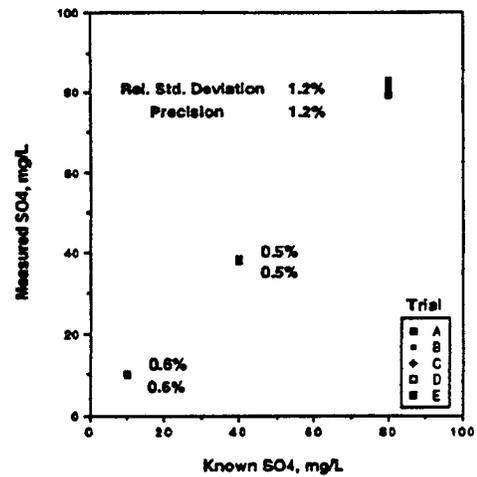
Figure 1: Precision and reproducibility test on anion concentrations determined by ion chromatography. Five trials of two measurements each on the four anions are used to calculate relative standard deviation and precision for each of three known concentrations. Lower precision (higher percentage) and higher relative standard deviation for F and Cl are probably the result of interference from the "water dip". All samples were spiked with concentrated eluent to try to eliminate this interference. a) Fluoride. b) Chloride. c) Nitrate reported as mg/L nitrogen. d) Sulfate.
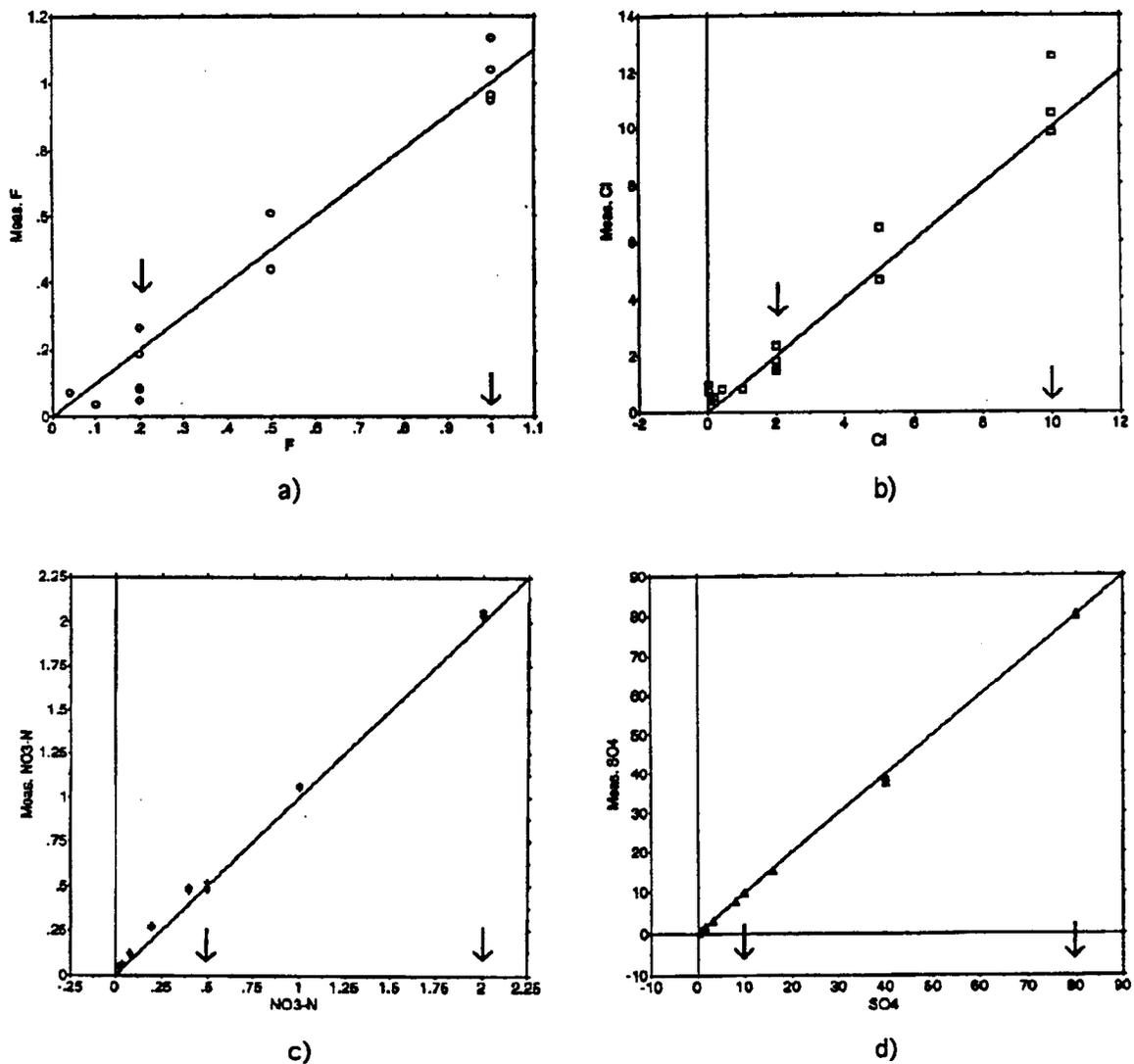
Figure 2: Determination of detection limits on anion concentrations determined by ion chromatography. One to two trials of two measurements each on four anions are used to assess how far below the lower of two calibration standards (concentrations shown by arrows on each graph) one can trust chromatography results. The one-to-one correlation line is shown on each graph. a) Fluoride. b) Chloride. c) Nitrate as mg/L nitrogen. d) Sulfate.
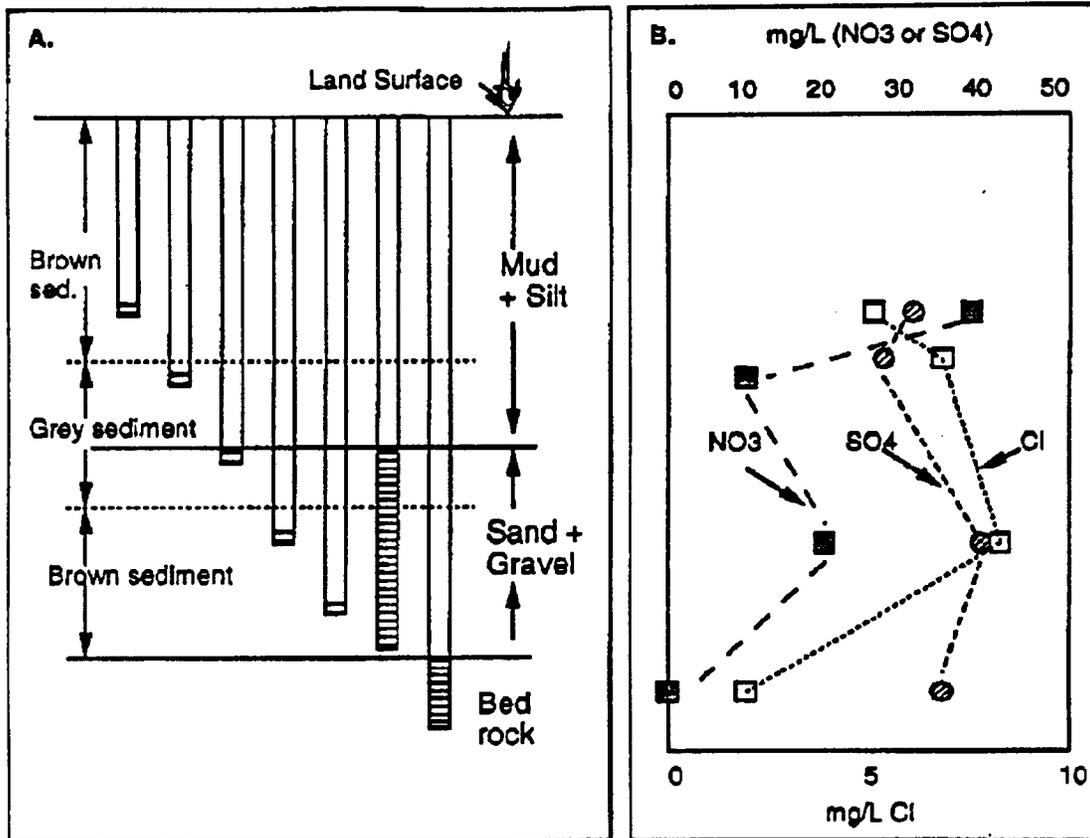
Figure 3: a) Schematic well nest at GEMS, showing screened intervals, depths of wells, and color of alluvial sediment (C. Mennicke, personal communication, 1992). b) Concentrations of NO_3, SO_4 and Cl change with depth. (NO_3 is reported as NO_3, not NO_3-N. Conversion factor is $NO_3/4.5$ = NO_3-N.) Higher NO_3 concentrations correspond crudely to oxidized (brown) sediment. The color change within the sand and gravel alluvium suggests that there may be chemical stratification within that unit.

a)

b)

IV.C.9
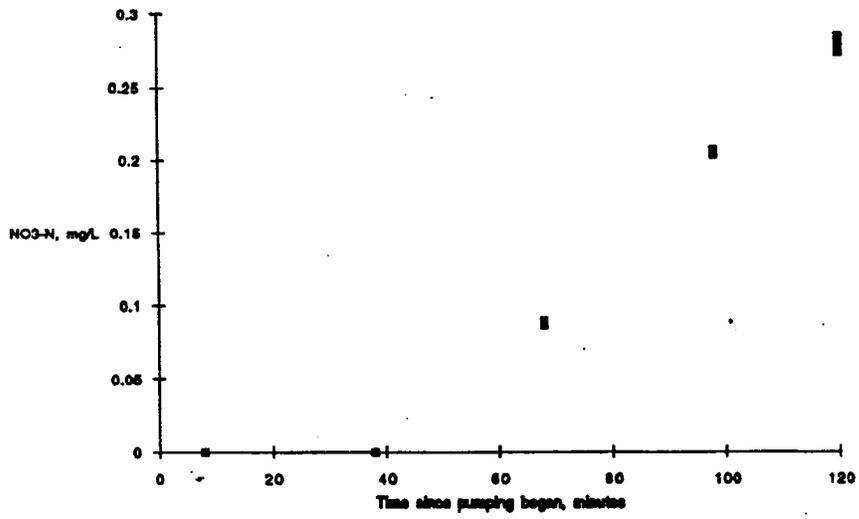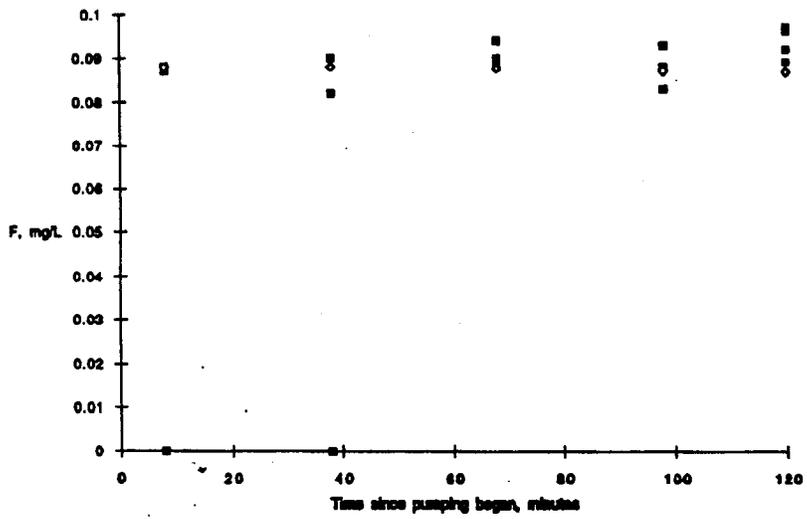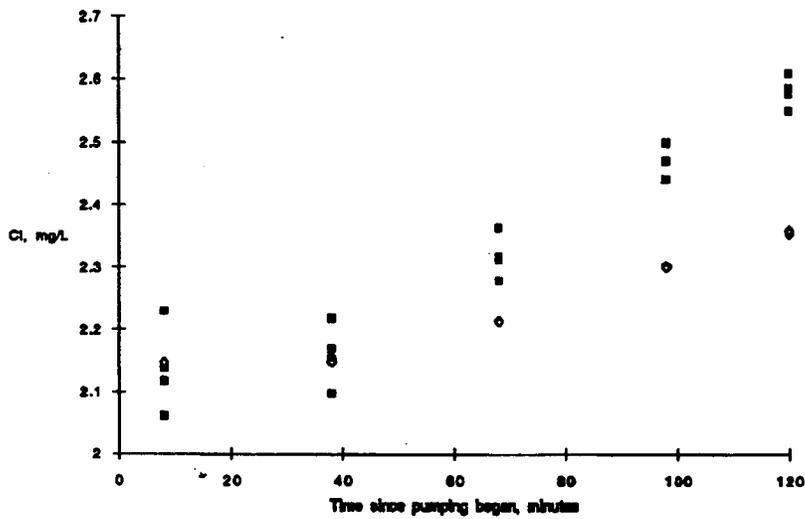
c)
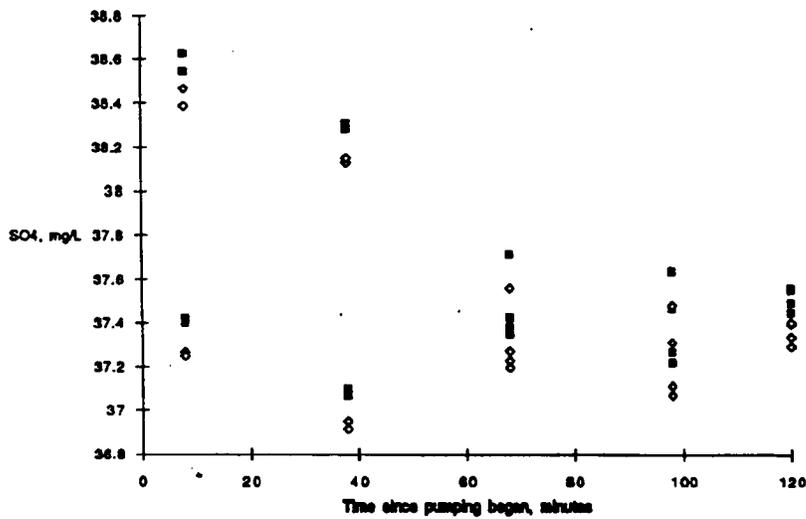
d)

Figure 4: Variation in anion concentrations during bedrock pumping test, and predictions of concentrations of F, Cl and SO$_4$ based on NO$_3$-N content. For each anion, an aliquot from two bottles was analyzed twice, resulting in four values for each anion for each time step (filled squares). Predicted results (unfilled diamond) are discussed in the text. a) NO$_3$-N. b) F. c) Cl. d) SO$_4$.
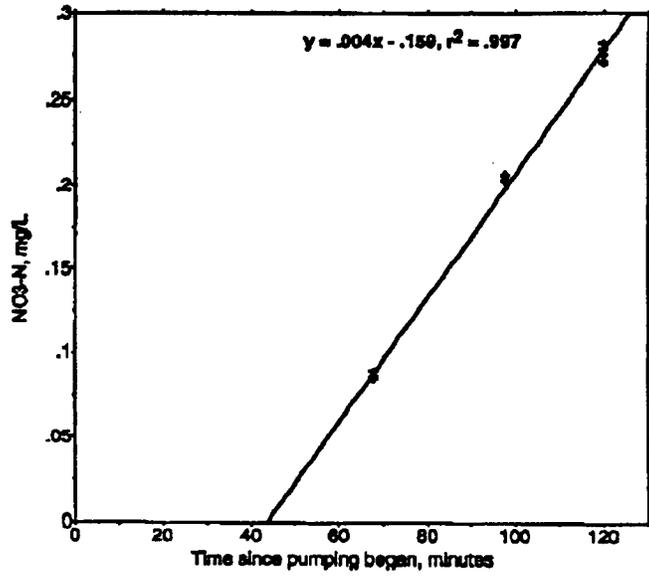
a)
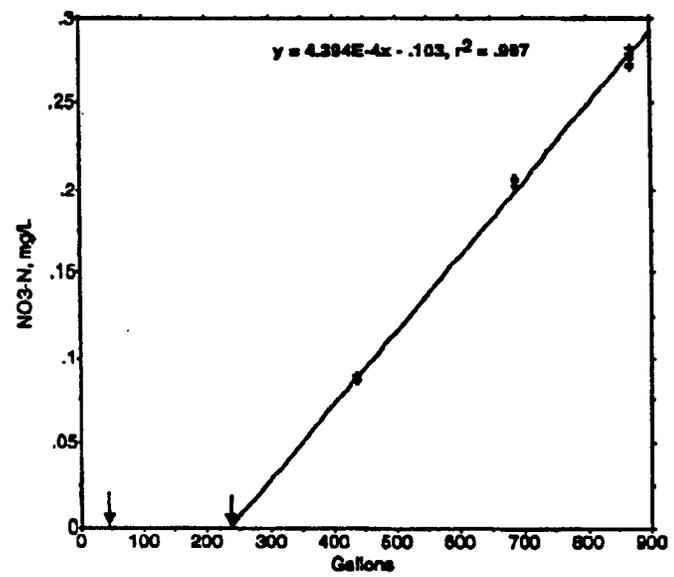
b)

Figure 5: Best fit line to those samples containing detectable NO₃-N. Lines for both NO₃-N *versus* time (a) and *versus* gallons of water produced (b) have very high correlation coefficients, and predict that leakage from the alluvium was produced from the bedrock well beginning at about 38 or 39 minutes. The first two samples, at time 8 minutes and 38 minutes, showed undetectable NO₃-N. These two samples are shown as arrows on 5b.

Table 1: *Partial Chemical Analyses of Ground Water at GEMS*
(concentrations in mg/L except as noted and except pH)

Well ID-->	GEMS 01	GEMS NE 25'	GEMS NE 35'	BEDROCK
Depth, m	21.3	7.62	10.7	24.0
Temp., °C	15.7			16.4
pH	6.89	6.77	6.79	7.08
Alkalinity, (as HCO3)	324	217	205	393
F	0.1	0.1	0.1	0.1
Cl	9.7	5.9	6.9	3.5
NO3-N	4.96	8.73	2.42	n.d.
SO4	43.0	29.5	27.5	38.0

n.d.: Not
  detected.

D. DRILLING AND SAMPLING ACTIVITIES

Introduction

Geologic site characterization is an important issue that must be addressed if details of contaminant transport in the subsurface are to be understood and predicted. Ideally, the formation heterogeneities at a site must be characterized at several scales. This section deals with the smallest practical scale: core samples with cross-sectional dimensions of a few inches. Historically, there has been great difficulty in obtaining relatively undisturbed cores of unconsolidated coarse sand and gravel. Prior to 1991, twenty five wells had been installed at GEMS in the Kansas River alluvium with hollow stem auger techniques. Six of these wells were cored through about 30 feet of coarse sand and gravel at depths of 40-70 feet using various techniques. A modified Waterloo sampler (Zapico, 1987; Zapico et al., 1987) was employed with good success, using drilling mud in the auger flights to control heave and help hold in the sample. However, the use of heavy drilling mud has disadvantages (potential to contaminate the aquifer and cores) and recovery without sample loss is difficult since the procedure is very sensitive to vibration and other mechanical forces. Without the use of drilling mud, the modified Waterloo sampler design was unsatisfactory because of relatively low recovery percentages. In order to address this limitation, new sampler designs were developed and field tested. The most promising design did not require drilling mud, achieved a very high recovery percentage, and was not as sensitive to vibration and mechanical forces during recovery. The new design (McElwee et al., 1991) incorporates an inflatable bladder, located in the drive shoe, which closes off the end of the sampler. The deflated rubber bladder lies behind a plastic sample liner as the core begins to enter the sampler. Near the end of the 5 foot sample drive, a piston extension triggers a release mechanism and allows a four inch retraction of the plastic liner, resulting in the bladder being in direct contact with the sediment. The bladder is then inflated from the surface with nitrogen gas, closing off the bottom of the sampler and allowing recovery with minimal opportunity for sediments to fall out. Using this sampler, we usually have been able to achieve about 85% recovery out of a possible 90% (drive shoe loss is .5 feet out of 5 feet due to bladder length and placement). The remaining 5% loss is due to compaction, premature piston movement, or wall friction preventing material movement into the sampler. After recovery the cores are taken to the laboratory for storage until measurement of hydraulic conductivity, porosity, density and particle-size fraction can be done.

Drilling Procedure

All except a few of the monitoring wells at GEMS have been installed with hollow-stem auger techniques. A review of hollow-stem auger techniques and equipment is given by Hackett (1987). Auger flights with 3 1/4 inch inside diameter and 6 5/8 inch outside diameter were used. The deepest wells at the site are about 70 feet. A typical installation would proceed by drilling to about 35 feet with a knock-out plate installed in the auger head in place of a pilot bit (Perry and Hart, 1985; Hackett, 1987). At that point, the plate would be knocked out by the pilot bit attached to drill rods then drilling and sampling could proceed to the desired depth. If no sampling is intended for that well, the plate may be left in until the completion depth is achieved. Alternately, if samples of the first thirty-five feet of silt and clay are desired, a split-spoon sampler with an overshoot mechanism for attachment inside the auger flights may be used. Typically, these split-spoon samplers are two feet in length and must be retrieved after every two feet of drilling.

Heaving sands or sandblows (Minning, 1982; Perry and Hart, 1985; Keely and Boateng, 1987; and Hackett, 1987) are a severe problem at this site in the zone of sand and gravel (35-70 ft.). It is absolutely essential to maintain greater hydrostatic pressure inside the auger flights than in the formation when coring in heaving sands. The water level inside the auger flights is maintained higher than the ambient water table by adding water at critical times (mainly, when tools are moved within the flights or the flights are moved). If a greater hydrostatic head within the auger flights is not maintained at critical times, several feet of sediment may quickly enter the flights, with the result that the possibility of obtaining an undisturbed sample at that depth is lost. Adding water to maintain a higher head in the flights may affect the chemistry and biota of an aquifer, so an investigator must balance this concern with the need to control heaving sands.

At GEMS, we are mainly interested in the sand and gravel aquifer (although we have taken continuous silt and clay samples for the first thirty-five feet at four of the well locations scattered over the site). Before knocking the plate out of the auger head at about 35 feet, the auger flights are filled with water from existing wells at the site. There is no known contamination at GEMS, so we simply pump water from a nearby well into the flights. Thus, we are not adding water of a dramatically different chemical composition to the aquifer. The pilot bit with drill rods is installed and drilling continues to about 40 feet. Below 40 feet, we typically want to obtain continuous samples. The sampler is designed to obtain a five foot core. Sampling occurs over the five foot interval

in front of the auger head before drilling down the next flight. Before sampling, the pilot bit must be withdrawn and the sampler inserted and driven beyond the auger head. Figure 1 summarizes the steps involved in obtaining a sample. Due to the close fit of the pilot bit and the sampler in the flights, there is great potential to induce heaving sands during removal of the pilot bit and retrieval of the sampler, so water is added to the flights at these critical times.

Drilling and Sampling - 1991

During the summer of 1991 four additional wells were drilled, sampled and completed (three of which were required by the terms of this project). This brings the total to twenty-nine wells at GEMS. Table 1 is a summary of pertinent information about all these wells. The latitude, longitude, and elevation data given in Table 1 were obtained through a cooperative surveying exercise with the 1st Battalion of the 127th Field Artillery of the Kansas Army National Guard. All the wells drilled during the summer of 1991 were cored from the surface to the bedrock, using the techniques outlined above. The split-spoon sampler was used for approximately the first thirty-five feet and then the bladder sampler was used until we hit bedrock at approximately seventy feet.

The samples of silt and clay from the first thirty-five feet were examined visually and detailed written logs of the visible physical features were prepared. At that point the silt and clay samples were discarded, since no further work was planned on them. In future years, we plan to take more samples and run hydraulic conductivity measurements on them while they are still fresh. We currently do not have the appropriate equipment for these very low-conductivity samples; however, we plan to buy the appropriate equipment in the next year.

Starting at approximately thirty-five feet, the bladder sampler was used to collect samples of the sand and gravel. Table 2 summarizes the sample recovery for all holes drilled in this time period (00-1, 1-7, 8-1, and 10-1). Other data about these wells can be found in Table 1. The overall recovery was about 80% which is about 5% lower than we were expecting. Due to the physical construction of the sampler (length and position of the bladder), six inches is always lost on the end of each sample. This means that 90% is the maximum recovery under ideal conditions. We usually lose another 5% due to compaction and other factors mentioned above, so 85% is about what we hope for typically.

The additional loss of 5% this season was due to a number of factors. In a couple of holes we had problems with cobbles blocking the sampler throat. In one extreme instance a two inch cobble (the sampler is only 1.5 inches in diameter) blocked the

entrance of the sampler and was recovered with the sampler. Another factor affecting recovery was the fact that we were testing driving mechanisms. Two holes were driven with a hydraulic hammer on the drill rig (00-1 and 1-7), one was driven with an electric jackhammer (8-1), and one was driven with an air jackhammer (10-1). The hole driven with the air jackhammer (10-1) had the best recovery and it is our evaluation from the field experience that the air jackhammer works best. We intend to drive future holes with the air jackhammer which we have purchased. We believe the increased recovery and ease of driving is due to the increased weight, power, and frequency of the air jackhammer.
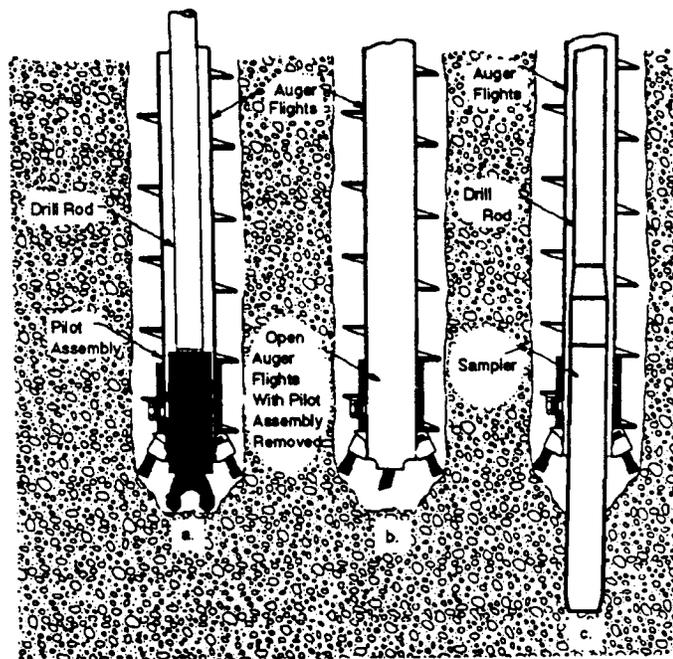
Figure 1. Sequential steps showing borehole
advancement with pilot assembly and collection
of a formation sample (after Riggs 1983).

Table 1

Well Data

Well Number	Latitude (North)	Longitude (West)	Elevation (ft)	Depth (ft)	Screen Length (ft)
0-1			829.424	71	30.00
0-2			829.291	46	2.29
0-3	39°00' 56.214"	95°12' 21.274"	829.393	36	2.44
0-4			829.132	25	2.50
0-5			829.413	65	2.29
0-7			829.414	54	2.29
*0-6	39°00' 55.083"	95°12' 21.137"	829.913	81	5.00
4-1	39°00' 55.260"	95°12' 21.141"	829.188	70	30.00
8-1	39°00' 55.418"	95°12' 21.095"	830.487	66	
00-1	39°00' 55.566"	95°12' 20.998"	829.188	58	2.50
10-1	39°00' 55.781"	95°12' 21.006"	828.668	57	
1-1			828.432	47	2.50
1-2	39°00' 55.493"	95°12' 20.756"	829.156	37	2.00
1-3			829.483	28	2.12
1-4			829.424	20	4.75
1-5			829.407	60	30.00
1-6			829.763	56	2.40
1-7	39°00' 55.803"	95°12' 21.838"	829.224	70	30.00
A1	39°00' 55.651"	95°12' 21.334"	828.488	32	
5-2	39°00' 55.694"	95°12' 21.008"	829.592	71	37.88
5-1	39°00' 55.998"	95°12' 21.018"	829.283	67	2.52

A2	39°00' 56.108"	95°12' 21.115"	829.868	26	
2-1			829.407	38	1.88
2-2	39°00' 56.323"	95°12' 20.950"	829.386	48	1.83
2-3			829.384	27	2.06
2-4			829.368	20	4.62
2-5			829.408	70	30.00
2-6			829.224	66	30.00
2-7			829.202	56	2.60

KGS Reference Mark: Latitude-North 39°00' 55.629"
Longitude-West 95°12' 21.274"   Elevation 827.563

* Well diameter is 5 inches; all other wells are 2 inches in diameter.

Table 2

Sample Recovery Analysis

Well Number	Segment Number	Segment Length (ft)	Head Space (ft)	% of Segment Length
Procedure: Hydraulic Hammer				
00-1	19	5.00	0.2031	4.06
00-1	20	5.00	0.2864	5.73
00-1	21	5.00	0.3542	7.08
00-1	22	4.67	2.8750	61.56
00-1	23	5.00	1.3229	26.46
00-1	24	5.00	0.2083	4.14
00-1	25	4.00	0.6771	16.93
00-1 Totals		33.67	5.9270	17.60
		Theoretical Recovery		82.40
		Bladder Loss		10.00
		Actual Recovery		72.40
Procedure: Hydraulic Hammer				
1-7	20	4.875	0.3229	6.62
1-7	21	4.833	0.3854	7.97
1-7	22	5.00	0.3229	6.46
1-7	23	5.00	0.3333	6.67
1-7	24	5.00	0.3958	7.92
1-7	25	5.00	4.3334	86.67
1-7	26	5.00	0.5000	10.00
1-7	27	5.00	1.3438	26.88
1-7 Totals		39.708	7.9375	19.99
		Theoretical Recovery		80.01
		Bladder Loss		10.00
		Actual Recovery		70.01
Procedure: Electric Jackhammer				
8-1	20	4.30	0.4583	10.66

8-1	21	5.00	0.6042	12.08
8-1	22	5.05	0.5312	10.52
8-1	23	5.00	0.3646	7.29
8-1	24	5.05	0.8125	16.09
8-1	25	5.00	0.5208	10.04
8-1	26	5.00	0.9792	19.58
8-1 Totals		34.40	4.2655	12.40
		Theoretical Recovery		87.60
		Bladder Loss		10.00
		Actual Recovery		77.60
Procedure: Air Jackhammer				
10-1	19	5.00	0.2083	4.17
10-1	20	5.05	0.1667	3.33
10-1	21	Numbering Omission		
10-1	22	5.10	0.2396	4.79
10-1	23	5.00	0.4583	9.17
10-1	24	4.95	0.2292	4.53
10-1	25	4.95	0.4583	9.23
10-1	26	4.95	0.7917	15.94
10-1 Totals		35.00	2.5521	7.29
		Theoretical Recovery		92.71
		Bladder Loss		10.00
		Actual Recovery		82.71
Well Totals		142.78	20.6821	14.48
		Theoretical Recovery		85.52
		Bladder Loss		10.00
		Actual Recovery		75.52
Bladder Loss - 10% of the total segment length, 14.28 ft, is lost due to the bladder mounting dimensions.				

E. LABORATORY ACTIVITIES
Laboratory Procedures and Methods

The cores recovered from the drilling and sampling summarized in the previous section of this report were taken to the laboratory for measurement of hydraulic conductivity in a constant-head permeameter. Prior to measurement, cores are stored under refrigeration to keep bacterial growth and evaporation to a minimum. The procedures and methods used in analyzing the core samples are essentially the same as those described in Butler et al. (1991) and Jiang (1991), with the exception of the changes noted below.

A new apparatus was developed to more accurately and efficiently calibrate the pressure transducers used in the permeameter. The calibration apparatus consists of metal pipe into which pressure transducers can be inserted with an air-tight seal, a rubber bladder to increase the volume of gas within the system, and a high-accuracy pressure transducer (Druck PTX 620 pressure transmitter) to serve as a pressure standard Nitrogen gas can be introduced into or released from the system in small amounts, simultaneously changing the pressure on both the pressure transducers and the pressure standard, while readings are recorded by a datalogger. The pressure transducers are then calibrated against the pressure standard. This new system can be used to calibrate both the pressure transducers used in the permeameter (0-5 psig) and the pressure transducers used in the field for slug and pumping tests (0-25 psig). Up to four pressure transducers can be calibrated at one time.

A Dwyer Series 650-2 temperature transmitter has been installed next to the thermometer in the permeameter. Water temperature is recorded by the datalogger at the same interval as water pressure in the outflow tubes of the permeameter, thus enabling temporal variations in viscosity values to be incorporated into the hydraulic conductivity measurements.

To more accurately determine the head drop over the cores, an instrument incorporating a dial caliper has been constructed and mounted on the permeameter. Water levels in glass-topped manometer tubes, which measure head at the top of each core and at the constant head boundary, can be read to the nearest .001 inch; readings are generally reproducible to better than .05 inch. This device allows us to use smaller head drops over the cores without increasing the percent error in our calculations.

Occasionally, a decrease in head at the constant head boundary is experienced due to lack of flow from the upper reservoir. To reduce the frequency of this occurrence, a new reservoir was installed that drains from the bottom rather than relying on a siphon tube exiting from the reservoir top.

X-rays are taken of each core sample to aid in the determination of changes in grain size and the identification of sedimentary structures. An aluminum filter was used to improve resolution at the edges of the core (Baker and Friedman, 1969). Using the X-rays as a guide, the core is cut into segments which are as homogeneous as possible within the 4 to 8 inch limit on segment size imposed by the permeameter setup. To inhibit organic growth, the core segments are then wrapped in plastic and aluminum foil and refrigerated until they are placed in the permeameter.

The amount of Thymol added to the water used in the permeameter has been increased to .1 g/l to further inhibit the growth of organic matter.

In order to keep the Reynolds number below one and reduce the possibility of non-laminar flow, the head drop over the core is kept as small as possible. This also decreases the entrainment of fine material as water moves through the core. The head drop is typically set at approximately .5 inches and increased if no flow occurs after 12 to 24 hours. Using this small head drop, cores take a minimum of 36 hours to saturate and stabilize, with some core segments requiring four to five days.

During the drying process, which precedes particle density analysis and dry sieving, clay-sized particles tend to coat larger grains and form sand-sized aggregates. This will cause the weight percentages of the larger grain sizes to be overestimated at the expense of the fines. To more accurately determine the weight percent of fine material in the core, the samples are wet-sieved with a 53 micron sieve after the particle density analysis. The weight percent of fine material is determined by comparing the dry weight of the sample before and after wet sieving. The coarse fraction is then dry-sieved to complete the grain size analysis. Even though some material is lost during the permeameter tests and the repacking process, this method of determining the amount of fine material should still be reasonably accurate, since most of the material that is lost is clay and silt sized.

No photographs are taken of the sediment before sieving.

Results and Discussion

Hydraulic conductivity values have been obtained for 50 of 51 segments from GEMS well 00-1, both in the undisturbed state (Figure 1) and after being dried and repacked (Figure 2). A comparison of the original and repacked hydraulic conductivity values is presented in Figure 3. The segment from depth 14.27-14.41 m below datum is composed of material that appears to be wood, so no permeameter test was run on that segment.

The undisturbed cores have an arithmetic mean conductivity of 20.16 m/day, with a sample standard deviation of 24.26 m/day. Values range from a minimum of .06 m/day

to a maximum of 94.28 m/day. There is no apparent trend in hydraulic conductivity with depth.

The repacked cores exhibit a higher mean conductivity and greater variability than the undisturbed cores. Values range from .04 m/day to 185.43 m/day with a mean of 44.82 m/day and standard deviation of 44.65 m/day.

For 45 of the 50 segments, the repacked hydraulic conductivity is greater than the original measurement. This is most likely due to the elimination of fine layers and redistribution of fine material during the repacking process, i.e. the repacked cores are generally more homogeneous than the undisturbed cores. In some cases, it is possible that the repacked cores could be less homogeneous than the undisturbed cores. Layers can be created within the core if a poorly sorted sediment is not sufficiently mixed while being repacked into the sample tube. For example, a one centimeter layer of fine material was noted at the top of the repacked sample 001-24-7 (depth 20.37- 20.56 m). For future repacks, we plan to use a sediment sample splitter to produce numerous small, homogeneous amounts of material to introduce into the sample tube to help eliminate this problem.

Decreases in Hydraulic Conductivity with Time

We have found that for many cores hydraulic conductivity increases (as the core completely saturates), reaches a maximum, and then decreases as the test continues. An example of this phenomenon for one core segment is illustrated in Figure 4. Possible explanations for this decrease in conductivity include biological growth, movement of fines, and mineral deposition. Maintaining the concentration of the biocide Thymol and employing as low a flow rate through the core as practical should reduce the influence of the first two possible factors. Calcite deposits have been observed on the plastic tubing, thermometer, and temperature transmitter of the permeameter, so a simulation using PHREEQE (Parkhurst et al., 1980) was run to determine the nature and amount of mineral material that might be deposited during the hydraulic conductivity tests.

The water in use in the permeameter is taken from the same site and depth from which the cores are taken to ensure as much as possible that the water will be in chemical equilibrium with the cores during the permeameter experiments. The water does experience some changes, however, before it is used in the permeameter: increased temperature, decreased partial pressure of PCO_2, and addition of Thymol. These changes may cause the water to precipitate mineral material in order to regain equilibrium.

Chemical analyses of water samples from GEMS are available from the fall of 1990 and the summer of 1991, and two of these samples are from the same depth from which water for the permeameter is collected. Both samples have similar chemical characteristics.

The PHREEQE simulation was performed by first creating a solution matching the temperature, pH and chemical composition of the two well water samples. Alkalinity was input as HCO3-, aqueous nitrogen gas was removed from the data base, and the pe was set at 9.0. The pe and pH were allowed to be determined by the reaction. The most abundant constituents of the coarse fraction in the cores are quartz and K-feldspar, so the saturation indices of quartz and microcline were adjusted to match the silica and potassium contents of the water samples. This resulted in the solution being slightly oversaturated with respect to quartz and undersaturated with respect to microcline. The solution was then equilibrated with laboratory temperatures (22 degrees C) and surface partial pressure of PCO2 (log PCO2 = -3.5). Thymol was added as a reaction to the computer simulated solution, and the solution was equilibrated with calcite to determine the amount of calcium carbonate that might be deposited.

The changes in alkalinity, pH, and pe that take place in the water according to the PHREEQE simulation are shown in Figure 5. The changes in the saturation index (log IAP/KT) of calcite are shown in Figure 6. The simulation shows that when well water is equilibrated with surface temperatures and pressures, calcite should precipitate. Calculations indicate that ten gallons of GEMS well water (approximately the amount used in the permeameter at one time) precipitate 3.56 cubic centimeters of calcite. What is not presently know is the kinetics of the situation. PHREEQE assumes all reactions reach equilibrium instantaneously. It is unclear how much of the calcite precipitates during the time the water is left to equilibrate with laboratory conditions (two weeks minimum) and how much is deposited in the cores and on the permeameter.

Future chemical analyses are planned to compare the calcium carbonate content of the water before and after the equilibration period in the lab, and before and after running a permeameter experiment. These analyses will allow us to better determine if deposition of calcite in the cores is contributing to the observed decrease in hydraulic conductivity with time.
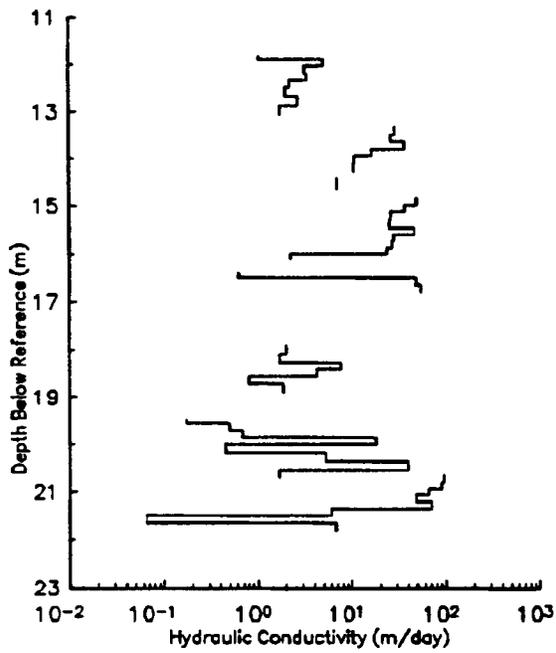
Figure 1. Profile of the original
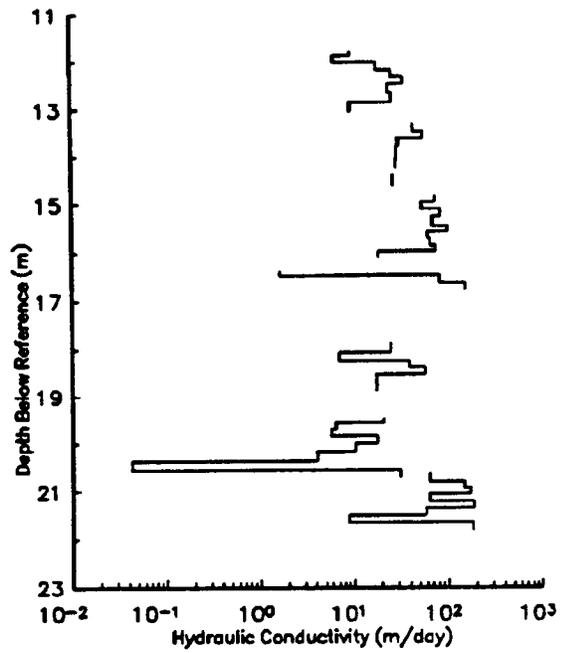hydraulic conductivity (K) at GEMS well 001

Figure 2. Profile of the repacked
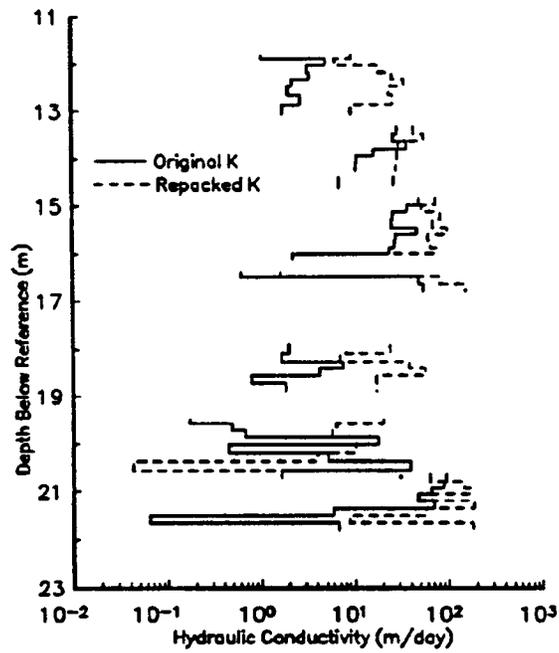hydraulic conductivity (K) at GEMS well 001

Figure 3. Profiles of the original and repacked
hydraulic conductivity (K) at GEMS well 001

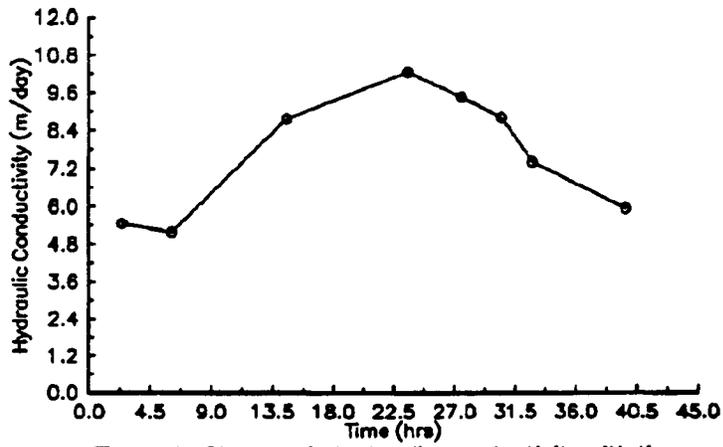Figure 4. Changes in hydraulic conductivity with time.
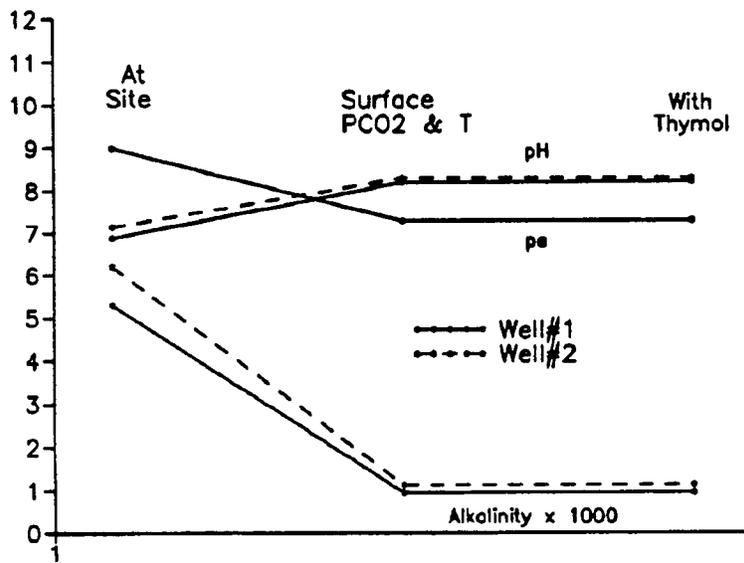Segment 5, Sample 24, Well OO-1

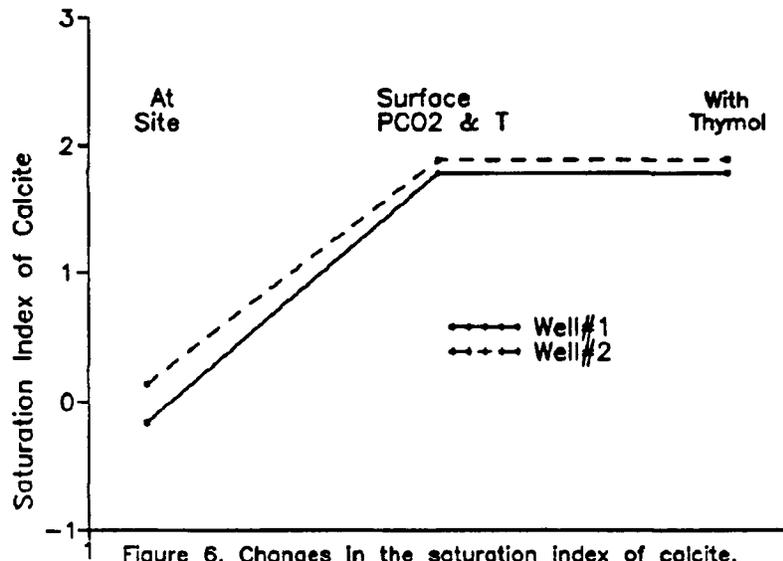Figure 5. Changes in alkalinity, pH and pe.

IV.E.6

Figure 6. Changes in the saturation index of calcite.
(SI = log ion activity product/equilibrium constant)

F. WIRELINE LOGGING ACTIVITIES

Geophysical logging had been one of the planned activities for the first year of this project. Unfortunately, delays in the bidding process moved logging activities into the second year of this project. A geophysical service company (AGE Co. of Austin, Texas), however, has now been awarded the bid and will perform the logging in early July of this year. The contract specifies that ten wells at GEMS will be logged using natural gamma and induction tools. The results of the logging survey will be discussed in the report of the activities of the second year of this project.

G. HIGH-RESOLUTION SEISMIC REFLECTION STUDY
Introduction

Seismic-reflection surveys have been extensively used for more than 60 years to image the subsurface for petroleum exploration. The successful use of the technique in shallow engineering applications, however, depends on several key conditions. First and foremost is the existence of acoustic velocity and/or density contrasts between geologic units in the subsurface. The second relates to the ability of the near-surface to propagate high-frequency seismic signal. Finally, the acquisition parameters and recording equipment must be compatible with the proposed target, resolution requirements, and environmental constrains of the survey. The application of shallow, high-resolution seismic reflection methods to specific geologic situations or problems requires a thorough understanding of the basic principles (Appendix B).

Shallow high-resolution seismic-reflection profiles can be useful in characterizing shallow structures significant to a variety of hydrogeologic settings. High-resolution seismic reflection has only recently developed as a practical and effective method for identifying zones of low permeability (Birkelo et al., 1987; Merey et al., in press), unconsolidated layers above bedrock (Steeples and Miller, 1990, Grantham, 1990), and mapping shallow (<30 m) bedrock surfaces (Hunter et al., 1984; Miller et al., 1989; Miller et al., 1990). The shallow seismic-reflection technique is inexpensive (relative to drilling) and can often decrease the need for drilling by an order of magnitude. While the seismic-reflection method can identify variations in the bedrock surface and stratigraphic relationships, it can give only estimates of depth. Explicit identification of lithologies requires confirmation drilling.

This section of the report displays and interprets seismic-reflection data acquired and processed to determine the feasibility of delineating stratigraphic or structural features of potential hydrogeologic significance at or above the top of a 70 ft deep bedrock surface. A series of walkaway noise tests (Appendix D) and two 200 ft CDP seismic lines were acquired in the Kansas River valley at the GEMS site (Figure 1). The walkaway tests included five different sources and seven analog low cut filter settings with a total apparent spread length of approximately 96 ft. The 200 shot point CDP survey with 2 ft station spacings was conducted using a downhole 30.06 rifle, 100 Hz geophones, 280 Hz analog low cut filters, and a Geometrics 2401x 48 channel seismograph. The data were acquired and processed with the bedrock surface as the primary target.

Data Acquisition

All data for this study were acquired with an EG&G Geometric's 2401x seismograph. The Geometric's seismograph amplifies, filters (analog), digitizes the analog signal into a 15-bit word, and stores the digital information in a demultiplexed format. The selected low cut filters have a 18 dB/octave rolloff from indicated -3 dB points. The 1/5 ms sampling interval resulted in a 5000 Hz sampling frequency recording 1024 samples for a record length of 204 ms. The Geometrics 2401x is a 48 channel floating point seismograph.

A variety of field parameters and equipment were tested to insure optimization of recorded data. The sources for the testing included downhole 30.06 and 50 caliber rifles (Steeples et al., 1987), 12 and 8 gauge auger gun (Healey et al., 1991), and 7.3 kg sledge hammer (Neitzel, 1958). The receivers for the entire study were single Mark Products L-40A 100 Hz geophones with two wired in series for the production portion of the survey. The receivers were placed in a 2 ft in-line array to attenuate source-generated air coupled wave.

The production seismic profile was preceded by an extensive series of tests (Appendix D). Proper matching of high- and low-cut filters for acoustic characteristics and targets at this site allowed optimization of the seismograph's dynamic range. Source-to-receiver offsets on walkaways ranged from 1 to 96 ft with receivers spaced at 1 ft intervals. Reflections, direct wave, refractions, ground roll, and air-coupled wave can all be easily identified on walkaway data (Appendix D). A typical walkaway noise test record is shown in Figure 2 (30.06 rifle). Reflections can be interpreted on unprocessed data recorded with 140 Hz and higher lowcuts. All aspects of the testing were instrumental in fine-tuning the acquisition parameters and equipment for the CDP portion of this study and in determining the potential of several variations in the acquisition process.

Production data for this study were acquired using the 30.06 downhole rifle, 2-100 Hz geophones in series, 2 ft station spacings, 8 ft source to nearest receiver distance, 280 Hz low cut and 1000 Hz high cut analog filters. The 280 Hz analog low cut filter shaped the pre-amplified spectra, enhancing the higher frequency components of the recorded energy. The near source-to-receiver offset would have allowed the recording of any intra-alluvial reflection with sufficient signal strength to set the seismographs least significant bit. The quality of bedrock and intra-alluvial reflections suggest the acquisition parameters and equipment were matched for this site and the associated geologic target. Parameters were selected to enhance the bedrock reflection recorded

during the walkaway tests. The bedrock reflection can be easily interpreted on most field files across the line.

Data Processing

Data processing was done on an Intel 80486-based microcomputer using *Eaves-dropper*, a set of algorithms marketed by Interactive Concepts Incorporated. The processing flow was similar to those used in petroleum exploration (Table 1). The main distinctions relate to the conservative use and application of correlation statics, precision required during velocity and spectral analysis, extra care during muting operations, and lack of deconvolution.

The air-coupled wave and the cyclic nature of the direct wave energy was not removable with spectral filtering and was not sufficiently attenuated during the 24 fold CDP stacking process to allow reflections shallower than bedrock to become apparent. F-k filtering improved the coherency and signal-to-noise of reflecting events above the bedrock surface. F-k filtering improved slightly the signal-to-noise ratio on stacked data.

For most basic shallow, high-resolution seismic reflection data the processing steps/operations are a simple scaling down of established petroleum based processing techniques and methods. However, processes such as deconvolution have basic assumptions that are violated by most shallow data sets. Migration is another operation that due to non-conventional scaling (vertical and/or horizontal) many times may appear to be necessary when in actuality geometric distortion may be simple scale exaggeration. Operations performed on data for this report have been carefully executed with no restrictive assumptions and with care not to create artifacts.

Results

Unequivocal identification of reflection energy on field files is essential for accurate interpretation of CDP stacked sections. Many of the raw field files acquired for the production portion of the survey have a confidently identifiable reflection event at approximately 65 ms (Figure 3). The 65 ms reflection has a dominant frequency of approximately 140 Hz and an apparent NMO velocity of around 3000 ft/sec. These characteristics represent an approximate depth to the reflector of 70 ft and a vertical resolution potential of about 5 ft. The signal-to-noise ratio on the raw file is sufficient to confidently identify bedrock reflections on most files at offsets longer than about 50 ft. The air coupled wave is the highest amplitude event on most files and increases the background noise of near-vertically incident reflection energy arriving later in time.

Analysis of processed field files improves confidence in interpretations of CDP-stacked sections (Figure 3). Digital filtering, first arrival muting, appropriate trace balancing, bad trace editing, f-k filtering, and trace balancing were key processes in improving the pre-stack appearance of reflections interpretable on raw field files. The reflection event identifiable at approximately 65 ms is less evident and possesses almost a 40% drop in dominant frequency on files recorded during the production portion of the study in comparison to walkaway files. This drop in overall signal quality predicates care and a conservative approach to interpretations of coherent energy on stacked data.

The event interpretable at 8 ft of offset and 30 ms is suggested to be the reflection from the clay/gravel interface at approximately 30 ft (Figure 3). An uphole velocity check shot (Grantham, 1990) allows confident correlation between the time seismic section and depth of events present above the bedrock surface (Figure 4). The event is high amplitude and possess some apparent hyperbolic curvature, especially on processed field files. However, the event has characteristics that make it difficult to confidently rule out an alternate interpretation that identifies it was a refracted arrival. Due to the hyperbolic nature of the event and the coherency at offsets at least as short as 8 ft, it will be interpreted as the clay/gravel reflector on CDP stacked data.

The bedrock reflection is coherent on field files at offset from 30 to 96 ft (Figure 3). On all files the bedrock reflection is at least interpretable at offset in excess of 80 ft. At offsets longer than about 75 ft the pull-up and associated stretch necessary to correct for non-vertical incidence is sufficient to drop the dominant frequency by as much as 25%. To reduce the detrimental effects of the NMO stretch, a stretch mute can be applied. However, if the stretch is reduced to less than 15%, information at offsets greater than 50 ft are muted leaving only the very close offset energy. Due to the minimal amount of reflected energy returning from the bedrock surface at offsets less than 50 ft, an excessive amount of stretch was necessary to produce an interpretable section. The reflection wavelets were allowed to stretch almost 50% before muting was permitted. The effects of this are evident on moved-out field files. The allowance of excess stretch was a necessary trade off on this data set to maintain sufficient coherency on the bedrock reflection.

Coherent events can be interpreted across the entire CDP stacked section (Figure 5). The stacked section possesses nominal 24 CDP fold as a result of the 48 channel recording system and selected recording geometry. The dominant frequency of most CDP stacked reflection energy is between 100 and 175 Hz. The stacking velocity ranged from 1900 to 3500 ft/sec. Variation in the depth to the clay/gravel interface at approximately 30 ft is no greater than 2 ft across the 170 ft of CDP line acquired for this study. The bedrock reflection possesses a decrease in dominant frequency resulting from the over-

stretching of reflection wavelets necessary to compensate for non-vertical incidence. Anomalies on the bedrock surface, such as the one interpreted at CDP location 270 could represent localized topographic relief on the bedrock surface of as much as 7 ft. Drill data from the area has encountered apparent relief of no greater than approximately two feet. Source-to-receiver offsets were not conducive to the recording of reflections from interfaces deeper than about 70 ft. Reflection events from within the Pennsylvanian sediments are interpretable on the stacked section at times greater than 80 ms but do not possess the coherency and wavelet consistency that is possible, due to the focused nature (70 feet or less) of this survey.

Only subtle indications of reflections from within the gravel portion of the section can be interpreted (Figure 5). Between CDP's 290 and 340 there is some indication of a reflection at a time of 42 ms. The event could be interpreted as a lens type feature with erosional termination at CDP 310 and 330 resulting in a 'hole' in the center of the lens. This interpretation is speculative but is a possibility in an alluvial setting such as this. This lens feature is probably less than 5 ft thick with an areal extent of no greater than 50 ft. The gravel portion of the section (between 30 and 70 ft) is for the most part acoustically transparent.

The most significant feature interpretable on the bedrock surface is present between CDP 260 and 300 (Figure 5). This feature appears to be a small bedrock mound with an associated low possibly filled with bedrock rubble. The significance of this event can not be fully ascertained without drilling/coring. The maximum change in bedrock elevation across this feature is about 6-7 ft. A defocusing of seismic energy is evident in the 80 ms reflection as a result of the severity of the dip on the bedrock between CDP 260 and 300. Another feature between CDP 360 and 400 could represent another bedrock rubble zone with undulations in the bedrock surface and associated fill. Confident interpretations of reflections associated with intra-alluvial features initially requires detailed confirmation drilling to establish key criteria for evaluation.

Conclusions

Shallow seismic reflection can be used to delineate structural features present between the clay/gravel interface at about 30 ft and the bedrock surface at slightly more than 70 ft. The close proximity and total number of boreholes on this site would suggest any feature that could potentially alter the hydrologic characteristics of this site between the ground and bedrock surface would have been detected. If the interpretations of the bedrock surface are accurate, the feature at CDP 270 represents a previously undiscovered bedrock high and low. The subtle event interpreted just below the

clay/gravel interface at CDP 330 could represent a localized non-permeable zone capable of significantly altering the local hydrologic properties. The presence of the deeper reflection events allows confidence in the interpretations of relative topographic change on the bedrock surface as a result of actual elevation change and not related to near-surface irregularities.

The data quality on this line was severely decreased in areas where the near-surface had been altered by surface traffic and/or drilling activities. Due to the extremely close spacing of boreholes and borehole activities much of the ground surface has been non-uniformly altered. The high resolution seismic method is very sensitive to near-surface conditions. Improvement in signal-to-noise and dominant frequency would be possible in this area if data were acquired in relatively undisturbed locations.

Recommendations

Several confirmation boreholes are essential to the verification of the interpretations presented here. The features interpreted are related to acoustic contrasts in the subsurface. The boreholes should be located at CDP stations 250, 275, 285, 350, and 380. The hole at 250 and 350 represent localized norms. The hole at 275 allows interpretation of the high associated with the low at 285. The borehole at 380 should allow identification of the source of the second reflection at 55 ms splitting off the bedrock reflection at 60 ms. Without the earth truth possible through drilling, there is no way to confidently designate the geologic significance of seismically detected features.

Future seismic lines acquired in this area should possess station spacing of no greater than 1 ft, directing efforts toward containment of more of the air coupled wave. All recorded reflection information with offsets greater than 75 ft possessed characteristics of wide-angle reflection and when corrected for non-vertical incidence display excessive wavelet stretch. At this site near-vertical incident energy is essential and extremely low levels of recorded air-couple wave and direct wave ring are important to the eventual resolution and signal-to-noise ratio of the resulting data set.
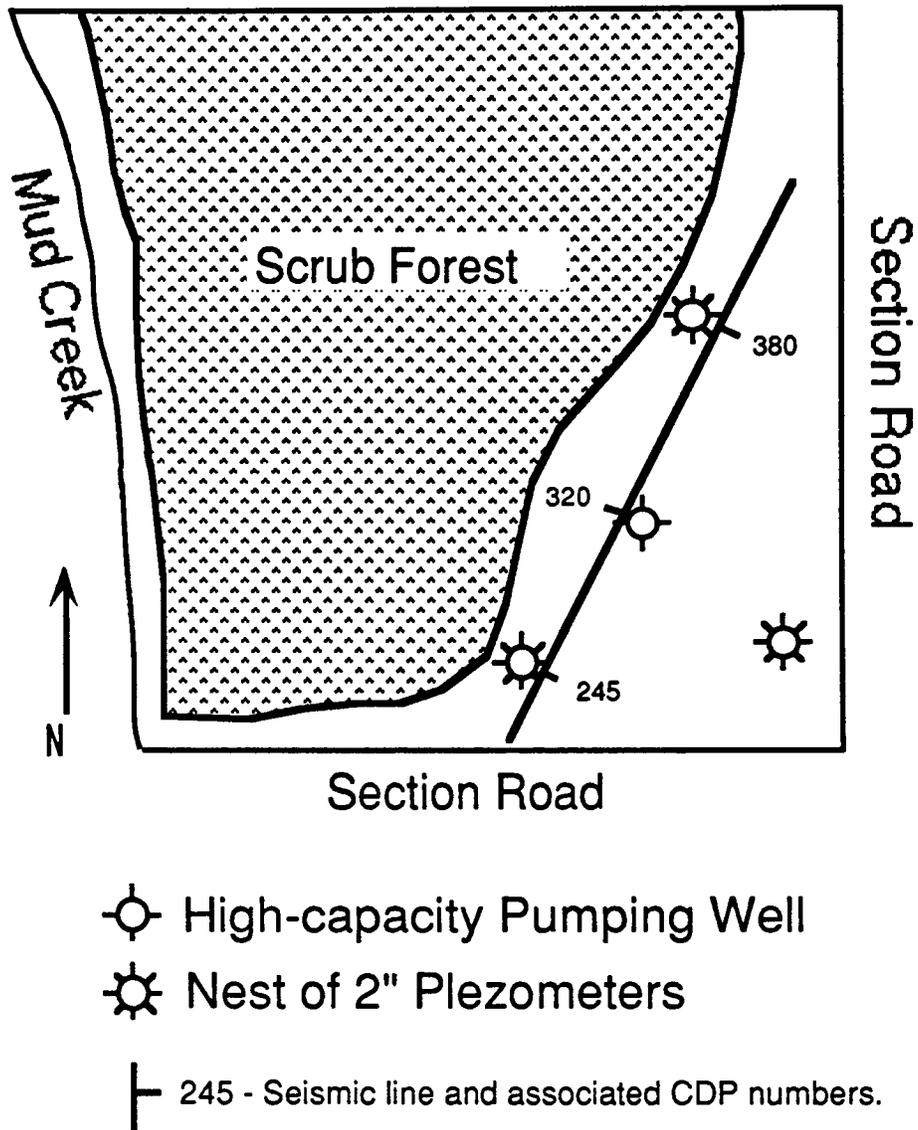
Figure 1. Site map showing relative location of seismic line with respect to existing well locations.
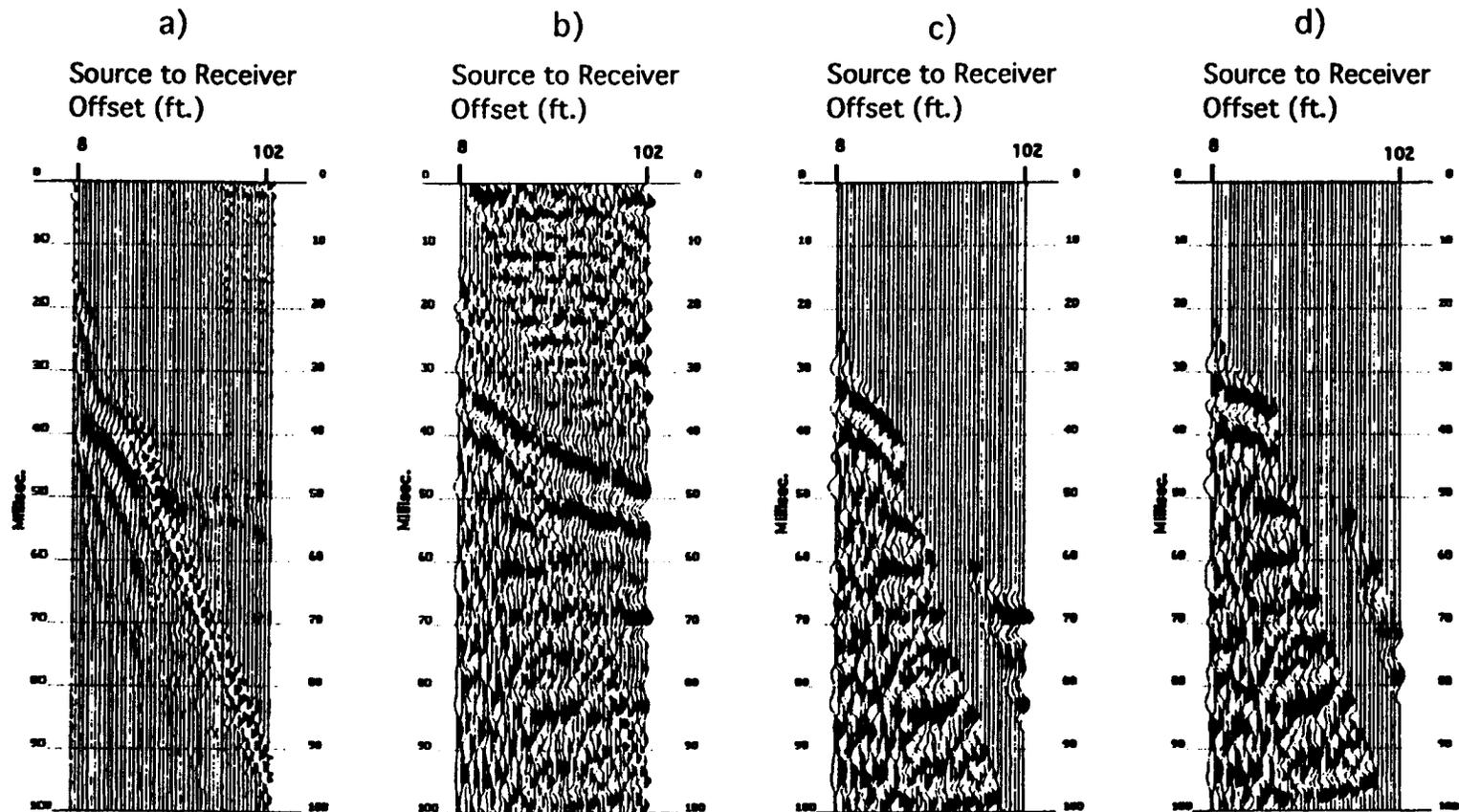
Source to Receiver Offset (ft.)

a)   b)

Figure 2. A typical walkaway noise test record with the downhole 30.06 rifle. a) represents the raw field file with a 25 ms AGC scale, b) represents a) with a 100 Hz digital low cut filter. These data were recorded with analog low cuts at 200 Hz.

Figure 3. Selected field file displaying the processing sequence. a) raw field file normalized,
  b) f-k filtered, AGC scaled to 25 ms, and digital filtering 125 to 250 Hz, c) appropriate
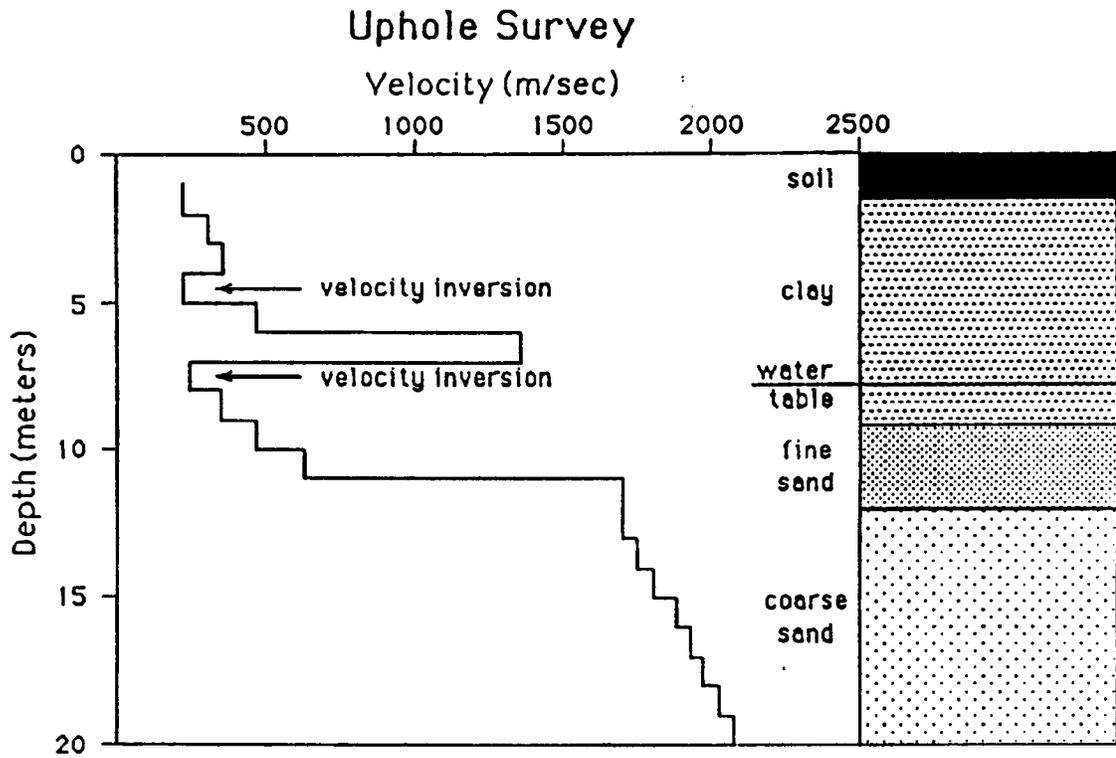 muting and trace balancing, d) moved out to adjust for non-vertical incidence.

Figure 4. Uphole survey and associated geologic cross-section (from Grantham, 1990).
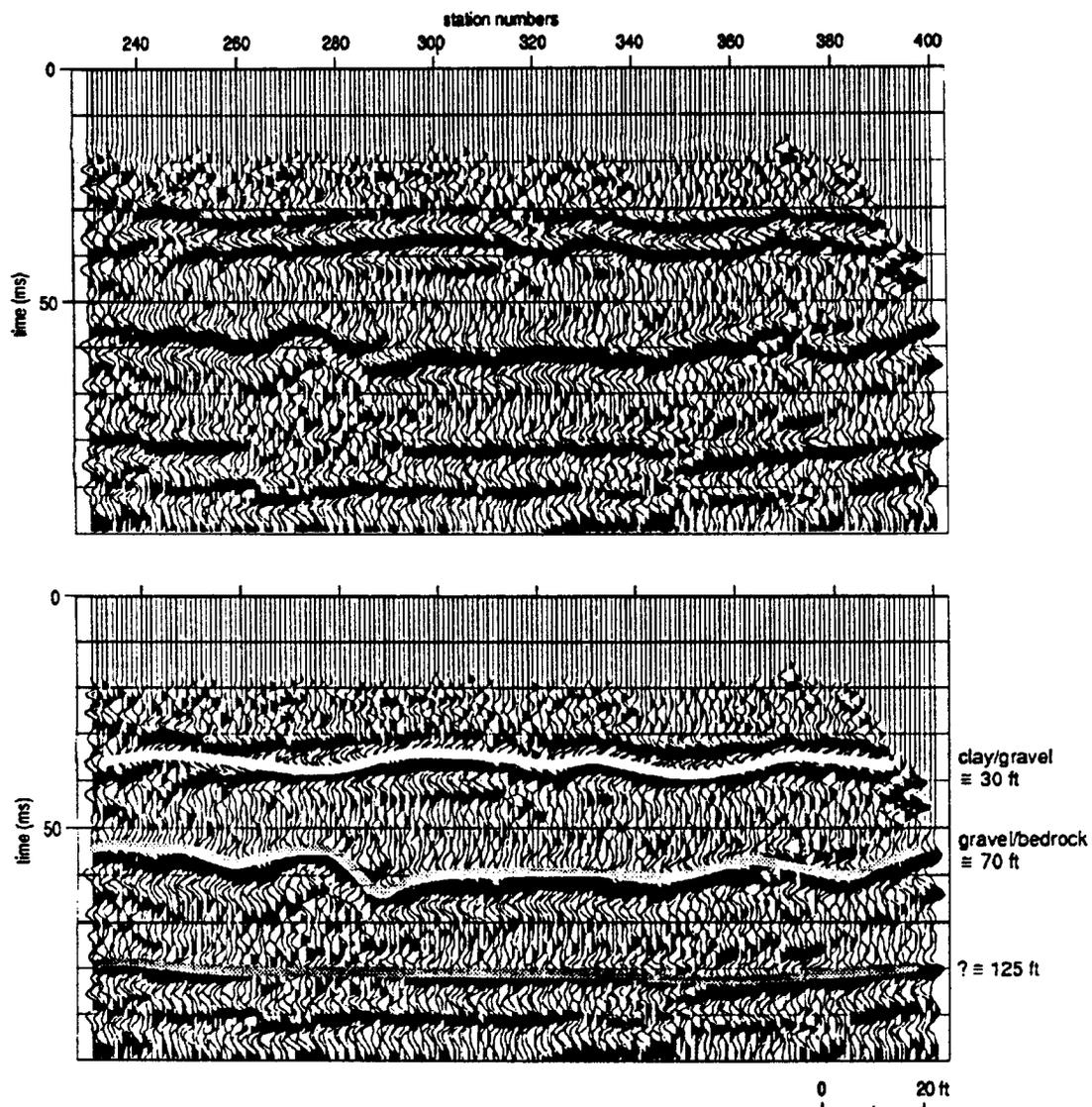
r

Figure 5. CDP stacked, 24 fold seismic reflection section from GEMS. At least three reflection events are easily interpretable on the stacked section. The interpretation suggest several feature of acoustic significance that could influence the hydrologic setting.

TABLE 1

format from SEG2 to KGSSEGY

preliminary editing

trace balancing

first arrival muting

surgical muting

assign geometries

sort into CDPs

velocity analysis

spectral analysis

surface consistent statics

residual statics

digital filtering

secondary editing

CDP stack

amplitude normalization

display

Table 1   Processing flow for CDP stacked data in Figure 5. Parameters were
determined by analysis of each prior step as well as through iterative
analysis of particular operations.